THÈSE DE DOCTORAT
DOCTORATE THESIS

SUSTAINABLE SMART CITY MOBILITY ENABLED BY MULTI-LEVEL COOPERATIVE DECISION-MAKING FOR CONNECTED AUTONOMOUS VEHICLES

SHAN HE

Université de technologie de Compiègne
Heudiasyc, UMR CNRS 7253

MEMBRES DU JURY

RAPPORTEURS	Nadine PIAT	Professeur à SUPMICROTECH-ENSMM
	Olivier SIMONIN	Professeur à l'INSA Lyon
EXAMINATEURS	Vincent FREMONT	Professeur à l'École Centrale de Nantes
	Youcef MEZOUAR	Professeur à SIGMA-Clermont
	Pedro CASTILLO-GARCIA	Directeur de recherche CNRS, Heudiasyc UMR CNRS/UTC
DIRECTEUR	Lounis ADOUANE	Professeur à l'Université de Technologie de Compiègne (UTC)

16 DÉCEMBRE 2025

SPÉCIALITÉ: Automatic Control and Robotics
ÉCOLE DOCTORALE: ED71 « Sciences pour l'Ingénieur »

Shan HE: *Sustainable Smart City Mobility Enabled by Multi-Level Cooperative Decision-Making for Connected Autonomous Vehicles*,
Thèse de Doctorat, 16 Décembre 2025

ABSTRACT

Connected Autonomous Vehicles (CAVs), equipped with cooperative decision-making capabilities, are regarded as a future development trend in intelligent urban transportation systems. Studies show that CAVs offer significantly greater applicability and effectiveness in managing complex situations such as unsignalized intersections or round-about crossing, primarily due to their ability to perform cooperative decision-making and intelligent coordination, which enhance both traffic efficiency and safety. The objective of this PhD thesis is to develop a CAV-based cooperative multi-risk assessment and management architecture for unsignalized intersections to optimize traffic flow at both the microscopic-level (interactions between several local vehicles) and macroscopic-level (interactions of CAV according to global road flows). At the microscopic level, a Multi-Risk Management Cooperative Optimization approach based on a Predicted Inter-Distance Profile (MRMCO-PIDP) is developed to efficiently manage the risk of collision between CAVs. This method is further extended to enhance the negotiation mechanism and optimization process by enabling adaptation to distributed decision-making. To address uncertainties arising from various environmental factors—such as localization errors, communication delays, and, more critically, communication loss—a PIDP-based Probabilistic Uncertainty Interval (PIDP-PUI) method is proposed to support robust collaborative decision-making mainly under degraded communication conditions. At the macroscopic level, due to the large volume of vehicles often leading to an exponential increase in computational complexity, a conflict-path-checking and risk management graph method is introduced to substantially reduce the computational burden of intersection management, thereby making the approach viable for real-world implementation. Building on this foundation, in complex traffic scenarios, effectively mitigating the congestion remains a critical challenge. To this end, a Congestion-Sensitive Flow Fusion (CSFF) model is proposed to analyze the causes of congestion from a traffic flow perspective and to provide target speeds for different directions to alleviate it. By integrating the macroscopic and the microscopic levels, the MRMCO-PIDP method and the proposed CSFF model are fused to achieve both collision avoidance and congestion mitigation, ultimately reducing average waiting delays and congestion rates. Further, in order to intensively validate the proposed decision-making architectures and optimization processes, a precise simulator has been developed, and a series of stochastic scenarios have been generated for evaluation. The simulation results demonstrate the effectiveness and the robustness of the proposed methods in handling complex and uncertain traffic conditions.

Keywords: Multi-Vehicle Systems (MVS), Connected Autonomous Vehicles (CAV), Cooperative Navigation, Cooperative Risk-Assessment and Management, Hybrid Centralized – Decentralized Control Architecture, Decision-Making under Uncertainty, Traffic flow management in localized intersections.

RÉSUMÉ

Les Véhicules Autonomes et Connectés (CAVs), dotés de capacités de prise de décision coopérative, sont considérés comme une tendance de développement majeure pour les systèmes de transport urbain intelligents. Les études démontrent que les CAVs offrent une applicabilité et une efficacité accrue pour la gestion des situations/environnements complexes comme les intersections et ronds-points non signalisés. Ceci est principalement dû à leur capacité à exécuter une prise de décision coopérative et une coordination intelligente, améliorant à la fois l'efficacité du trafic et la sécurité. L'objectif de cette thèse de doctorat est de développer une architecture coopérative d'évaluation et de gestion multi-risques, basée sur les CAVs, pour les intersections non signalisées, afin d'optimiser le flux de trafic aux niveaux à la fois microscopique (interactions entre plusieurs véhicules locaux) et macroscopique (interactions des CAVs en fonction des flux routiers globaux).

Au niveau microscopique, une approche d'Optimisation Coopérative de Gestion Multi-Risques basée sur le Profil de Distance Inter-Véhiculaire Prédit (MRMCO-PIDP) est développée pour gérer efficacement le risque de collision entre les CAVs. Cette méthode est ensuite étendue pour améliorer le mécanisme de négociation et le processus d'optimisation en permettant une adaptation à la prise de décision distribuée. Pour répondre aux incertitudes provenant de divers facteurs environnementaux — tels que les erreurs de localisation, les délais de communication et, plus critique encore, la perte de communication — une méthode d'Intervalle d'Incertitude Probabiliste basée sur le PIDP (PIDP-PUI) est proposée pour soutenir une prise de décision collaborative robuste dans des conditions de communication dégradées.

Au niveau macroscopique, étant donné le grand volume de véhicules en interaction, ceci entraîne souvent une augmentation exponentielle de la complexité de calcul, une méthode basée sur un graphe de gestion des risques et de vérification des chemins de conflit est introduite pour réduire substantiellement la charge de calcul de la gestion de l'intersection, rendant ainsi l'approche viable pour une mise en œuvre dans le monde réel. Sur cette base, dans des scénarios de trafic complexes, l'atténuation efficace de la congestion demeure un défi critique. À cette fin, un modèle de Fusion de Flux Sensible à la Congestion (CSFF) est proposé pour analyser les causes de la congestion du point de vue de la théorie des flux de trafic et pour fournir des vitesses cibles pour les différentes directions de l'intersection dans l'objectif de minimiser les risques de congestion.

En intégrant les niveaux macroscopique et microscopique, la méthode MRMCO-PIDP et le modèle CSFF proposé sont fusionnés pour réaliser à la fois l'évitement des collisions et l'atténuation de la congestion, réduisant ainsi les délais d'attente moyens et les taux de congestion. De plus, afin de valider de manière approfondie les architectures de prise de décision et les processus d'optimisation proposés, un simulateur précis a été développé, et une série de scénarios stochastiques a été générée pour l'évaluation. Les résultats de simulation démontrent l'efficacité et la robustesse des méthodes proposées dans la gestion de conditions de trafic complexes et incertaines.

Mots-clés : Systèmes Multi-Véhicules (MVS), Véhicules Autonomes et Connectés (CAV), Navigation Coopérative, Évaluation et Gestion Coopérative des Risques, Architecture de Contrôle Hybride Centralisée – Décentralisée, Prise de Décision sous Incertitude, Gestion des flux de trafic à des intersections localisées.

PUBLICATIONS

[1] S. He and L. Adouane, “Multi-scale cooperative decision-making in unsignalized intersections integrating traffic flow dynamics,” in *2026 IEEE Intelligent Vehicles Symposium (IV)*, Detroit, United States, 2026.

[2] S. He and L. Adouane, “Safe cooperative decision-making in uncertain unsignalized intersection based on probabilistic and predictive risk assessment strategy,” in *2025 IEEE Intelligent Vehicles Symposium (IV)*, 2025, pp. 1140–1147. DOI: 10.1109/IV64158.2025.11097798.

[3] S. He and L. Adouane, “Contextual-graph topology for efficient and real-time cooperative intersection management,” *IFAC-PapersOnLine*, vol. 59, no. 3, pp. 151–156, 2025, 12th IFAC Symposium on Intelligent Autonomous Vehicles IAV 2025, ISSN: 2405-8963. DOI: https://doi.org/10.1016/j.ifacol.2025.07.026. [Online]. Available: https://www.sciencedirect.com/science/article/pii/S2405896325003659.

[4] S. He and L. Adouane, “Energy-efficient cooperative decision-making for cavs: a traffic flow optimization approach,” in *2025 20th Annual System of Systems Engineering Conference (SoSE)*, 2025, pp. 1–6. DOI: 10.1109/SoSE66311.2025.11083785.

[5] S. He and L. Adouane, “A hybrid coordinated decision-making method for cavs at unsignalized intersection,” in *2024 European Control Conference (ECC)*, 2024, pp. 3769–3776. DOI: 10.23919/ECC64448.2024.10591063.

[6] S. He and L. Adouane, “A dynamic multi-risk management based on cooperative optimization architecture for cavs at unsignalized intersection,” *IFAC-PapersOnLine*, vol. 58, no. 18, pp. 71–77, 2024, 8th IFAC Conference on Nonlinear Model Predictive Control NMPC 2024, ISSN: 2405-8963. DOI: https://doi.org/10.1016/j.ifacol.2024.09.012. [Online]. Available: https://www.sciencedirect.com/science/article/pii/S2405896324013910.

[7] S. He and L. Adouane, “Reactive cooperation of multi-vehicle system for efficient intersection crossing based on pidp speed space assessment,” in *2024 13th International Workshop on Robot Motion and Control (RoMoCo)*, 2024, pp. 142–148. DOI: 10.1109/RoMoCo60539.2024.10604427.

[8] S. He and L. Adouane, “Energy efficiency of cavs in unsignalized intersections based on cooperative risk-assessment strategy,” in *Proceedings of the Symposium on Technological Systems, Sustainability and Safety (TS3 2024)*, Paris, France, 2024.

[9] S. He and L. Adouane, “Multi-scale cooperative traffic flow coordination for cavs at unsignalized intersections,” *Transportation Research Part D: Transport and Environment*, 2025, Submitted for publication, under review.

ACKNOWLEDGMENTS

It's wild how time flies.

It feels like just yesterday, but it's already been over three years since I landed back in France on April 14, 2022, to chase this PhD. Looking back on these three years, it's really been a journey—full of struggles, some real pain, but also a lot of joy.

I'll be the first to admit I'm a master procrastinator. I have this terrible habit of putting things off until I absolutely can't anymore, and only then do I find the motivation to get it done. As it turns out, that's a horrible quality for a PhD student.

I wasted so much time just trying to figure out how to even start. It's a strange thing to say, because my research topic and my thesis title were set from day one. The destination was always clear. But I was completely lost on how to get there—what path to take, what methods to use. I was just... stuck.

I owe so much to my supervisor, Lounis. He is a true gentleman. He showed me incredible patience, especially with my… lazy before deadlines. Whenever I was academically lost, he pointed me in the right direction. When I was just plain lost in life, he offered guidance. Without his support and mentorship, especially during those tough first two years, I honestly don't think I would have produced enough to ever finish this PhD. Being his student has been an absolute honor.

On top of the academic struggles, life threw some curveballs, too. My grandfather passed away in the summer of 2022. Because of all the pandemic restrictions in China, I could not return to China at that time and couldn't even go home for his funeral. To be honest, I'd had this sinking feeling ever before I left for France... a fear that something like this might happen. I just didn't think it would be so soon.

And as the saying goes: when it rains, it pours.

This PhD was supposed to be a joint program between UTC and Cranfield University, which meant I was supposed to move to the UK after 18 months. But in late 2023, my ATER application, a key part of the visa, was repeatedly rejected. Eventually, the British university had to cancel my offer and pull my funding.

This threw my life into chaos. I would be broke after two months, had to ask my parents for money just to get by, and was suddenly facing the very real possibility of not being able to finish my PhD at all.

Once again, Lounis came to the rescue. He actively pursued and secured two rounds of short-term funding and a new one-year contract at UTC for me to ensure the continuity of my PhD. This was a massive relief, both financially and mentally. I honestly can't thank him enough. I'm also so grateful to all the UTC staff and my colleagues at Heudiasyc who helped me navigate that mess.

I'm also not exactly what you'd call a social butterfly. My go-to way to relax is just planting myself in front of my computer and gaming. So I'm incredibly thankful for my French colleagues—Kévin, Hugo, and Sara. They pulled me out of my shell and invited me, the "foreigner" in the office, to experience the real France. We explored everything: the food and wine, the forests and castles, the history and culture... a world that is as deep as it is beautiful. They also helped me untangle all the little problems of daily life here.

And, of course, a huge thanks to Elisa from Italy (and her Tiramisu and Spritz!), and to my Mexican friends—Alexanjo, Alex, Salvador, and the two Armandos (and their tequila and tacos!).

Looking back, it's funny. If that UK visa had gone through smoothly, I would have missed out on meeting all these amazing people. Maybe it was a blessing in disguise, after all.

I also need to thank my friends who were there for me all along: Yang Kang, Pian Yuwei, Dr. Wei Siyi, and so many others, my colleagues, Emmanuel, Thibault, Lyes, Mi Chunlin, Zhu Chengrui, Chen Wenlong, Li Lei, Shen Siyi, and so many others.

And finally, the most important thank you of all: to my parents and my family. Thank you for the lessons you taught me, for your belief in my education, and for the financial support that made this all possible. Thank you for backing me completely when I decided to go for this PhD, and for trusting me to find my own way, even when I was lost about the future. Home has always been my safe harbor in every storm, and knowing you were there for me was the anchor that kept me steady while I was all alone on another side of the world.

Last of all... a small thanks to myself, for somehow managing to stick it out. It's been a long road, but it is not the conclusion, it is the opening of a new chapter.

CONTENTS

ACRONYMS

AIM: Autonomous Intersection Management

ASA: Adaptive Simulated Annealing

CAVs: Connected Autonomous Vehicles

CRMG: Contextual Risk Management Graph

CRMG-PIDP: Contextual Risk Management Graph based on PIDP

CSFF: Congestion-Sensitive Flow Fusion

DCFC: Dynamic Collision-Free Cooperation

D-MRMCO: Dynamic Multi-Risk Management Cooperative Optimization

ETTC: Extended Time-to-Collision

FCFS: First-Come-First-Served

FSM: Finite State Machine

HDVs: Human-Driven Vehicles

IM: Intersection Manager

MFD: Macroscopic Fundamental Diagram

MRMCO-PIDP: Multi-Risk Management Cooperative Optimization based on PIDP

MVS: Multi-Vehicle System

PC: Probability Collective

PI: Potential Interval

PIDP: Predicted Inter-Distance Profile

PIDP-PUI: PIDP based Probabilistic Uncertainty Interval

PO-MDP: Partially Observable Markov Decision Process

RSS: Responsibility-Sensitive Safety

SCOU: Safe Cooperative Optimization under Uncertainty

TFCM-CAVs: Traffic Flow Coordination Method for CAVs

TTC: Time-To-Collision

UAPR: Uncertainty-Adaptive Planning Rate

V2I: Vehicle-to-Infrastructure

V2V: Vehicle-to-Vehicle

V2X: Vehicle-to-Everything

LIST OF FIGURES

LIST OF TABLES

GENERAL INTRODUCTION

CONTEXT OF THE PHD THESIS

Despite the long-standing goals of Intelligent Transportation Systems (ITS) to enhance safety, efficiency, and sustainability, significant challenges persist, particularly in the context of ambitious initiatives like the “Vision Zero”. At the heart of this challenge lie urban intersections, which act as the primary bottlenecks for the entire transportation network. From a safety perspective, they are the epicenters of urban accidents due to inherent conflict points between crossing traffic flows. From an efficiency standpoint, existing management paradigms, reliant on traffic signals or stop signs, are fundamentally passive and non-cooperative. This enforces inefficient stop-and-go dynamics, resulting in significant delays, energy waste, and pollutant emissions, which is contrary to the demands of modern green and efficient mobility. Consequently, the traditional intersection management framework itself has become the main impediment to improving the overall performance of urban traffic systems, highlighting the urgent need for a new paradigm capable of active, real-time, and fine-grained cooperative control.

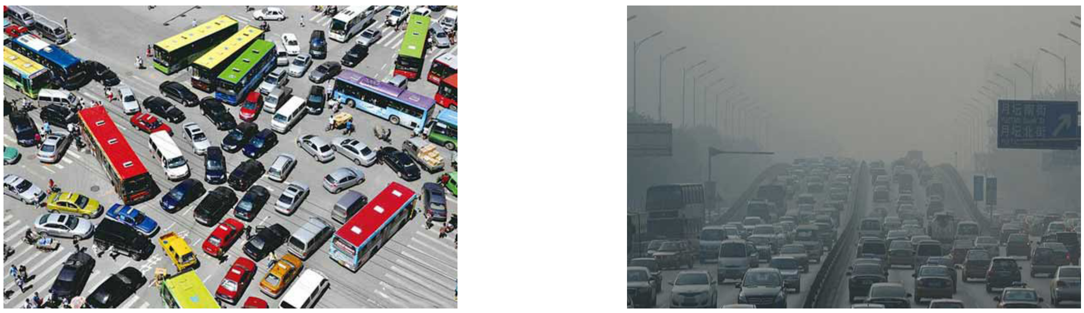

(a) Time waste (b) Pollution

Traffic congestion at intersection

The emergence of Connected and Autonomous Vehicles (CAVs) presents a transformative opportunity to dismantle this long-standing bottleneck. Equipped with advanced onboard sensors and high-precision actuation, and provided with shared environmental awareness through connectivity, these vehicles can transcend their roles as isolated agents and operate as a cohesive, intelligent collective. The true paradigm shift, however, lies in their capacity for cooperative decision-making. Instead of passively adhering to the rigid, predetermined rules of traffic signals, CAVs can proactively negotiate and optimize their spatio-temporal trajectories in real-time. This ability to collaboratively plan for a shared objective allows for the replacement of inefficient stop-and-go dynamics with a fluid, on-demand coordination scheme, directly targeting the core safety and efficiency challenges inherent to intersections. It is precisely these capabilities that make CAVs uniquely suited for the dynamic and unstructured nature of unsignalized intersections, where their full cooperative potential can be unleashed, offering a level of optimization far beyond what is achievable at traditionally signalized crossings.

However, focusing the cooperative capability solely on the vehicles within the local confines of an intersection is insufficient to solve the full spectrum of urban traffic challenges. In complex urban networks, phenomena such as “ghost traffic jams” are often the result of cascading effects that originate far from the point of congestion and are invisible from a purely local perspective. To meaningfully address systemic issues like city-wide congestion, it is imperative to look beyond the immediate vicinity of the intersection and consider the surrounding, holistic traffic flow. A truly effective solution must therefore bridge the gap between macroscopic traffic flow dynamics and microscopic CAV control, integrating both scales to enable genuine urban-level traffic management.

Within this context, our research is conducted at the Heudiasyc Laboratory (UMR CNRS/UTC 7253) of the Université de Technologie de Compiègne (UTC) and supervised by Prof. Lounis ADOUANE, aiming to investigate multi-level cooperative decision-making and planning approaches for CAVs in smart city environments.

PROBLEM STATEMENT

The foundational paradigm for modern cooperative driving has shifted from discretized resource allocation protocols, which often lead to inefficient stop-start cycles, toward the joint optimization of continuous spatio-temporal trajectories. This approach allows for fluid and highly efficient vehicle coordination. However, the success of this paradigm hinges on surmounting three interconnected, multi-layered challenges that define the current scientific frontier.

First, at the most fundamental level of vehicle interaction, there is a need for a more holistic risk assessment model. While predictive metrics like the Predicted Inter-Distance Profile (PIDP) have surpassed reactive ones like Time-to-Collision (TTC), they are predominantly designed with pairwise vehicle dynamics in mind. This intrinsic limitation prevents a truly comprehensive understanding of collective risk in dense, multi-agent scenarios, where danger can emerge from complex group interactions rather than simple one-to-one conflicts.

Second, this coordination must operate within the real world, which is inherently uncertain. Even with a perfect multi-vehicle risk model, decision-making is plagued by imperfect sensor data and unpredictable behaviors. This forces a critical dilemma: relying on probabilistic methods that optimize for average performance but lack the hard safety assurances required for certification, or employing robust, set-based methods (e.g., Responsibility-Sensitive Safety (RSS)) that provide verifiable guarantees but often impose severe performance penalties due to worst-case conservatism. Navigating this trade-off between optimality and certifiable safety remains a major unresolved issue.

Finally, solving the local coordination problem, even robustly, is a necessary but insufficient condition for true urban mobility improvement. Vehicle-level optimization is inherently myopic, ignoring the broader network context. Effective intersection management is deeply coupled with macroscopic traffic flow dynamics, where upstream demand and downstream congestion dictate local performance. Without unifying these scales, locally optimal maneuvers can inadvertently trigger system-level inefficiencies, such as propagating traffic waves.

Therefore, the central challenge addressed by this thesis is the development of a unified cooperative decision-making framework that is simultaneously collective in its risk assessment, robust against uncertainty without being overly conservative, and aware of the macroscopic traffic context in its planning.

MAIN OBJECTIVES AND CONTRIBUTIONS

To address the multifaceted challenges identified in the previous section, this thesis aims to propose a comprehensive, multi-layered cooperative decision-making framework for CAVs at unsignalized intersections. The research is structured around four primary objectives, each building logically upon the last to construct a solution that is robust, scalable, and system-aware.

1. **To Develop a Collective Risk Management Framework for Multi-Vehicle Coordination**. The foundational objective is to move beyond simplistic pairwise risk assessment. The work begins by establishing a baseline coordination mechanism for two-vehicle scenarios, leveraging the PIDP metric to analyze interaction dynamics and assign priorities, which are then translated into acceleration or deceleration commands for safe and rapid passage (cf. Section 3.2.1). This fundamental model is then systematically extended from this dyadic case to address the more complex and realistic scenarios involving three, four, or more vehicles (cf. Section 3.2.2). The key contribution here is the development of a method to manage collective risk, where the interactions among multiple agents are considered simultaneously, rather than as a mere aggregation of separate pairwise conflicts. The main contribution regarding this aspect is given in Chapter 3, and has been published in [1], [2], [3]. Contributions about CAVs' energy consumption optimization based on this framework has been published in [4], [5].

2. **To Design a Robust Decision-Making Strategy under Environmental Uncertainty.** Building upon the deterministic coordination framework, the second objective is to enhance its robustness against real-world uncertainties, such as communication latency and localization errors. This research gives special consideration to the most critical failure mode: complete communication loss. To tackle this, a novel hybrid methodology is proposed. This approach synergizes the strengths of probabilistic models, which capture the likely evolution of vehicle states, with the conservative guarantees of set-based interval analysis (cf. Section 4.2). The resulting contribution is a decision-making strategy that can gracefully degrade and maintain a high level of safety even when some CAVs disconnect from the local network. The main contribution regarding this aspect is given in Chapter 4, and has been published in [6].

3. **To Ensure Computational Scalability in Dense Traffic Scenarios**. With a robust multi-agent framework established, the next challenge is to ensure its real-time feasibility in dense, continuous traffic flows. The computational burden of conventional risk assessment methods grows combinatorially with the number of vehicles, posing a significant scalability bottleneck. To overcome this, the third objective is to develop a method to drastically reduce this computational load. This is achieved by first analyzing the topological structure of the intersection to classify potential conflict types (cf. Section 5.2.1). Based on this classification, the algorithm can intelligently prune the set of interactions that require explicit risk calculation, effectively filtering out non-conflicting vehicle pairs (cf. Section 5.2.2). The contribution is an efficient risk assessment scheme that allows the framework to scale to high-density traffic without compromising real-time performance. The main contribution regarding this aspect is given in Section 5.2, and has been published in [7].

4. **To Integrate Microscopic Vehicle Control with Macroscopic Traffic Flow Management**. Finally, having addressed the local, microscopic challenges of robustness and scalability, the ultimate objective of this thesis is to bridge the gap between local vehicle coordination and network-level traffic management. This involves first defining a new metric for congestion specifically tailored to CAVs at unsignalized intersections from a macroscopic perspective (cf. Section 5.3.1). A model is then developed to translate high-level traffic management goals into tangible commands for CAVs on the corresponding direction (cf. Section 5.3.3). The key contribution is a multi-scale control architecture where macroscopic guidance speeds, generated to alleviate emerging congestion, are directly incorporated into the microscopic decision-making framework. This integration enables the system to not only resolve local conflicts but also to actively contribute to the mitigation of large-scale traffic congestion. The main contribution regarding this aspect is given in Section 5.3. The results associated with this contribution are submitted for publication in [8] "*Transportation Research Part D: Transport and Environment*".

MANUSCRIPT ORGANIZATION

In accordance with the research themes outlined above, this thesis is organized into five chapters. The outline of this manuscript is depicted in Figure 2. Chapter 1 provides a comprehensive review of the state of the art, aiming to discuss the current research landscape and, more specifically, to identify the existing gaps in multi-risk cooperative decision-making and planning for CAVs within the Smart City context. Chapter 2 introduces foundational methodologies from related fields that are pertinent to the approaches developed in this thesis. Finally, the core methods proposed in this thesis are presented in detail from Chapter 3 to Chapter 5. The specific contents are as follows:

1. **Chapter 1 - From Smart Cities to Connected Autonomous Vehicles Cooperative Decision-Making**

   This chapter establishes the scientific context for the thesis. It begins by positioning CAVs as a critical enabler within the broader Smart City paradigm. It then reviews the evolution of autonomous decision-making, starting from the foundational challenges of single-vehicle motion planning. This basis is subsequently extended to complex multi-vehicle cooperative strategies, particularly for unsignalized intersections. Finally, the chapter bridges these microscopic interactions with the challenges of macroscopic urban traffic flow, identifying the key research gaps that this thesis aims to address.

2. **Chapter 2 - Theoretical Foundations and Methodological Review for CAVs**

   This chapter provides a methodical review of key concepts, spanning from microscopic vehicle control—encompassing behavioral decision-making, risk assessment, and motion planning—to the broader challenges of cooperative intersection management. Crucially, it examines state-of-the-art approaches for handling uncertainty and for integrating local vehicle dynamics with macroscopic traffic flow theories. This chapter establishes the essential methodological context required to appreciate the novel contributions presented in the subsequent sections.

3. **Chapter 3 - Multi-Risk Assessment and Management Cooperative Optimization at Unsignalized Intersection**

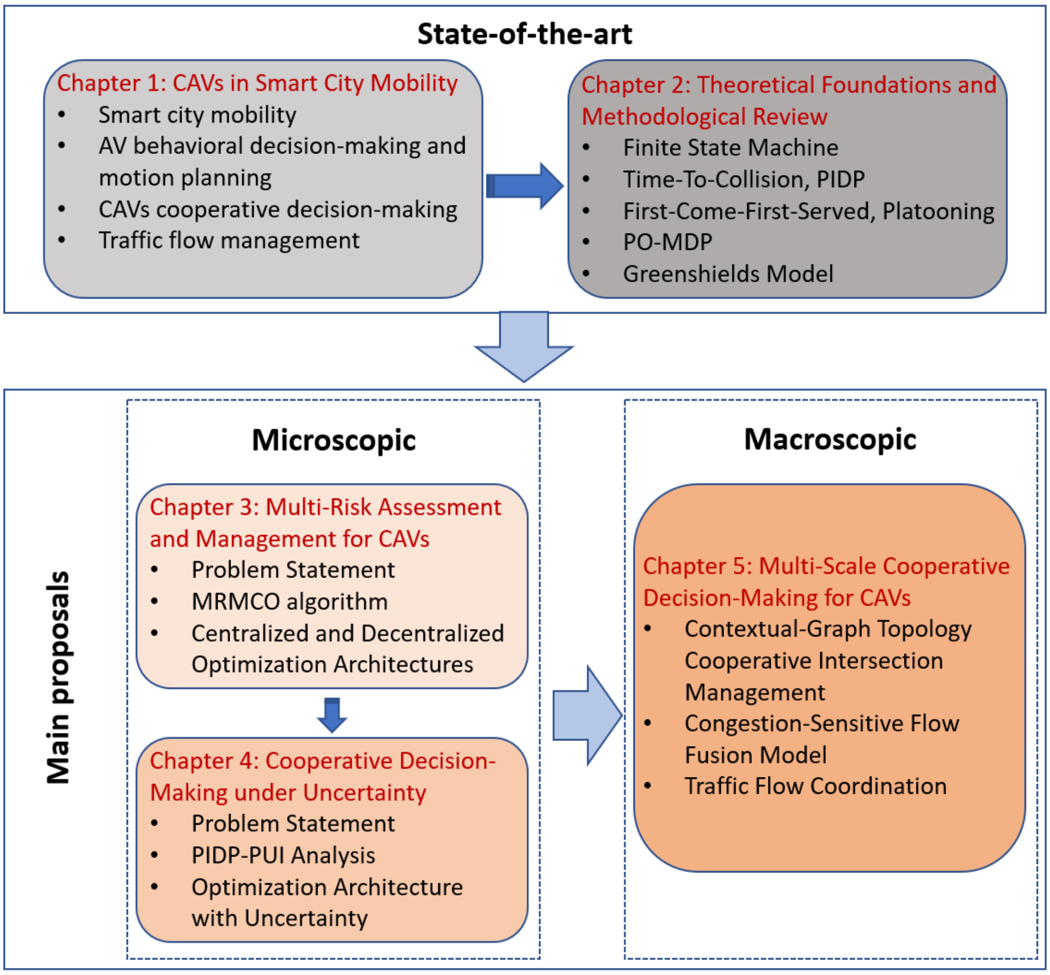

Figure 2: The outline of the PhD manuscript

This chapter presents the thesis' foundational contribution: a novel framework for Multi-Risk Assessment and Management at unsignalized intersections. This chapter moves beyond simple pairwise interactions to address complex, simultaneous conflicts. It introduces a methodology that extends the PIDP to effectively manage collective risk. It is then implemented and evaluated within two distinct cooperative optimization architectures: one centralized and one decentralized, establishing a robust solution for safe and efficient multi-vehicle coordination.

4. **Chapter 4 - Cooperative Decision-Making Method for CAVs under Uncertainty**

   This chapter confronts the critical challenge of decision-making under uncertainty. Building on the deterministic models, this chapter introduces a novel hybrid methodology, termed Probabilistic Uncertainty Interval Analysis, which fuses the efficiency of probabilistic forecasting with the guarantees of set-based methods. This approach is integrated with the PIDP risk assessment framework to compute risk against a bounded interval of potential vehicle positions, rather than a single trajectory. The result is a robust cooperative framework capable of ensuring safety during high-risk events, with a specific focus on managing communication loss at intersections.

5. **Chapter 5 - Multi-Scale Cooperative Decision-Making for CAVs**

   This chapter elevates the research from the vehicle level to the network level by developing a multi-scale cooperative decision-making framework. To address the computational challenges of high-density traffic, it first introduces a method to significantly reduce the computational load of risk assessment. Building on this scalable foundation, the chapter then presents a novel architecture that integrates the microscopic cooperative controller with macroscopic traffic flow dynamics. This hybrid approach enables the system to manage not only local vehicle conflicts but also to address systemic-level of risk and congestion in complex urban scenarios.

General conclusion and main contributions in the PhD thesis are summarized at the end of the manuscript, along with perspectives.

1 FROM SMART CITIES TO CONNECTED AUTONOMOUS VEHICLES COOPERATIVE DECISION-MAKING

This chapter introduces the background and motivation of the study, focusing on the growing challenges of urban traffic systems and the urgent demand for sustainable and intelligent mobility solutions. It outlines the evolution of smart city mobility from both micro- and macro-level perspectives, linking individual vehicle behaviors with large-scale traffic flow management. The chapter also reviews the development of autonomous and connected vehicle technologies, particularly their decision-making and motion planning foundations, which together establish the basis for cooperative and efficient transportation systems.

1.1 GLOBAL TRANSPORTATION CHALLENGES AND SMART MOBILITY VISION

1.1.1 *Challenges and Complexities of Urban Traffic Systems*

Urban traffic management is a cornerstone of modern city planning, addressing the intricate challenges posed by the increasing density and mobility demands of urban populations. As cities worldwide continue to grow, the complexity of managing traffic flows escalates, leading to significant economic, environmental, and social consequences. Intersections, as critical nodes within urban traffic networks, play a pivotal role in determining the efficiency, safety, and sustainability of transportation systems.

The rapid urbanization and population growth in metropolitan areas have exacerbated traffic-related challenges, particularly in densely populated cities. According to data from the *TomTom Traffic Index (2024)*[9], traffic congestion in Bordeaux leads to an average annual time loss of 113 hours per driver during rush hours, corresponding to an estimated economic loss of approximately 1582 € per person per year. Moreover, the average travel time per 10 kilometers in Bordeaux reaches 31 min and 8 s. Similar patterns are observed in Paris, where drivers lose around 101 hours annually, incurring an average cost of 1442 € per person, with a mean travel time of 28 min and 53 s per 10 kilometers. The data presented in Table 1.1 highlight the magnitude of urban traffic challenges across European cities, where congestion not only disrupts daily commutes but also undermines economic productivity and overall urban livability.

Beyond economic impacts, traffic congestion exacerbates safety risks. The National Highway Traffic Safety Administration (NHTSA) in the United States reported that human error accounts for 94% of traffic crashes, based on a survey of 2,189,000 incidents [10]. Intersections, where conflicting vehicle movements converge, are particularly prone to accidents, making them a focal point for traffic management strategies aimed at enhancing safety.

Environmentally, urban traffic is a major contributor to greenhouse gas emissions, posing a significant threat to public health and sustainability. Transport accounts for around one-fifth of global CO_2 emissions; it is now the second-largest source of global greenhouse gas emissions [11]. Three-quarters of this is from road transport in 2020 [11], [12]. Most of this

Table 1.1: TomTom 2024 Traffic Index – Top 8 Most Congested Cities in the Europe [9]

World Rank	City	Country	Avg. Travel Time per 10 km	Congestion Level	Time Lost per Year (rush hours)
5	London	U.K.	33 min 17 s	32%	113 h
24	Bordeaux	France	31 min 08 s	33%	113 h
45	Paris	France	28 min 53 s	30%	101 h
58	Edinburgh	U.K.	27 min 24 s	40%	94 h
63	Marseille	France	27 min 14 s	31%	93 h
92	Nice	France	25 min 29 s	29%	84 h
94	Liverpool	U.K.	25 min 15 s	35%	86 h
96	Nantes	France	25 min 06 s	32%	96 h

comes from passenger vehicles — cars and buses — contributing 45.1%. The other 29.4% comes from trucks carrying freight. A substantial portion of these emissions, however, can be attributed to non-essential fuel consumption caused by traffic congestion, which forces vehicles to operate inefficiently through frequent idling, acceleration, and deceleration cycles. These emissions contribute to air pollution, increasing the risk of heart disease and stroke, and underscore the urgency of meeting ambitious targets, such as the 60% reduction in transport emissions by 2050 set by the 2011 Transport White Paper [13].

Socially, traffic congestion affects quality of life by increasing travel times, reducing accessibility, and contributing to stress and health issues. In cities like London and Paris, where drivers spend significant time in traffic. At the same time, unreasonable congestion management policies implemented by governments may impose substantial additional costs on people's daily lives [14]. Such effects are particularly pronounced among low-income urban residents, potentially exacerbating existing social inequalities [15]. Moreover, the high accident rates at intersections, driven by human error, pose ongoing safety concerns for all road users, including vulnerable groups such as pedestrians and cyclists.

Smart City Mobility has increasingly been recognized as a promising direction for addressing urban traffic congestion and improving overall transportation efficiency [16]. By integrating digital infrastructure, real-time data analytics, and intelligent coordination mechanisms, smart cities aim to optimize traffic flow, enhance safety, and reduce environmental impact [17], [18]. Rather than merely managing congestion, this paradigm envisions a holistic urban mobility ecosystem that connects vehicles, infrastructure, and users in a sustainable and adaptive manner.

Building upon the discussions of current traffic challenges and cooperative vehicle decision-making, the next subsection will focus on the concept of Smart City Mobility, exploring how intelligent infrastructure and connected autonomous vehicles can collectively shape the future of urban transportation systems.

1.1.2 *The Smart City Vision: Micro- and Macro-Level of Urban Traffic*

The smart city concept was born in the early 1990s [19]. American IT companies invented the term to describe new Information Communication Technology (ICT) tools aimed at responding to the problems of large metropolises, i.e., solving problems related to traffic and transport management.

Among the various dimensions of the smart city, smart mobility is considered one of the most critical pillars. It represents the integration of advanced transportation systems, intelligent infrastructure, and communication technologies to achieve efficient, safe, and low-emission urban mobility. Through the deployment of sensors, Internet of Things (IoT) devices [20], [21], and intelligent transport systems [22], [23], cities can collect and analyze real-time information about vehicle flows, road conditions, and environmental factors, thereby enabling adaptive traffic control and improved coordination among mobility services [24], [25]. The implementation of 5G networks and big-data-driven platforms further supports the seamless exchange of information between vehicles and infrastructure, laying the foundation for a more responsive and sustainable transportation network [26], [27].

While these technological advancements have significantly improved local traffic control and urban mobility management, it is important to emphasize that focusing solely on micro-level dynamics—such as individual intersections, roundabouts, or vehicle interactions along specific road segments—is insufficient to fully address the complexity of modern urban transportation systems. Urban mobility is inherently a multi-scale phenomenon, where micro-level vehicle behaviors interact with macro-level traffic flow patterns that reflect collective trends across entire networks. Therefore, achieving truly efficient and sustainable smart city mobility requires an integrated perspective that combines micro-level decision and control mechanisms with macro-level, traffic flow analysis. This holistic approach provides deeper insights into congestion propagation, mobility demand distribution, and system-wide coordination, thereby enabling more effective urban traffic management and planning.

In this context, Connected and Autonomous Vehicles (CAVs) have emerged as a pivotal element in the realization of smart mobility [28]. As an integral component of smart city ecosystems, CAVs enable continuous communication with their surroundings—vehicles (Vehicle-to-Vehicle, V2V), infrastructure (Vehicle-to-Infrastructure, V2I), and even pedestrians (Vehicle-to-Pedestrian, V2P)—through Vehicle-to-Everything (V2X) technologies. This interconnectivity facilitates real-time decision-making, enhances safety, and contributes to traffic efficiency by reducing human error and enabling cooperative driving strategies [29]. Moreover, CAVs play a key role in reducing environmental impacts by supporting optimized routing, smoother traffic flow, and integration with electric mobility infrastructures [30], [31]. Their deployment is therefore expected not only to improve mobility performance but also to reshape urban planning, redefining how people, goods, and services move within cities.

In summary, the smart city framework provides the digital and infrastructural foundation for the sustainable transformation of urban mobility. Within this framework, CAVs represent a critical technological and systemic evolution toward safer, cleaner, and more efficient cities. The following section will therefore focus on the development of autonomous driving technologies and the distinctive characteristics of Connected and Autonomous Vehicles.

1.2 AUTONOMOUS VEHICLES: DECISION-MAKING AND MOTION PLANNING

Within the broader framework of smart cities, CAVs constitute a fundamental component of smart mobility, enabling efficient, safe, and sustainable transportation. At the core of this ecosystem lies the autonomous vehicle — the technological foundation upon which CAVs are built. This section will begin by introducing the historical development of autonomous vehicles, followed by a discussion of their control architecture, decision-making methods, and motion planning.

1.2.1 *Development of Autonomous Vehicles*

Historically, vehicles evolved from purely mechanical machines operated by humans to intelligent systems capable of perception, reasoning, and autonomous control. This transformation has been propelled by advances in automation, robotics, and artificial intelligence, as well as by societal demands for safer, cleaner, and more efficient mobility (cf. Figure 1.1). The vision of automated driving dates back to early mechanical experiments, but significant progress emerged during the late 20th century through initiatives such as the EUREKA PROMETHEUS Project in Europe [32] and the DARPA Grand Challenges in the United States [33], which established the technological milestones of modern autonomous navigation. Today, autonomous vehicles integrate sophisticated sensing, decision-making, and control mechanisms that enable them to operate with minimal or no human intervention.

The Society of Automotive Engineers (SAE) formalized the classification of vehicle automation into six levels (0–5) [35] (cf. Figure 1.2). Levels 0–2 are generally regarded as driver assistance systems, where the human driver remains primarily responsible for monitoring and control.

1. **Level 0 (No Automation)**: The driver performs all driving tasks; the vehicle provides only basic warnings or alerts without active control.

2. **Level 1 (Driver Assistance)**: The system can assist with either steering or acceleration/braking, but the driver must remain fully engaged and responsible.

3. **Level 2 (Partial Automation)**: The vehicle simultaneously manages steering and speed under specific conditions, though constant driver supervision is still required.

These stages established the technological foundation for higher automation. Progress since the DARPA Grand Challenges has driven the transition toward conditional and full automation, represented by Levels 3–5.

1. **Level 3 (Conditional Automation)**: The system handles all driving tasks within a defined domain, but the driver must take over when requested.

2. **Level 4 (High Automation)**: The vehicle operates autonomously in specific, geofenced environments without human intervention, though only within its design limits.

3. **Level 5 (Full Automation)**: A fully autonomous capability under all road and environmental conditions—no human control or fallback required.

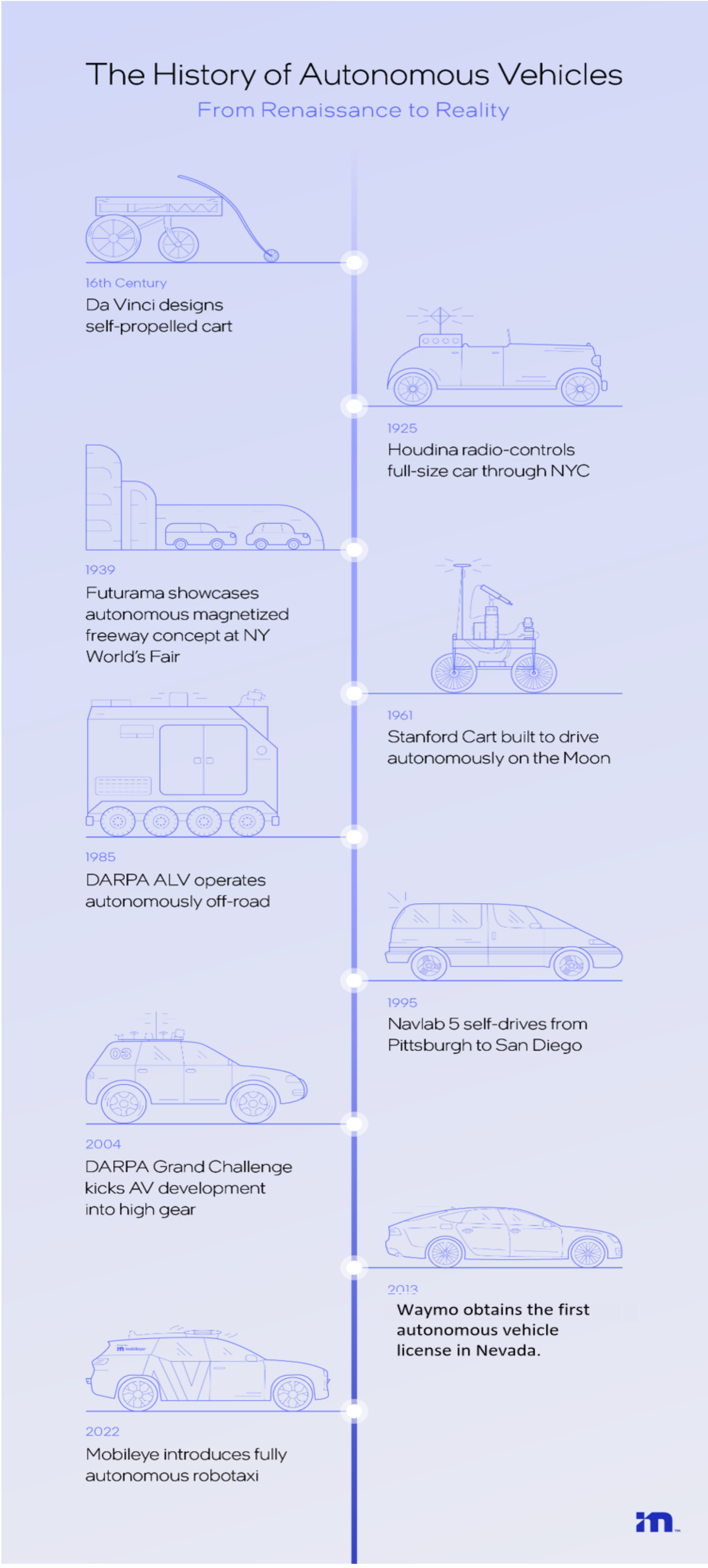

Figure 1.1: The history of autonomous vehicles [34]: from early mechanical designs and conceptual visions to fully automated robotaxi

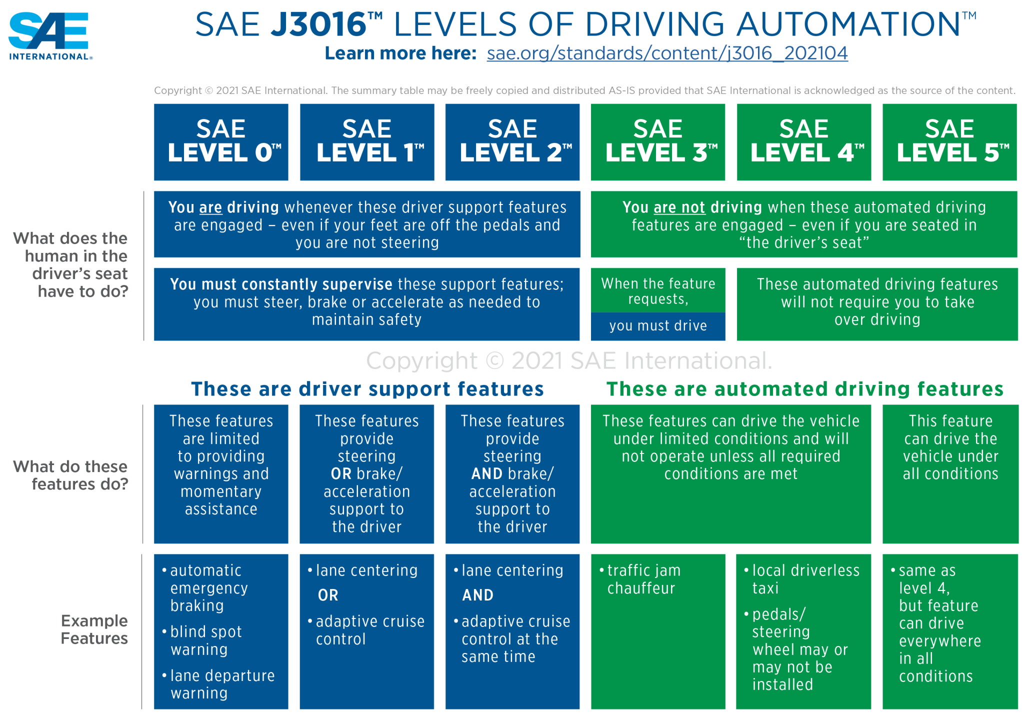

Figure 1.2: SAE Levels of Driving Automation J3016_202104 (Copyright© 2021 SAE International) [36]

In recent decades, the commercial sector has accelerated the development and deployment of autonomous driving technologies. Level 3 systems, such as Mercedes's Drive Pilot, have been introduced under well-defined operational conditions as regulatory frameworks worldwide evolve to enable higher automation [37]. Building upon this foundation, companies like Google's Waymo and General Motors' Cruise have launched Level 4 services, offering fully autonomous operation within geofenced urban areas [38], [39].

Ongoing research continues to expand operational domains, improve system robustness, and enhance safety assurance, with the long-term objective of achieving full automation [40], [41]. Autonomous vehicles thus mark a profound paradigm shift—advancing safety, efficiency, and sustainability while reshaping future urban mobility and infrastructure design.

1.2.2 *Overview of Autonomous Vehicles Control Architecture*

The control architecture of an autonomous vehicle is a complex and hierarchical system that integrates multiple subsystems to achieve safe, efficient, and intelligent driving behavior [40], [42], [43]. This architecture serves as the backbone of autonomy, enabling the vehicle to perceive its environment, make informed decisions, and execute control commands in real time.

In general, the control architecture can be decomposed into three fundamental components: perception, decision-making, and control [41], [44] (cf. Figure 1.3). The perception layer is responsible for interpreting raw sensor data and constructing an accurate representation of the surrounding environment [45], [46]. The decision layer utilizes this environmental understanding to plan specific tasks, activate an appropriate behavior, resolve

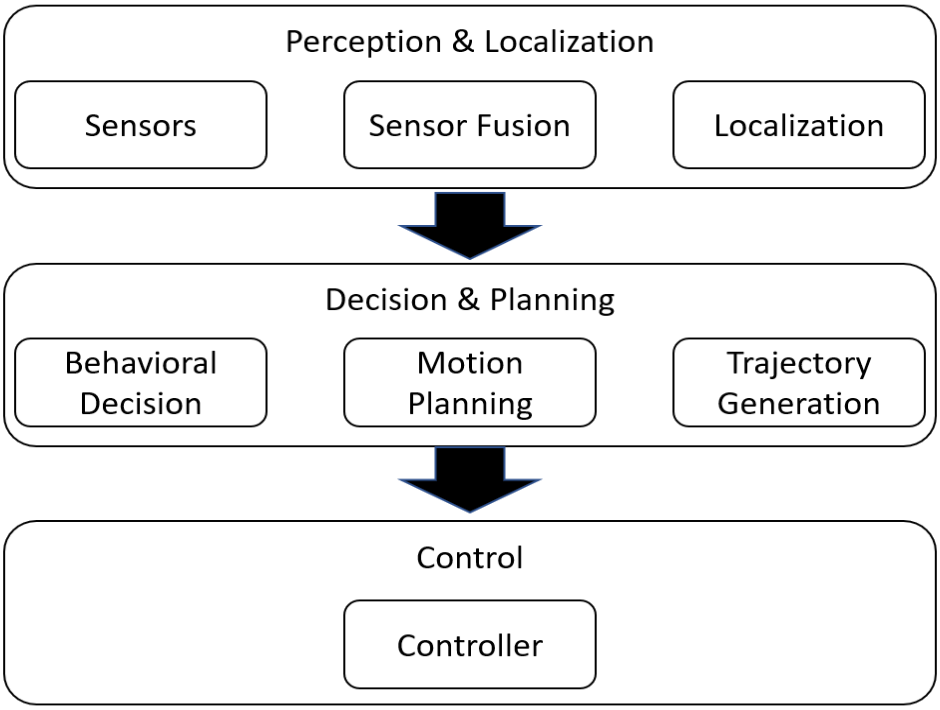

Figure 1.3: Overall Control Architecture of Autonomous Vehicles

conflicts, and generate feasible trajectories [47], [48]. Finally, the control layer converts planned motions into executable control signals delivered to the vehicle's actuators [42], [49].

a) Perception

The perception system of autonomous vehicles relies on a suite of complementary sensors that collectively enable environmental awareness, object detection, and localization [45], [50]. Active sensors such as LiDAR and Radar provide precise range and velocity information independent of illumination, while passive sensors—including RGB and infrared cameras—capture rich semantic and visual cues essential for classification and scene understanding [46], [51]. However, each modality has inherent limitations in cost, resolution, or environmental robustness, necessitating sensor fusion. Localization integrates GNSS, IMU, and HD map data to ensure accurate global positioning even in urban environments [52], [53]. Multi-modal fusion (cf. Figure 1.4) combines active ranging, passive imaging, and positioning information to maintain perception continuity under varying lighting and weather conditions. Through redundancy and cross-validation, these integrated sensing frameworks enhance robustness and reliability, forming the perceptual foundation of autonomous driving [40], [44].

b) Decision-Making

The decision-making process in autonomous driving follows a hierarchical framework that translates perception data into safe and efficient driving strategies [55]. At the behavioral level, the system plans routes and selects driving maneuvers by combining rule-based logic

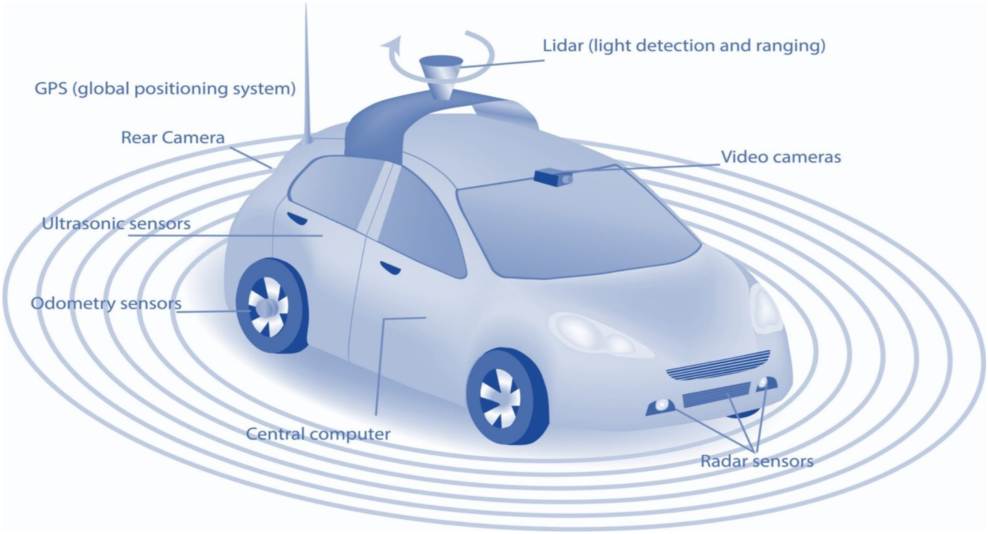

Figure 1.4: Sensors used in Autonomous Vehicles [54]

with probabilistic reasoning to address uncertainty [56]. The motion planning layer then generates feasible trajectories through search- and optimization-based methods that respect vehicle dynamics and adapt to surrounding obstacles in real time [57], [58]. In multi-agent contexts, game-theoretic and learning-based models enable interactive decision-making, allowing vehicles to anticipate and negotiate with other road users [59], [60]. Safety assurance is ensured through formal verification and runtime monitoring, which evaluate decision outputs against traffic regulations and physical constraints, activating predefined fallback behaviors when risks arise [61].

c) Control

The control layer translates planned trajectory decisions into vehicle movement through longitudinal and lateral control systems (cf. Figure 1.5). For example, the model-based controllers, using PID for steady-state and MPC for transient scenarios like emergency deceleration, adjust throttle and braking to adapt to road conditions and vehicle states [62]. Steering control combines look-ahead path following with predictive strategies, compensating for tire slip during aggressive maneuvers to optimize directional accuracy [63]. By-wire systems enable precise electronic control of throttle, braking, and steering, with sub-100ms response latencies and redundant architectures for fail-operational safety [64]. Fault management employs graduated responses, from parameter adaptation to system reconfiguration, with real-time monitoring and adaptive control for reliability [65].

While perception and control remain fascinating and technically challenging areas within autonomous driving research, the primary focus of this thesis lies in cooperative decision-making. Therefore, the following sections will concentrate on reviewing and analyzing representative decision-making and motion planning methods commonly employed in autonomous driving systems.

1.2.3 *Decision-Making*

Decision-making is a core functional module in autonomous driving systems, responsible for determining what the vehicle should do under varying traffic conditions, social contexts,

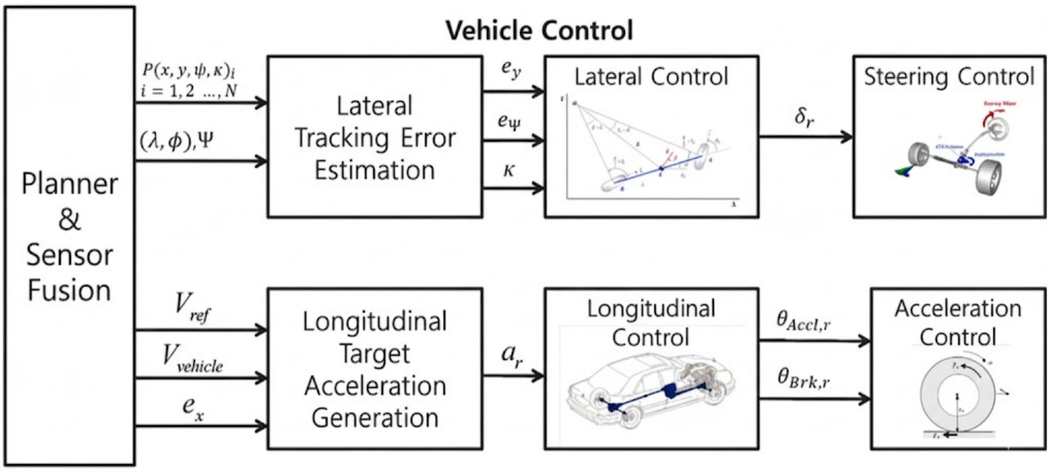

Figure 1.5: Control of Autonomous Vehicles [66]

and operational constraints. Positioned upstream of motion planning, decision-making synthesizes environmental perception, prediction, and high-level intent to produce structured driving behaviors that align with safety, legality, efficiency, and social acceptability.

A complete decision-making architecture typically encompasses three hierarchical layers. The Behavioral Decision Layer operates under traffic laws and driving conventions to select high-level maneuvers—such as lane keeping, overtaking, yielding, or merging—based on route goals and traffic semantics. Above this, the Interactive Layer addresses complex multi-agent scenarios by modeling and anticipating the behaviors of surrounding vehicles. It enables cooperative or competitive strategies in settings like intersections, roundabouts, or lane changes, where negotiation and timing are critical. Finally, the Risk Management Layer provides a safety supervisory mechanism by evaluating the potential risk associated with each planned action. This includes assessing the likelihood of collisions, behavioral uncertainty, or policy deviation, and issuing mitigative adjustments when necessary.

These layers form a tightly integrated stack that enables autonomous vehicles to make rational, context-aware decisions in dynamic, uncertain, and socially interactive environments. Decision-making not only drives system-level safety and efficiency, but also bridges the gap between reactive control and long-term autonomous intent.

a) Behavioral Decision

The Behavioral Decision Layer plays a pivotal role in the autonomous driving architecture by bridging strategic routing with low-level motion planning. Its primary function is to determine high-level maneuvers—such as lane changes, merges, or yielding—based on contextual understanding, traffic rules, and real-time environmental dynamics (cf. Figure 1.6) [67]. This layer emphasizes what action to take and when to take it, operating within a scenario-driven framework guided by road semantics and mission objectives. To ensure regulatory compliance and socially acceptable behavior, the behavioral layer is closely integrated with a rule engine that encodes both static laws and dynamic traffic conditions. Driving policies—ranging from conservative to assertive—modulate decision thresholds, influencing how the vehicle responds under uncertainty or interaction pressure. The interplay between hard constraints (e.g., stop signs) and soft policies (e.g., comfort margins) ensures both safety and adaptivity [67].

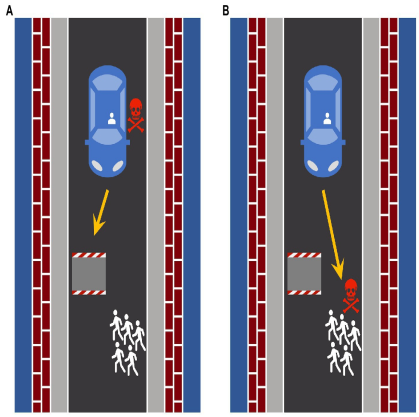

Figure 1.6: Behavior decision-making [75]

Building upon this foundation, a wide range of methodologies have been developed to realize behavioral decision-making, each offering distinct advantages in interpretability, flexibility, and adaptability. Finite State Machines (FSMs) remain widely used for their simplicity and deterministic control but are limited in highly interactive environments [68]. Probabilistic frameworks such as Partially Observable Markov Decision Processes (PO-MDPs) handle uncertainty by reasoning over belief states to derive optimal actions [69], [70]. Data-driven methods—including Graph Neural Networks (GNNs) [71], [72], which model multi-agent spatial-temporal dependencies, and Large Language Models (LLMs) [73], [74], which enable natural-language-grounded reasoning—have further expanded behavioral reasoning toward social awareness and transparency. End-to-end learning approaches directly map sensory inputs to high-level maneuvers, reducing manual rule engineering. In modern practice, hybrid architectures that combine symbolic reasoning with learning-based adaptability are increasingly favored, offering both interpretability and robustness for real-time behavioral decision-making in diverse and uncertain driving environments.

b) Interaction-Aware

The Interaction-Aware Layer elevates the decision-making framework beyond ego-centric planning by enabling socially contextualized coordination among multiple traffic agents. In complex real-world scenarios—such as highway merging, intersection negotiation, and roundabout yielding—autonomous vehicles must consider not only their own objectives and constraints but also the intentions, behavioral patterns, and likely reactions of surrounding road users. This layer addresses the inherently interactive nature of traffic, where each agent's behavior can influence and be influenced by others, demanding reasoning that accounts for reciprocal dependencies [76].

Key functionalities of this layer include intent recognition and trajectory prediction of nearby agents, adaptive planning under partial regulation (such as in unprotected turns), and behavior modeling that captures cooperative or adversarial dynamics. The Interaction-Aware Layer differs from the Behavioral Layer by emphasizing continuous adaptation rather than one-shot maneuver selection and by managing temporal coupling between agents' actions. It is particularly relevant in dense or ambiguous scenarios where compliance with static rules alone is insufficient for safe and efficient navigation.

Various algorithmic paradigms support this form of interaction reasoning. Game-theoretic frameworks, such as Stackelberg games and level-k reasoning, model multi-agent interactions as strategic games where each agent anticipates and reacts to others' decisions. Monte Carlo Tree Search (MCTS) [77], when combined with predictive models, enables forward simulation of possible action sequences under uncertainty, balancing safety and exploration. Spatio-temporal GNNs represent agents and their relations as dynamic graphs, allowing policy inference based on structural context and enabling scalable, real-time coordination in dense traffic [78]. Probabilistic generative models—such as mixture density networks and Gaussian process policies [79], [80], [81]—further support multi-modal future prediction, essential for risk-aware planning in uncertain environments.

Beyond passive interaction inference, the emergence of V2X communication technologies has enabled explicit coordination among connected agents. Protocols based on cellular V2X (C-V2X) allow vehicles to exchange planned maneuvers, priorities, and cooperative intentions in real time. This capability supports consensus-based planning, particularly valuable in tightly coupled scenarios like joint merging, platooning, or intersection negotiation without traditional right-of-way structures.

c) *Risk Assessment*

The Risk Assessment and Management Layer forms the safety backbone of autonomous driving architectures, continuously evaluating when an action might become unsafe and how urgently intervention is needed. Rather than generating trajectories or selecting maneuvers, its responsibility is to identify potential threats based on future states, quantify their severity, and trigger mitigation strategies before risk thresholds are breached.

Risk assessment in autonomous driving primarily relies on deterministic kinematic indicators and probabilistic prediction models. Deterministic methods, such as Time to Collision (TTC) [82], Predicted Inter-Distance Profile (PIDP) [83] or Post-Encroachment Time (PET) [84], evaluate the temporal or spatial proximity of potential conflicts based on current vehicle states, offering fast and interpretable risk estimation for real-time decision-making. In contrast, probabilistic approaches estimate the likelihood of collision by considering uncertainty in motion prediction and environmental perception-Probability Collective (PC) Algorithm [85]-thereby providing a more comprehensive view of safety under dynamic or partially observable conditions.

Further technical details and formulations of these risk assessment methods will be discussed in Section 2.2. Several representative motion planning approaches commonly employed in autonomous driving systems will be introduced in next subsection, highlighting how they ensure safe and efficient vehicle behavior.

1.2.4 *Motion Planning*

Motion planning is a fundamental element of autonomous driving and mobile robotics, responsible for determining not only where an agent should go but also how it should move safely and efficiently within its physical and dynamic limits. It integrates key tasks such as path planning, trajectory generation, kinodynamic and dynamic constraint handling, and multi-objective optimization, forming a continuous pipeline that directly connects high-level decision-making with low-level control. Beyond feasibility, motion planning also considers risk assessment to evaluate potential hazards and uncertainties in dynamic, partially observable environments (cf. Figure 1.7). As real-world traffic scenarios grow

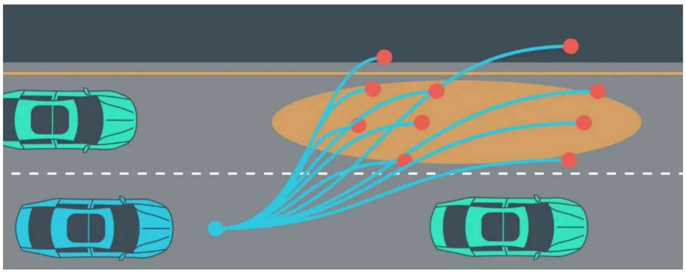

Figure 1.7: Motion planning for autonomous vehicles

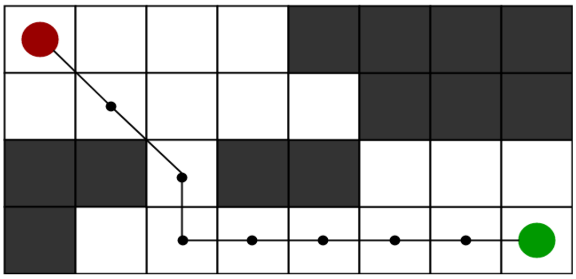

Figure 1.8: A* algorithm example

increasingly complex and interactive, motion planning must operate in real time, balancing safety, efficiency, and comfort while adapting to changing conditions. In this sense, it serves as a crucial bridge between behavioral intent and executable vehicle actions in autonomous systems.

a) Search-based Methods

Search-based methods constitute a foundational paradigm in path planning, characterized by their systematic exploration of discretized representations of the robot's configuration space [86]. By leveraging combinatorial search strategies, they guarantee completeness, ensuring a solution is found if one exists, and often provide provable optimality under admissible cost functions. This rigorous mathematical formalism enables transparent decision-making, making them indispensable for safety-critical applications, including structured environment navigation and systems requiring deterministic guarantees.

Classical methods include progressive adaptations: Dijkstra's algorithm establishes the baseline with exhaustive optimal traversal [87], while A* introduces heuristic guidance for efficiency without sacrificing optimality (cf. Figure 1.8) [88]. Dynamic environments are addressed by D* replanning and LPA*'s reuse of historical data, both of which enable real-time adaptation [89], [90]. For kinematically constrained systems, Hybrid A* bridges discrete search with continuous state-space exploration, and State Lattice methods employ precomputed motion primitives to ensure dynamically feasible trajectories [91], [92]. Together, these variants form a hierarchical framework balancing theoretical robustness with practical scalability across robotics domains.

Figure 1.9: Rapidly-exploring Random Trees [57]

b) Sampling-based Methods

Sampling-based methods constitute a powerful class of motion planning algorithms particularly effective in high-dimensional and continuous configuration spaces. Instead of exhaustively exploring discretized grids, they generate feasible paths by randomly sampling states and incrementally constructing connectivity structures such as trees or graphs. Their probabilistic formulation provides strong scalability, flexibility, and computational efficiency, making them suitable for complex, dynamically constrained environments. These approaches are widely used in robotic manipulation, mobile navigation, and autonomous driving, offering probabilistic completeness and, in asymptotically optimal variants, convergence toward optimal solutions [44].

Representative algorithms include PRM [93], which builds a multi-query roadmap connecting randomly sampled collision-free configurations; Rapidly-exploring Random Trees (RRT) (cf. Figure 1.9) [94] and its extensions—RRT* [95], Informed RRT* [96], and RRT-Connect [97]—which improve exploration efficiency and path optimality through rewiring, heuristic sampling, and bidirectional expansion. FMT [98] accelerates planning with lazy collision checking and dynamic programming, while BIT* [99] integrates graph-search principles with batch sampling for high-quality solutions. More recent approaches, such as Non-Uniform Tree Sampling (NUTS) [100], adapt sampling density based on environmental complexity to enhance efficiency in heterogeneous domains.

c) Parametric Curve-based Methods

Parametric curve-based methods form a key category of motion planning techniques that generate smooth, dynamically feasible trajectories using parameterized curves [42], [49]. Unlike sampling-based or graph-search methods, they inherently incorporate kinematic and curvature constraints, making them especially suitable for non-holonomic systems such as car-like autonomous vehicles. These methods naturally produce geometrically and dynamically continuous paths—ensuring smooth curvature and heading transitions critical for vehicle stability and comfort [42], [49].

Common curve representations include Dubins [101] and Reeds–Shepp [102] paths for shortest or time-optimal motion under curvature limits, clothoid curves [103] for continuous curvature transitions in high-speed maneuvers, and polynomial-based forms like Bézier [104] and B-splines [105] (cf. Figure 1.10) for flexible, locally controllable path generation. In practice, these curves are often combined with discrete search planners—such as Hybrid A* [91]—to balance global optimality and smoothness, refining trajectories via curvature-

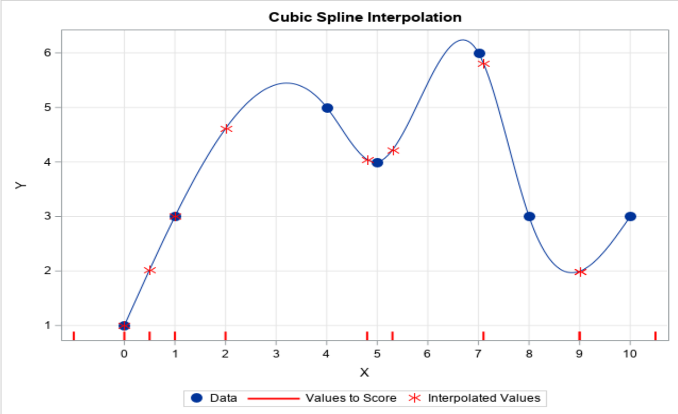

Figure 1.10: Spline curve

constrained interpolation [48]. This hybrid integration makes parametric curve-based methods essential in structured driving environments, urban navigation, and automated parking applications.

This section has presented an overview of autonomous vehicles, including their technological evolution, system architecture, and the key components involved in decision-making and motion planning. Building upon this foundation, the next section will extend the discussion to CAVs, examining their control architectures, cooperative decision-making mechanisms, and how these capabilities enable advanced smart city traffic management strategies derived from cooperative driving principles.

1.3 CONNECTED AUTONOMOUS VEHICLE: FROM COOPERATIVE DECISION-MAKING TO INTELLIGENT TRAFFIC MANAGEMENT

It is widely anticipated that the widespread adoption of autonomous vehicles will help alleviate urban traffic congestion, as their standardized and rule-abiding driving behaviors are expected to outperform those of most human drivers. However, real-world deployment of robotaxi fleets has shown that the lack of cooperative intent, limited situational awareness, and overly conservative driving strategies of current single-vehicle systems often fail to deliver the expected efficiency gains. In dense urban settings, these limitations can even worsen congestion, as vehicles hesitate or fail to coordinate effectively with surrounding traffic [106].

Recent CAV research reflects a clear shift toward cooperative and networked architectures, acknowledging that standalone perception and decision-making suffer from line-of-sight restrictions, sensor occlusions, and environmental degradation—as demonstrated by incidents involving early autonomous systems from Tesla and Uber [107]. Moreover, isolated connected vehicles depend on high penetration rates to achieve notable improvements in safety and efficiency. These challenges have motivated the development of multi-vehicle cooperative systems, such as the EU Horizon 2020 COSAFE project [108], which leverage shared sensing, computation, and decision-making among vehicles and infrastructure.

As cyber-physical systems integrating autonomous intelligence with vehicular communication networks, CAVs enable real-time information exchange through V2V and V2I communication, forming a control architecture that enhances perception, planning, and actuation (cf. Figure 1.11). Through cooperative perception and coordinated motion, CAVs can reduce collision probability, smooth traffic flow via platoon-based harmonization, and

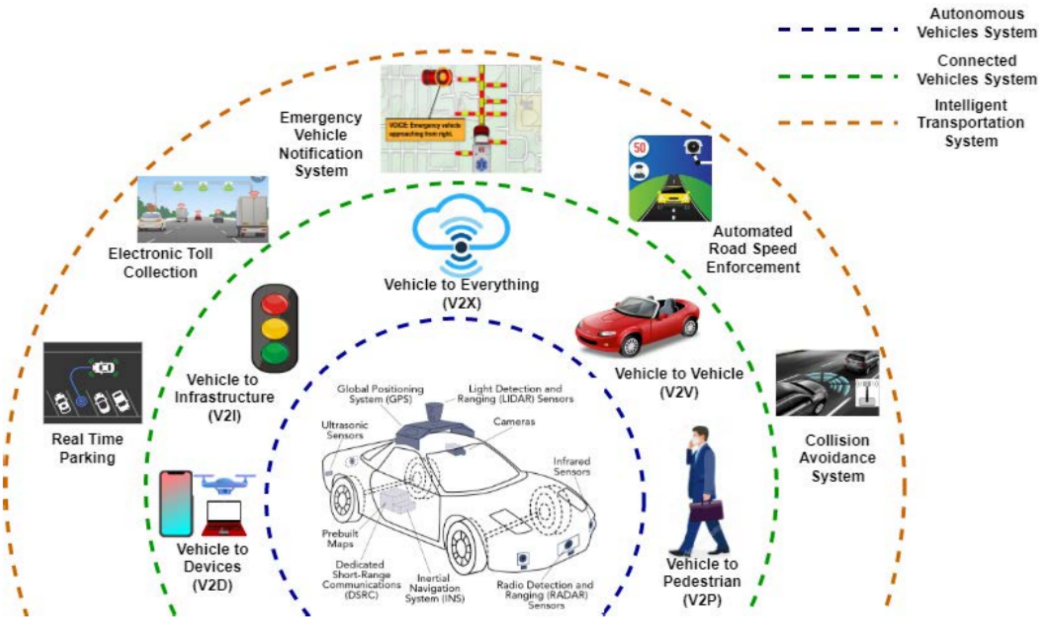

Figure 1.11: Overview of connected automated system vehicle infrastructure [111]

optimize routing through infrastructure-mediated coordination. These capabilities position CAVs at the intersection of multi-agent robotics and intelligent transportation systems, marking them as a cornerstone of next-generation smart mobility frameworks [109], [110].

1.3.1 *Cooperative CAVs Architecture: Centralized vs. Decentralized*

Cooperative CAV architectures typically comprise several synergistic layers: communication, cooperative decision-making and planning, perception, location, and control (cf. Figure 1.12):

- **Communication layer:** Intelligent V2X networks integrate millimeter-wave DSRC and 5G technologies to enable low-latency (<100 ms) and high-reliability communication, ensuring stable message exchange even in dense traffic environments [112].
- **Perception layer:** Multi-vehicle and infrastructure sensing—combining cameras, LiDAR, radar, and fixed sensors—fuses data to build an extended and more accurate environmental model beyond single-vehicle capability [113].
- **Decision-making and planning layer:** CAVs exchange real-time intentions and environmental assessments to coordinate trajectories and optimize collective behavior using consensus and decentralized optimization [114].
- **Localization layer:** Cooperative localization fuses GNSS, V2X-based relative positioning, and infrastructure corrections (e.g., RTK-GNSS, SLAM) to achieve centimeter-level accuracy and maintain consistent global positioning in complex urban environments [115].

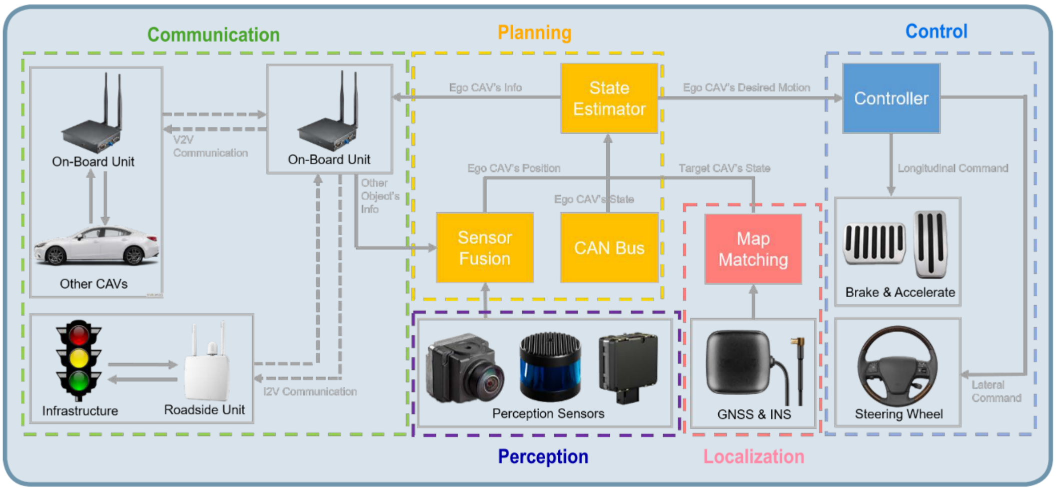

Figure 1.12: General architecture of a MVS with communication, perception, localization, planning and control modules [117]

- **Control layer:** Local controllers execute coordinated maneuvers through real-time throttle, steering, and braking adjustments, supported by cooperative schemes such as CACC and platoon control to ensure safe, smooth motion [116].

In practical applications, the architecture of CAVs systems can be further categorized into centralized and decentralized (distributed) frameworks, depending on how the decision-making and planning layer is organized. While the perception, communication, localization, and control layers share similar principles, the distinction lies in where and how decision-making authority is implemented—either concentrated within a central infrastructure or distributed among individual vehicles. This structural difference fundamentally defines the system's computational topology, communication dependency, and coordination mechanisms.

In a centralized architecture, portions of the perception, localization, and decision-making processes are offloaded to a central controller or infrastructure-based planner. The central unit aggregates vehicle and environmental data through high-throughput networks such as 5G V2I or edge–cloud systems, enabling global optimization across multiple agents [118]. This architecture provides strong coordination and overall efficiency but also introduces scalability bottlenecks and vulnerability to communication delays, handover interruptions, and single-point failures, as well as significant demands on infrastructure computation and bandwidth [119], [120].

Conversely, a decentralized architecture assigns perception, localization, and decision-making to each vehicle's on-board intelligence. CAVs rely on local sensing and V2V/V2I communication to make real-time cooperative decisions, offering robustness, scalability, and fault tolerance without a central authority [121], [122]. This setup supports parallel computation and flexible coordination but requires sophisticated consensus and conflict-resolution algorithms to maintain global consistency and efficiency under dynamic traffic conditions [123], [124], [125].

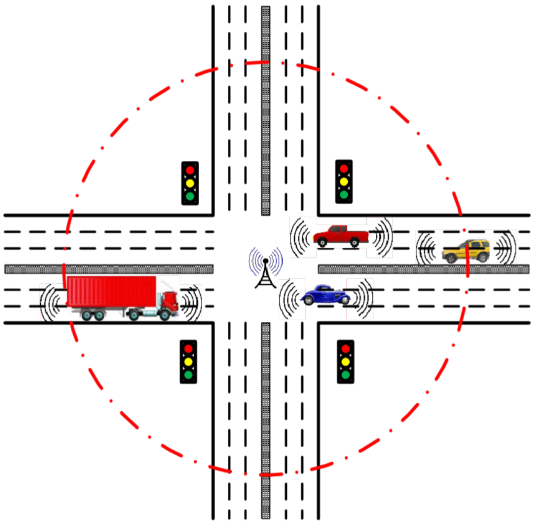

Figure 1.13: Conventional signalized intersection [126]

1.3.2 *Cooperative Decision-Making Approaches in CAVs at Intersection*

CAVs have demonstrated broad applicability across urban transportation systems. Through cooperative sensing, communication, and decision-making, CAVs enable coordinated platooning on highways, adaptive signal control via V2I communication, dynamic routing and shared mobility services, energy-efficient driving, and city-level traffic flow optimization through large-scale data fusion and predictive control [5], [127], [128]. These applications collectively enhance safety, sustainability, and operational efficiency, positioning CAVs as a cornerstone technology in the evolution toward intelligent urban mobility.

Within these diverse applications, urban intersections represent one of the most common and critical environments, where multiple traffic streams converge and interact (cf. Figure 1.13). Traditional signalized intersections, governed by fixed or adaptive Signal Phase and Timing (SPaT) plans, rely heavily on driver compliance and pre-defined timing cycles. While effective under moderate and predictable traffic, these systems often exhibit inefficiencies such as idle delays, energy waste, and limited adaptability to dynamic flow variations [129], [130]. Their reactive nature prevents real-time optimization, and human-driven vehicles further introduce behavioral uncertainty that constrains smooth coordination [131].

In contrast, CAVs' inherent information-sharing and cooperative decision-making capabilities provide the foundation for more adaptive and efficient traffic management. By exchanging intent, trajectory, and environmental data through V2V and V2I communication, CAVs can dynamically negotiate priority and coordinate movements at intersections without relying on fixed signal cycles. Consequently, unsignalized intersections have emerged as the most representative scenario to demonstrate the full potential of cooperative CAV systems. CAV coordination and decision-making strategies in unsignalized intersection environments (cf. Figure 1.14) will be focused on.

At the core of unsignalized intersection management lies the challenge of safely and efficiently coordinating multiple vehicles within a shared conflict zone. Unlike signalized intersections governed by fixed phase schedules, unsignalized scenarios require real-time negotiation and adaptive coordination among vehicles. Traditional rule-based and centralized scheduling approaches provide limited scalability under heterogeneous traffic

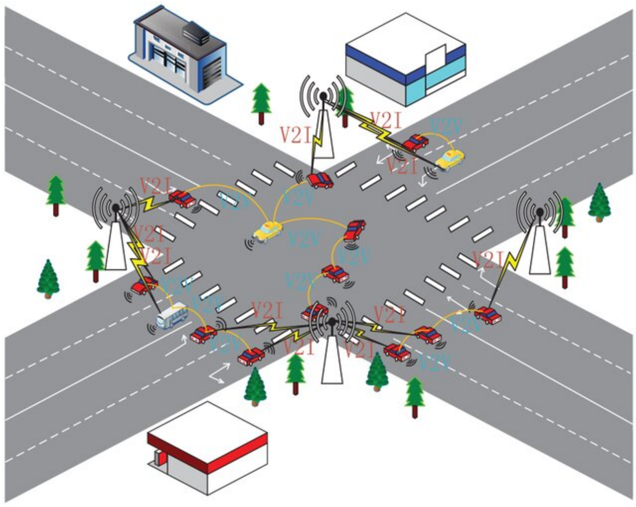

Figure 1.14: General unsignalized intersection model with V2V & V2I communication[132]

conditions. CAVS can communicate intentions, predict trajectories, and execute coordinated maneuvers, enabling new forms of intelligence and cooperative optimization. Consequently, CAV-enabled intersection management has evolved into several key methodological paradigms, including centralized reservation-based, decentralized consensus, and spatial-temporal or platoon-based strategies, each offering distinct advantages in safety, efficiency, and adaptability.

a) Reservation-based Systems

Centralized architecture represents one of the earliest and most established paradigms for unsignalized intersection management, where a central controller collects vehicle states and intentions to optimize trajectories and avoid conflicts. This architecture offers a global view that enables near-optimal coordination and safety but requires high communication and computation capacity, limiting scalability under dense traffic. Among such approaches, Autonomous Intersection Management (AIM) stands as the most representative reservation-based centralized method.

The reservation paradigm (cf. Figure 1.15), first proposed in the seminal AIM framework [133], models intersection access as a time-slot allocation problem [134]. Vehicles request entry reservations, which are granted by a central manager based on conflict-free scheduling rules such as First-Come-First-Served (FCFS) or priority-based schemes that may consider turning maneuvers or emergency vehicles [135]. Conceptually similar to slot management in air or rail systems, this approach leverages V2X communication to coordinate vehicle access dynamically. Subsequent extensions integrate feasible speed profiles to ensure smooth, dynamically consistent trajectories [136] and expand the paradigm to network-wide applications, where slot-based coordination regulates corridor- or region-level flows. Simulation studies show that reservation-based control can significantly outperform traditional signalized systems, often approaching theoretical limits of intersection efficiency [137].

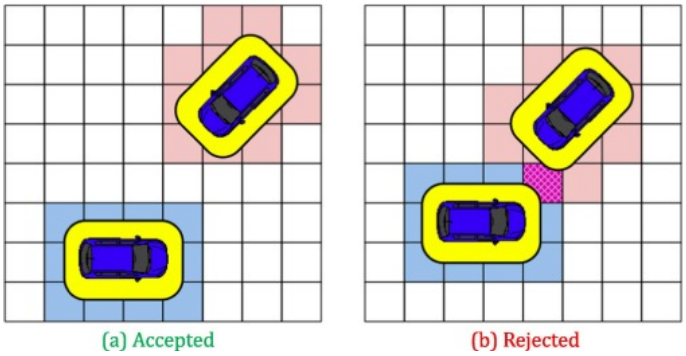

Figure 1.15: Reservation system at intersection [138]: (a) Accept if the requested reservation area is conflict-free; (b) Reject if the requested reservation area conflicts with an existing one

b) Consensus-based Coordination

Decentralized control shifts decision-making to individual CAVs, allowing vehicles to negotiate locally through sensing and V2X communication. This enhances robustness and scalability but can lead to conservative behaviors or deadlocks without centralized coordination.

Among such approaches, consensus-based methods enable vehicles to iteratively agree on crossing times or safety margins through local communication, ensuring conflict-free passage without a central scheduler. For instance, decentralized iLQR frameworks using consensus-based optimization [139], [140], [141] allow each vehicle to compute feasible trajectories independently while maintaining global consistency. Similarly, Distributed Model Predictive Control (DMPC) achieves real-time consensus on trajectory updates under limited communication [142]. Despite their scalability, these approaches remain sensitive to latency and convergence challenges in dense traffic.

c) Optimization-based Scheduling

Intersection management can be formulated as an optimization problem, targeting objectives such as total travel time, vehicle delay, or conflict overlap while respecting safety and kinodynamic constraints [143]. Classical methods often employ Mixed-Integer Linear Programming, dynamic programming, or combinatorial optimization tools. For instance, [144] proposes a linear-programming model with a rolling-horizon approach that minimizes average vehicle delay under safe time interval constraints, achieving reductions in delay of up to 76% compared with FCFS control. In a different direction, [145] develops a convex optimal control framework that successively optimizes crossing sequence and velocity trajectories via second-order cone programming, jointly minimizing travel time and energy consumption while maintaining real-time computational efficiency. Further extending applicability, [146] incorporates pedestrian phases into reservation-based optimization frameworks, demonstrating robust multi-modal scheduling in signal-free environments. Although these optimization-based strategies offer strong theoretical performance and fine-grained control, their scalability remains constrained in high traffic-volume scenarios due to computational demands.

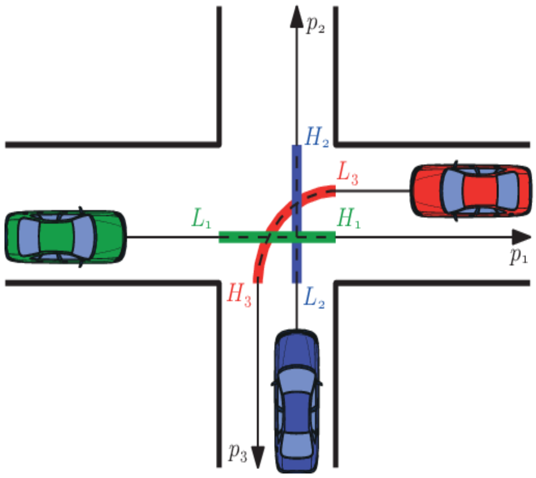

Figure 1.16: Space-based conflict detection with 3 CAVs at unsignalized intersection [147]

d) Spatio-Temporal Planning Approaches

Spatio-temporal planning provides a geometric and kinematic framework for managing unsignalized intersections by reasoning about vehicle interactions within a joint time–space domain [148], [149], [150]. Although it belongs to the broader family of optimization-based methods, its focus differs: instead of jointly optimizing multiple control objectives, it concentrates solely on resolving spatio-temporal conflicts between vehicles. By explicitly modeling interactions in both time and space, this approach enables transparent safety verification and interpretable conflict resolution.

Two complementary principles guide spatio-temporal planning: temporal separation, where vehicles are allocated non-overlapping time intervals in shared conflict zones; and spatial separation, where vehicles follow geometrically distinct trajectories that avoid overlap even with partial time coincidence. These principles are often implemented through time–space graphs, in which each vehicle's motion is represented as a trajectory curve in a two-dimensional time–space plane (cf. Figure 1.16). Potential collisions correspond to curve intersections, and planning becomes an optimization problem of adjusting timing, sequencing, or local paths to eliminate these intersections. Efficient formulations based on graph search, mixed-integer optimization, or convex relaxation are used to derive dynamically feasible and collision-free schedules, providing both safety guarantees and improved traffic throughput.

e) Platooning Strategies

Platooning strategies exploit the natural advantages of grouping CAVs into convoys that traverse intersections cooperatively. Instead of treating each vehicle as an independent agent, the system manages platoons as collective units, thereby reducing the dimensionality of the control problem and enhancing overall efficiency [151]. Platooning provides a scalable and effective mechanism for unsignalized intersection management, leveraging convoy coordination to increase throughput and reduce delays. Nevertheless, its success depends on reliable intra-platoon communication, precise control of inter-vehicle spacing, and adaptive mechanisms for handling mixed traffic with both platooned and individual vehicles.

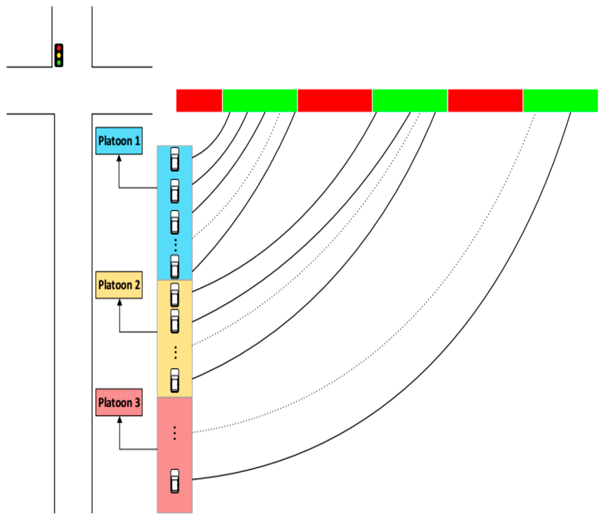

Figure 1.17: Platoon formation coordination [153]

Platoon-based intersection management typically begins with the formation of vehicle groups en route to the intersection. Vehicles traveling in the same direction or performing compatible maneuvers (e.g., vehicles proceeding straight or executing coordinated turns) dynamically join into a platoon through V2V communication. Once the intersection is crossed, the platoon may dissolve back into individual vehicles or reconfigure into new formations (cf. Figure 1.17) [152]. This grouping mechanism reduces the number of negotiation entities with the intersection manager, lowering communication and scheduling overhead.

This section has introduced the fundamental architecture of CAVs and several representative cooperative control frameworks. These approaches primarily operate at the micro-level, focusing on vehicle interactions and traffic coordination within localized areas such as intersections or roundabouts. In the next chapter, attention will shift toward the macro-level of traffic management—specifically, the regulation of traffic flow around intersections and roundabout. By integrating both micro- and macro-level perspectives, we aim to establish a multi-layered understanding of intelligent urban traffic management within the broader context of smart city mobility.

1.4 MACRO-SCALE BENEFITS: FROM INTERSECTION-LEVEL CONTROL TO CONTINUOUS FLOW THEORIES

Macroscopic urban traffic flow management constitutes a vital component of Smart City Mobility, complementing micro-level vehicle coordination by providing a broader, system-oriented perspective on urban transportation. Through macroscopic analysis, traffic phenomena such as intersection congestion, flow propagation, and network-wide mobility patterns can be understood at an aggregate level rather than through isolated vehicle interactions. Therefore, in this section, we will use this higher-level viewpoint to introduce the adoption of multi-scale analytical frameworks, allowing the integration of microscopic decision-making models with macroscopic traffic dynamics.

At the macroscopic level, traffic flow theory provides the foundational framework for understanding the collective dynamics of urban mobility systems. Its core lies in revealing the intrinsic relationships among the three fundamental parameters of flow (q), density (k),

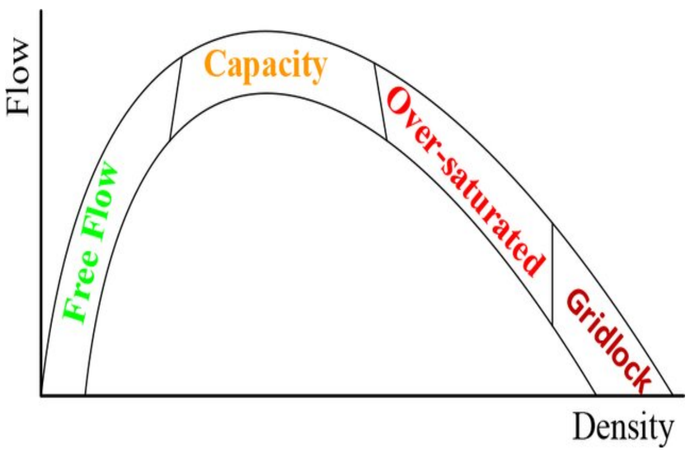

Figure 1.18: Network macroscopic fundamental diagram [161]

and speed (v), which together characterize the aggregate behavior of vehicular movement. This relationship, often referred to as the fundamental diagram, serves as the cornerstone of macroscopic traffic analysis, enabling quantitative evaluation of roadway capacity, congestion onset, and system performance under varying traffic conditions.

Several classical models have been proposed to capture these relationships under different traffic regimes. The Greenshields model introduces a linear speed–density relation and represents the most fundamental description of traffic flow behavior [154]. The Greenberg model, featuring a logarithmic form, provides improved accuracy in congested traffic conditions [155], while the Underwood model [156], based on an exponential function, better characterizes free-flow conditions. Extending beyond static relationships, the continuous flow models—such as the Lighthill–Whitham–Richards (LWR) model [157], [158]—treat traffic as a compressible fluid, describing shockwave formation and propagation through partial differential equations. At a larger scale, the Macroscopic Fundamental Diagram (MFD) [159], [160] generalizes these principles to network-level analysis, revealing stable relationships between vehicle accumulation and overall network productivity (cf. Figure 1.18), thus offering a powerful tool for city-wide traffic management and control.

Macroscopic optimization approaches for traffic management generally fall into two complementary categories. The first group, rooted in fundamental diagram and MFD theory, focuses on regulating macroscopic variables such as density and flow through perimeter control and route guidance to maintain system-wide equilibrium [162], [163]. The second group, based on control and optimization theory, employs frameworks such as optimal control to dynamically optimize signal timings, ramp metering, or vehicle trajectories using predictive traffic flow models (e.g., LWR, or MFD) [164], [165]. Together, these approaches form the methodological foundation for network-level traffic flow optimization in smart cities.

Both macroscopic and microscopic modeling approaches play a complementary role in supporting intersection management. Macroscopic theories inform the evaluation of capacity and systemic efficiency, while microscopic models enable detailed simulation of vehicle interactions within conflict zones. Their integration provides a multi-scale perspective that bridges the gap between theoretical traffic flow analysis and the practical design of intersection control strategies.

1.5 CONCLUSION

This chapter reviewed the evolution of urban mobility from traditional traffic systems toward intelligent and cooperative approaches within smart cities. It first discussed the main challenges of urban transportation and emphasized the importance of adopting a multi-level perspective that connects micro-level vehicle behavior with macro-level traffic flow dynamics. The smart city vision was introduced as a conceptual foundation for integrating these perspectives and supporting more systematic urban mobility analysis.

The discussion then focused on autonomous vehicles and CAVs, outlining their architectures and the corresponding decision-making and motion planning methodologies. Various cooperative strategies were examined, particularly those applied to unsignalized intersections, where coordination and efficiency are critical.

Finally, the chapter extended the discussion to macro-scale traffic theories—such as fundamental diagrams and network-level flow models—illustrating how they complement micro-level studies and enable multi-layered understanding of urban traffic. Overall, this chapter provided a state-of-the-art overview of existing research, forming the conceptual basis for subsequent discussions on large-scale cooperative traffic management and flow optimization.

2 THEORETICAL FOUNDATIONS AND METHODOLOGICAL REVIEW FOR CAVS

While Chapter 1 provided an introduction of the field, this chapter offers a focused examination of the core theories and specific methods essential for advancing cooperative decision-making in CAVs. The primary goal is to establish a solid foundation for the novel framework proposed in this thesis.

To achieve this, this chapter is going to present a detailed review of key existing methods from the literature. This analysis is crucial for two reasons: it highlights the current capabilities and limitations of state-of-the-art solutions, and it provides a direct basis for comparison to validate the contributions of our proposed approach. Ultimately, this chapter serves as the essential preparatory groundwork, bridging established knowledge with the innovations to follow.

2.1 BEHAVIORAL DECISION-MAKING

As one of the core components of this thesis, decision-making plays a pivotal role in enabling intelligent and cooperative behavior among autonomous and connected vehicles. Within this context, particular emphasis is placed on two key aspects: behavioral decision-making and risk assessment. This section focuses on the former, presenting representative approaches used for high-level behavior generation in autonomous driving systems, including Finite State Machine (FSM)-based and optimization-based decision-making methods.

2.1.1 *Finite State Machine*

Finite State Machine models represent one of the earliest and most intuitive approaches to behavioral decision-making in autonomous driving systems. They provide a structured way to describe discrete driving behaviors and their logical transitions, enabling interpretable and computationally efficient decision processes [68], [166].

In an FSM framework, the vehicle's operational behavior is decomposed into a finite set of states, each corresponding to a specific driving intention, such as *lane keeping*, *car following*, *lane changing*, *overtaking*, or *stopping*. Transitions between these states are governed by predefined logical rules derived from environmental perception and traffic regulations.

Formally, an FSM is defined as a 5-tuple:

$$\mathscr{M} = \{S, A, T, O, \delta\}$$

where:

- S is the finite set of discrete behavioral states;
- A denotes the set of possible driving actions;
- $T : S \times A \to S$ represents the state transition function;

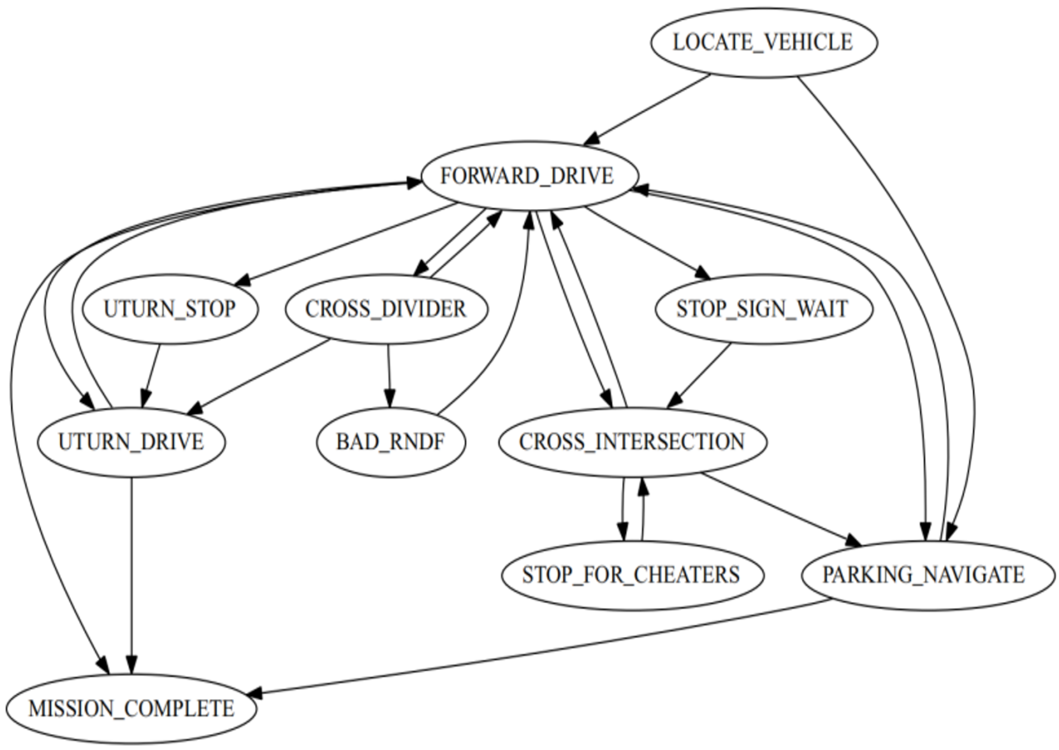

Figure 2.1: Example of FSM state transition diagram

- O is the set of environmental observations (e.g., distance to leading vehicle, lane availability);
- δ is the decision policy defining transitions according to conditions derived from O.

In practical applications, each behavioral state encodes a high-level driving objective that guides lower-level motion planning and control. For instance, in a typical highway scenario, the *lane keeping* state maintains lane alignment and constant velocity, while the *car following* state dynamically adjusts the vehicle speed to preserve a safe inter-vehicle distance. When the system detects that the front vehicle is moving slower than a predefined threshold and the adjacent lane is free, the FSM triggers a transition to the *lane changing* state. These transitions are implemented through deterministic conditional rules such as:

$$\text{if } (d < d_{\text{safe}}) \text{ and } (\Delta v > 0) \Rightarrow s_{t+1} = \textit{Car Following},$$

$$\text{if } (d_{\text{left}} > d_{\text{safe}}) \text{ and } (\Delta v_{\text{left}} < 0) \Rightarrow s_{t+1} = \textit{Lane Changing}.$$

This rule-based structure ensures both transparency and traceability, making FSMs particularly attractive for safety-critical systems where interpretability and regulatory compliance are required.

A representative example of a FSM is illustrated in Figure 2.1, showing the sequence of behavioral states an autonomous vehicle may experience during a typical mission. The initial states include `LOCATE_VEHICLE` (localizing the vehicle), `FORWARD_DRIVE` (driving forward), and `UTURN_STOP` (stopping before the U-turn line). The vehicle then transitions through various task-specific states such as `CROSS_DIVIDER` (crossing traffic-dividing sections), `STOP_SIGN_WAIT` (waiting at a stop sign), and `CROSS_INTERSECTION` (handling intersection traversal). Upon mission completion, the system enters the `MISSION_COMPLETE` state. Exceptional conditions, such as navigating within parking areas (`PARKING_NAVIGATE`) or operating on an unmatched route file (`BAD_RNDF`), are also explicitly handled through dedicated transitions. This FSM structure effectively captures the scenario-driven decision logic of autonomous driving, ensuring interpretable and structured behavioral control under complex traffic environments.

The FSM approach offers several notable advantages: it is easy to design and implement, computationally lightweight, and highly interpretable for verification and validation purposes. These properties have led to its wide adoption in early autonomous driving platforms, such as Tesla's Autopilot, Baidu Apollo's behavioral layer, and CARLA's *BehaviorAgent* used in simulation studies.

2.1.2 *Optimization-based Decision-Making*

Optimization-based methods have emerged as a prominent and widely adopted approach in the field of decision-making for autonomous vehicles, encompassing a wide spectrum of techniques and applications. The overall architecture typically involves a sequential pipeline of state estimation, environment prediction, motion planning, and feedback control. Within this framework, the planning module translates the complex task of driving into a formal mathematical problem, which is then solved to yield an optimal vehicle trajectory or behavior.

Given the extensive breadth of this domain, a comprehensive treatise on the entire pipeline is beyond the scope of this section. Instead, we will concentrate our discussion on the most pivotal aspect of this paradigm: the formulation of the decision-making task as a well-defined optimization problem. This formulation is critical as it directly encodes the desired driving behavior—balancing safety, efficiency, and comfort—into a mathematical structure composed of cost functions and constraints. To provide a concrete and illustrative example of this process, we will focus on the construction of the optimization objectives and their representation in the objective function.

Defining appropriate optimization objectives is a central component of optimization methods, directly influencing the quality, safety, and efficiency of planned motions. These objectives specify what the planner should prioritize—such as minimizing travel time, energy consumption, or trajectory curvature—and are typically embedded within a cost function that guides the search or optimization process [167].

In practice, optimization objectives vary depending on the task context, platform dynamics, and environmental constraints [168]. For autonomous vehicles, common objectives include minimizing jerk or acceleration for ride comfort, reducing energy expenditure for efficiency, and maintaining safe distances from obstacles or road boundaries [167]. In multi-agent systems, additional terms may be introduced to promote coordination, fairness, or communication efficiency [169]. Well-defined objectives enable planners to generate behaviors aligned with high-level goals while ensuring feasibility under real-world physical and safety constraints. They also allow for multi-objective formulations, where competing criteria—such as time vs. comfort—are balanced through weight tuning or Pareto optimization [170]. These objectives broadly encompass five fundamental categories:

- **Time-Optimality**: Minimizing traversal duration, essential for emergency vehicles and racing drones.

- **Energy Efficiency**: Reducing energy consumption per unit distance, crucial for mobile robots with limited battery capacity.

- **Comfort-Centric Smoothness**: Constraining jerk and curvature for passenger comfort in autonomous vehicles [171].
- **Path Tracking Precision**: Minimizing deviation from reference trajectories, vital for industrial AGVs (Automated Guided Vehicles) in precision tasks.
- **Dynamic Feasibility**: Enforcing kinodynamic constraints (e.g., acceleration/torque bounds) through inequality constraints.

a) Time-Optimality

Time-optimality refers to the objective of minimizing the total travel or maneuver completion time while ensuring safety and dynamic feasibility. In decision-making and motion planning, this criterion seeks the fastest trajectory that satisfies kinematic, dynamic, and collision-avoidance constraints. Such formulations are particularly relevant for intersection crossing, merging, and lane-changing scenarios, where minimizing time improves overall traffic throughput and efficiency. The corresponding objective function can be expressed as:

$$\min\ (t_f - t_0) \tag{2.1}$$

where t_0 and t_f denote the start time and the final time. In the intersection crossing scenarios, they could be replaced by the times at which vehicles enter and leave the intersection.

b) Energy Efficiency

Energy-efficiency objectives aim to minimize the total energy or fuel consumption during a vehicle's maneuver or over a driving horizon. In optimization-based decision-making and motion planning, this is commonly achieved by penalizing high acceleration, jerk, or power demand, which are directly correlated with energy usage. The cost function can therefore be formulated as follows[172]:

$$f_{fuel}(t) = \int_{t_0} \frac{1}{\eta}(\frac{1}{2}\rho C_d A v(t)^3 + mgC_r v(t) + mv(t)|a(t)| + F_{idle})dt \tag{2.2}$$

where $f_{fuel}(t)$ is the total fuel consumption, η is drivetrain efficiency, ρ is air density, m is vehicle mass, A is frontal area of the vehicle, g is gravitational acceleration, C_d is aerodynamic drag coefficient, C_r is rolling resistance coefficient, $a(t)$ is acceleration, and F_{idle} is idle fuel consumption. The larger acceleration/deceleration is, the more fuel consumption is.

To avoid the trivial solution where the vehicle minimizes energy consumption by remaining stationary (i.e., reducing velocity to zero) in equation (2.2), which may arise when velocity is treated as an optimization variable, it is advisable to reformulate the cost function from total energy or power consumption to energy consumption per unit distance (e.g., fuel per kilometer):

$$P_{fuel}(t) = \frac{f_{fuel}(t)}{\int_{t_0} v(t)dt} \tag{2.3}$$

This adjustment ensures a more realistic and meaningful optimization objective by directly linking energy efficiency to actual mobility performance. The approach is particularly effective in optimization scenarios where the total travel distance is not fixed.

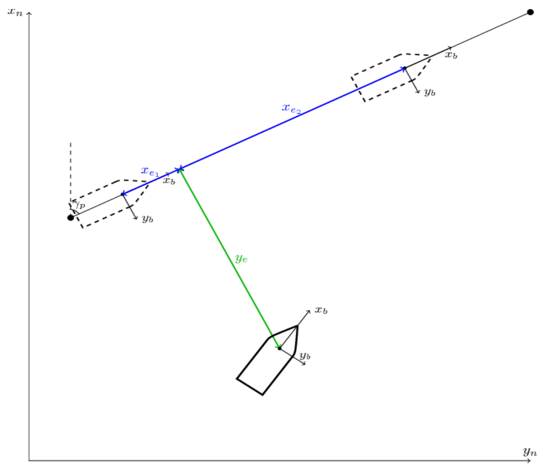

Figure 2.2: Illustration of the path-tracking [173]

c) Comfort-Centric Smoothness

Comfort-centric smoothness objectives are typically constructed by penalizing the magnitude of acceleration and jerk in the cost function. This is achieved by integrating squared terms of these quantities over time, thereby encouraging gradual variations in motion and smooth control inputs:

$$\min \int_{t_0} |\frac{d^2 v(t)}{dt^2}| dt \tag{2.4}$$

d) Path Tracking Precision

Path-tracking precision objectives are formulated by penalizing deviations between the vehicle's actual trajectory and a predefined reference path. This is commonly achieved by minimizing the lateral and longitudinal tracking errors, often expressed as squared distance terms integrated over time to ensure accurate and stable trajectory following (cf. Figure 2.2:

$$\min \int_{t_0} \|p(t) - p_{ref}(t)\|^2 dt \tag{2.5}$$

where $p(t)$ is the trajectory of vehicle, $p_{ref}(t)$ is the reference trajectory.

e) Multi-Objective Optimization

Multi-objective synergy is achieved through weighted sum optimization and Pareto-optimal frontier analysis:

$$J_{\text{total}} = \sum_{i=1}^{n} w_i J_i \tag{2.6}$$

where J_i and w_i are the cost function of the $i-th$ objective and its corresponding weight. Each objective category exhibits distinct trade-offs:

- Time-optimality may compromise passenger comfort.
- Energy efficiency could extend travel duration.

- Aggressive tracking may violate dynamic constraints.

In summary, this section reviewed key approaches in behavioral decision-making, including FSM-based and optimization-based methods, which enable autonomous vehicles to select appropriate maneuvers under diverse traffic conditions. While these techniques focus on determining what actions to take, the next section will address how safe these actions are—introducing risk assessment methodologies that evaluate and manage potential hazards in autonomous driving decision processes.

2.2 RISK ASSESSMENT

This section focuses on risk assessment, a crucial component of decision-making in autonomous driving. It introduces classical metrics such as Time-to-Collision and its extensions, followed by a detailed discussion of the PIDP-based approach for evaluating collision risks in dynamic environments.

2.2.1 *Time to Collision and Extended TTC*

Time-To-Collision (TTC) [82] is the foundational and one of the most famous risk assessment metrics, which estimates the remaining time until a collision would occur if both the ego vehicle and the obstacle maintain current speeds and directions. Its simplicity and real-time responsiveness make it a staple in emergency braking and forward collision warning systems. The definition of TTC in co-linear is as follows (cf. Figure 2.3a):

$$TTC = \frac{x_{lead}(t) - x_i(t) - 2r}{\dot{x}_{lead}(t) - \dot{x}_i(t)} \tag{2.7}$$

where $x_{lead}(t)$ is the position of the leading vehicle, and $x_i(t)$ is the position of ego vehicles. $\dot{x}(t)$ is velocity, r is the safety radius. The definition is extended to a non-collinear form as follows (cf. Figure 2.3b):

$$\begin{aligned} &\left[\left(x_i(t) + \dot{x}_i(t) \cdot TTC_{ij}\right) - \left(x_j(t) + \dot{x}_j(t) \cdot TTC_{ij}\right)\right]^2 \\ &+ \left[\left(y_i(t) + \dot{y}_i(t) \cdot TTC_{ij}\right) - \left(y_j(t) + \dot{y}_j(t) \cdot TTC_{ij}\right)\right]^2 = (2r)^2 \end{aligned} \tag{2.8}$$

While the conventional TTC metric provides an instantaneous estimate of collision risk based solely on the current relative distance and velocity between two vehicles, it neglects higher-order motion dynamics such as acceleration or steering. To address this limitation, the Extended TTC (ETTC) was introduced as a higher-order temporal metric that incorporates both the kinematic and dynamic evolution of interacting vehicles over time.

The ETTC extends the TTC formulation by considering the predicted future motion of each vehicle, typically modeled through constant acceleration dynamics. For two vehicles j and k, the ETTC can be computed by solving the quartic equation that expresses the equality of their predicted positions at the collision instant:

$$\begin{aligned} &[x_k + v_{xk} \cdot ETTC_{kj} + \tfrac{1}{2}a_{xk} \cdot ETTC_{kj}^2 - (x_j + v_{xj} \cdot ETTC_{kj} + \tfrac{1}{2}a_{xj} \cdot ETTC_{kj}^2)]^2 \\ +&[y_k + v_{yk} \cdot ETTC_{kj} + \tfrac{1}{2}a_{yk} \cdot ETTC_{kj}^2 - (y_j + v_{yj} \cdot ETTC_{kj} + \tfrac{1}{2}a_{yj} \cdot ETTC_{kj}^2)]^2 = (R_k + R_j)^2, \end{aligned} \tag{2.9}$$

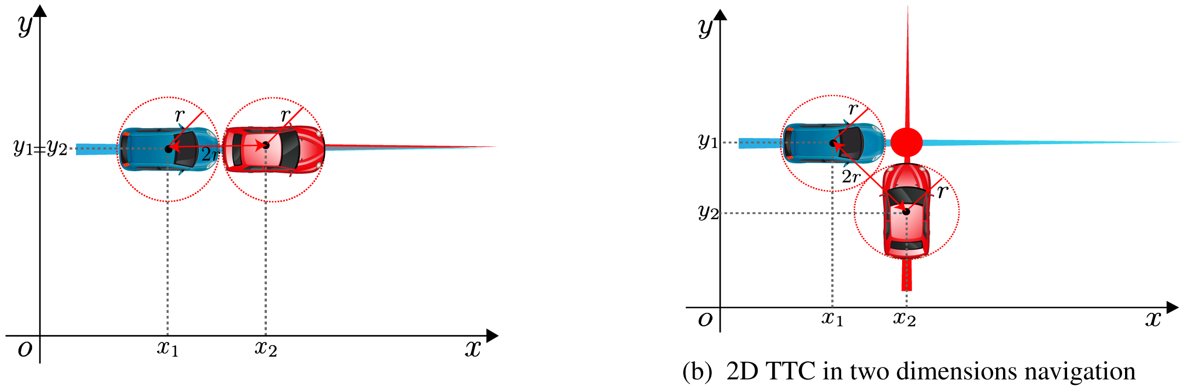

(a) 2D TTC in co-linear navigation case

(b) 2D TTC in two dimensions navigation case

Figure 2.3: A collision of two vehicles based on circle area [174]

where (x_j, y_j) and (x_k, y_k) denote the initial positions of vehicles j and k, (v_{xj}, v_{yj}) and (v_{xk}, v_{yk}) are their respective velocity components, and (a_{xj}, a_{yj}), (a_{xk}, a_{yk}) their accelerations. R_j and R_k represent the effective radii of the safety envelopes surrounding each vehicle.

Solving equation (2.9) yields the time values at which the two vehicles' boundaries may come into contact; among these, the smallest positive real root corresponds to the valid ETTC value, indicating the remaining time before a potential collision occurs.

The ETTC thus generalizes the TTC by accounting for the vehicles' future kinematic states and motion trends, enabling a more realistic and predictive assessment of collision risk in dynamic traffic scenarios. However, since equation (2.9) is quartic, multiple solutions (including complex or negative roots) may exist, and only positive real solutions are physically meaningful. If no real positive solution exists, no future collision is predicted under the assumed motion model.

Several extensions of ETTC have been proposed to handle special cases. For instance, when the relative velocity between two vehicles approaches zero, the ETTC may become undefined or uninformative. In such cases, additional indicators such as the Minimal Safety Margin—representing the residual spatial distance between vehicles—can be used to complement the temporal evaluation of risk. Moreover, while ETTC assumes rectilinear motion, real-world vehicle trajectories are often curvilinear, particularly at intersections or roundabouts.

In summary, the ETTC provides a more comprehensive temporal risk metric than TTC by integrating acceleration and curvature effects, thus serving as a foundation for more sophisticated collision prediction and cooperative risk assessment methods in connected and autonomous driving contexts.

2.2.2 *Time Exposed TTC and Time Integrated TTC*

These metrics, which are also extensions of the TTC measure, provide additional information beyond the basic temporal proximity evaluation. The Time Exposed Time-to-Collision (TET) represents the duration during which the vehicle remains within a safety distance smaller than a predefined threshold TTC^*, while the Time Integrated Time-to-Collision (TIT) denotes the integral of the TTC profile below that same threshold (see Figure 2.4).

These extensions are primarily used for monitoring vehicle following behavior, such as in platooning scenarios [175], but can also be combined with other safety indicators such

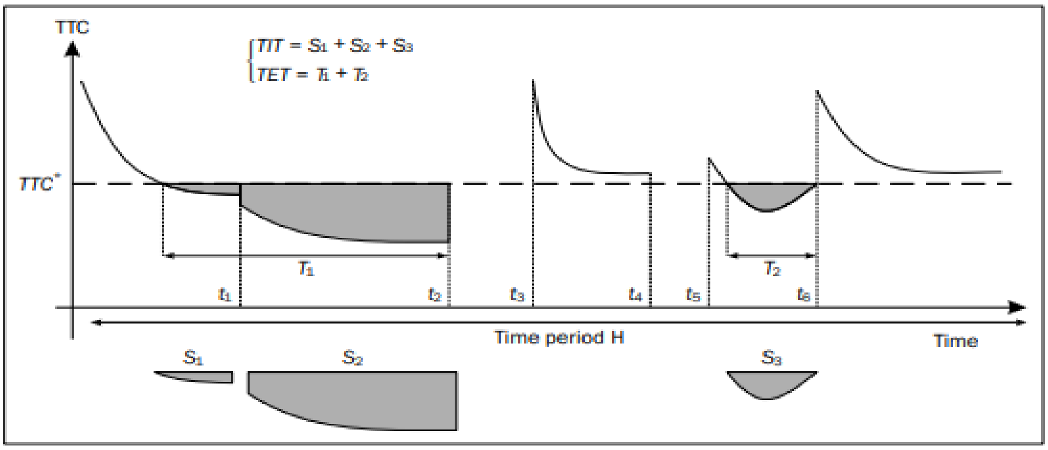

Figure 2.4: Example of determining TET and TIT [177]

as the Deceleration Rate to Avoid a Crash (DRAC) [176], which quantifies the minimum deceleration required to prevent a collision. In [177], TET and TIT are merged into a single indicator representing the overall probability of collision. Such metrics are particularly useful for a posteriori evaluation of vehicle maneuvers, serving as a foundation for model calibration or learning-based safety assessment.

2.2.3 *Predicted Inter-Distance Profile*

The Predicted Inter-Distance Profile (PIDP) metric is used for the evaluation and execution of overtaking maneuvers on highways or multi-risk management at unsignalized intersection crossings, depicts how the distance between two vehicles or a vehicle and an obstacle will change over a future time frame [178], [179]. If the information of the ego-vehicle and other vehicle (path, speed profiles, etc.) is known, and assuming these factors remain constant during a certain time horizon of prediction, the evolution of the inter-vehicle distance PIDP between them is feasible to be projected. In the dynamic environment, PIDP will be recalculated every time at the end of the control process and when the speed policy changes.

Figure 2.5 illustrates the definition of the PIDP framework. The computation of the inter-vehicle distance $p(t)$ is given as follows:

$$p(t) = \sqrt{(x_i(t) - x_j(t))^2 + (y_i(t) - y_j(t))^2} \tag{2.10}$$

where $x(t)$ and $y(t)$ are vehicles coordination information. $p(t)$ represents the variation of the inter-vehicle distance over time, and its time-dependent profile serves as an intuitive representation of the PIDP.

The safety distance should be declared if PIDP is applied to check the collision relation between two vehicles or vehicles and an obstacle. The safety distance d_{safety} is the minimum distance between two vehicles without collision, which is defined as:

$$d_{safety} = r_i + r_j + Margin \tag{2.11}$$

where r_i and r_j are the safety radius of respectively vehicle i and j, $Margin$ is a certain distance to guarantee to take into account the different uncertainties linked to the communication system as well as the capacity of maximum braking of the vehicles.

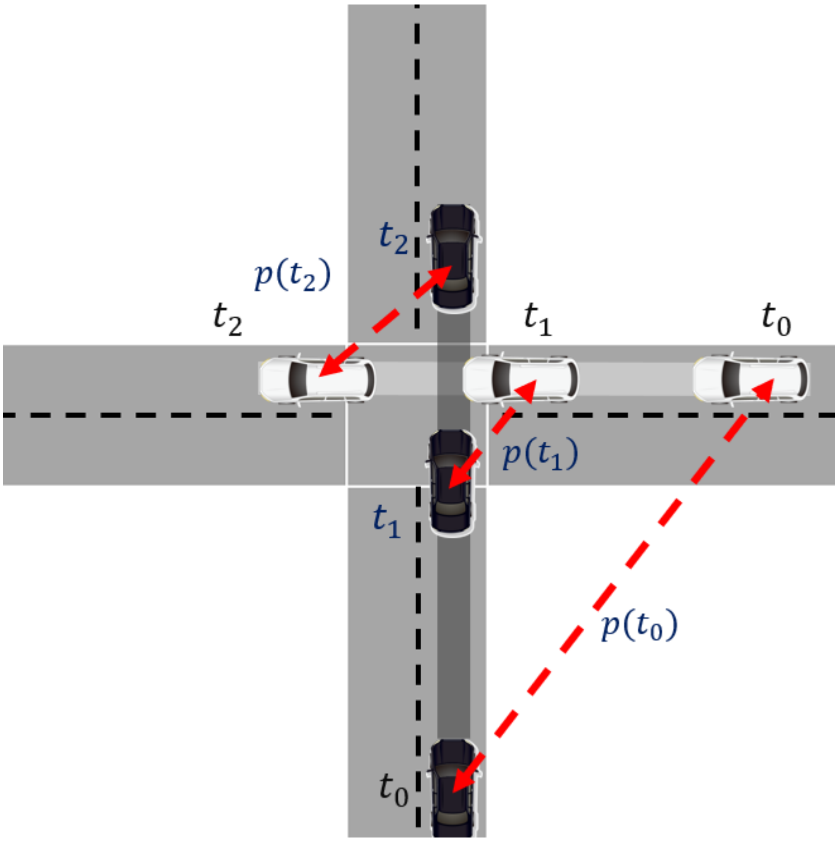

(a) Predicted inter-distance

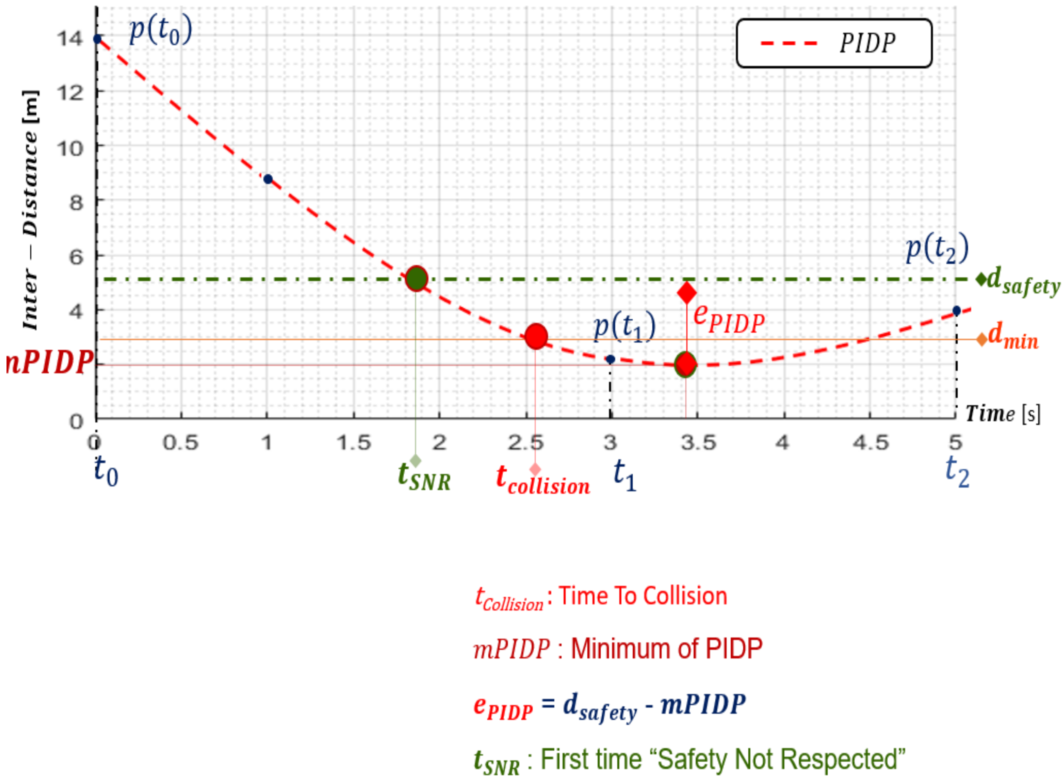

(b) $PIDP(t)$ curve

Figure 2.5: Definition of Predicted Inter-Distance Profile

mPIDP (cf. Figure 2.5) is the minimum value of the PIDP, which is the shortest distance between the two vehicles in the future. If *mPIDP* is smaller than the safety distance d_{safety}, it means that if neither speed nor path changes, the two vehicles have the risk of collision. For convenience, we define *ePIDP* (cf. Figure 2.5) as the difference between *mPIDP* and d_{safety}:

$$\begin{cases} mPIDP = & min(PIDP) \\ ePIDP = & mPIDP - d_{safety} \end{cases} \tag{2.12}$$

If *ePIDP* is positive, it indicates that current strategies do not have risk of collision, and if it is negative, it signifies the presence of collision risk exists in the future. The smaller *ePIDP* is, the greater the risk of collision. $ePIDP_{ij}^{po}$ and $ePIDP_{ij}^{ne}$ are defined as:

$$\begin{cases} ePIDP_{ij}^{po} = ePIDP_{ij}, & if \quad ePIDP_{ij} \geq 0 \\ ePIDP_{ij}^{ne} = ePIDP_{ij}, & if \quad ePIDP_{ij} < 0 \end{cases} \tag{2.13}$$

Time to Safety Not Respected and Collision is another time-scale metric used to describe the urgency of collision risk between two vehicles based on their PIDP curve. It is defined as "the time at which the distance between two vehicles first falls below the safe distance" (cf. Figure 2.5). The smaller t_{SNR} is, the more urgent the collision risk is. If there is no risk of collision, the value of t_{SNR} is equal to positive infinity.

Having established the fundamental principles of risk assessment that underpin safe and reliable decision-making, the discussion now transitions to motion planning, where these assessed risks are integrated into the generation of smooth, efficient, and dynamically feasible trajectories for autonomous vehicles.

2.3 MOTION PLANNING

Following the discussion on decision-making and risk assessment, this section focuses on motion planning, particularly on speed planning techniques that ensure smooth, safe, and dynamically feasible vehicle motion [180]. It presents several representative approaches—including Spatio-Temporal (ST) graph–based planning, Speed Lattice–based planning, and Quintic Spline curve generation—which together form the algorithmic foundation for generating continuous and optimized velocity profiles in autonomous driving.

2.3.1 *Spatio-Temporal Graph–based Speed Planning*

Spatio-temporal (ST) graph–based speed planning is a representative methodology for generating feasible and safe velocity profiles in autonomous driving [181], [182]. The core idea is to transform the longitudinal motion planning problem into a search task over a discretized two-dimensional space, where the horizontal axis represents time t, and the vertical axis denotes the longitudinal distance along a reference path s. Each point (s,t) in this space represents a possible position of the ego vehicle at time t, and a continuous trajectory $s(t)$ defines a specific velocity profile.

Dynamic obstacles, such as preceding vehicles or pedestrians, can be projected into this ST domain as forbidden regions. These regions are defined by the predicted spatio-temporal occupancy of obstacles and represent states that would lead to potential collisions if entered by the ego vehicle. Therefore, the task of velocity planning becomes one of finding a continuous, collision-free path in the ST plane from the initial point (s_0, t_0) to the goal (s_T, T).

The ST-graph planning procedure typically follows four key stages:

1. **Discretization of the ST space:** The time horizon $[0, T]$ is discretized into uniform steps Δt, and the longitudinal distance range $[0, S_{\max}]$ is discretized with resolution Δs. Each node in the ST graph thus represents a feasible vehicle state (s_i, t_j).

2. **Sampling and Edge Construction:** Neighboring nodes are connected by directed edges representing feasible motion segments. Each edge must satisfy vehicle kinematic constraints such as maximum acceleration and jerk:

$$v = \frac{\Delta s}{\Delta t}, \quad a = \frac{\Delta v}{\Delta t}, \quad |a| \leq a_{\max}.$$

3. **Graph Search:** A path search algorithm (e.g., Dynamic Programming, Dijkstra, or A*) is used to find a collision-free and smooth trajectory. The cost function typically integrates multiple criteria:

$$J = w_v (v - v_{\text{ref}})^2 + w_a a^2 + w_j j^2 + w_t t,$$

where v_{ref} denotes the reference velocity, and w_v, w_a, w_j, and w_t are weighting coefficients.

4. **Trajectory Smoothing:** The resulting discrete trajectory is then refined through polynomial fitting (e.g., fifth-order polynomial) or Quadratic Programming (QP) optimization to ensure continuity of velocity, acceleration, and jerk.

The ST-graph method has several advantages: it explicitly handles dynamic obstacles, ensures time-dependent safety, and provides intuitive visualization of temporal conflicts. However, its main limitations lie in computational cost and the need for post-processing to ensure trajectory smoothness.

2.3.2 *Speed Lattice–based Planning*

Speed lattice–based planning extends the idea of sampling-based trajectory generation into a structured, discrete search framework in the velocity domain [183], [184]. Instead of directly optimizing a continuous velocity function, this method constructs a lattice—a discretized graph of candidate velocity states—that allows efficient exploration of dynamically feasible trajectories under vehicle constraints.

a) Core Principle

The method begins by defining a discrete set of terminal velocity points $\{v_i\}$ or acceleration values $\{a_i\}$, sampled within feasible physical limits. For each sampled state, a parameterized polynomial or spline curve is generated to represent a dynamically feasible velocity trajectory:

$$v(t) = a_0 + a_1 t + a_2 t^2 + a_3 t^3,$$

subject to boundary conditions such as $v(0) = v_0$, $a(0) = a_0$, and $v(T) = v_T^i$. Each candidate curve thus corresponds to a node in the speed lattice, while feasible transitions between curves form the graph edges.

b) Algorithmic Workflow

The overall planning process can be summarized as follows:

1. **Sampling:** Discretize the velocity or acceleration domain within admissible limits and sample candidate terminal states.
2. **Trajectory Generation:** For each sample, compute the corresponding velocity profile using polynomial fitting or time-scaling laws that satisfy kinematic and comfort constraints (e.g., bounded acceleration and jerk).
3. **Evaluation and Search:** Each trajectory segment is evaluated by a cost function balancing smoothness, efficiency, and comfort. Dynamic Programming (DP) or best-first search is applied over the lattice to select the sequence of segments with the minimal cumulative cost.
4. **Refinement:** The best candidate path is smoothed through local optimization (e.g., quadratic programming) to produce the final continuous velocity curve.

Speed lattice methods are especially suited to structured driving environments such as highways or intersections, where dynamic feasibility and comfort are critical. Compared with ST-graph planners, they provide superior control continuity and adaptability to complex vehicle models. However, their computational demand increases with lattice resolution, and global optimality is not guaranteed.

2.3.3 *Quintic Spline Curve Generation*

Quintic spline interpolation is widely adopted in motion and velocity planning due to its ability to generate smooth, dynamically feasible trajectories that satisfy boundary conditions on position, velocity, and acceleration. By constructing fifth-order polynomials between successive waypoints, the planner ensures continuity not only in position and velocity but also in higher-order derivatives such as acceleration and jerk. This property is particularly critical for autonomous vehicles, as it directly influences ride comfort, mechanical wear, and safety.

When the initial and terminal conditions of a velocity profile are specified—including velocity, acceleration, and jerk (the derivative of acceleration)—together with the total transition time, a quintic spline interpolation can be employed to construct a smooth trajectory. The method formulates the velocity profile as a fifth-order polynomial of time:

$$v(t) = a_0 + a_1 t + a_2 t^2 + a_3 t^3 + a_4 t^4 + a_5 t^5 \tag{2.14}$$

where the coefficients $a_0, a_1, \ldots, a_5$ are determined by imposing boundary conditions at the start and end of the interval. Specifically, the known initial values of velocity, acceleration, and jerk define constraints on $v(0), \dot{v}(0)$, and $\ddot{v}(0)$, while the target terminal conditions define constraints on $v(T), \dot{v}(T)$, and $\ddot{v}(T)$, T denoting the total duration of the maneuver. Solving this system of six linear equations yields the coefficients of the quintic polynomial, thereby producing a velocity profile that guarantees continuity up to the second derivative.

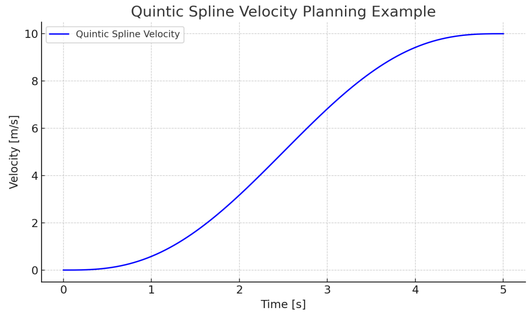

Figure 2.6: Quintic spline curve example

Given the boundary condition that:

$$\begin{cases} v(0) = v_0 \\ \dot{v}(0) = \dot{v}_0 \\ \ddot{v}(0) = \ddot{v}_0 \\ v(T) = v_T \\ \dot{v}(T) = \dot{v}_T \\ \ddot{v}(T) = \ddot{v}_T \end{cases} \tag{2.15}$$

so, the coefficients $\{a_k\}_{k=0}^{5}$ are:

$$\begin{cases} a_0 = v_0, \\ a_1 = \dot{v}_0 \\ a_2 = \frac{1}{2}\ddot{v}_0 \\ a_3 = \frac{-3T^2\ddot{v}_0+T^2\ddot{v}_T-12T\dot{v}_0-8T\dot{v}_T-20v_0+20v_T}{2T^3} \\ a_4 = \frac{\frac{3}{2}T^2\ddot{v}_0-T^2\ddot{v}_T+8T\dot{v}_0+7T\dot{v}_T+15v_0-15v_T}{T^4} \\ a_5 = \frac{-T^2\ddot{v}_0+T^2\ddot{v}_T-6T\dot{v}_0-6T\dot{v}_T-12v_0+12v_T}{2T^5} \end{cases} \tag{2.16}$$

Equivalently, the six boundary conditions yield the linear system:

$$\underbrace{\begin{bmatrix} 1 & 0 & 0 & 0 & 0 & 0 \\ 0 & 1 & 0 & 0 & 0 & 0 \\ 0 & 0 & 2 & 0 & 0 & 0 \\ 1 & T & T^2 & T^3 & T^4 & T^5 \\ 0 & 1 & 2T & 3T^2 & 4T^3 & 5T^4 \\ 0 & 0 & 2 & 6T & 12T^2 & 20T^3 \end{bmatrix}}_{\mathscr{A}(T)} \begin{bmatrix} a_0 \\ a_1 \\ a_2 \\ a_3 \\ a_4 \\ a_5 \end{bmatrix} = \begin{bmatrix} v_0 \\ \dot{v}_0 \\ \ddot{v}_0 \\ v_T \\ \dot{v}_T \\ \ddot{v}_T \end{bmatrix}.$$

Solving $\mathscr{A}(T)a = b$ yields the closed-form coefficients equation (2.15) listed above.

An example is shown as Figure 2.6, this approach ensures that the planned velocity trajectory transitions smoothly between the prescribed boundary conditions while avoiding discontinuities in acceleration or jerk, which are detrimental to both vehicle dynamics and passenger comfort.

At this point, the discussion has covered several key motion planning techniques commonly used in autonomous driving, with a particular focus on speed planning and smooth trajectory generation. These approaches bridge the gap between high-level decision-making and low-level vehicle control, ensuring both safety and efficiency in navigation. Building on this foundation, the next section will turn to CAVs cooperative decision-making, examining how these principles are applied and extended in realistic unsignalized intersection scenarios.

2.4 AUTONOMOUS INTERSECTION MANAGEMENT AND COOPERATIVE TRAFFIC CONTROL

This section focuses on representative cooperative traffic control strategies for unsignalized intersections, which aim to coordinate multiple CAVs safely and efficiently without relying on traditional traffic signals. The following subsections provide a concise overview of First-Come-First-Served scheduling, Reservation-based, and Leader–Follower platooning methods, outlining their key principles, coordination mechanisms, and practical considerations in cooperative intersection management.

2.4.1 *First-Come-First-Served Scheduling*

a) Core Idea and System Architecture

The First-Come-First-Served (FCFS) scheduling algorithm is one of the most intuitive and foundational centralized approaches for managing traffic at an unsignalized intersection [133]. The core principle is predicated on fairness and simplicity: vehicles are granted passage in the strict order of their arrival or request submission.

This methodology relies on a centralized decision-making entity, typically referred to as an Intersection Manager (IM) or a Roadside Unit (RSU). The IM possesses a comprehensive view of the intersection's state, including all approaching vehicles that are within its communication range. It acts as an arbiter, processing requests sequentially and ensuring that no two vehicles are assigned conflicting spatiotemporal paths. Each CAV must communicate with the IM to request a reservation before it is permitted to cross.

b) Algorithm Workflow

The FCFS protocol can be broken down into a clear, step-by-step process, which is initiated by the CAV and arbitrated by the IM.

1. **Request Transmission:** As a CAV approaches the intersection control area, it transmits a reservation request to the IM. This request message contains essential information, including:
   - Vehicle ID and physical dimensions (length, width).
   - Its current state vector: position, velocity, and acceleration.
   - The intended maneuver (e.g., proceeding straight, turning left, or turning right).
   - An Estimated Time of Arrival (ETA) at the intersection's entry point.

2. **Request Queuing:** Upon receiving the request, the IM validates it and places it into a chronological queue. This queue strictly adheres to the FCFS principle, ensuring that the earliest valid request is always at the front.

3. **Spatiotemporal Simulation & Conflict Check:** The IM dequeues the request at the head of the queue. It then performs a simulation to project the vehicle's spatiotemporal trajectory—its path through space and time—across the intersection. The IM maintains a database of all previously approved reservations. The critical task is to check if the newly simulated trajectory conflicts with any of these existing reservations. A conflict is defined as two vehicles occupying the same spatial region at the same point in time.

4. **Reservation Decision (Approve or Delay):** Based on the conflict check, the IM makes a binary decision:
   - **Approval:** If no conflict is detected, the IM approves the request. It reserves the spatiotemporal path for the vehicle and broadcasts a confirmation message back to the CAV, which includes the approved entry time and the required velocity profile.
   - **Delay:** If a conflict is detected, the request is denied. The IM calculates the minimum delay required for the vehicle to avoid the conflict and communicates this information back to the CAV. The CAV must then adjust its speed and may need to submit a new request with a revised ETA.

5. **Trajectory Execution:** Once a CAV receives its approval and reservation details, it adjusts its trajectory to meet the specified time and speed constraints, ensuring it traverses the intersection safely according to the centrally managed plan.

The FCFS-based coordination scheme provides implementation simplicity and safety guarantees through centralized management. However, it suffers from efficiency limitations due to its rigid sequencing, where slow vehicles can obstruct traffic flow. The architecture also presents reliability concerns as central manager failure would disable the entire intersection, with additional scalability challenges in dense traffic conditions.

2.4.2 *Reservation-based Methods*

The reservation-based method, first introduced by Dresner and Stone [185], has been widely applied in CAV coordination at intersections, significantly improving traffic efficiency and safety [186], [187]. Its core idea is to abstract the physical intersection into a discrete grid of tiles (or slots) in space and discrete steps in time. A vehicle's passage is treated as a request to reserve a specific sequence of these spatiotemporal slots.

This approach relies on a central IM that acts as a resource manager. The IM maintains a master ledger of all slots and their booking status, ensuring that no single slot is ever allocated to more than one vehicle at the same time, thus guaranteeing safety (cf. Figure 2.7).

The workflow is a negotiation process between a CAV and the IM. First, an approaching CAV transmits a detailed request, including its intended path and desired speed profile. The IM receives this request and discretizes the vehicle's continuous trajectory into a specific sequence of spatiotemporal slots it needs to occupy. This results in a list of

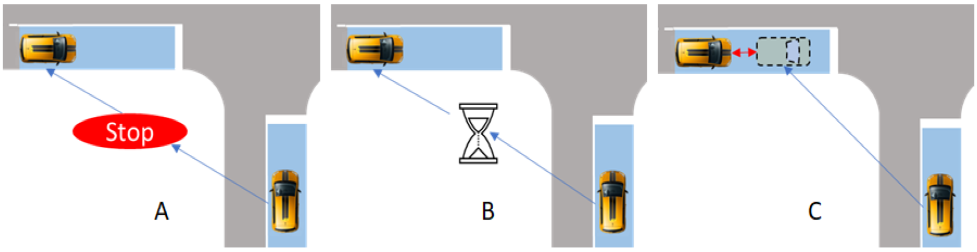

Figure 2.7: Protocols of Reservation-based method: (A)—Stop and Go, (B)—Reservation, (C)—Virtual Platoon [188]

required slots, e.g., `{(tile_A, time_1), (tile_B, time_1), (tile_B, time_2), (tile_C, time_2), ...}`.

Next, the IM checks this sequence against its master reservation ledger. If all requested slots are free, the reservation is approved, the slots are marked as "occupied", and a confirmation is sent to the CAV. If any slot is already booked, the request is denied; a sophisticated IM might then provide a counter-offer with the earliest available time for the same trajectory. Upon receiving confirmation, the CAV must precisely execute its approved schedule, and as it vacates each slot, that resource is released back into the available pool.

The primary advantage of the reservation-based method is its high efficiency and formal safety guarantee, achieved by allowing non-conflicting paths to be used simultaneously. However, this granularity imposes a significant computational and communication burden on the central Intersection Manager, which can become a bottleneck in dense traffic. Furthermore, the method is susceptible to issues from the discretization process and inherits the vulnerabilities of any centralized system, such as having a single point of failure.

2.4.3 *Leader-Follower Platooning*

a) Core Idea and System Architecture

In contrast to centralized methods, distributed approaches delegate decision-making authority to the vehicles themselves. The Leader-Follower Platooning strategy is a prominent example, designed to enhance efficiency by reducing control complexity [151].

The core idea is to organize vehicles with similar routes into tightly-coordinated groups called platoons. Within each platoon, a single vehicle is designated as the Leader, while all others are Followers. The key insight is that only the Leaders of different platoons need to engage in complex negotiations for right-of-way. The Followers simply execute a car-following logic to maintain a constant spacing from the vehicle ahead. This approach relies entirely on V2V communication, eliminating the need for a central IM.

b) Algorithm Workflow

The process involves platoon dynamics before, during, and after the intersection crossing.

1. **Platoon Formation:** As vehicles approach an intersection, they use V2V communication to discover neighbors with the same intended maneuver. Vehicles with compatible routes dynamically form a platoon. The vehicle at the front naturally

assumes the role of the Leader. The Followers then switch their control logic to a car-following model (e.g., Constant Time Gap control).

2. **Leader-to-Leader Negotiation:** Once platoons are formed, only the Leaders from conflicting traffic streams need to communicate and negotiate. This dramatically reduces the number of agents involved in the decision-making process from all vehicles to just a few Leaders.

3. **Priority Resolution:** The Leaders determine the right-of-way based on a shared, pre-defined set of priority rules. These rules must be simple and unambiguous to ensure consistent outcomes. Common examples include:
   - **Road Hierarchy:** Platoons on major roads have priority over those on minor roads.
   - **Platoon Size:** Longer platoons may be given priority to maximize throughput.
   - **Arrival Time:** The Leader that first reaches a virtual “decision line” may gain priority.
   - **Emergency Status:** Any platoon containing an emergency vehicle receives absolute priority.

4. **Maneuver Execution:** The platoon whose Leader wins the negotiation (the high-priority platoon) proceeds through the intersection as a single unit. The Leaders of lower-priority platoons command their respective platoons to yield, typically by slowing down or stopping before the intersection entry point. The Followers in all platoons simply maintain their formation relative to their preceding vehicle.

5. **Platoon Dissolution:** After the platoon has cleared the intersection, the Leader can broadcast a “dissolve” message, allowing all vehicles to revert to independent driving mode. This step is crucial for ensuring flexibility in the road network beyond the intersection.

Platoon-based coordination enhances intersection throughput via grouped vehicle movements with minimal gaps and reduces control complexity by concentrating decision-making at the leader level. Its distributed structure improves robustness by eliminating single-point failure. However, this approach incurs overhead from dynamic platoon formation and dissolution, which is less suitable for light traffic. Priority mechanisms may also create unfair delays for single vehicles or small platoons, and performance gains are highly dependent on sustained traffic density, diminishing under irregular flow conditions.

This section highlighted key strategies for cooperative intersection control, emphasizing structured coordination among CAVs to improve safety and efficiency in unsignalized intersection. As real-world environments often involve uncertainty from sensing errors, communication delays, and human interactions, the next section focuses on cooperative decision-making under uncertain and dynamic conditions.

2.5 COOPERATIVE DECISION-MAKING UNDER UNCERTAINTY

Uncertainty in perception, communication, and environment dynamics poses significant challenges for cooperative decision-making among CAVs. To handle such incomplete or imprecise information, two representative approaches are introduced in this section. The

Partially Observable Markov Decision Process (PO-MDP) framework models decision-making under partial observability [69], [70], [189], while Robust and Set-Theoretic Methods ensure safety through bounded uncertainty representations [190], [191]. Together, they provide complementary insights for achieving reliable and resilient CAV coordination in uncertain environments.

2.5.1 *Partially Observable Markov Decision Process*

When making decisions in real-world traffic, a CAV rarely has access to the complete and perfect state of its environment. Sensor measurements are inherently noisy, the intentions of other drivers are hidden, and communication links can be unreliable. To address these challenges, the PO-MDP provides a principled mathematical framework for planning under uncertainty. It is a generalization of the standard Markov Decision Process that explicitly accounts for imperfect state information.

a) Core Idea: Belief-State Planning

The fundamental distinction of a PO-MDP is that the agent does not know the true state of the world. Instead, it maintains a belief state, denoted as $b(s)$, which is a probability distribution over the set of all possible world states. This belief encapsulates the agent's uncertainty about the true state, based on the history of its past actions and observations. Rather than mapping a known state to an action, a PO-MDP policy maps this belief state to an action. The decision-making process thus becomes a cycle of acting, observing, and updating the belief.

b) Formal Definition of a PO-MDP

A PO-MDP is formally defined as a tuple of 7 elements $(\mathscr{S}, \mathscr{A}, \mathscr{T}, \mathscr{R}, \Omega, \mathscr{O}, \gamma)$:

1. **States ($\mathscr{S}$):** A finite set of all possible states of the world. In cooperative driving, a state $s \in \mathscr{S}$ would typically include the precise kinematic information (position, velocity, acceleration) of all vehicles, as well as hidden variables like the intentions of human drivers (e.g., aggressive, cautious, yielding) or the operational status of other CAVs.

2. **Actions ($\mathscr{A}$):** A finite set of actions available to the ego vehicle. An action $a \in \mathscr{A}$ could be a low-level control command (e.g., accelerate, decelerate, turn) or a high-level maneuver (e.g., proceed, yield, request merge).

3. **Transition Function ($\mathscr{T}$):** $\mathscr{T}(s, a, s') = P(s'|s, a)$ defines the probability of the world transitioning from state s to state s' after the ego vehicle takes action a. This function models the uncertainty in the environment's dynamics, such as the unpredictable reactions of human drivers.

4. **Reward Function ($\mathscr{R}$):** $\mathscr{R}(s, a)$ is a scalar function that defines the immediate reward (or cost) received after taking action a in state s. The reward function encodes the goals of the agent, such as reaching a destination quickly, maintaining safety, ensuring passenger comfort, and adhering to traffic rules.

5. **Observations (Ω):** A finite set of observations the agent can perceive from its sensors. An observation $\omega \in \Omega$ is the agent's only window into the state of the world.

It could be raw sensor data (e.g., LiDAR point cloud) or processed information (e.g., a list of detected objects with their estimated positions and velocities).

6. **Observation Function ($\mathscr{O}$):** $\mathscr{O}(\omega|s',a) = P(\omega|s',a)$ gives the probability of receiving observation ω if the world has just transitioned to state s' after the agent took action a. This function models the uncertainty inherent in the agent's sensors (e.g., sensor noise, occlusions, detection failures).

7. **Discount Factor (γ):** $\gamma \in [0,1)$ is a factor that balances the importance of immediate rewards versus future rewards.

c) The PO-MDP Decision-Making Cycle

The agent operates in a continuous "belief-action-observation" loop:

1. **Action Selection:** At time t, the agent is in a belief state b_t. It selects an action a_t that is optimal with respect to this belief, aiming to maximize the expected long-term discounted reward. This is determined by a policy $\pi(b_t) = a_t$.

2. **State Transition and Observation:** After executing a_t, the world transitions from the true (but unknown) state s_t to a new state s_{t+1} according to the transition function $\mathscr{T}$. The agent then receives a new observation ω_{t+1} according to the observation function $\mathscr{O}$.

3. **Belief Update:** This is the crucial step where the agent integrates the new information. It updates its belief from b_t to b_{t+1} using Bayesian inference. The updated belief $b_{t+1}(s')$ for each possible new state s' is calculated as:

$$b_{t+1}(s') = \eta \cdot P(\omega_{t+1}|s',a_t) \sum_{s\in\mathscr{S}} P(s'|s,a_t) b_t(s)$$

where η is a normalizing constant to ensure the new belief is a valid probability distribution. This update step allows the agent to reduce its uncertainty about states that are consistent with its latest observation and increase its uncertainty about those that are not.

The goal of a PO-MDP solver is to find an optimal policy π^* that maps any belief state to the action that maximizes the expected cumulative reward. It is employed to infer the driving intentions of surrounding vehicles and to determine the optimal path and speed of the ego vehicle [192]. However, finding an exact solution is computationally intractable for all but the smallest problems. In practice, online planning algorithms like MCTS are often used. These methods perform a forward search from the current belief state to find the best immediate action, making them suitable for real-time applications like autonomous vehicles.

2.5.2 *Robust and Set-Theoretic Methods*

While probabilistic frameworks like PO-MDP aim to find policies that are optimal on average, they rely on accurate knowledge of probability distributions, which can be difficult to obtain in practice. An alternative paradigm for decision-making under uncertainty is offered by robust and set-theoretic methods. Instead of modeling uncertainty with probabilities, this approach models it as belonging to a bounded, deterministic set [193]. The goal is then to find a control policy that guarantees safety and performance for any possible realization of the uncertainty within that set. This provides a worst-case, formally verifiable guarantee of safety.

a) Bounded Uncertainty and Worst-Case Guarantees

The foundational philosophy of set-theoretic methods is to move away from stochastic descriptions and towards a deterministic, set-based representation of uncertainty. The core assumption is that while we do not know the exact value of an uncertain variable (e.g., the exact position of another vehicle, the precise intention of a human driver), we can bound its possible values within a well-defined set.

This approach is particularly powerful for safety-critical systems like CAVs, where one is often more concerned with avoiding catastrophic failure in the worst possible case than with optimizing performance for the average case. The decision-making problem is thus transformed into finding a strategy that is robust against all adversarial possibilities allowed by the uncertainty sets.

b) Set-Theoretic Representation of Uncertainty

In this framework, all sources of uncertainty are modeled using sets. Let $x(t)$ be the state of a vehicle at time t. An uncertain state is not a single point but a set $X(t)$ where the true state is known to lie, i.e., $x(t) \in X(t)$. Common representations for these uncertainty sets include:

- **Polytopes:** Defined by a set of linear inequalities, $X = \{x \mid Ax \leq b\}$. They can represent complex shapes but operations can be computationally expensive.
- **Ellipsoids:** Defined by a quadratic inequality, $X = \{x \mid (x-c)^T P^{-1}(x-c) \leq 1\}$, where c is the center and P is a positive definite matrix defining the shape. Operations on ellipsoids are often computationally efficient.
- **Zonotopes:** A special class of polytopes that are computationally efficient to work with. They are particularly useful for representing the evolution of linear systems under uncertainty.

Sources of uncertainty that are modeled this way include:

1. **State Uncertainty:** The initial state of the ego vehicle and other agents is known only to lie within a certain set, e.g., due to localization errors.
2. **Sensing Uncertainty:** Sensor measurements of other objects are not perfect points but are represented as sets that contain the true object state.
3. **Model Uncertainty:** The dynamic models of vehicles are not perfect. Disturbances and unmodeled dynamics are assumed to be bounded within a set.
4. **Behavioral Uncertainty:** The future actions or intentions of other agents (especially human drivers) are modeled as a set of possible control inputs they might apply.

c) Reachability Analysis for Collision Avoidance

The primary tool used in set-theoretic decision-making is reachability analysis. The goal is to compute the set of all possible states a system can reach over a future time horizon, given the uncertainties [194].

FORWARD REACHABLE SET: Given a vehicle's dynamics $\dot{x} = f(x,u,w)$, where x is the state, u is the control input, and w is a disturbance bounded in a set $\mathscr{W}$, the forward reachable set $\mathscr{R}(t)$ is the set of all possible states $x(t)$ that the vehicle can be in at time t, starting from an initial set of states X_0.

COLLISION AVOIDANCE AS A SET-INVARIANCE PROBLEM: In a multi-vehicle scenario, robust collision avoidance is formulated as a constraint that the reachable sets of any two vehicles must not intersect at any point in time. Let $\mathscr{R}_i(t)$ be the forward reachable set of vehicle i at time t, and let its physical occupancy at state x be the set $\mathscr{B}(x)$. The safety constraint is:

$$\left(\bigcup_{x\in\mathscr{R}_i(t)} \mathscr{B}(x)\right) \cap \left(\bigcup_{y\in\mathscr{R}_j(t)} \mathscr{B}(y)\right) = \emptyset, \quad \forall t \in [0,T], \forall i \neq j \tag{2.17}$$

This simply states that the set of all possible physical locations for vehicle i must be disjoint from the set of all possible physical locations for vehicle j at all times.

THE DECISION-MAKING PROCESS: The planning problem becomes finding a sequence of control inputs (a policy) for the ego vehicle that ensures this non-intersection constraint is satisfied for the entire planning horizon, regardless of the behavior of other agents (as long as their behavior stays within their pre-defined uncertainty sets). This is often formulated as a minimax optimization problem or solved using techniques from robust control, such as finding an invariant set or using Hamilton-Jacobi-Isaacs reachability.

Set-theoretic methods offer unparalleled safety assurances by guaranteeing collision-free operation under a well-defined set of uncertainties, a feature highly desirable for autonomous systems. It has been widely adopted in ACC, V2X communication, and multi-agent collision avoidance [195], [196], [197]. This robustness comes at the cost of potential over-conservatism, as the controller must always plan for the absolute worst-case scenario, which may be extremely unlikely to occur in practice. Consequently, the performance (e.g., travel time) may be suboptimal compared to methods that optimize for average-case performance, and the computational complexity of propagating sets forward in time remains a significant, though actively researched, challenge.

2.6 MACRO–MICRO INTEGRATION: TRAFFIC FLOW THEORIES FOR CAV COORDINATION

To effectively coordinate CAVs at a large scale, it is essential to understand the collective dynamics of traffic flow. While individual CAVs operate based on micro-level control laws, their combined behavior gives rise to macro-level phenomena such as congestion and shockwaves. This section reviews fundamental traffic flow theories that bridge this macro-micro gap, providing the theoretical basis for designing scalable CAV coordination strategies. We begin with the foundational single-regime model, progress to a more nuanced multi-phase theory, and conclude with a network-level perspective.

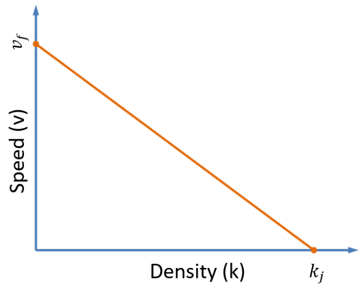

Figure 2.8: Greenshields speed-density model

2.6.1 *Greenshields' Traffic Flow Model*

The study of traffic flow has long been a critical area in transportation engineering, aiming to optimize road capacity and enhance safety. Among the pioneering models, the Greenshields traffic flow model, proposed by Bruce D. Greenshields in 1935 [154], stands as a foundational approach to understanding the relationship between traffic density and speed. The Greenshields model is based on observations of real-world traffic data and postulates a linear relationship between vehicle speed and traffic density. It establishes a simple mathematical relationship between the three primary variables of traffic flow:

- **Flow (q):** The number of vehicles passing a point per unit of time (e.g., vehicles/hour).
- **Density (k):** The number of vehicles per unit length of roadway (e.g., vehicles/km).
- **Speed (v):** The average speed of vehicles in the traffic stream (e.g., km/h).

These variables are linked by the fundamental equation of traffic flow:

$$q = kv \tag{2.18}$$

$$v = v_f(1 - \frac{k}{k_{jam}}) \tag{2.19}$$

$$q = v_f * k(1 - \frac{k}{k_{jam}}) \tag{2.20}$$

where q is the traffic flow (veh/h or veh/s), k is traffic density (veh/km or veh/m), v is the average vehicle speed (km/h or m/s). v_f is the free-flow speed, k_{jam} is the jam density. The simplicity of this linear relationship allows for an intuitive representation of traffic states, transitioning from free-flow conditions to congested scenarios. Despite its basic assumptions, the Greenshields model has provided a cornerstone for subsequent traffic flow theories. This section leverages the Greenshields model as a baseline to explore traffic flow optimization in the context of CAVs, aiming to address modern challenges at unsignalized intersections and beyond.

equation (2.18) is the definition of traffic flow. equation (2.19) is the speed-density relationship, when the traffic density approaches zero ($k \longrightarrow 0$), the flow rate also tends toward zero ($q \longrightarrow 0$) since there are virtually no vehicles on the roadway (cf. Figure 2.9). Conversely, under congested conditions where vehicle movement becomes restricted ($k \longrightarrow k_{jam}$), the flow rate similarly decreases to zero ($q \longrightarrow 0$).

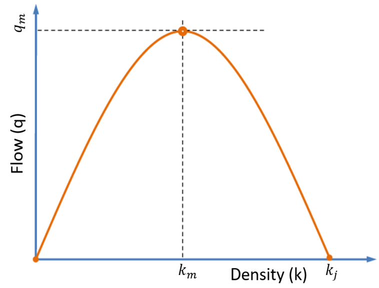

Figure 2.9: Greenshields flow-density model

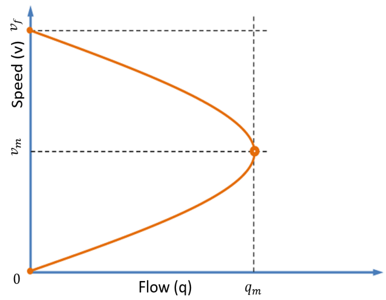

Figure 2.10: Greenshields speed-flow model

Equation (2.20) is the flow-density relationship, when the flow rate approaches zero ($q \longrightarrow 0$), two distinct situations may arise (cf. Figure 2.10): (1) the roadway contains almost no vehicles ($k \longrightarrow 0$), allowing the few present to travel at free-flow speed ($v \longrightarrow v_f$); or (2) the roadway is so congested ($k \longrightarrow k_{jam}$) that vehicle movement is effectively restricted ($v \longrightarrow 0$). In fact, substituting a given flow value into the fundamental relation yields two possible speed values: the lower one corresponds to unfavorable traffic conditions, while the higher one represents favorable conditions. When the flow rate reaches the road capacity, these two speeds converge to the same value, which corresponds to the optimal traffic speed, and the corresponding traffic flow is the maximum flow (q_{max}). By taking the derivative of the flow equation (2.20) and setting it to zero, the maximum flow (q_{max}) and its corresponding vehicle density can be calculated as:

$$q_{max} = \frac{v_f k_{jam}}{4} \iff k = \frac{k_{jam}}{2} \tag{2.21}$$

which means that the maximum flow occurs when the density is half of the jam density. Figure 2.11 summarizes the three pairwise relationships among speed–density, speed–flow, and flow–density within a single diagram. These pairwise relations represent different perspectives of the fundamental speed–flow–density relationship and thus serve distinct purposes in traffic flow analysis. For example, the speed–density relation links a driver's choice of speed to the concentration of vehicles in the surrounding environment. The Greenshields model has been so successful that it has been widely adopted to characterize the states of both highway and urban traffic systems [198], [199].

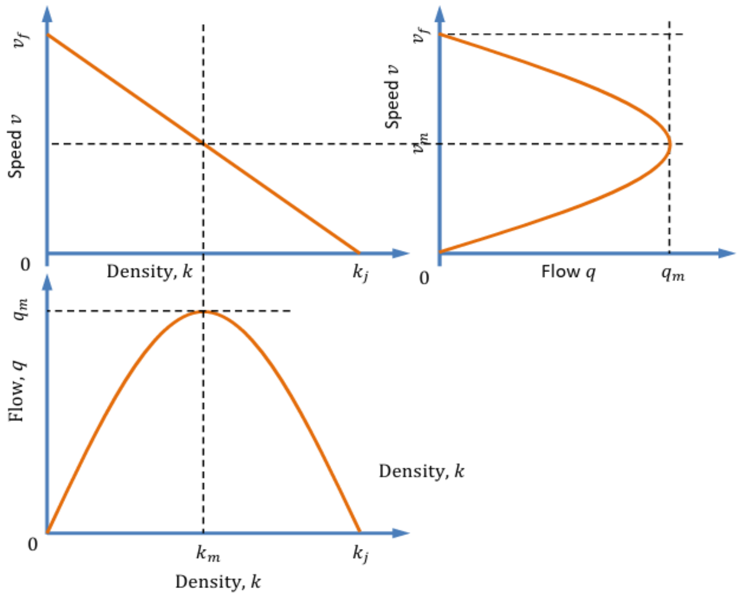

Figure 2.11: Greenshields flow-density-speed model

2.6.2 *Three-Phase Traffic Theory*

Empirical observations have revealed complex traffic phenomena, such as capacity drop and stop-and-go waves, that cannot be explained by single-regime models like Greenshields' model. The Three-Phase Traffic Theory, developed by Boris Kerner [200], provides a more nuanced framework by classifying traffic into three distinct phases:

1. **Free Flow (F):** This is the uncongested state, characterized by high speeds and low densities. Drivers can maneuver with little to no influence from other vehicles. In the flow-density plane, this phase corresponds to a line of data points with a high, near-constant speed.

2. **Synchronized Flow (S):** This phase represents a congested state where vehicles travel at a significantly reduced but relatively homogeneous speed over a substantial road segment. The defining characteristic of synchronized flow is the absence of a fixed downstream bottleneck. Crucially, within this phase, a wide range of flow values can be observed for the same density, causing the data points to occupy a two-dimensional region in the flow-density plane. This phase is responsible for the "capacity drop" phenomenon, where the maximum flow observed in the congested state is lower than the roadway capacity.

3. **Wide Moving Jam (J):** This is the classic, fully developed traffic jam. It is a region of extremely high density and very low (near-zero) speed that propagates upstream at a characteristic, constant velocity. Unlike synchronized flow, the flow-density relationship within a wide moving jam is deterministic, forming a distinct line on the flow-density diagram.

The theory is defined by the phase transitions between these states, most notably the traffic breakdown from Free Flow to Synchronized Flow (**F** $\rightarrow$ **S**) and the subsequent formation of a Wide Moving Jam within the synchronized phase (**S** $\rightarrow$ **J**). For CAV coordination, this theory is critical because it implies that congestion is not a monolithic state. Strategies designed to prevent the initial F $\rightarrow$ S transition (e.g., by smoothing vehicle interactions) will be fundamentally different from those designed to dissolve wide moving jams.

2.6.3 *The Macroscopic Fundamental Diagram*

While the previous theories describe traffic on individual road segments, the Macroscopic Fundamental Diagram (MFD) extends these concepts to the network level [160], [201]. The MFD describes the aggregate behavior of an entire urban region or network by relating two key variables:

- **Network Accumulation (n):** The total number of vehicles present within the network boundaries at a given time. This is analogous to density (k) at the link level.
- **Network Production (P):** The total vehicle-kilometers traveled per unit time within the network. This is analogous to flow (q) at the link level and is often measured as the product of the trip completion rate and the average trip length.

Empirical and simulation studies have shown that for urban networks where congestion is distributed relatively homogeneously, a well-defined, concave MFD exists. This MFD curve has a distinct shape: an ascending part where production increases with accumulation, a peak representing the network's maximum production capacity, and a descending part where excessive accumulation leads to gridlock and a sharp drop in network production (cf. Figure 1.18).

The existence of an MFD has profound implications for large-scale CAV coordination. It provides a simple yet powerful model for network-wide traffic control. By monitoring the network's state (i.e., its current position on the MFD), a traffic management system can implement control strategies to maintain accumulation near the critical value (n_{crit}) that maximizes overall network throughput. It has been widely used in dynamic congestion analysis of large-scale networks [202]. CAVs can play a dual role in this paradigm: they can act as mobile sensors providing high-quality real-time data to construct and validate the MFD, and they can serve as actuators to implement network-level control strategies, such as perimeter control or dynamic route guidance, with high precision.

2.7 CONCLUSION

This chapter presented an in-depth review of the theoretical and methodological foundations underpinning cooperative decision-making and motion planning in CAVs. It summarized key approaches in behavioral decision-making, risk assessment, and motion planning, together with representative cooperative strategies for intersection management and decision-making under uncertainty. In addition, the discussion bridged micro-level vehicle coordination along with macro-level traffic flow modeling, highlighting the necessity of multi-scale perspectives for understanding and improving urban mobility.

While the literature has made significant progress, important gaps remain. Existing methods still struggle to ensure real-time, computationally efficient multi-vehicle risk management in dynamic, unsignalized intersections. Moreover, research on microscopic CAV cooperation and macroscopic traffic flow optimization has largely evolved in parallel, with limited integration between the two domains.

To address these challenges, the next part of this thesis focuses on developing an integrated framework for cooperative decision-making in CAVs. The work presented herein first introduces our cooperative strategies for multi-vehicle coordination at intersections. It then builds upon this foundation by extending these concepts to address the complexities of uncertain environments. A subsequent part will further connect these microscopic methods with macroscopic traffic flow principles, forming a unified multi-level perspective on smart city mobility.

3 MULTI-RISK ASSESSMENT AND MANAGEMENT FOR CAVS

Intersections are widely recognized as one of the primary causes of urban traffic congestion, while CAVs are broadly regarded as a promising solution to this challenge. Compared with traditional signalized intersections, unsignalized intersections offer greater potential to exploit the technological advantages of CAVs, including rapid reaction, precise control, and collective decision-making.

However, fully leveraging these advantages requires solving a complex cooperative decision-making problem. When multiple autonomous vehicles converge at an intersection, they must reach consensus on who proceeds, when, and how to avoid collisions while minimizing total delays. Each vehicle operates as an intelligent agent with its own objective—crossing quickly and safely—yet also with the ability to consider the objectives of others. A fundamental trade-off arises between overly cautious behaviors, which may cause congestion, and overly aggressive strategies, which may compromise safety. The core challenge, therefore, lies in designing a decision-making framework that enables vehicles to act in a prosocial manner, sharing information and adjusting their plans to preserve the collective benefit, without relying on centralized control such as traffic signals.

3.1 PROBLEM STATEMENT

We address the problem of cooperative decision planning for multiple autonomous vehicles at an unsignalized intersection. The goal is to enable a group of CAVs approaching a common intersection to negotiate their crossing order and trajectories autonomously, in a decentralized manner, so that safety is ensured and overall traffic performance is improved. The key questions include: How can vehicles share and use information about their intended movements to avoid conflicts? What decision-making strategy allows them to agree on a crossing sequence efficiently? How can we ensure that the solution scales with many vehicles without imposing excessive computational burdens? By formulating this as a cooperative multi-agent planning problem, we seek a strategy that balances safety and efficiency, taking full advantage of CAV capabilities.

The following subsection outlines the fundamental assumptions and foundational methods, which collectively define its operational boundaries and theoretical foundation.

3.1.1 *Fundamental Assumptions*

All CAVs are assumed to possess a high degree of autonomy. Communication among CAVs, as well as between CAVs and intersection infrastructure, follows a common protocol that is fully compatible across agents. Through this communication, vehicles are able to exchange and share information regarding their predicted trajectories, velocities, and other relevant states. Owing to this information sharing, each vehicle gains a better understanding of the behaviors and decisions of others, and consequently tends to select strategies that maximize collective benefit, except in cases where such choices would severely compromise its own objectives. Vehicle velocities and trajectory profiles are not fixed or unique but are instead iteratively updated throughout the decision-making process. Each vehicle continuously explores alternative velocity plans, identifying strategies better suited to the current traffic context. Once a strategy is confirmed to be more advantageous than the vehicle's existing plan, the vehicle adopts it, updates its corresponding velocity and trajectory, and subsequently broadcasts this updated information to all nearby CAVs.

3.1.2 *Related Work and Challenges*

In contrast to discrete spatio-temporal scheduling approaches such as FCFS and its variants [135] (cf. Section 2.4.1), continuous trajectory optimization methods enable a more refined and efficient form of cooperative coordination among connected vehicles. Scheduling-based methods generally formulate intersection cooperation as a discrete resource allocation problem, where vehicles are granted access to the conflict zone based on temporal slots or priority queues. Although such "stop-and-go" strategies guarantee safety, they inherently sacrifice traffic efficiency and vehicle dynamic smoothness, leading to suboptimal throughput and frequent acceleration–deceleration behaviors. In contrast, trajectory optimization approaches operate in a continuous spatio-temporal domain, where the optimal trajectories of multiple vehicles are jointly optimized under safety and kinematic constraints (cf. Section2.3.1). This formulation allows vehicles to coordinate through smooth velocity adjustments, achieving collision-free interaction without full stops and thus improving both safety and traffic flow efficiency.

Within this family of optimization-based approaches, risk assessment plays a critical role in ensuring cooperative safety. Conventional TTC/ETTC metrics (cf. Section 2.2.1), which are reactive by nature, can only indicate the time remaining before a potential collision but fail to characterize its severity or adapt to complex, dynamic interaction scenarios [174]. By contrast, the PIDP metric provides a richer and more predictive representation of risk, simultaneously estimating the time of potential collision and its intensity, thereby offering a continuous and differentiable risk landscape suitable for optimization frameworks [203] (cf. Section 2.2.3).

Nevertheless, most existing risk metrics, whether TTC- or PIDP-based, are inherently designed for pairwise vehicle interactions, limiting their applicability to complex multi-vehicle coordination tasks. This observation motivates our work: to develop a novel multi-vehicle cooperative decision-making framework that extends the PIDP formulation toward collective risk assessment and management, enabling real-time, predictive, and dynamically consistent coordination among multiple connected autonomous vehicles.

3.1.3 *Formulation of Searching Space*

It is chosen in our research investigations to consider the path of the vehicles are known, only their linear velocities are predicted or controlled online. Further, it is important to mention, that the proposed approaches, could consider variable paths, but it is not included in this work. Since the paths of vehicles passing through the intersection are solely determined by their starting positions and destination directions, the only available control parameter is the navigation speed. CAVs should make their decisions within a limited time interval and coordinate their navigation actions.

We have introduced the speed profiles generation method in section 2.3.3. We generate speed profile based on each vehicle's initial speed, the legal maximum speed at the intersection, and dynamic constraints such as the vehicle's maximum acceleration and deceleration.

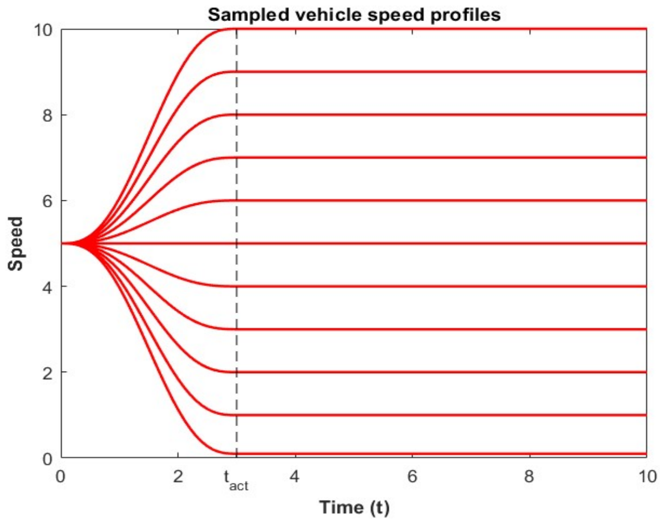

Figure 3.1: Speed profiles in searching space [204]

Typically, based on the current speed profile, a discrete set of candidate target speeds is generated to represent the possible choices available to the vehicle at its present state. Each target speed is then used to construct a corresponding speed profile that satisfies the vehicle's dynamic constraints. We refer to each such speed profile as a distinct strategy. The subsequent decision-making process identifies the most suitable strategy from this set, considering both the newly generated candidates and the previously executed strategy. To ensure sufficient coverage of feasible options, the candidate target speeds are uniformly sampled within the range of attainable velocities, determined by the vehicle's capacity to accelerate or decelerate over a given time horizon.

An example is shown as Figure 3.1. The velocity values are uniformly sampled between a minimum velocity v_{min} and a maximum velocity v_{max}. The set of N_s sampled velocities, denoted as $\{v_i\}_{i=0}^{N_s-1}$, is given by:

$$\begin{aligned} v_{max} &= min(v_{max}, v_{legal}) \\ v_{min} &= max(v_{min}, 0) \\ v_i &= v_0 + i\Delta v \\ \Delta v &= \tfrac{v_{max}-v_{min}}{N_s-1} \end{aligned} \tag{3.1}$$

where v_{legal} is the maximum legal speed around the intersection.

3.1.4 *Unsignalized Intersection Model*

For different intersections, variables such as size, speed limits, and the extent of infrastructure coverage vary. Consequently, the best solution is to combine these parameters and establish an independent intersection model, rather than treating them as data that CAVs need to explore on their own. This approach ensures that CAVs operate within a well-defined context, facilitating more effective and efficient decision-making and optimization.

Therefore, let's consider an unsignalized intersection as shown in Figure 3.2 in this work. It consists of 1 infrastructure and 4 areas:

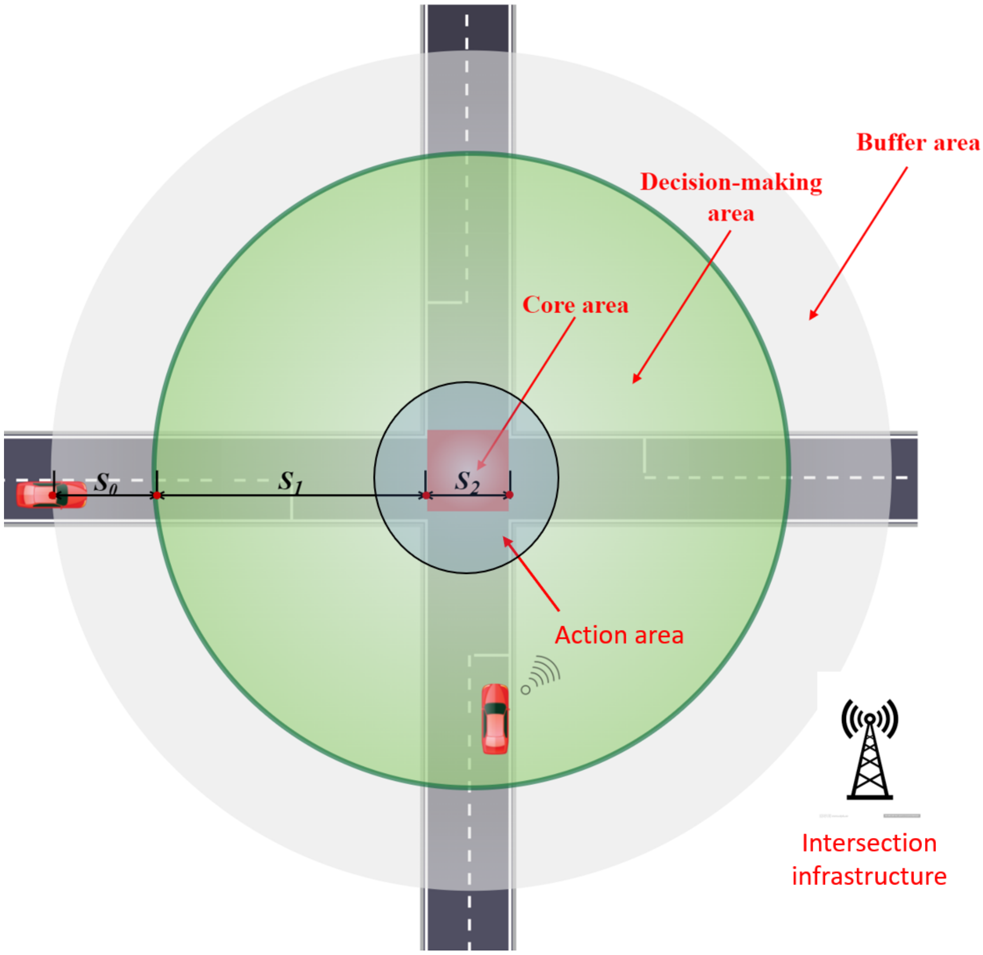

Figure 3.2: General Unsignalized Intersection Model: S_0 represents the ring width of the buffer area. S_1 represents the ring width of the decision-making area. S_2 denotes the width of the intersection core region

1. The Core area is the center of the intersection, vehicles interact in this area with safety strategies.

2. The Action area is a small area near the center of the intersection, vehicles in this area have the highest priority (w.r.t. the other CAVs outside this region) and only broadcast their strategies in the communication process, their strategy will not be changed.

3. The Decision-making area is a large area near the intersection, vehicles in this area are included in the cooperative decision-making process.

4. The Buffer area is the area for vehicles approaching the intersection to build communication with the infrastructure of the intersection and the other CAVs if available for V2V communication.

S_0 represents the ring width of the buffer area, which denotes the distance from the buffer area to the decision-making area. S_1 represents the ring width of the decision-making area, corresponding to the distance from the decision-making area to the intersection core region. S_2 denotes the width of the intersection core region. The infrastructure is designed to collect CAVs' information and broadcast it to all CAVs around the intersection.

3.2 MULTI-RISK MANAGEMENT COOPERATIVE OPTIMIZATION BASED ON PIDP

The foundation of any cooperative trajectory optimization framework lies in its ability to accurately assess and manage collision risk. As established in Section 2.2.3, the PIDP offers a significant advantage over reactive metrics by providing a continuous, predictive, and differentiable risk landscape, making it highly suitable for optimization-based planners.

However, the utility of PIDP in its standard form—and indeed, most conventional risk metrics—is largely confined to quantifying the risk of a pairwise interaction (i.e., between two vehicles). At a busy, multi-leg unsignalized intersection, vehicles are rarely faced with a single, simple conflict. Instead, they are confronted with a complex and coupled "multi-risk" environment. A single vehicle may, for example, face a potential lateral collision from the right while simultaneously managing a potential rear-end conflict from behind and a crossing conflict from the front. In such scenarios, simply identifying multiple pairwise risks is insufficient. A decision to resolve one conflict (e.g., braking to yield to one vehicle) could inadvertently exacerbate another. This creates a critical gap: a method is needed that does not just assess risk, but manages and optimizes the resolution of these competing, simultaneous conflicts.

To bridge this gap, this section introduces the Multi-Risk Management Cooperative Optimization based on PIDP (MRMCO-PIDP). This framework is developed as a comprehensive extension of the PIDP concept, evolving it from a powerful assessment metric into a full-fledged management methodology. It is specifically designed to rapidly identify and execute optimal collision-avoidance strategies, not just for two-vehicle interactions, but for complex, expandable multi-vehicle and multi-risk coordination scenarios.

3.2.1 *Unsignalized Intersection Collaboration between two CAVs*

When discussing the coordination of CAVs at intersections, the problem is primarily concerned with a dual objective: enabling vehicles to traverse the shared conflict space safely and efficiently. Before optimizing for efficiency (e.g., minimizing travel time), the non-negotiable prerequisite of safety must be guaranteed. Let us, therefore, first address the foundational challenge of how vehicles can cooperate to ensure a safe passage through the intersection.

At an intersection, if a potential collision occurs between vehicles traveling in the same direction, the solution is generally straightforward — the leading vehicle may accelerate or the following vehicle may decelerate to avoid a rear-end collision. When the potential collision is not a same-direction rear-end type, two alternative strategies are usually feasible: one vehicle can decelerate to yield and allow the other to pass first, or it can accelerate to clear the intersection quickly. Both approaches are considered viable solutions. However, the goal is to find a feasible solution to avoid the collision as soon as possible, rather than to find a solution only. Let's start the method from the easiest example: collision avoidance between two vehicles.

When the vehicle has the risk of collision with others, it will select the increased speed profile or the decreased speed profile based on the current speed profile, and calculate the new $PIDP(t)$ curves with respect to the conflicting vehicle. The decision to accelerate or decelerate is determined based on the numerical values of both obtained $ePIDP_{ij}$ (where i is the index of the ego-vehicle and j is the other CAV, the method to get the *ePIDP* is introduced in Section 2.2.3). In order to explain the basic working of the proposed MRMCO-PIDP for a simple situation of two vehicles in conflict, let us give an example of possible encountered situation as shown in Figure 3.3. In this Figure, the superscript of "*in*" and "*de*" are the abbreviation of "increased speed" and "decreased speed". The following method is used to select the better strategy between "increased speed" and "decreased speed", and mark the corresponding $ePIDP_{ij}$ as $ePIDP_{ij}^{opt}$:

1. If $ePIDP^{in} > 0 > ePIDP^{de}$, it means the increased speed profile doesn't have collision but the decreased still presents a risk of collision. Selecting the increased one is better to find the feasible solution faster.

2. If $ePIDP^{de} > 0 > ePIDP^{in}$, the decreased speed profile is a better choice and the reason is the same as the previous one.

3. If both values are positive or both are negative, the solution with the larger *mPIDP* is selected, since the change in velocity is the same, the larger the change in the mPIDP of the strategy, the faster the strategy resolves collisions.

In Figure 3.3, the blue curve is the initial speed profile and corresponding $PIDP(t)$ curve. From the Figure 3.3b, it is easy to find that the current *mPIDP* is smaller than the safety distance d_{safety}, which means it has risk of collision in the future. Then, it generates the predicted accelerated and decelerated speed profiles, corresponding to the red and pink curves respectively in Figure 3.3a, and corresponding $PIDP(t)$ curves in Figure 3.3b.

From Figure 3.3, it can be readily observed that in this example $ePIDP^{in}$ is positive while $ePIDP^{de}$ is negative, which corresponds to the case that the increased speed profile is a better choice. Therefore, for the current ego vehicle, accelerating through the intersection is more effective than decelerating in reducing the joint waiting time of the two vehicles.

3.2.2 *MRMCO-PIDP: From Single-Risk to Multi-Risk Management*

After introducing the simplest method, MRMCO-PIDP, suitable for resolving conflicts between two vehicles, we further extend this approach to address multi-vehicle collision

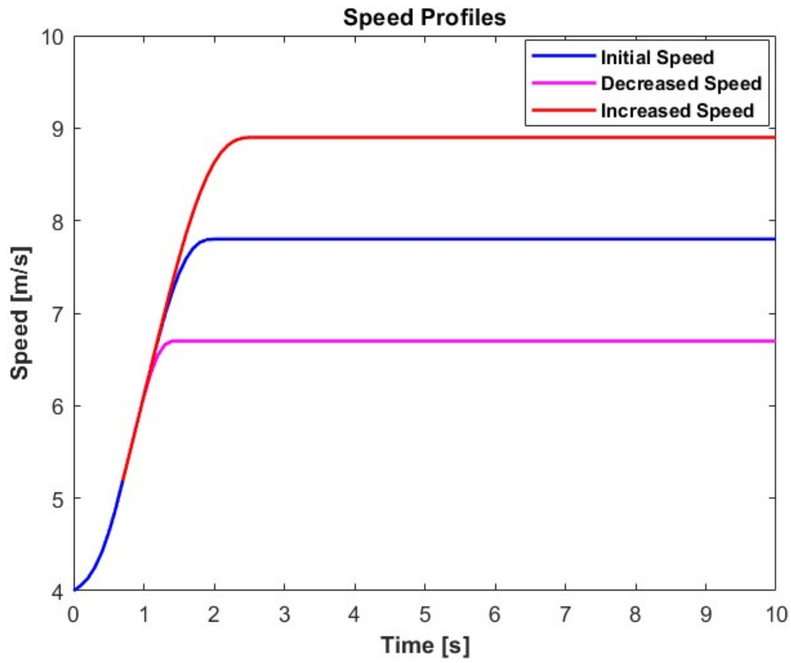

(a) Speed

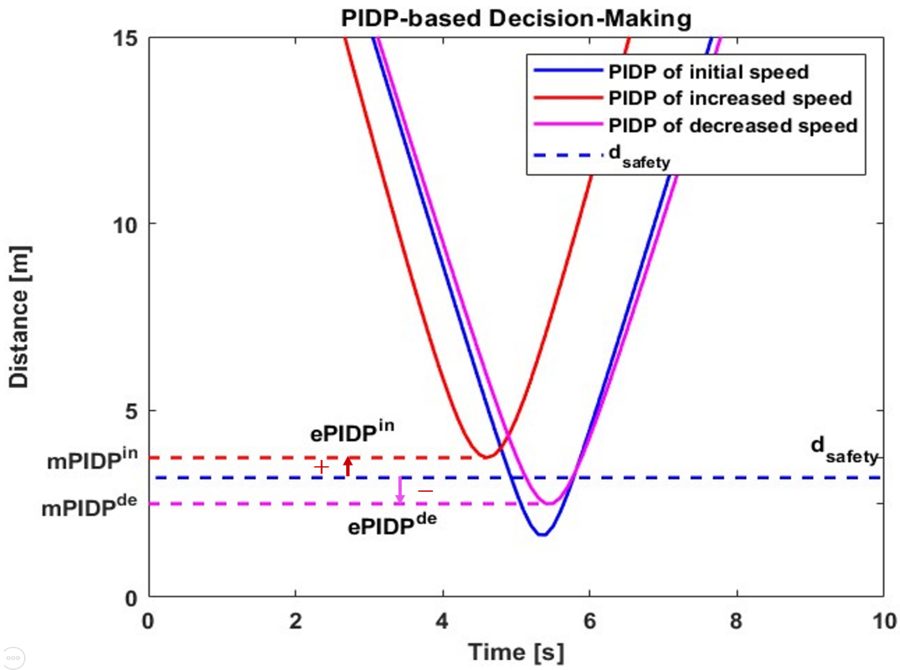

(b) $PIDP(t)$

Figure 3.3: $PIDP$-based decision-making: (a) is the speed profiles of the initial speed profile, increased speed profile, and decreased speed profile; (b) is the $PIDP(t)$ curves corresponding to (a)

risk scenarios. For a single CAV, it is possible to face potential conflicts with multiple other vehicles simultaneously while passing through an intersection. If we directly apply the MRMCO-PIDP described in Section 3.2.1, a special situation may arise in which the vehicle, after negotiating with different conflicting counterparts, obtains inconsistent strategies—such as being required to accelerate for one vehicle and to decelerate for another conflicting vehicle. Clearly, a vehicle cannot accelerate and decelerate simultaneously. Therefore, it becomes necessary to reassign a unified strategy for that vehicle.

Let us consider the special scenario we introduced before and extend the MRMCO-PIDP from single-risk to multi-risk management. The details of the MRMCO-PIDP algorithm is given in Algorithm 1.

The extension is designed to deal with this kind of problem. In this case, each vehicle should make a balance between accelerating and decelerating. The final decision of vehicle i is represented as $Decision_i$:

$$Decision_i = \sum_{j \in C_i} (s_{ij} * |ePIDP_{ij}^{opt}|) \tag{3.2}$$

$$s_{ij} = \begin{cases} 1 & \text{if } ePIDP_{ij}^{opt} = ePIDP_{ij}^{in} \\ -1 & \text{if } ePIDP_{ij}^{opt} = ePIDP_{ij}^{de} \end{cases} \tag{3.3}$$

s_{ij} indicates the motion of $ePIDP_{ij}^{opt}$, if the optimized speed profile is the increased speed, $s_{ij} = 1$, otherwise $s_{ij} = -1$. $ePIDP_{ij}^{opt}$ is the optimized $ePIDP$ between vehicle i and vehicle j through the introduced method.

If $Decision_i$ is positive, the increased speed profile will be selected as the current favorite strategy; otherwise, the decreased speed profile will be selected as the current favorite strategy. C_i is the set of vehicles who has the risk of collision with vehicle i. This Algorithm is updated each sample time to select successively the most suitable increase or decrease of velocity.

Note that this algorithm is only used to quickly find feasible solutions when vehicles are at risk of collision.

When considering cooperative decision-making for CAVs at intersections, the perspective of a single vehicle is insufficient to achieve true "cooperation". Therefore, the following section builds upon the foundation of the proposed MRMCO-PIDP method to extend its application from a single-agent decision-making context to a functional, multi-agent cooperative framework. Results will be shown in Section 3.4.

3.3 MULTI-VEHICLE OPTIMIZATION ARCHITECTURE: FROM CENTRALIZED TO DECENTRALIZED

In the previous section, we introduced the fundamental principles of the MRMCO-PIDP algorithm and explained how the PIDP can be adapted for risk assessment and management in CAVs. However, the decisions derived from this method represent only a locally optimal solution for the individual vehicle making the decision. Such solutions fail to account for the collective behavior of all CAVs in the vicinity of the intersection, and thus cannot guarantee that the newly selected strategy is not only beneficial for the ego vehicle but also optimal for the surrounding traffic system as a whole. This limitation motivates the need for an architecture in which vehicles can actively negotiate with other CAVs, ensuring that the resulting strategies are not merely ego-centric improvements but also enhance the overall

Algorithm 1 MRMCO-PIDP Algorithm

Input ego vehicle i and its current favorite speed profile $v(t)_i^{favorite}$
Generate increased speed profile $v(t)_i^{in}$ and decreased speed profile $v(t)_i^{de}$ for vehicle i
for each vehicle j at risk of collision with vehicle i **do**
    Calculate $ePIDP_{ij}^{in}$ and $ePIDP_{ij}^{de}$
    $ePIDP_{ij} = max(ePIDP_{ij}^{in}, ePIDP_{ij}^{de})$ \\ The strategy with the larger $ePIDP$ will be chosen
    if $ePIDP_{ij} == ePIDP_{ij}^{in}$ **then**
        \\ If the increased speed is accepted
        $s_{ij} = 1$
    else
        \\ If the decreased speed is accepted
        $s_{ij} = -1$
    end if
    \\ Get the final behavioral decision
    $decision_i = \sum_{j \in CL_i}(s_{ij} * |ePIDP_{ij}|)$
    if $decision_i > 0$ **then**
        \\ If the final behavioral decision is acceleration
        $v(t)_i^{favorite} \leftarrow v(t)_i^{in}$
    else
        \\ If the final behavioral decision is deceleration
        $v(t)_i^{favorite} \leftarrow v(t)_i^{de}$
    end if
end for
Output favorite speed profile $v(t)_i^{favorite}$

efficiency and safety of all CAVs approaching the intersection. In this section, we turn to the design of unsignalized intersection infrastructure and the corresponding cooperative optimization architecture for CAVs. We begin with a relatively straightforward centralized architecture, and subsequently extend the framework to decentralized architecture that offer greater practical relevance and reduced computational complexity. The simulation results of two architectures will be shown in Section 3.4.

3.3.1 *Objective Function*

In order to quantitatively evaluate whether a proposed speed strategy benefits not only the ego vehicle but also the collective performance of all CAVs at the intersection, it is essential to establish an objective function capable of assessing each candidate strategy. Such a function enables systematic comparison across the set of feasible alternatives to identify the most advantageous solution. To enhance the role of the objective function, it is therefore necessary to revisit the primary objectives of the proposed method and explicitly align the evaluation criteria with these overarching goals:

1. Collision-free decision-making with multi-risk in CAVs.
2. CAVs take the least total time to pass the intersection.

Building upon the methodologies for objective function construction reviewed in Section 2.1.2, and the overarching goals outlined above, the objective function is designed as follows:

$$J(S) = J_{Colli} + J_{Time} \tag{3.4}$$

[1]

For the Collision-free part, the method we apply is linked to the use of PIDP, which is introduced in Section 2.2.3.

$$\begin{aligned} J_{Colli} = &W_{Dist} \sum_{i=1}^{N_v} \sum_{j \in V_i} ePIDP_{ij}^{po} \\ &+ W_{Penalty} \sum_{i=1}^{N_v} \sum_{j \in C_i} (-ePIDP_{ij}^{ne}) \end{aligned} \tag{3.5}$$

where V_i is the set of vehicles that intersect with the path of vehicle i. $ePIDP_{ij}^{po}$ is the $ePIDP$ between vehicle i and j when its value is positive. $ePIDP_{ij}^{ne}$ is the $ePIDP$ between vehicle i and j when its value is negative. W_{dist} and $W_{Penalty}$ are positive coefficients. $W_{Penalty}$ is a value that tends to infinity, which is a penalty function when vehicles have negative $ePIDP$.

For the least total passing time part, the predicted exiting time and average speed are applied. The cost function is written as:

$$\begin{aligned} J_{Time} = &W_{Spd} \sum_{i=1}^{N_v} \int_{t_i^{enter}}^{t_i^{exit}} (v_{max} - v_i(t)) \\ &+ W_T \sum_{i=1}^{N_v} (t_i^{exit} - t_i^{enter}) \end{aligned} \tag{3.6}$$

where t_i^{enter} is the time when vehicle i enters the decision-making area (cf. Figure 3.2), t_i^{exit} is the predicted time when vehicle i exits the action area. v_{max} is the maximum legal speed near the intersection, $v_i(t)$ is the speed profile of vehicle i. W_{Spd} and W_T are positive coefficients.

3.3.2 *Dynamic Collision-Free Cooperation: A Centralized CAVs Coordination Method*

In cooperative decision-making at unsignalized intersections, safety constitutes the foremost requirement. Once safety is guaranteed, additional emphasis is placed on ensuring that the proposed methods achieve solutions that are as close to optimal as possible. As outlined in Section 1.3.1, the centralized architecture represents one of the earliest and most extensively investigated paradigms in this domain. It relies on an intersection manager that collects the state information of all CAVs and subsequently allocates passage times or generates feasible trajectories. This approach provides the strongest safety guarantees and offers the greatest potential to reach a globally optimal solution, albeit at the cost of significant computational and communication demand. Therefore, as a starting point, we introduce a centralized cooperative decision-making and optimization framework for CAVs at intersections, within which the proposed MRMCO-PIDP method is applied to validate its effectiveness. We refer to this approach as the Dynamic Collision-Free Cooperation (DCFC) decision-making approach.

1 Energy cost is also an important part for objective function, more details are given in Appendix A.

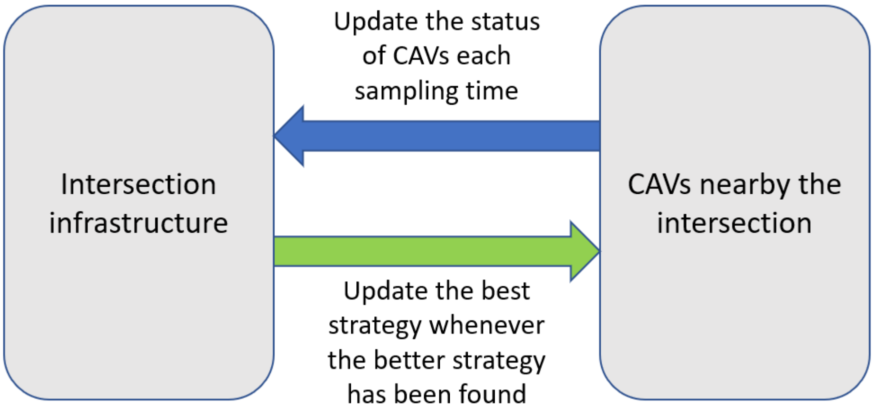

Figure 3.4: Coordination model between CAVs and the intersection infrastructure

a) V2I Coordination Model

The V2I model between the intersection infrastructure and the surrounding CAVs is illustrated in Figure 3.4. In this centralized framework, the decision-making process is executed entirely within the intersection infrastructure (cf. Figure 3.2), which serves as the control hub of the system. The infrastructure continuously gathers real-time information from all approaching CAVs, including their positions, velocities, and predicted trajectories, and computes an optimized conflict-free strategy that ensures safety while seeking to minimize overall delay or energy consumption. Once a new best strategy is obtained, it is immediately broadcast to the relevant CAVs through low-latency V2I communication. Upon receiving the updated commands, CAVs promptly adjust their dynamics by modifying speed profiles and trajectories according to the prescribed plan. This architecture ensures strong safety guarantees by leveraging a global perspective at the infrastructure level, while enabling coordinated vehicle behaviors that are otherwise difficult to achieve through decentralized decision-making strategy.

b) Centralized Optimization Process

Details of the proposed centralized optimization process is introduced in this section. The overall workflow of the algorithm is detailed in Algorithm 2. The optimization process is executed in a time-based cycle; it runs each sampling period, CAVs' states (e.g., position, speed, acceleration) and the best combined strategy will be updated also.

Within this optimization framework, the intersection infrastructure continuously collects information from the surrounding CAVs, including but not limited to their current states, planned speed profiles, and intended exit directions. Subsequently, the central decision-making system generates three possible speed trajectories for each vehicle, acceleration, deceleration, and keeping speed, based on their current velocity (the trajectory generation method follows Section 3.1.3). Considering that each vehicle has three potential strategies, the total number of possible combined strategies is 3^N when N CAVs are present at the intersection (cf. Figure 3.5).

For all possible combined strategies, the system computes the $PIDP(t)$ and the corresponding J_{Colli} (cf. equation (3.5)). Any strategies with J_{Colli} values greater than that of the currently executed strategy are discarded, since a larger J_{Colli} indicates a higher collision

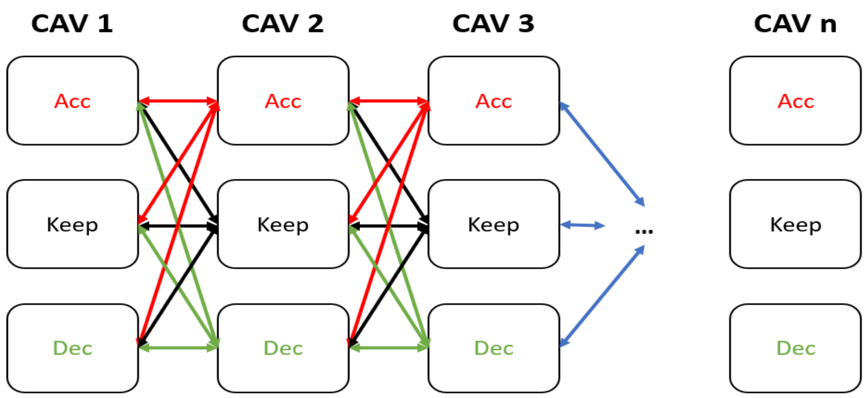

Figure 3.5: Generation of combined strategies. Each vehicle has “Acc”, “Keep”, and “Dec” three strategies while it doesn’t have reached its minimum or maximum speed. Therefore, for all N CAVs, there are 3^N total combinations of strategies at each sample time

risk. This ensures that any newly adopted combined strategy provides improved safety compared to the current one.

In the second step, the system evaluates the J_{Time} for all remaining strategies and selects the one with the minimal cost as the current optimal strategy S_{cur} and corresponding cost J^{cur}. If the J^{cur}_{Time} is smaller than the previously best adopted strategy (J^{best}_{Time}), it will be accepted to replace the previous best, and broadcast to all CAVs in the vicinity of the intersection, else, go next sampling period.

If no combined strategy passes the first-round filtering, the strategy with the minimum J_{Colli} is directly adopted as the current optimal solution and broadcast to all CAVs at the intersection. But this is a transitional solution, the better solution will be found next sampling period.

3.3.3 *Dynamic Multi-Risk Management Cooperative Optimization: A Decentralized CAVs Negotiation Architecture*

While the centralized cooperative decision-making framework provides a structured way to coordinate CAVs at unsignalized intersections, its reliance on global information exchange and centralized computation introduces limitations in terms of scalability, communication load, and single-point failures. Moreover, the computational burden of a centralized architecture is extremely high and increases exponentially with the number of vehicles, which imposes stringent performance requirements on the intersection infrastructure. As a result, deploying such approaches in real-world traffic systems may prove challenging. To overcome these issues and enhance adaptability in large-scale or highly dynamic environments, it is essential to consider decentralized architectures. In such a framework, each vehicle is endowed with local decision-making capabilities, relying on onboard sensing and inter-vehicle communication to achieve cooperative behavior. This subsection therefore introduces the decentralized cooperative decision-making approach, which we name Dynamic Multi-Risk Management Cooperative Optimization (D-MRMCO), highlighting how it contrasts with the centralized paradigm and how it addresses the aforementioned limitations.

Algorithm 2 Dynamic Collision-Free Cooperation (DCFC) decision-making and optimization process

while Set of vehicles inside the buffer area is not empty **do**
  Input CAVs and their planned trajectory
  Check the risk of collision based on $PIDP(t)$ \\ cf. Section 2.2.3
  Generate Δv for each CAV in the decision-making area and corresponding "Acc", "Dec", and "Keep" speed profiles
  Generate all situations resulting **S** from all possible combinations of behaviors of these CAVs and calculate their cost **J** \\ There are 3^N different combinations
  if $\exists$ combined strategy $S \in \mathbf{S}$, which makes $J_{Colli}(S) \leq J_{Colli}^{best}$ **then**
    \\ Safer strategies have been found
    Remove all the combined strategies whose $J_{Colli} > J_{Colli}^{best}$ from the strategy list
    \\ Strategies with higher risk should be removed from the possible strategy set
  else
    \\ Cannot find a strategy safer than the best strategy
    Select the combined strategy S^{trans} with minimum J_{Colli} \\ Get the most safety strategy from the current strategy set
    $S^{best} \leftarrow S^{trans}$
    $J^{best} \leftarrow J^{trans}$
    Output the new best strategy S^{best} to CAVs
    Break this optimization cycle and wait for the next sampling period
  end if
  Select the current best cost J^{cur} from all combined strategy cost list **J**, and corresponding strategy S^{cur}
  if $J_{Time}(S^{cur}) < J_{Time}^{best}$ **then**
    \\ If the current best strategy has less cost than the best strategy
    $S^{best} \leftarrow S^{cur}$ \\ Accept the current best strategy as the best strategy
    $J^{best} \leftarrow J^{cur}$
    Output the new best strategy S_{best} to CAVs
  end if
  Wait for the next sampling period
end while

a) Distributed CAVs Communication and Negotiation Framework

In contrast to centralized approaches, decentralized cooperative decision-making relies on a fundamentally different communication and negotiation architecture. Since vehicles interact directly through V2V and V2I channels without the oversight of a central coordinator, it is crucial to define a standardized synchronization scheme and timing protocol that can be universally adopted by all CAVs. Such a protocol ensures that information is exchanged and processed consistently across agents, thereby preventing delays, conflicts, or errors arising from mismatched message handling. Building on this requirement, this section introduces a refined communication and negotiation timing protocol together with the corresponding optimization framework, both of which aim to provide scalable, efficient, and reliable coordination in decentralized traffic environments.

The communication and negotiation protocol timing are illustrated in Figure 3.6. It consists of three distinct processes: the preparation process, the optimization process, and the negotiation process. In the preparation process, CAVs attempt to establish connections

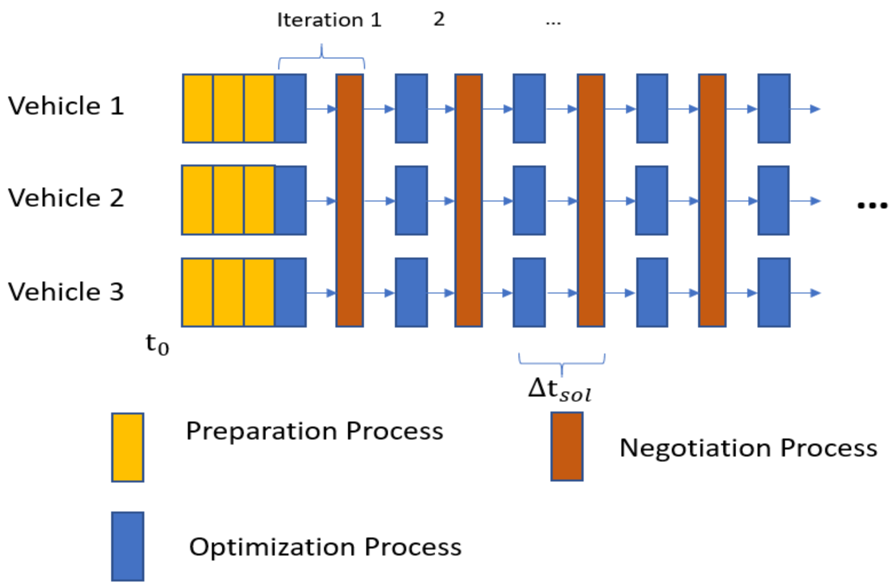

Figure 3.6: Communication and negotiation protocol timing

with the intersection infrastructure and share their information with one another. During the optimization process, the proposed MRMCO is executed to determine a better ego strategy for each vehicle. At this stage, the strategy generated by each vehicle aims to maximize its own benefit rather than the collective welfare. In the negotiation process, CAVs exchange their strategies with one another, and each vehicle uses the current strategies of the others as reference inputs in the next sampling period's optimization process to compute the corresponding PIDP. The selected strategy with maximizing its own benefit is then accepted by all CAVs. The optimization and negotiation processes are repeated at each sampling period.

Figure 3.7 illustrates the overall framework of the decentralized D-MRMCO approach, which consists of two main components: the CAVs and the intersection infrastructure. In this system, the infrastructure no longer performs centralized decision-making; instead, it is simplified to serve as an entity that provides the intersection map and facilitates information exchange among CAVs. All decision-making processes are thus carried out autonomously by the CAVs themselves. The details of the proposed D-MRMCO approach is given in Algorithm 3.

On the CAV side, each vehicle first retrieves the intersection map information from the infrastructure and performs an initial path planning. Subsequently, based on its current velocity and the speed strategies of surrounding vehicles, it generates a set of candidates speed profiles. The proposed MRMCO method is then applied to determine, in real time, the speed profile that best aligns with the vehicle's current strategy. The CAV's actuator executes the motion in accordance with the selected strategy, and the updated strategy is subsequently transmitted to the infrastructure, which then broadcasts it to all neighboring CAVs to ensure consistent situational awareness. In this process, we abandon the traditional approach of global optimization based on a predefined objective function, and instead interpret the iterative adjustment of each CAV's future strategy, driven by the states of other CAVs, as an Equilibrium Convergence Process. Through continuous adjustments, all agents eventually reach a configuration where no further modification is necessary, that is, the system achieves an equilibrium condition. Typically, when the iterative update

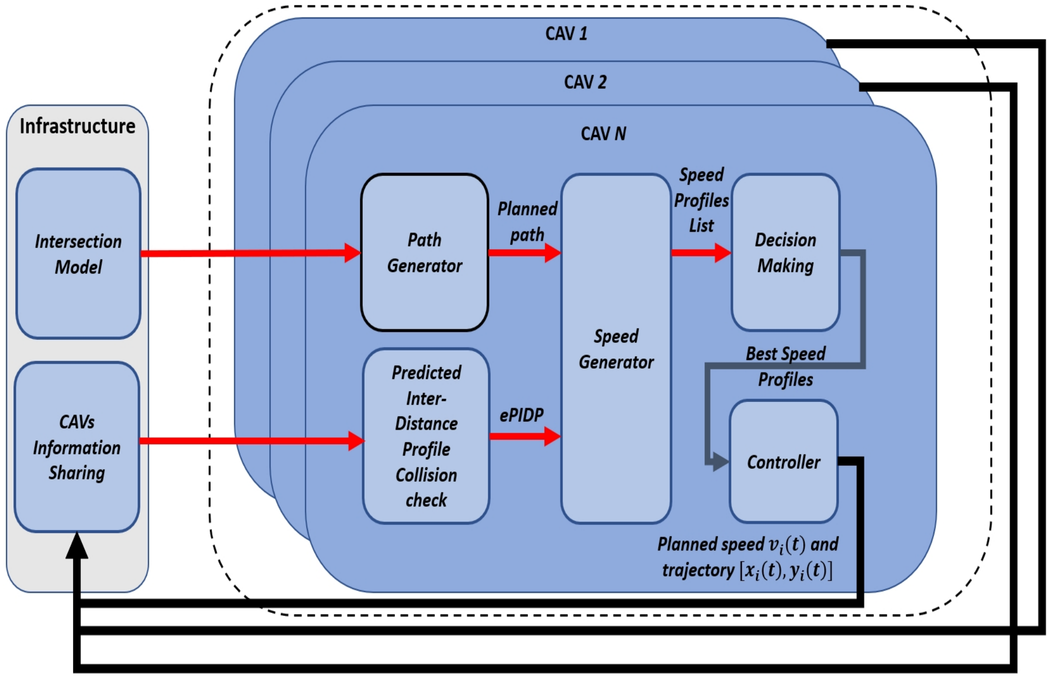

Figure 3.7: Overall framework of the decentralized D-MRMCO approach

rule remains unchanged, the final converged equilibrium state is determined by the initial conditions of the system.

In this context, relying on the fixed set of velocity samples introduced in Section 3.1.3 would impose significant constraints on the results, as these sampled target velocity points are finite and fixed, rather than continuous and dynamically variable. Thus, a dynamic adjustment of the target velocity is required. With this in mind, we introduce the following extensions building upon the foundation laid in Section 3.2. We have to find a certain increased and decreased target speed. We built a link between the *ePIDP* and the target speed when CAVs have the risk of collision:

$$v_i^{gap} = K_p * \sum_{j}^{N_v} ePIDP_{ij}^{ne} \tag{3.7}$$

where K_p is the proportional coefficient. v^{gap} refers to the increment or decrement in target speed during MRMCO-PIDP. $ePIDP_{ij}^{ne}$ is the absolute value of $ePIDP_{ij}$ if and only if it is negative, otherwise, $ePIDP_{ij}^{ne}$ is 0. It is written as:

$$ePIDP_{ij}^{ne} = \begin{cases} |ePIDP_{ij}| & \text{if } ePIDP_{ij} < 0 \\ 0 & \text{if } ePIDP_{ij} \geq 0 \end{cases} \tag{3.8}$$

The target speed for the ego vehicle could be written as:

$$v^{target} = \begin{cases} v_i^{tar} + v_i^{gap} & \text{if } decision_i > 0 \\ v_i^{tar} - v_i^{gap} & \text{if } decision_i \leq 0 \end{cases} \tag{3.9}$$

where v_i^{tar} is the current target of vehicle i, v^{target} is the new target speed of the vehicle. Then, the speed profile will be regenerated based on vehicle's current dynamic status and the target speed.

Algorithm 3 Dynamic MRMCO optimization process

Input information of all CAVs nearby the intersection
while Set of vehicles inside the buffer area is not empty **do**
  for all vehicle i in the vehicle set V **do**
    Generate increased speed profile $v(t)_i^{in}$ and decreased speed profile $v(t)_i^{de}$ for vehicle i
    for each vehicle j at risk of collision with vehicle i **do**
      Calculate $ePIDP_{ij}^{in}$ and $ePIDP_{ij}^{de}$
      $ePIDP_{ij} = max(ePIDP_{ij}^{in}, ePIDP_{ij}^{de})$ \\ The strategy with the larger $ePIDP$ will be chosen
      if $ePIDP_{ij} == ePIDP_{ij}^{in}$ **then**
        \\ If the increased speed is accepted
        $s_{ij} = 1$
      else
        \\ If the decreased speed is accepted
        $s_{ij} = -1$
      end if
    end for
    \\ Get the final behavioral decision
    $decision_i = \sum_{j \in CL_i}(s_{ij} * |ePIDP_{ij}|)$
    Calculate the speed gap v_i^{gap}
    \\ Recalculate gap speed
    if $decision_i > 0$ **then**
      \\ If the final behavioral decision is acceleration
      $v_i^{tar} \leftarrow v_i^{tar} + v_i^{gap}$
    else
      \\ If the final behavioral decision is deceleration
      $v_i^{tar} \leftarrow v_i^{tar} - v_i^{gap}$
    end if
    Generate the speed profile based on the v_i^{tar} and update it as the new favorite speed profile $v(t)_i^{favorite}$
    Output favorite speed profile $v(t)_i^{favorite}$ and share it to other CAVs
  end for
end while

b) Stochastic Perturbation Mechanism for Restoring Convergence

Although the proposed distributed decision-making framework demonstrates strong convergence properties under general conditions, it may still encounter difficulties in specific initial configurations. In certain cases, the iterative process defined by the local update rules may fail to reach a feasible solution or require an excessive number of iterations before achieving equilibrium. Such situations typically arise when the system becomes trapped in a suboptimal or non-convergent state, preventing further progress toward a stable solution. To address this limitation and enhance the robustness and general applicability of the proposed method, a stochastic perturbation mechanism is introduced. This mechanism enables the system to escape infeasible or stagnant configurations by introducing controlled randomness into the iterative process. Building upon this idea, we further adapt the simulated annealing algorithm to design an enhanced approach, referred to as the Adaptation of Simulated Annealing (ASA) Algorithm, to guide the distributed optimization toward feasible and globally convergent solutions, or a better optimal solution.

The Simulated Annealing (SA) algorithm is a stochastic global search optimization algorithm. It makes use of randomness as part of the search process. This approach provides a mechanism for the algorithm to potentially escape local optima and approach a global optimum. The Metropolis Criterion [205] is the main idea that allows the SA to accept the non-optimal solution as the current best solution.

The details of the ASA Algorithm is given in Algorithm 4. J is the objective function. T is the temperature, it is designed as:

$$T = d_i - r_{action} \tag{3.10}$$

where d_i is the distance of vehicle i to the center of the intersection (cf. Figure 3.2). r_{action} is the radius of the Action area.

Algorithm 4 Adaptive Simulated Annealing (ASA) Algorithm

Input ego vehicle i and its current favorite speed profile $v(t)_i^{favorite}$
Generate a random speed profile $v(t)_i^{SA}$
$\Delta J = J(v(t)_i^{SA}) - J(v(t)_i^{favorite})$ \\ Calculate the cost error
if $\Delta J < 0$ **then**
    \\ If the current method has better cost
    $v(t)_i^{favorite} \leftarrow v(t)_i^{SA}$
    \\ Accept this strategy as the favorite strategy
else if $exp(-\frac{\Delta J}{T}) > rand$ **then**
    \\ If the current method is worse than the favorite method but it satisfies the Metropolis Criterion
    $v(t)_i^{favorite} \leftarrow v(t)_i^{SA}$
    \\ Accpet this strategy as the favorite strategy
end if
Output favorite speed profile $v(t)_i^{favorite}$

The ASA algorithm is activated only when some CAVs fail to find a feasible solution, or when the system has already reached a convergent solution but attempts to explore a better one. Its core optimization mechanism remains based on the previously proposed MRMCO framework, but it is only used for the decentralized architecture.

3.4 SIMULATION RESULTS

In order to validate the effectiveness of the proposed MRMCO-PIDP method, it is necessary to conduct simulation-based verification. Simulation validation offers the distinct advantage of generating a large number of scenarios, allowing for the comprehensive testing of the method's performance under a multitude of diverse conditions prior to its practical deployment on autonomous vehicles in real world. It therefore represents an indispensable intermediate step, aimed at demonstrating the approach's robustness range, identifying its limitations, and ensuring a level of reliability, as evidenced by the large volume of trials performed.

Our simulations are based on algorithmic verification performed in MATLAB. In this chapter, as we are not considering uncertainties arising from external disturbances or noise, we assume ideal conditions. Specifically, all V2V and V2I communication is considered to be latency-free, and all information is assumed to be perfectly known. The parameters listed in Table 3.1 constitute the common configuration adhered to in all simulations. To validate the effectiveness of the proposed algorithm and framework, different simulations will be introduced in the following sections. All the simulation videos in chapter can be found in https://youtu.be/RnQEfH9Jwfk.

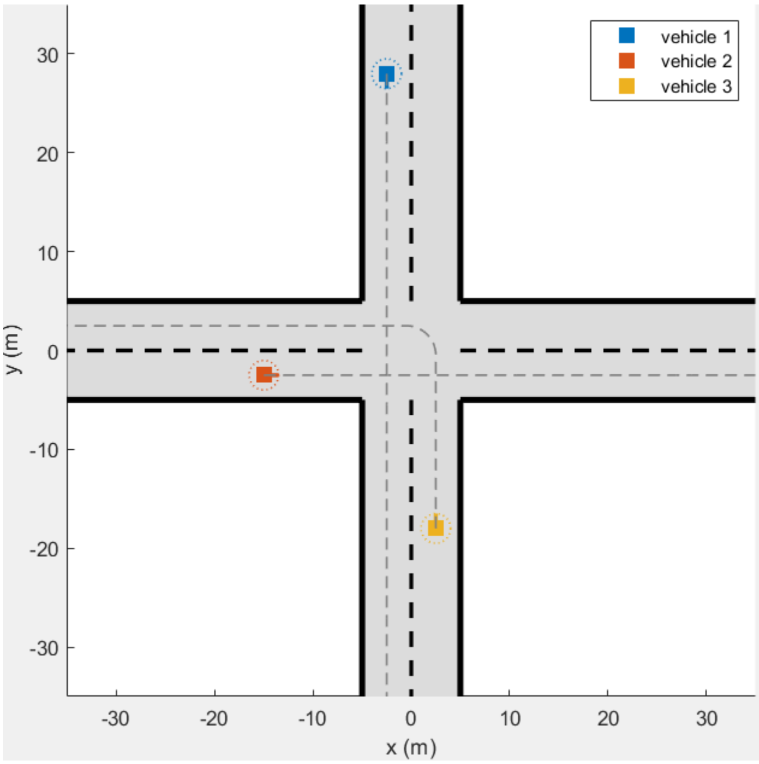

Figure 3.8: Simulation scenario with 3 CAVs

3.4.1 *Evaluation of Computational Efficiency*

In this section, the feasibility and computation efficiency of the proposed algorithm and framework will be validated, their performance will be assessed under different scenarios and results will be compared with ε-PC algorithm [206], which is a distributed multi-agent optimization as the coordination of probabilistic decision variables among agents, enabling

Table 3.1: Parameters of vehicles and simulation

Parameters	Value	Parameters	Values
a_{max}	$3[m/s^2]$	r_{safety}	1.5[m]
$[v_{min}, v_{max}]$	[0,10][m/s]	T_{sample}	0.1[s]
$Margin$	0.2 $[m]$	$T_{horizon}$	10[s]

convergence to globally optimal solutions and has been theoretically demonstrated to have the capability of reaching the global optimum.

We begin by considering a scenario at an unsignalized intersection involving 3 CAVs, as illustrated in Figure 3.8 and their initial states are given in Table 3.2, where the dashed lines indicate their intended paths. It is evident that the path of each vehicle intersects with those of the other two, implying that a potential collision risk exists between any two vehicles in the scenario.

As this section is primarily focused on validating the effectiveness of the proposed MRMCO-PIDP method, we will not employ the complete multi-risk management framework at this stage. Instead, the MRMCO-PIDP decision-making logic will be embedded within the ε-PC framework to supersede its native decision-making component. A more comprehensive validation of the entire proposed framework will be presented in a subsequent section.

Table 3.2: Initial state of each vehicles

Parameters	Value	Parameters	Values
v_1	$3.5[m/s]$	(x_1, y_1)	[-2.5, 28] $[m]$
v_2	6 $[m/s]$	(x_2, y_2)	[-15, -2.5] $[m]$
v_3	5 $[m/s]$	(x_3, y_3)	[2.5, -18]$[m]$

Figures 3.9 and 3.10 depict the velocity profiles and inter-vehicle distances planned by the ε-PC and MRMCO-PIDP algorithm, respectively. Table 3.3 summarizes the key simulation results.

As observed in Figures 3.9b and 3.10b, both the ε-PC and MRMCO-PIDP algorithms are capable of finding safe and feasible solutions. However, the MRMCO-PIDP algorithm, while maintaining safe inter-vehicle headways, further compresses the minimum distance between vehicles, thereby enhancing the spatial utilization of the intersection.

Figures 3.9a and 3.10a illustrate the velocity profiles planned by the ε-PC and MRMCO-PIDP algorithms, respectively. In conjunction with Table 3.3, it becomes evident that although the MRMCO-PIDP method finds a feasible solution, it exhibits the limitation discussed in Section 3.3.3: its potential to converge to a sub-optimal solution rather than the global optimum. (This issue has been resolved in the Section 3.3.3, and simulation results will be given in Section 3.4.2.) This deficiency is directly responsible for the behavior observed in Figure 3.10a, where vehicle 1 is unable to accelerate to pass the intersection before vehicle 3. Consequently, this results in a higher average passing time for the MRMCO-PIDP algorithm compared to the ε-PC algorithm. While the average passing time of the MRMCO-PIDP solution is suboptimal in the current framework compared to ε-PC, Table 3.3 highlights its crucial advantage: the execution time is less than 5% of that required by the ε-PC algorithm. This result provides a direct proof of the method's preliminary viability, confirming its ability to simultaneously satisfy the two critical requirements: finding a feasible solution and being sufficiently fast.

Table 3.3: Results analysis with 3 CAVs

Algorithm	Execution time	Number of iterations	Avg. Passing time	Max Passing time
ε-PC	22.01 $[s]$	15	4.43 $[s]$	5.70 $[s]$
$MRMCO-PIDP$	0.98 $[s]$	15	5.17 $[s]$	7.30 $[s]$

Table 3.4: Initial state of each vehicles

Parameters	Value	Parameters	Values
v_1	$6[m/s]$	(x_1, y_1)	[-11, -2.5] $[m]$
v_2	6 $[m/s]$	(x_2, y_2)	[2.5, -25] $[m]$
v_3	4 $[m/s]$	(x_3, y_3)	[2.5, -29]$[m]$
v_3	5 $[m/s]$	(x_3, y_3)	[-2.5, 10]$[m]$
v_3	4 $[m/s]$	(x_3, y_3)	[-27, -2.5]$[m]$

Table 3.5: Results analysis with 5 CAVs

Algorithm	Execution time	Number of iterations	Avg. Passing time	Max Passing time
ε-PC	82.47 $[s]$	20	3.26 $[s]$	4.90 $[s]$
$MRMCO-PIDP$	4.13 $[s]$	34	3.22 $[s]$	4.90 $[s]$

To further validate the viability of the proposed method, we increased the number of vehicles to 5 and repeated the experiment. The initial states of the vehicles are presented in Table 3.4 and the scenario is illustrated in Figure 3.11. The corresponding results are shown in Figures 3.12 and 3.13, and Table 3.5.

Comparing the results, it is evident that the MRMCO-PIDP method can still rapidly find a feasible solution even in this more complex environment. Furthermore, the MRMCO-PIDP algorithm outperforms the ε-PC algorithm in terms of both execution time and the final average passing time. Notably, its execution time remains less than 5% of that required by the ε-PC algorithm.

Based on the comparative results from the 3-vehicle and 5-vehicle simulations, we conclude that the proposed MRMCO-PIDP algorithm possesses the capability to rapidly find feasible, collision-free solutions in complex unsignalized intersection scenarios, and is extremely computationally efficient, requiring less than 5% of the execution time of the ε-PC algorithm. Critically, this demonstrates that the method's performance is scalable, showing no significant degradation as the number of interacting vehicles increases.

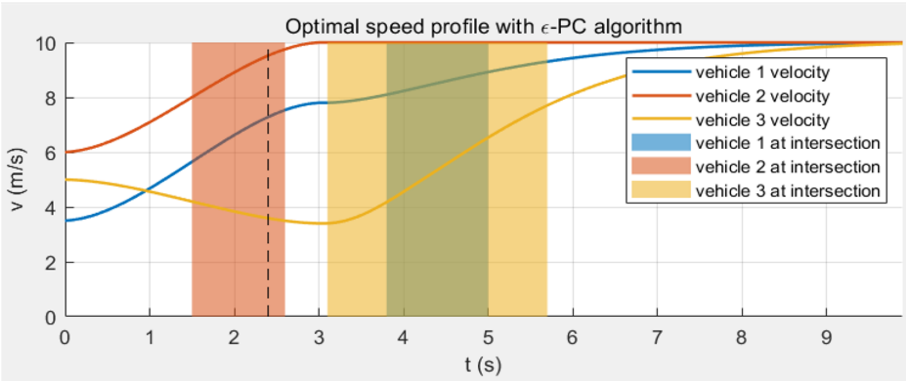

(a) Speed profiles

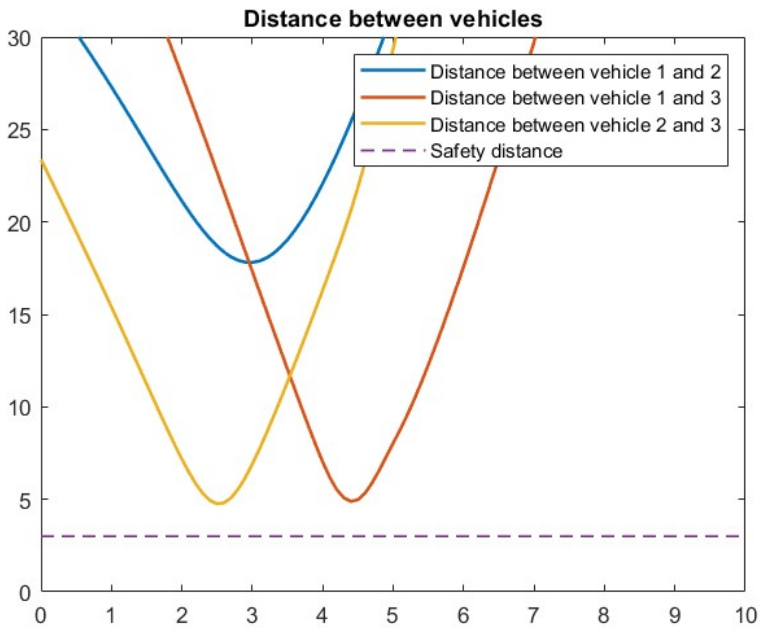

(b) Distance between two vehicles

Figure 3.9: ε-PC algorithm result

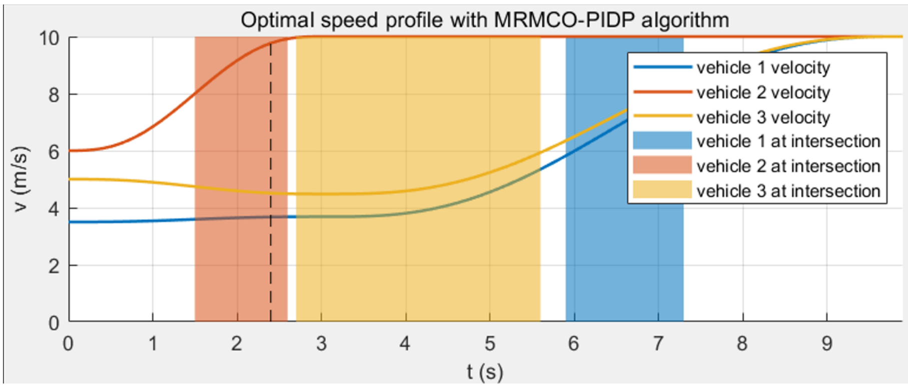

(a) Speed profiles

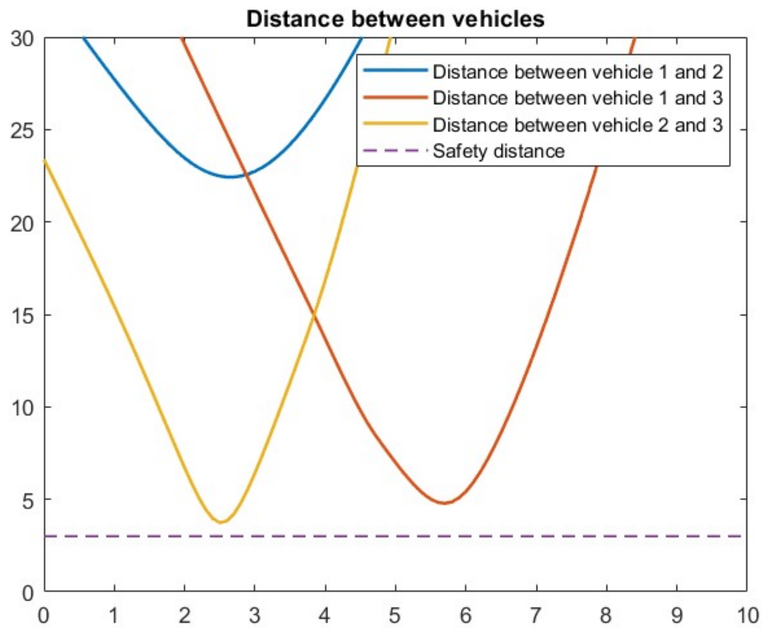

(b) Distance between two vehicles

Figure 3.10: MRMCO-PIDP algorithm result

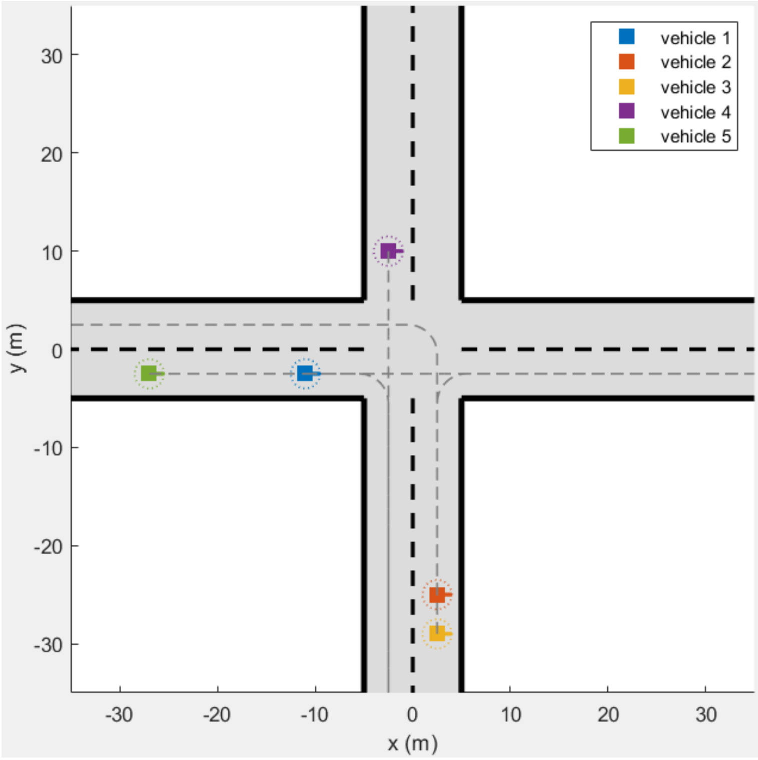

Figure 3.11: Simulation scenario with 5 CAVs

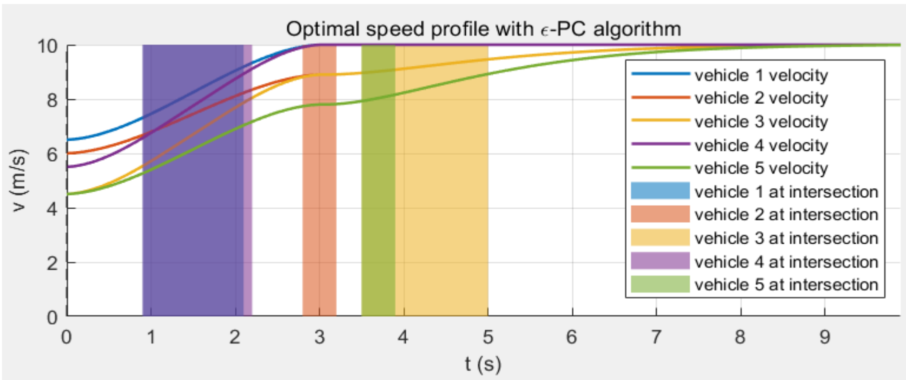

Figure 3.12: Speed profiles by ε-PC algorithm with 5 vehicles

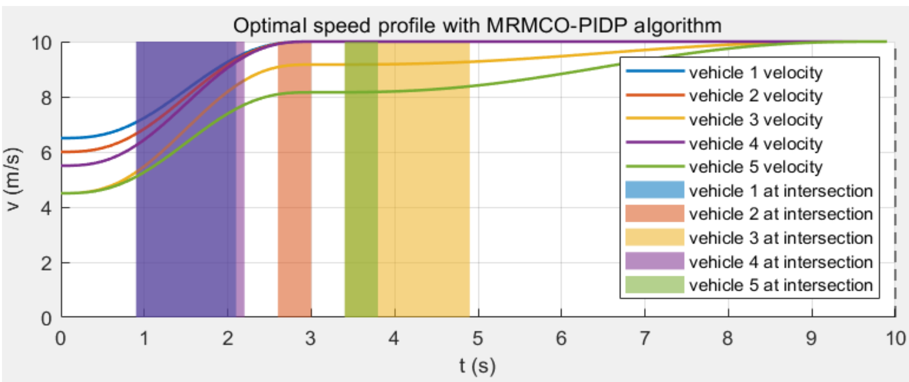

Figure 3.13: Speed profiles by MRMCO-PIDP algorithm with 5 vehicles

3.4.2 *Proposed Centralized vs. Decentralized Optimization Architecture*

Having established the feasibility of the core MRMCO-PIDP method through preliminary simulations (albeit conducted within the ε-PC framework), we now proceed to validate the two complete optimization architectures built upon it. This subsection will evaluate both the centralized Dynamic Collision-Free Cooperation (DCFC) decision-making framework and the decentralized Dynamic Multi-Risk Management Cooperative Optimization (D-MRMCO). We will commence this analysis, as before, using the fundamental 3 CAVs conflict scenario illustrated in Figure 3.8.

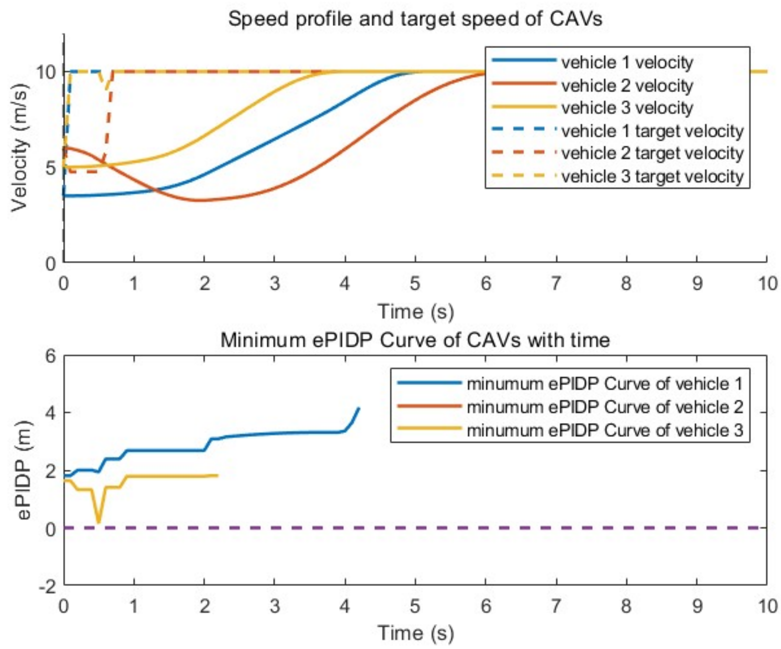

Figure 3.14: Speed profiles and *ePIDP* list by DCFC algorithm with 3 vehicles

The simulation results are presented in Figure 3.14, Figure 3.15, and Table 3.6. It is evident from Table 3.6 that the centralized DCFC algorithm is outperformed by the decentralized D-MRMCO algorithm in terms of both execution time and average passing time, this is an understandable outcome, given that D-MRMCO was developed as a direct refinement of the DCFC. Furthermore, the *ePIDP* curves in Figures 3.14 and 3.15 reveal that the DCFC algorithm's spatial utilization of the intersection is also significantly lower than that of D-MRMCO.

However, an analysis of the velocity profiles reveals a critical trade-off. The trajectory planned by the centralized DCFC algorithm is notably smoother, and it is devoid of the sharp velocity fluctuations observed in the D-MRMCO algorithm during its initial negotiation phase. This aligns with the characteristic advantages of a centralized architecture, where a strong, unified computational framework can significantly enhance overall system stability.

As before, the simulation is extended to the scenario to a 5-vehicle mutual conflict, again using the scenario configuration depicted in Figure 3.11. The experimental results are presented in Figure 3.16, Figure 3.17, and Table 3.7.

Upon analyzing the results, it becomes evident that the centralized DCFC algorithm achieves a superior optimization result compared to the decentralized D-MRMCO algo-

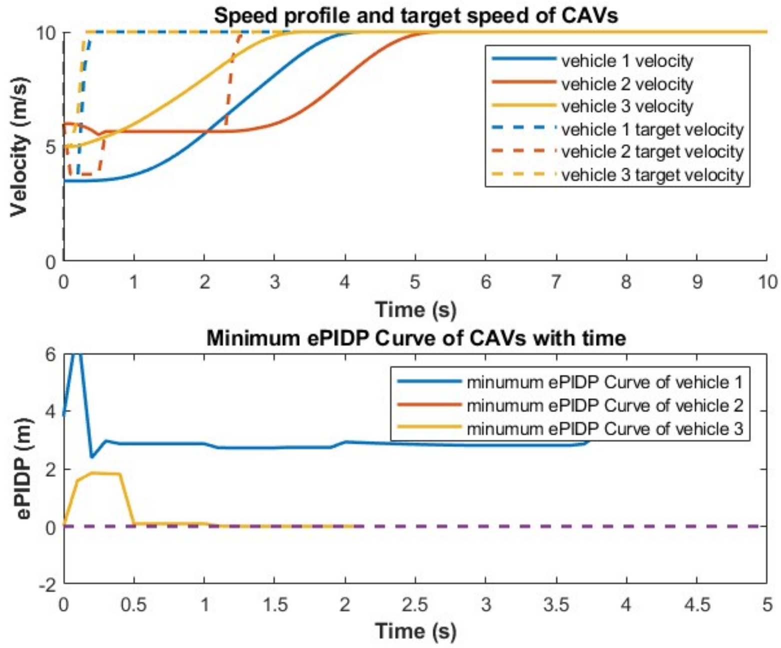

Figure 3.15: Speed profiles and *ePIDP* list by D-MRMCO algorithm with 3 vehicles

Table 3.6: Results analysis with 3 CAVs

Algorithm	Execution time	Avg. Passing time	Max Passing time
$DCFC$	4.18 $[s]$	4.53 $[s]$	5.30 $[s]$
$D-MRMCO$	0.52 $[s]$	4.00 $[s]$	4.90 $[s]$

Table 3.7: Results analysis with 5 CAVs

Algorithm	Execution time	Avg. Passing time	Max Passing time
$DCFC$	60.78 $[s]$	3.22 $[s]$	5.10 $[s]$
$D-MRMCO$	0.93 $[s]$	4.08 $[s]$	6.50 $[s]$

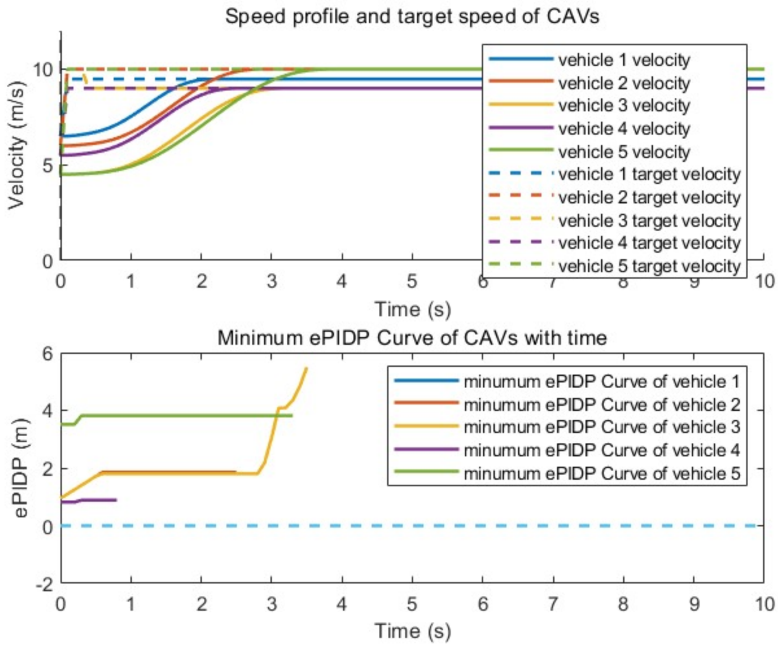

Figure 3.16: Speed profiles and *ePIDP* list by DCFC algorithm with 5 vehicles

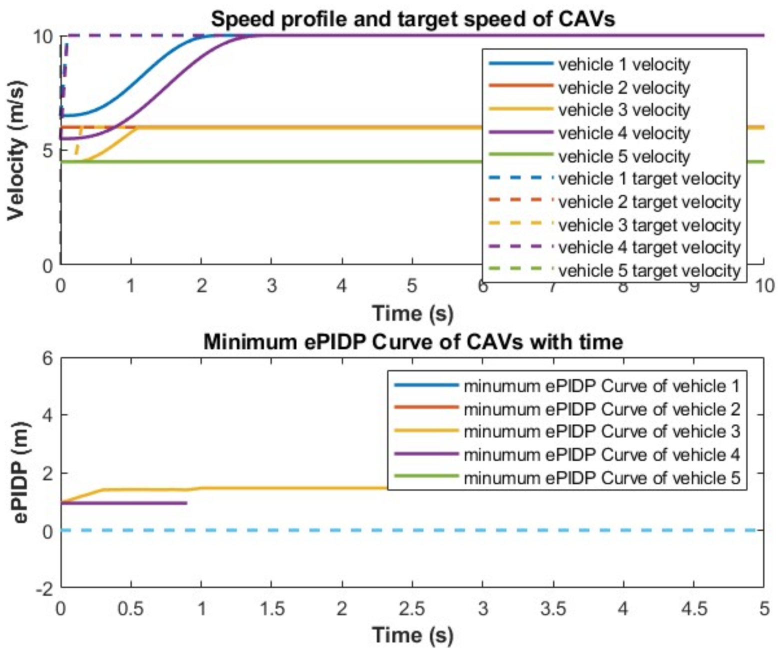

Figure 3.17: Speed profiles and *ePIDP* list by D-MRMCO algorithm with 5 vehicles

rithm. This advantage, however, comes at the cost of a significantly higher execution time. A comparison of execution time reveals the critical impact of scalability: as the number of vehicles increases from 3 to 5, the execution time of the DCFC algorithm explodes from 4.18 seconds to 60.78 seconds, a 15-fold increase. In stark contrast, the execution time of the D-MRMCO algorithm only increases from 0.52 seconds to 0.93 seconds, a growth of approximately 80%. This implies that while DCFC, as a centralized algorithm, may yield better performance in its final optimized solution, its computational cost grows exponentially with the number of vehicles requiring coordination. This severely restricts its potential for real-world application. Conversely, although the decentralized D-MRMCO algorithm cannot guarantee convergence to the global optimum, its extremely rapid execution time is an unparalleled advantage. Furthermore, this execution time appears to be approximately linearly correlated with the number of vehicles, rather than exhibiting the exponential growth of its centralized counterpart, rendering its practical implementation feasible.

3.5 CONCLUSION

This chapter proposed the Multi-Risk Management Cooperative Optimization based on PIDP (MRMCO-PIDP), a novel framework for multi-vehicle cooperative risk management at unsignalized intersections, which is capable of exceptionally rapid convergence to feasible solutions in complex scenarios involving mutual, overlapping collision risks among multiple vehicles. The approach utilizes the Predicted Inter-Distance Profile (PIDP) as its core risk assessment strategy. Building upon this foundation, the chapter detailed how this method is used to analyze the current intersection risk state and to efficiently derive these feasible solutions.

A foundational model for the unsignalized intersection was also established. This model was then integrated with the MRMCO-PIDP method, leading to the development of two distinct cooperative optimization architectures: the centralized Dynamic Collision-Free Cooperation (DCFC) framework and the decentralized Dynamic Multi-Risk Management Cooperative Optimization (D-MRMCO). This integration yielded promising results. Notably, the decentralized D-MRMCO architecture demonstrated excellent scalability, as its computational load does not grow significantly with the number of interacting vehicles. This finding is critical, as it confirms the method's feasibility for successful application in real-world smart urban transportation systems.

However, the initial assumptions of this chapter must be relaxed to account for the array of uncertainties inherent in CAV systems in the real world, such as communication noise, latency, and interruptions. It is therefore necessary to develop a more comprehensive system capable of making safe cooperative decisions in such environments. This challenge will be addressed in detail in the following chapter.

4 COOPERATIVE DECISION-MAKING METHOD FOR CAVS UNDER UNCERTAINTY

Building upon the cooperative decision-making framework developed for unsignalized intersections under deterministic conditions, this chapter extends the proposed architecture to environments characterized by uncertainty. In real-world traffic scenarios, various factors such as sensor noise, communication latency, localization errors, and unpredictable behaviors of surrounding vehicles introduce stochastic disturbances that cannot be ignored. These uncertainties may significantly affect the accuracy of trajectory prediction, conflict assessment, and the overall safety, precision and efficiency of cooperative strategies.

To address these challenges, the primary task is to effectively quantify the impact of such disturbances on a vehicle's risk assessment. To this end, we introduce a novel method, Probabilistic Uncertainty Interval (PUI) analysis. This technique leverages a vehicle's prior states to forecast a bounded interval of its potential future positions, rather than a single, deterministic path. We then integrate this concept with the PIDP framework. This fusion allows us to perform cooperative risk assessment under uncertainty by calculating the distance profile between a vehicle's planned trajectory and the predicted uncertainty interval of others. Based on this robust assessment, this chapter develops a cooperative decision-making framework that ensures each vehicle can cross the intersection with minimal risk, even in the presence of stochastic environmental factors.

4.1 PROBLEM STATEMENT

In real-world traffic environments, CAVs are inevitably exposed to various sources of external uncertainty, including but not limited to communication delays, sensor noise, and unexpected system disturbances. Among these factors, one of the most critical and challenging scenarios arises when communication loss occurs within the CAV network. In this chapter, we specifically consider such cases, where one or more CAVs suddenly disconnect from the network due to unforeseen causes. During the disconnection period, the affected vehicle can neither receive information from nearby CAVs nor transmit its own state or strategy preferences to others or to the intersection infrastructure. Consequently, the remaining connected CAVs must infer the possible future states and strategies of the disconnected vehicle based on its last known status and adjust their own decisions accordingly. The objective is to minimize the potential collision risk while maintaining the overall traffic efficiency of the intersection under these partial communication failure conditions.

4.1.1 *Related Work*

Addressing uncertainty in cooperative CAV planning has led to two dominant philosophies. Probabilistic approaches, such as PO-MDP (cf. Section 2.5.1), optimize for expected performance and efficiency but offer only soft, probabilistic safety assurances (e.g., chance constraints), which may be insufficient for safety-critical validation.

Conversely, robust and set-based methods (cf. Section 2.5.2), like Reachability Analysis or formal models like Responsibility-Sensitive Safety (RSS) [207], provide verifiable, worst-case safety guarantees. However, this often comes at the cost of excessive conservatism, which can significantly degrade traffic efficiency and passenger comfort by forcing overly cautious maneuvers.

This reveals a fundamental trade-off between optimality and certifiable safety. Therefore, a compelling research direction lies in developing a hybrid framework that can synergize the strengths of probabilistic approaches and robust and set-based methods—achieving high performance under nominal conditions while maintaining strong safety margins without undue conservatism.

4.1.2 *Fundamental Assumptions*

CAVs can obtain information from two primary sources: through V2V or V2I communication, and through their onboard sensors. The former approach heavily relies on the stability of the communication system but provides access to almost all relevant information, including other CAVs' trajectories, current states (such as position, speed, and acceleration), and intended speed strategies. The latter, in contrast, depends on the vehicle's own sensing capabilities, offering higher reliability but limited perception range—especially in urban environments or near intersections where obstacles may obstruct line-of-sight detection. In such cases, a CAV may be unable to detect vehicles approaching from other directions until it reaches the intersection, and can only obtain basic state information without directly inferring their future trajectories or intended speed profiles.

Therefore, we introduce the following assumption:

1. The disconnected vehicle loses communication with other CAVs at some point after establishing a connection with the intersection infrastructure but before entering the intersection.

2. The disconnected vehicle continues to comply with the intersection's maximum speed limit and basic kinematic continuity, ensuring that its velocity does not undergo abrupt changes.

3. The disconnected vehicle may recover from the failure and reconnect to the CAV network at a later time.

4. Although the disconnected vehicle cannot communicate with others, it can still be observed by nearby CAVs when it is within their sensing range. In such cases, the surrounding CAVs are able to obtain its current position, velocity, and acceleration information.

We classify the methods for obtaining vehicle state information according to the vehicle's connection status and spatial location, as summarized in Table 4.1. It can be observed that when a CAV is in a disconnected state and located outside the observation zone, its exact state cannot be determined either through communication or sensing. In such cases, the only feasible approach is to employ a predictor to estimate the vehicle's current state and its future progress. Therefore, as one of the key focuses of this chapter, we will discuss how CAVs can acquire and predict information about other CAVs under conditions of complete or partial communication loss.

If the CAV communication is enabled and reliable (considered known by each vehicle according to the Quality of Service (QoS) of the considered communication), the information from communications will be used for decision-making regardless of whether it is observable or not, because more information can be received from communication than from embedded sensors on the vehicles, or put in the infrastructure, as an RSU (Road Side Unit) for instance. If it is observable but communication disabled, the information from sensors will be used for decision-making even with noise. If it is neither communication enabled nor observable, a predictor will be used to generate a set of possible speed profiles and thus positions.

Table 4.1: Ways to acquire information from other vehicles

	Communication enabled	Communication disabled
Observed	Communication	Sensors
Unobserved	Communication	Predictor

4.2 PIDP-BASED PROBABILISTIC UNCERTAINTY INTERVAL ANALYSIS

In this section, we introduce a vehicle state predictor that is formulated based on a vehicle's prior state information. Building upon this, we will investigate how the PIDP and Probabilistic Interval methods can be jointly employed to analyze the uncertainty in vehicle position and velocity that arises specifically from communication loss. Furthermore, we will demonstrate how PIDP is utilized to correct the outputs of this unreliable predictor.

4.2.1 *Predictor for CAVs under Communication Loss*

Consider an unobservable CAV whose communication is disabled suddenly, while knowing that all its past information (position, speed, acceleration, planned speed profile, etc.) are recorded, but we have lost the means to obtain its future information during the disruption. In order to make decision to pass the intersection without collision, other CAVs have to predict the possible position and speed profile of the disconnected vehicles.

Based on the vehicle's speed prior to disconnection, and under the constraint of the maximum allowable speed near the intersection, a set of candidate set-point speeds $\overrightarrow{v_s}$ is sampled from the feasible kinematic interval of the disconnected vehicle, and the set-point speeds $\overrightarrow{v_s}$ should be sampled from all the speed space. A probability distribution vector $\overrightarrow{p_v}$, corresponding to each sampled speed will also be calculated, representing the likelihood that the disconnected vehicle will select this set-point speed. The set of speed profiles are generated based on its acceleration and set-point speeds (cf. Figure 4.1). These speed profiles represent all feasible ways for the vehicle to reach each potential target speed under basic motion continuity and dynamic feasibility constraints, thus encompassing the full range of possible speeds the vehicle may take after becoming disconnected from control.

$$\overrightarrow{v_s} = [v_{lb}, \ldots, v_{min} + n * v_{step}, \ldots, v_{ub}] \tag{4.1}$$

$$v_{step} = \frac{v_{ub} - v_{lb}}{N_s - 1} \tag{4.2}$$

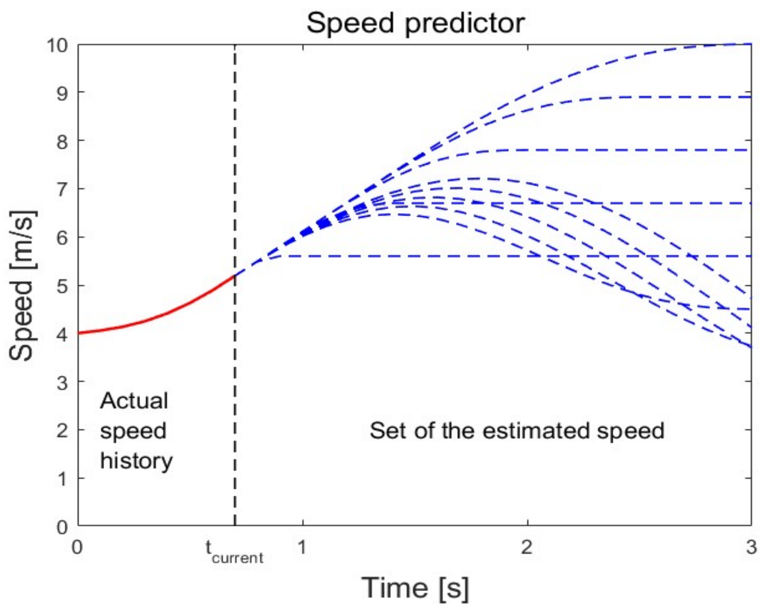

Figure 4.1: Predicted speed profiles of disconnected vehicle by predictor

where v_{step} is the speed sampling step. N_s is the number of samples. v_{lb} is the lower boundary of the potential interval of speed, and v_{ub} is the upper boundary of the potential interval of speed.

4.2.2 *PIDP-based Uncertainty Analysis*

After the disruption happened, all information of the disconnected vehicle cannot be obtained anymore. It implies that the predictor is required to generate different information distributions for the vehicle, such as speed and position, along with their corresponding probabilities. As introduced in the objective function (3.4), it is easy to find that the only important parameter of these objective functions is PIDP between two vehicles. Therefore, the potential interval of PIDP metric is proposed to transfer the uncertainty from speeds and positions to PIDP, then a PIDP-based Probabilistic Uncertainty Interval (PIDP-PUI) method is introduced to resolve it.

In Section 4.2.1, the potential interval of speed-based set-point speed predictor is introduced. $\overrightarrow{p_v}$ is the probability distribution vector corresponding to all sampled set-point speeds, which represents the probabilities with which a disconnected vehicle may adopt each of these sampled speeds. To obtain the potential interval of $PIDP(t)$ between the disconnected vehicle and the ego vehicle, we need to convert each sampled speed profile into its corresponding $PIDP(t)$ and combine them into a Potential Interval $PIDP_{PI}$ (cf. Figure 4.2), which is written as:

$$PIDP_{PI}(t) = \begin{bmatrix} PIDP_1(t) \\ \dots \\ PIDP_i(t) \\ \dots \\ PIDP_{N_s}(t) \end{bmatrix} \tag{4.3}$$

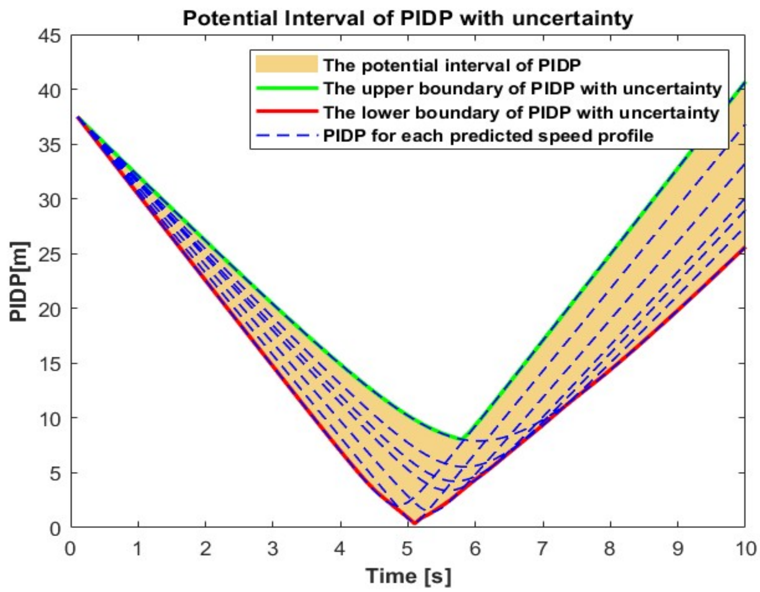

Figure 4.2: Potential Interval of PIDP

where $PIDP_i(t)$ is the PIDP trajectory corresponding to the i-th sampled set-point and its speed profile (cf. Figure 4.2). $PIDP_{PI}(t)$ is a matrix corresponding to the Potential Interval (PI) of PIDP.

Acquiring only the $PIDP_{PI}(t)$ is insufficient; the next step is to derive a representative predicted $PIDP(t)$ curve, $PIDP_{predicted}(t)$, to compute the objective function. Considering that the distribution of sampled set-points follows the corresponding probability distribution vector $\overrightarrow{p_v}$, the predicted $PIDP(t)$ can be described as the following formula by mathematical expectation:

$$PIDP_{predicted}(t) = \overrightarrow{p_v} * PIDP_{PI}(t) \tag{4.4}$$

where $\overrightarrow{p_v}$ is a row probability vector of length N_s whose elements are all non-negative real numbers summing to one, it denotes the probability distribution for each sampled case. The $PIDP_{predicted}$, generated by expectation-based method, consistently remains within the PI, and its reliability is determined by the probability distribution vector $\overrightarrow{p_v}$. The specific method for obtaining the probability distribution vector $\overrightarrow{p_v}$ can be found in existing studies on perception and prediction, which employ techniques such as sampling methods [208] or Bayesian inference [209], [210]. As the derivation of this vector is not the primary focus of the present work, it will not be detailed here.

Consequently, when the probability associated with the speed of the disconnected vehicle during the interruption period is generated by a reliable predictor (cf. Figure 4.3), the resulting curve will not deviate significantly from the actual one. Conversely, when it is generated by an unreliable predictor, the $PIDP_{predicted}(t)$ by mathematical expectation may significantly deviate from the actual curve, thereby failing to eliminate the risk of collision.

4.2.3 *Uncertainty Analysis with Unreliable Predictor*

The unreliable predictor refers to a prediction model that lacks sufficient confidence in its estimated trajectories and therefore fails to produce a probability distribution with a well-defined and dominant peak. In such cases, the predicted outcomes are highly

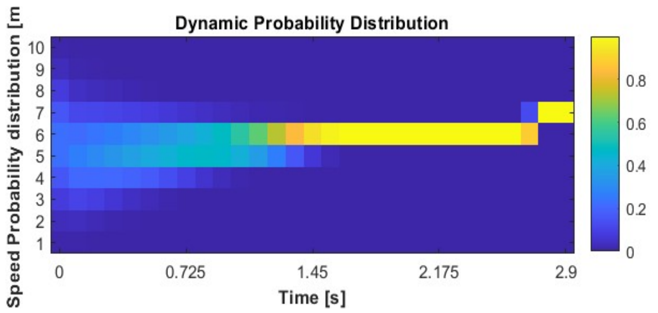

Figure 4.3: Probability distribution with reliable predictor. The predictor ultimately outputs a probability distribution characterized by a finite number of probability peaks, each representing a high likelihood of a corresponding vehicle choice or state

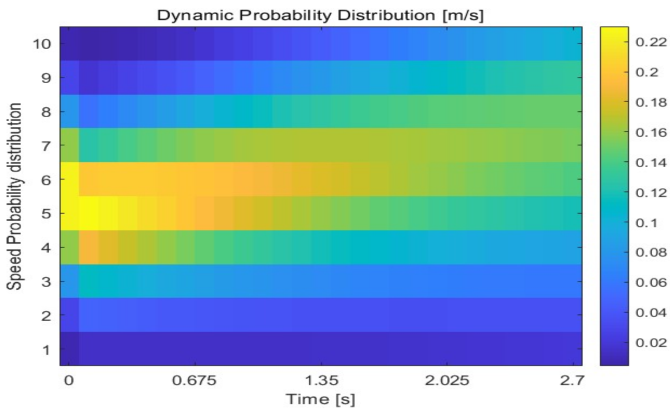

Figure 4.4: Probability distribution with unreliable predictor. This predictor ultimately fails to output a reliable probability distribution, instead converging to a uniform distribution

uncertain and dispersed across multiple possibilities, rather than concentrated around a plausible or most-likely trajectory (cf. Figure 4.4). This phenomenon corresponds to a probability distribution that exhibits low sharpness and poor resolution, which—according to the principles of probabilistic forecasting—indicates that the predictive model does not effectively differentiate between feasible and infeasible outcomes [211], [212]. As a result, its probability surface tends to be nearly flat or uniformly distributed, implying that the predictor is poorly calibrated and overestimates uncertainty. Well-calibrated and sharp probabilistic predictors have been shown to significantly improve decision-making safety and efficiency by providing interpretable and confidence-aware trajectory hypotheses [213]. Consequently, the reliability of a trajectory predictor depends not only on accuracy but also on the calibration and sharpness of its predicted probability distributions.

To address this limitation, the PIDP-PUI method is extended and integrated as a corrective mechanism. Instead of merely increasing confidence in predicted outcomes, the proposed extension leverages the PIDP-based risk assessment framework to reconstruct the probability distribution based on inter-vehicle interaction risks and contextual consistency. By embedding this risk-aware adjustment process into the prediction stage, the method transforms an uninformative, flat probability surface into a safety-oriented probabilistic representation. This not only mitigates the influence of unreliable predictions but also enhances the overall safety and robustness of the cooperative decision-making process under uncertainty.

It is the probability distribution vector $\overrightarrow{p_v}$ that is affected directly by the unreliable predictor. Therefore, a re-weighting function, based on the *mPIDP*, is designed to assign new weights to this probability distribution vector $\overrightarrow{p_v}$ in equation (4.4), thereby obtaining the new vector $\tilde{p_v}$:

$$PIDP_{PUI} = \tilde{p_v} * PIDP_{PI}(t) \tag{4.5}$$

$$\tilde{p_i} = \frac{p_i}{\sum_j f_j p_j} \tag{4.6}$$

$$f_i = e^{-\alpha ln(mPIDP_i + \varepsilon)} \tag{4.7}$$

$$\alpha = \alpha_{base} + \beta(\frac{1}{\max((d_{safety} - min(mPIDP)), \varepsilon)}) \tag{4.8}$$

where the $PIDP_{PUI}$ is the effective predicted $PIDP(t)$ curve of the CAV with uncertainty. $\tilde{p_v}$ is the reweighted probability distribution and $\tilde{p_i}$ is the reweighted probability of the $i-th$ sampled $PIDP(t)$ curve. f_i is the probability reweighing function for the $i-th$ sampled $PIDP(t)$ curve. α_{base}, β, and ε are positive constant coefficients.

Equations (4.5)–(4.8) outline the core formulations of the proposed PIDP-PUI method, which is designed to formally correct the output of an unreliable predictor by re-weighting its probability distribution based on an independent, risk-based analysis.

The final, adjusted risk profile, $PIDP_{PUI}$, is defined in equation (4.5). This equation represents the calculation of a new expected value (or weighted average) of all the sampled $PIDP(t)$ curves within the Potential Interval ($PIDP_{PI}(t)$). Critically, it does not use the original, unreliable probability vector, but instead employs the reweighted probability vector $\tilde{p_v}$ as the new set of weights. This ensures the final aggregated profile reflects a risk-corrected perception of the future. The mechanism is fundamentally a Bayesian-style update [209], where the original (prior) probability p_i is modified by a correction factor f_i, and then re-normalized. Equation (4.7) defines this critical correction factor f_i. It is designed as an inverse power-law relationship, $f_i = (mPIDP_i + \varepsilon)^{-\alpha}$, which is central to the method's logic: a high-risk sample (which yields a small $mPIDP_i$, or minimum distance) will generate an exponentially large weighting factor f_i.

This factor f_i is then used to update the distribution, as shown in equation (4.6). This step effectively boosts the final probability of any sample that f_i identified as high-risk, thereby overpowering the original, low-probability assignment from the unreliable predictor.

Finally, equation (4.8) makes the entire framework adaptive and risk-sensitive. The exponent α, which controls the aggressiveness of the reweighting, is not a fixed constant. Instead, it is dynamically modulated by the most severe risk in the entire set, $\min(mPIDP)$. As the overall situation becomes more dangerous (i.e., $\min(mPIDP)$ approaches d_{safety}, making the denominator of the fraction small), α increases significantly. This, in turn, makes the reweighting function f_i far more sensitive to changes in risk, forcing the system to react more decisively when it perceives a high-risk environment.

The fundamental idea behind these formulations is to diminish the influence of unreliable predictors on the final decision: the reweighting function f_i dramatically increases the weight of samples that, despite being assigned low probabilities by the predictor, pose a higher collision risk (small $mPIDP_i$), with larger overall risks (small $\min(mPIDP)$) yielding even larger reweighting factors via α.

4.3 SAFE COOPERATIVE OPTIMIZATION UNDER UNCERTAINTY

After introducing the use of the PIDP-PUI to address uncertainty issues represented by communication loss, this section presents the proposed centralized Safe Cooperative Optimization under Uncertainty (SCOU) architecture. The flowchart of the optimization architecture is illustrated in Figure 4.5, which operates in real-time at the infrastructure level.

If no communication loss occurs—meaning that the system does not experience strong uncertainty—the cooperative decision-making optimization framework proposed in Section 3.3.3 is sufficient to handle the problem. Therefore, in this chapter, we focus exclusively on cooperative decision-making and planning methods under conditions where uncertainty arises, particularly in scenarios characterized by communication loss.

The optimization loop remains active whenever CAVs are present around the intersection. Initially, essential information about each CAV, including entry and exit directions, dimensions, safety radius, and maximum acceleration and deceleration capabilities, is collected, stored, and configured as global variables. Conflict relationships among vehicles are identified based on their entry and exit directions. Subsequently, vehicle information is broadcast to all CAVs potentially involved in conflicts.

Before initiating each optimization loop, the algorithm checks for possible communication malfunctions among CAVs. If any malfunction is detected, the current global best costs for objective functions, J^{best}, J^{best}_{Colli} (cf. equation (3.5)), and J^{best}_{Time} (cf. equation (3.6)), are reset to handle uncertainties caused by communication loss.

The first step of the optimization loop involves generating accelerated, decelerated, and current speed profiles, based on each vehicle's current velocity and acceleration as described in Section 4.2.1. For vehicles that are unobservable and whose communication is disabled, a set of potential speed intervals must be predicted. For vehicles that are observable but have disabled communication, speed profiles are generated using sensor-measured velocity and acceleration (cf. Table 4.1).

In the second step, all potential combined strategies are evaluated, as detailed in Section 4.2.1. The $PIDP(t)$ for pairs of vehicles with potential conflict relationships are computed. For vehicles with disabled communication, $PIDP(t)$ values are replaced by $PIDP_{PUI}$.

Subsequently, the cost of the objective function for each combined strategy is calculated. All strategies whose J cost is equal to or lower than the current global best cost are retained, as they indicate equal or reduced collision risk. Among these selected strategies, those with the minimum J_{Colli} cost—representing the lowest imminent collision risk—are further identified.

The final step involves selecting the strategy with the minimal J_{Time}. If the selected strategy's J_{Time} exceeds the previous best cost J^{best}_{Time}, it is generally not accepted, as it implies a longer average crossing time compared to the previously planned strategy. However, an exception occurs if the selected strategy has a higher J_{Colli} than J^{best}_{Colli}. This situation indicates that unexpected events have increased collision urgency within the dynamic environment, necessitating acceptance of the current strategy to manage collision risks in the next optimization cycle.

If accepted, the current strategy is updated as the global best strategy, and its corresponding cost is set as the global best cost. If not accepted, all CAVs continue to follow their previously planned strategies. This concludes the current optimization cycle, and the next cycle begins at the subsequent sampling interval. Here, t denotes the current time, and t_{max} represents the maximum allowed time threshold for vehicles failing to find a feasible solution. If no improved solution is found over several consecutive optimization cycles, the result is considered to have converged. Simulation results will be shown in Section 4.4

4.4 SIMULATION RESULTS

Whereas the simulations in the previous chapter focused on validating the framework under ideal, deterministic assumptions, this section is dedicated to evaluating the overall proposed Architecture SCOU under uncertainty while using PIDP-PUI as a powerful multi-risk assessment under uncertainty.

The primary objective is to validate the central claim of this chapter: that the proposed approach can ensure safe cooperative decision-making, with a specific focus on the critical challenge of communication loss. We will utilize the same MATLAB-based verification platform and the common vehicle parameters established in Chapter 3 (see Table 3.1). The following simulations are specifically designed to demonstrate how the PIDP-PUI method effectively analyzes risk from uncertainty, and how it achieves the reliable PIDP-based safety cooperative decision-making with unreliable predictors under these degraded conditions. All the simulation videos in chapter can be found in https://youtu.be/yJjWv0xN9Kg.

4.4.1 *Typical Scenario Analysis*

The scenario is shown as Figure 4.6, some important parameters are given in Table 4.2. The communication interruption happened at 0.5 second for vehicle 1, and the duration of the interruption is 3.5s. Under this assumption, a 0.5s preparation period allows CAVs to complete initial mutual communications to acquire potential collision relationships and collision points, while a sustained 3.5s communication interruption ensures that a disconnected CAV remains in a state where its information cannot be directly obtained until it enters the intersection and the possibility to observe it with the vehicles' sensors. The path of vehicle 1 has cross points with the path of vehicle 3 and vehicle 4 (cf. Figure 4.6), they may have a risk of collision.

Table 4.2: Parameters of vehicles and simulation

Parameters	Value	Parameters	Values
$r_{observable}$	5 $[m]$	α_{base}	10
β	0.5	ε	1

To establish a validation baseline, a simple and **reliable predictor** is first considered. This test case simulates a best-case scenario where the uncertainty, while present, is well-behaved. The predictor is initialized with a uniform probability distribution across all potential speeds, representing maximum initial uncertainty. As time evolves and more (simulated) information is gathered, this distribution is designed to gradually converge toward a single, correct speed value, accurately reflecting the disconnected vehicle's true future state. This reliable convergence allows for a direct comparison of two decision-making strategies under uncertainty:

1. **The Expectation-Based Method (Baseline):** This approach, serving as a control, uses the mathematical expectation (the mean value) of the predictor's speed profiles to generate a single, deterministic $PIDP_{Predicted}$ curve.

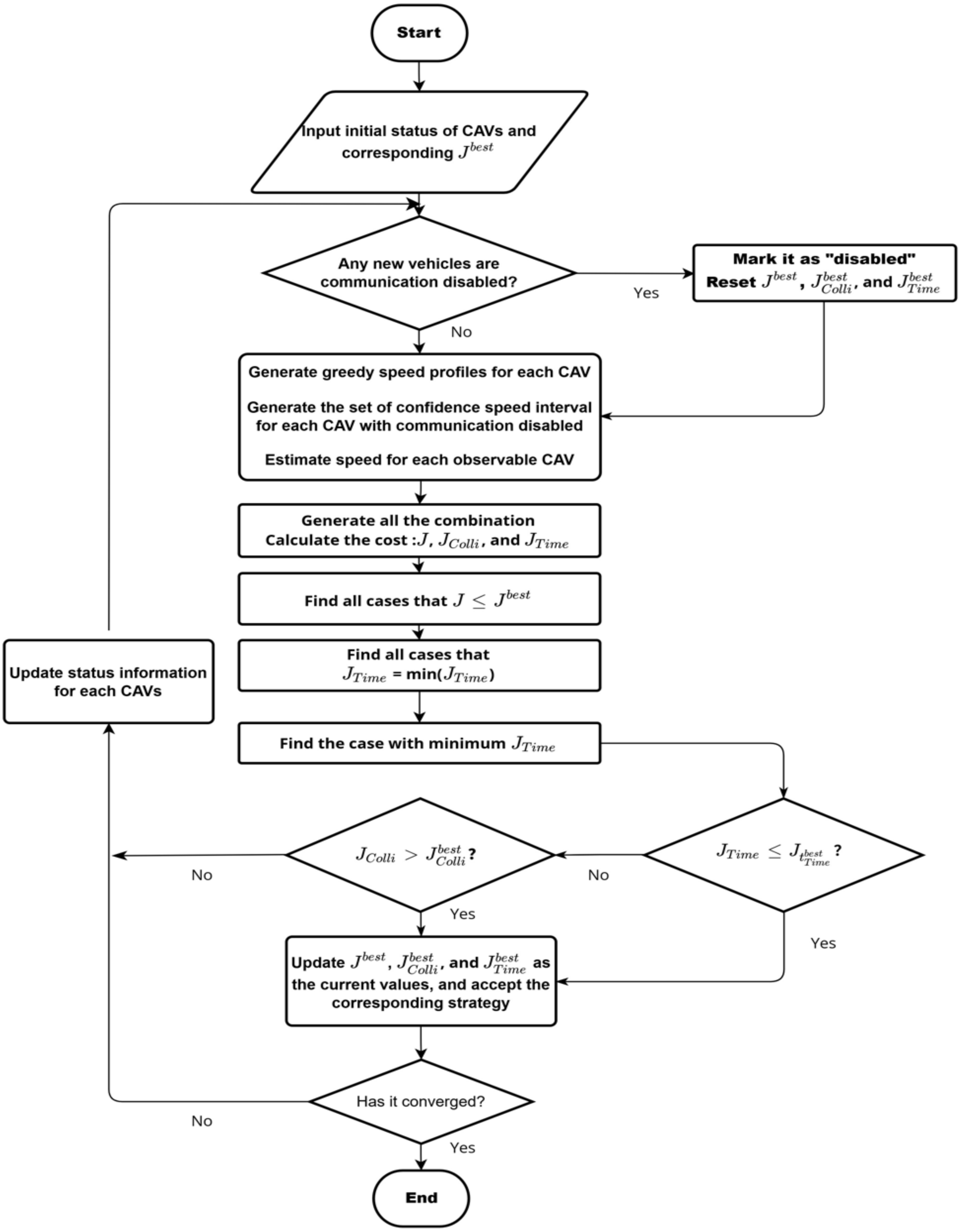

Figure 4.5: Safe Cooperative Optimization under Uncertainty flowchart

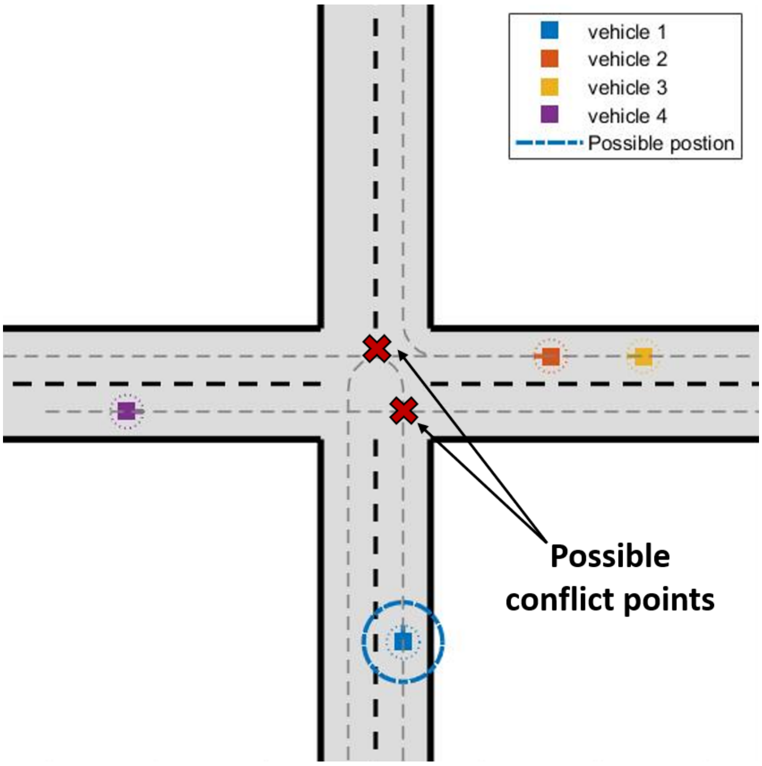

Figure 4.6: Typical unsignalized intersection with 4 vehicles

2. **The PIDP-PUI Method (Proposed):** This approach applies the full methodology developed in this chapter, ingesting the same probability distribution but using the risk-based re-weighting logic to generate the $PIDP_{PUI}$ curve.

These two resulting profiles are then independently used to perform safe cooperative decision-making, allowing for a clear assessment of the PIDP-PUI method's behavior when faced with trustworthy data.

The comprehensive results of this comparative analysis are presented in Figures 4.7 (Expectation-Based) and 4.8 (PIDP-PUI). These figures provide a complete overview of the simulation outcomes. Specifically, Figures 4.7a and 4.8a illustrate the planned speed profiles for the cooperating vehicles, where t_{obs} denotes the time at which the disconnected vehicle becomes observable again. The primary safety validation is depicted in Figures 4.7b and 4.8b, which plot the actual, ground-truth minimum inter-vehicle distance over time. Efficiency metrics are provided in Figures 4.7c and 4.8c, detailing the predicted exit time for each CAV and the resulting average, which corresponds to the expected time leaving the intersection estimated from the current speed profiles of the vehicles. Finally, the internal mechanisms of the uncertainty processing are visualized in Figures 4.7d and 4.8d, which represent the probability distribution across the different sampled speeds as it evolves over time.

An analysis of these results reveals several key insights. Most critically, both the Expectation-Based method and the PIDP-PUI method successfully find a collision-free solution, as confirmed by Figures 4.7b and 4.8b, where the real minimum distance always remains above the safety threshold. This outcome is expected, as the reliable predictor provides a high-fidelity forecast, and its mathematical expectation is, in this case, a trustworthy representation of the future. Consequently, the efficiency of both approaches is also comparable, with the average exit times remaining similar.

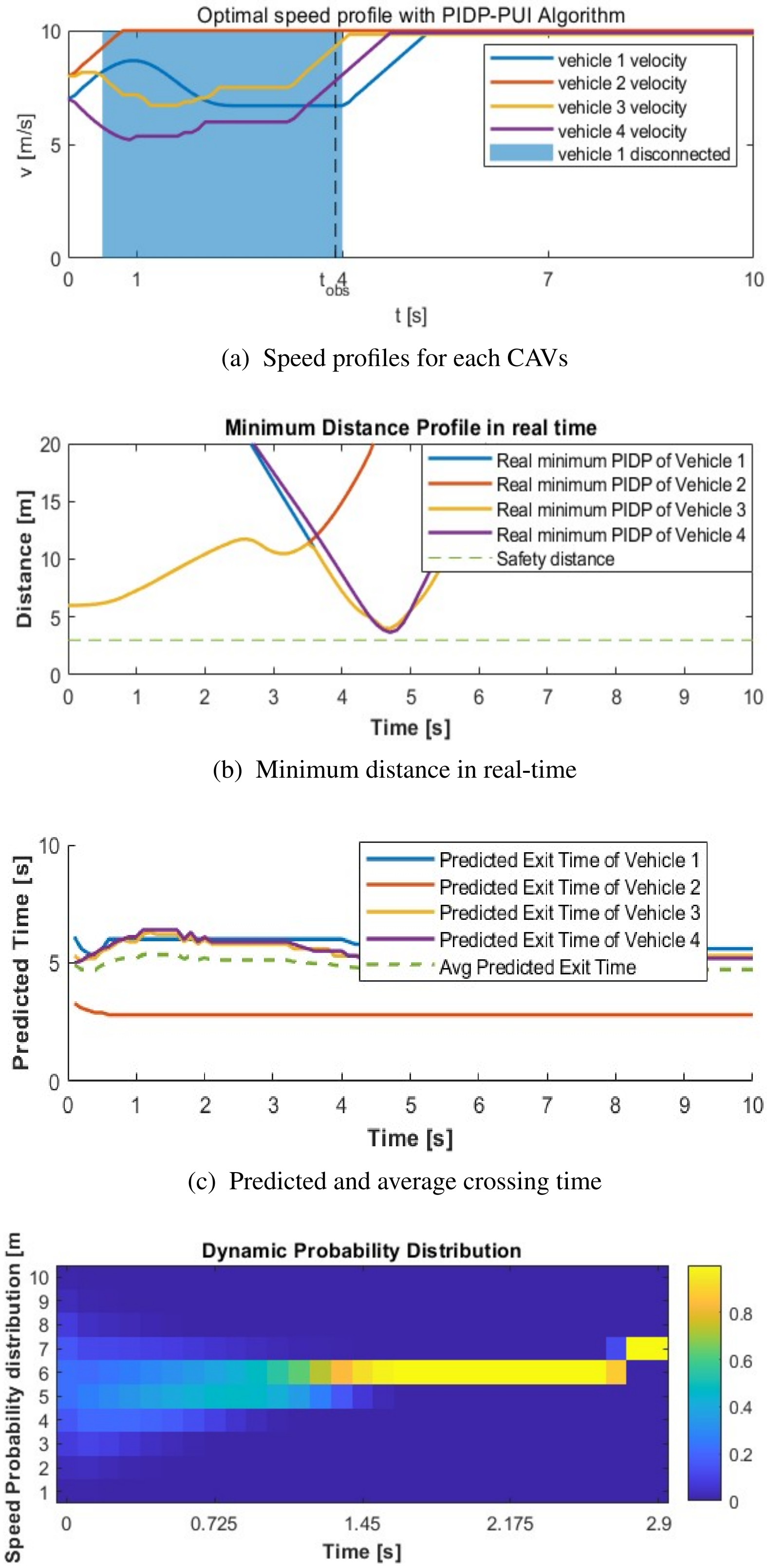

(a) Speed profiles for each CAVs

(b) Minimum distance in real-time

(c) Predicted and average crossing time

(d) Probability distribution corresponding to step time

Figure 4.7: Results of Expectation-Based method with a reliable predictor

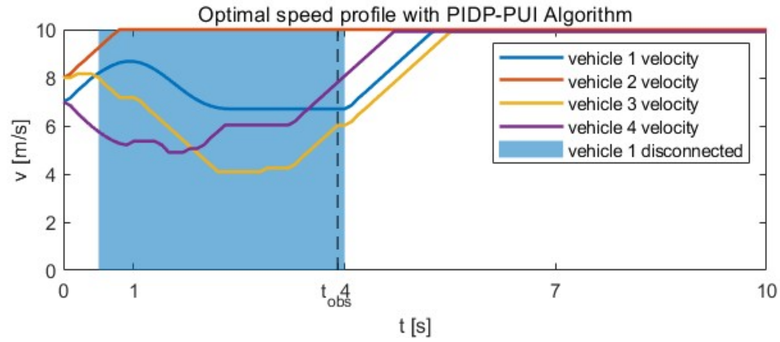

(a) Speed profiles for each CAVs

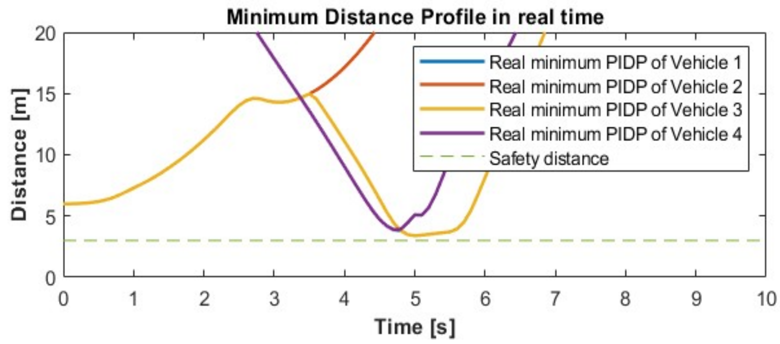

(b) Minimum distance in real-time

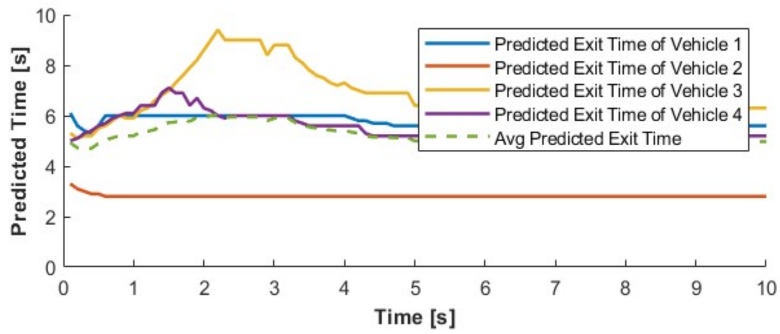

(c) Predicted and average crossing time

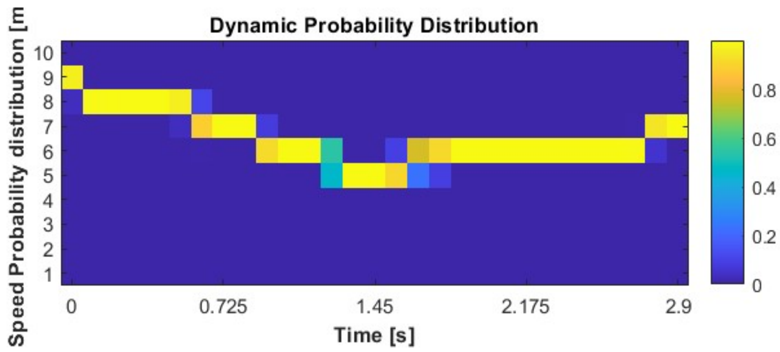

(d) Reweighted probability distribution corresponding to step time

Figure 4.8: Results of PIDP-PUI method with a reliable predictor

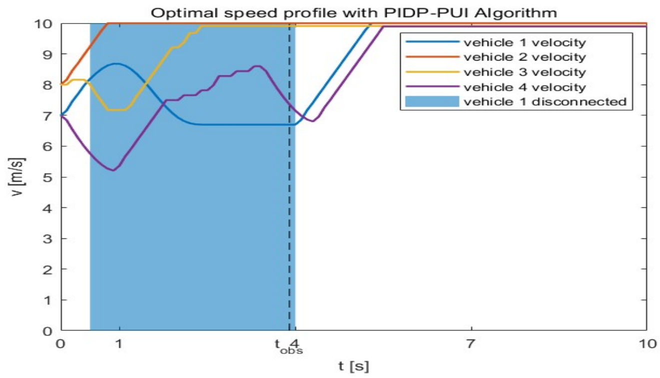

(a) Speed profiles for each CAVs

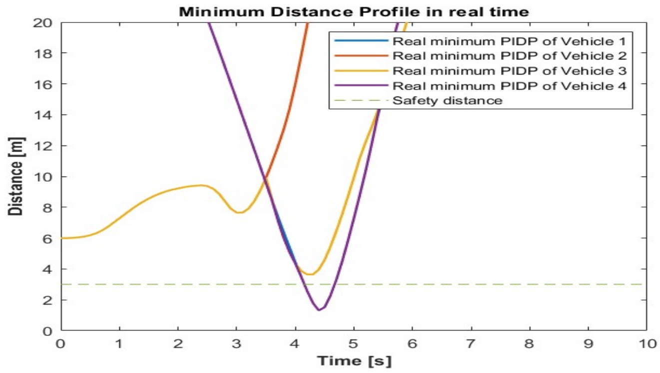

(b) Minimum distance in real-time

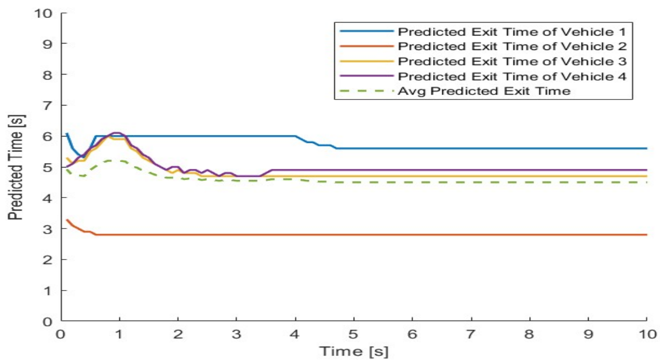

(c) Predicted and average crossing time

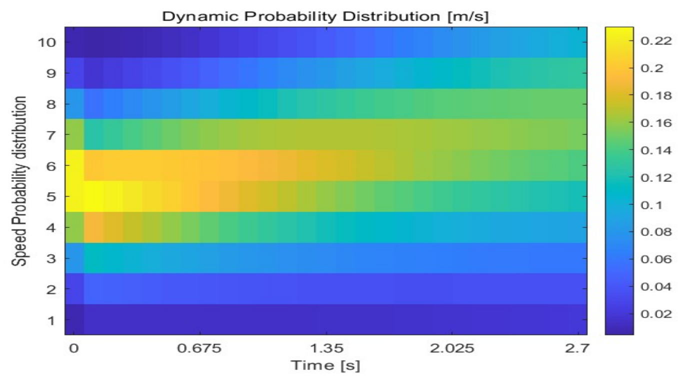

(d) Probability distribution corresponding to step time

Figure 4.9: Results of Expectation-Based method with an unreliable predictor

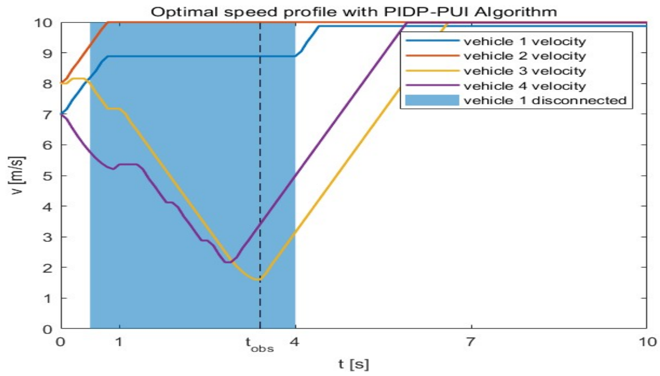

(a) Speed profiles for each CAVs

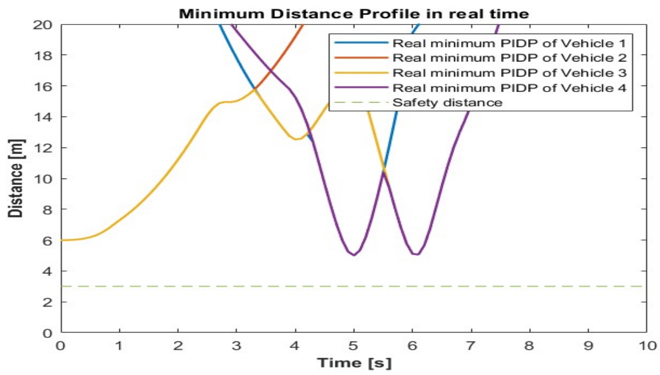

(b) Minimum distance in real-time

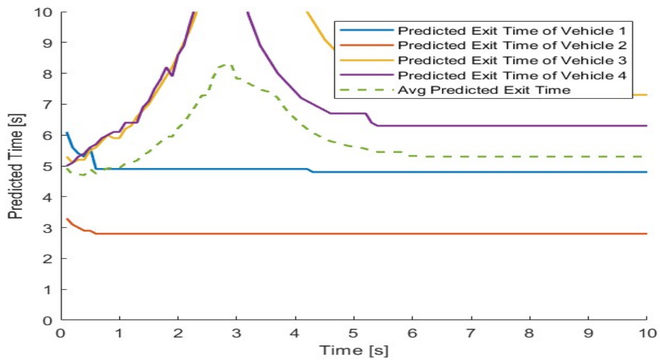

(c) Predicted and average crossing time

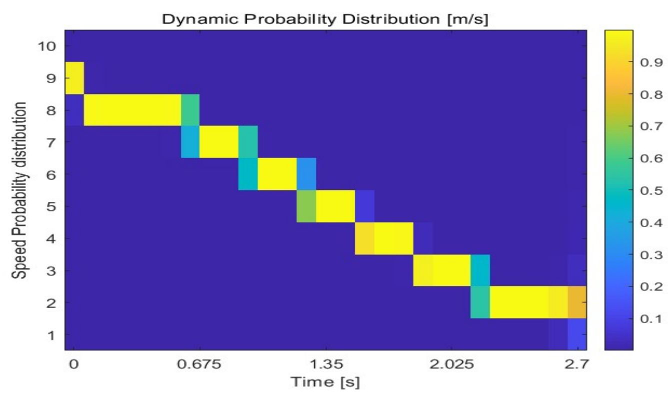

(d) Reweighted probability distribution corresponding to step time

Figure 4.10: Results of PIDP-PUI with an unreliable predictor

The most informative comparison, however, lies in Figures 4.7d and 4.8d. While the probability distribution given by the reliable predictor (Figure 4.7d) converges smoothly, the re-weighted distribution from the PIDP-PUI method (Figure 4.8d) is visibly different. This demonstrates that the PIDP-PUI mechanism is actively re-evaluating the risk of each sampled trajectory. In this reliable scenario, the re-weighting process correctly identifies that the high-probability path (the expected value) is indeed safe, and thus the resulting decision converges to a similarly safe and efficient solution. This benchmark test successfully validates two crucial points: 1) the PIDP-PUI framework correctly identifies and endorses a safe solution when the predictor is reliable, and 2) its more complex risk-assessment layer does not introduce unnecessary conservatism or performance degradation in a non-threatening environment. This establishes its baseline rationality before testing it against unreliable predictors.

Second, the validation is extended to the critical failure scenario: an unreliable predictor. This scenario is specifically designed to test the core hypothesis of this chapter—that the PIDP-PUI method can provide robust safety even when the underlying probabilistic forecast is uninformative or actively misleading. As visualized in Figure 4.9d, the probability distribution generated by this predictor over time lacks a clear or prominent peak, instead appearing diffuse or uniformly spread. This flat distribution strongly suggests that the predictor is "confused" and has low confidence, failing to identify a single, high-likelihood outcome for the disconnected vehicle's speed.

This is the critical failure case for conventional probabilistic methods. When the standard Expectation-Based $PIDP_{predicted}$ is derived from this uninformative distribution, it is calculated as a simple mathematical average of all possible speeds. This "average" speed, however, has no physical basis and is merely a statistical artifact of the predictor's failure. When this highly compromised $PIDP_{predicted}$ is used for decision-making, the consequences are catastrophic. As tragically demonstrated in Figure 4.9b, the real, ground-truth minimum distance between vehicles decisively falls below the safety distance, indicating that a collision occurs. This result proves that naïvely trusting the mathematical expectation of an unreliable predictor is fundamentally unsafe.

In stark contrast, the PIDP-PUI method demonstrates its designed robustness under these exact conditions. Although it receives the same uninformative probability distribution (Figure 4.9d) as the baseline, it does not use it directly. Instead, as shown in Figure 4.10d, the PIDP-PUI's re-weighting mechanism (defined in equations (4.7) and (4.8)) actively transforms this flat distribution. It identifies the high-risk, low-probability samples—those that the predictor ignored but which pose a severe collision threat—and exponentially boosts their probability weights. This process creates a new, distinct peak in the distribution, which no longer represents the predictor's probabilistic forecast, but rather the system's own assessment of the most significant risk.

The resulting $PIDP_{PUI}$ curve is then generated based on this new, risk-aware re-weighted distribution. The system's decision is now dominated by the high-risk samples, forcing on a more conservative and safe maneuver. The successful outcome is confirmed in Figure 4.10b: the real minimum distance successfully remains above the safety threshold, and the system achieves collision-free cooperative decision-making under uncertainty. This comparative test confirms the fundamental contribution of the PIDP-PUI method: it successfully diminishes the influence of the unreliable predictor, overrides its dangerous "average" recommendation, and robustly ensures safety.

4.4.2 *Statistical simulation with random communication loss*

While the fixed-scenario analysis demonstrated the mechanism of the PIDP-PUI's risk-correction, it does not quantify its overall reliability under varying conditions. To simulate the unpredictable nature of real-world communication loss, the validation must be extended from these specific case studies to a large-scale statistical analysis. In this subsection, simulations with thousands of random initial conditions are repeated to rigorously evaluate the proposed method's reliability and efficiency. To ensure these tests constitute a genuine stress test of the framework's robustness, the following challenging simulation setup is specified:

1. **Adversarial Behavior Model:** The disconnected vehicle's behavior is explicitly designed to defeat simple historical prediction. It will immediately change its speed profile upon disconnection, rather than following its previously planned speed. This ensures that other CAVs cannot easily predict its future state based on its previous status. The new speed set-point follows a uniform distribution between $[v_{min}, v_{max}]$, representing the full range of legal speeds and maximum unpredictability.

2. **Maximal Criticality Timing:** Communication disruptions are strategically timed to maximize their impact on decision-making. Interruptions are set to occur as the vehicle approaches the intersection (specifically, within the 3 seconds before it becomes observable). This window is the most critical: if the disruption occurs too early, the system has ample time to react; if it occurs too late, the interaction is already over. The vehicles experiencing disruptions, as well as the precise timing and duration of the interruptions, are all generated by a random function.

To quantify the performance across this vast set of stochastic trials, a new metric is defined: the Uncertainty-Adaptive Planning Rate (UAPR). The UAPR is formally defined as the task completion rate (i.e., the percentage of successful, collision-free intersection crossings) of a given decision-making approach under these randomized simulation tests. A higher UAPR indicates a stronger and more robust capability to handle the severe uncertainty caused by communication loss.

Figure 4.11 presents the resulting UAPR of the Expectation-Based method and the PIDP-PUI method, tested against both the reliable and unreliable predictors. The results starkly illustrate the core findings of this chapter.

As seen in Figure 4.11a, when the reliable predictor is used, the UAPR of both methods is similarly high. This is expected; because the predictor is trustworthy, its $PIDP_{predicted}$ closely approximates the true risk, and the $PIDP_{PUI}$ (while actively re-weighting) correctly converges to a similar, safe conclusion. This confirms that the PIDP-PUI method does not introduce unnecessary conservatism in well-behaved scenarios.

The critical distinction, however, is revealed in Figure 4.11b, which plots the UAPR when using the unreliable predictor. The UAPR of the Expectation-Based method sharply decreases, demonstrating its brittleness—it easily trusts the flawed mathematical expectation of the predictor, which, in a high number of random scenarios, leads to a catastrophic failure and a collision. In stark contrast, the UAPR of the PIDP-PUI method remains stable and high. This result statistically proves its robustness: the re-weighting mechanism consistently identifies and compensates for the predictor's failure, ensuring a safe outcome.

It is noted that the scenarios in this statistical simulation are generated entirely in a random way. As a result, a small subset of "unsolvable" scenarios inevitably emerges — for instance, initial conditions that are already in a state of unavoidable collision due to dynamic or kinematic constraints. Consequently, even an ideal decision-making strategy cannot resolve all possible cases, since certain randomly generated configurations are physically infeasible. Therefore, a 100% UAPR cannot be guaranteed, as it is not theoretically achievable under such stochastic and unconstrained scenario generation. The high and stable UAPR achieved by the PIDP-PUI method thus demonstrates a near-optimal handling of all solvable scenarios, proving its robustness in handling uncertainty.

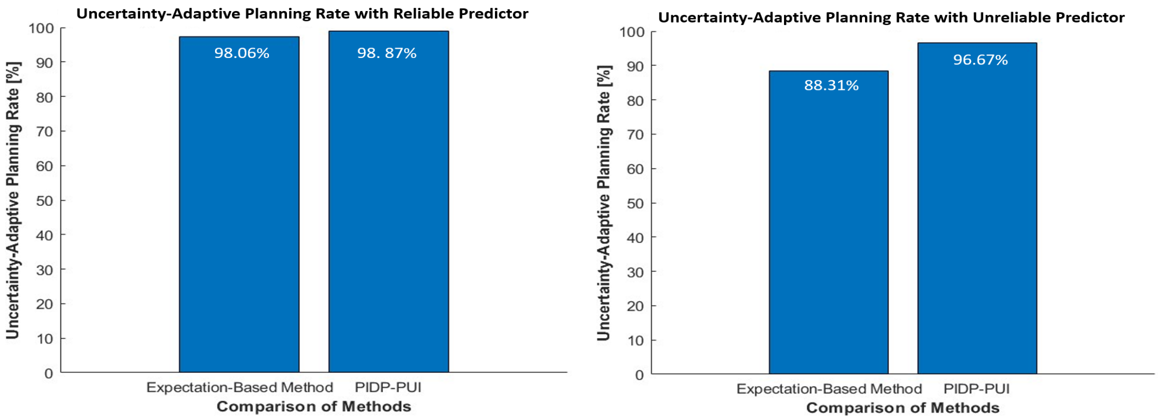

(a) With a reliable predictor (b) With an unreliable predictor

Figure 4.11: Statistical simulation results analysis

4.5 CONCLUSION

This chapter directly addressed the critical challenge of uncertainty, which was identified as the primary limitation of the deterministic framework developed in Chapter 3. To manage the stochastic disturbances inherent in real-world scenarios—particularly communication loss—this chapter formally introduced the concept of the Potential Interval (PI) of PIDP to bound the possible future states of a disconnected vehicle. Building upon this, a novel hybrid methodology, the PIDP-based Probabilistic Uncertainty Interval (PIDP-PUI), was proposed. This method integrates a risk-based re-weighting mechanism with the PIDP framework, enabling it to formally assess and correct the outputs of potentially unreliable state predictors, thereby supporting robust collaborative decision-making.

The efficacy of this PIDP-PUI method was validated through a series of extensive stochastic simulations. These experiments critically compared its performance against a standard expectation-based baseline, using both reliable and unreliable predictors. The results demonstrated that when a reliable predictor is available, the PIDP-PUI approach performs efficiently and comparably to the baseline, confirming it does not introduce unnecessary conservatism. However, when the predictor was unreliable, the expectation-based method was shown to be "brittle", failing to prevent collisions. In stark contrast, the proposed PIDP-PUI method demonstrated superior robustness, successfully identifying and overriding the flawed predictions to maintain a high safety margin and ensure collision-free operation under these degraded conditions.

However, it must be recognized that to comprehensively address the overall problem of urban intersection traffic, the cooperative decision-making optimization methods proposed in Chapters 3 and 4—which focus solely on a limited number of CAVs in the local vicinity—are inherently insufficient. A more macroscopic approach is required; one that can capture the collective behavior of all vehicles within the intersection's influence area in a smart city context. Therefore, the following chapter will introduce an approach that integrates microscopic vehicle decision-making with macroscopic traffic flow management. The goal is to gain a deeper understanding of, and more effectively solve, critical urban traffic issues such as congestion.

5 MULTI-SCALE COOPERATIVE DECISION-MAKING FOR CAVS

Building upon the previous chapters, where our focus was placed on vehicle-level cooperative decision-making at unsignalized intersections and under uncertain environments, this chapter extends the scope to deal with the macroscopic level of traffic flow states. While vehicle-level coordination provides the foundation for ensuring safety and efficiency at the microscopic scale, urban mobility cannot be fully understood without considering the aggregate behaviors that emerge when large volumes of vehicles interact across intersections and corridors. To promote the scalability of the proposed cooperative frameworks toward broader urban transportation systems, it becomes necessary to integrate traffic flow states into the proposed overall control architecture. Therefore, this chapter examines how cooperative intersection management can be contextualized within both macroscopic and microscopic traffic flow perspectives, providing a bridge between individual decision-making processes and system-wide traffic performance.

5.1 PROBLEM STATEMENT

Prior research has mainly focused on vehicle-level coordination, where each vehicle determines its optimal trajectory under cooperative frameworks to resolve conflicts and ensure smooth navigation through intersections. Although vehicle-level cooperative decision-making provides valuable insights for local intersection management, it does not fully capture the broader dynamics of urban traffic. In practice, intersection performance is strongly influenced by upstream and downstream traffic flow conditions, where congestion propagation, queue spillbacks, and demand fluctuations shape the overall system efficiency (cf. Section 2.6). Existing studies often treat intersection management and traffic flow modeling as separate problems, which limits the scalability of vehicle-level strategies to citywide traffic management [214]. Consequently, there is a pressing need to integrate microscopic decision-making with macroscopic traffic flow dynamics.

The problem addressed in this chapter can therefore be formulated as follows: how to extend cooperative vehicle-level decision-making frameworks at unsignalized intersections toward traffic flow–oriented planning that accounts for both local vehicle coordination and large-scale traffic dynamics. Specifically, the objective is to develop methodologies that bridge microscopic trajectory optimization with macroscopic traffic flow models, enabling scalable cooperative control strategies that enhance safety, reduce congestion, and improve overall urban mobility.

5.2 CONTEXTUAL-GRAPH TOPOLOGY FOR EFFICIENT AND REAL-TIME COOPERATIVE INTERSECTION MANAGEMENT

In Chapter 3, we introduced a framework that successfully addresses the intricate problem of ensuring safe, collision-free coordination for CAVs at the microscopic level. However, when elevating the perspective to a macroscopic scale to consider broader traffic flow dynamics, the number of interacting vehicles increases substantially. This escalation in vehicle count introduces a severe challenge of scalability; the computational burden associated with pairwise conflict checking and coordination, which is manageable at the micro-level, experiences a combinatorial explosion. This computational complexity becomes prohibitive for any purely microscopic method, rendering it intractable for real-time application in dense traffic scenarios. Therefore, a crucial prerequisite for achieving a genuine integration of macroscopic and microscopic control is to first devise a method that fundamentally reduces the computational complexity of conflict analysis for large vehicle populations.

To address these scalability challenges, we propose a shift in the computational paradigm. The fundamental insight is that instead of exhaustively evaluating the state of every vehicle against all others, it is more efficient to focus directly on the source of potential collisions. By leveraging graph-theoretic representations and conflict-path analysis, this approach abstracts the multi-vehicle problem to analyze the underlying conditions that lead to conflicts. This allows for a significant pruning of the decision space, which drastically reduces the computational burden and accelerates the decision-making process, thereby enhancing its applicability to continuous and dense traffic flow environments.

To make the method more comprehensible, we begin by introducing the required graph theory concepts, applied to deal with the addressed cooperative task.

Given a set of vehicles, denoted as $V = (v_1, v_2, ..., v_n)$. We construct an undirected graph $G = (V, E)$ to represent potential collision relationships among these vehicles. The construction follows these rules:

1. Vertex set (V): Each vertex in V corresponds to one vehicle in the buffer area (cf. Figure 3.2). For every vehicle v_i in the set, there is a corresponding vertex v_i in the graph. When a new vehicle enters the buffer area, it will be added to the set V, and it is similarly removed when a vehicle leaves the buffer area.

2. Edge set (E): For any pair of distinct vehicles v_i and v_j, if there is a potential collision risk ($ePIDP_{ij} < 0$), an undirected edge $e(i, j)$ is added to E. If no potential collision risk exists, no edge will be added to the edge set E. If a vertex is removed, which means, that the vehicle is outside of the action area (cf. Figure 3.2), its related edges will be removed from E too. When a new vertex is added, its related edges will be added to E.

5.2.1 *Contextual Risk Management Graph based on Conflicting Paths Checking*

In Chapter 3, we made an important assumption: in intersection traffic, once the entry and exit directions of a vehicle are determined, and lane changes are not considered, the vehicle's path is uniquely defined. Previously, in Section 2.2.3, we introduced how the PIDP method can be used to detect potential collision risks between vehicles. However, by removing the time variable t, we can retain only the position-based path, it is straightforward to observe that, under intersection conditions, if the paths of two vehicles do not contain a cross point, then under normal driving circumstances they cannot encounter a collision risk. Conversely, if their paths do contain a cross point, the PIDP method can subsequently be applied to determine whether a collision risk exists. Therefore, we can begin with the conflict mode of intersection vehicles to preliminarily identify which vehicle pairs are exposed to potential collision risks.

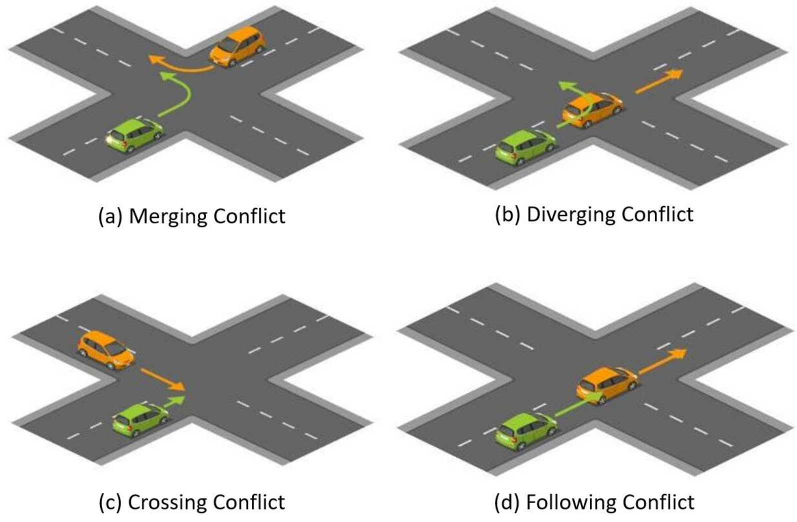

Figure 5.1: Four conflicting modes at intersection [7]

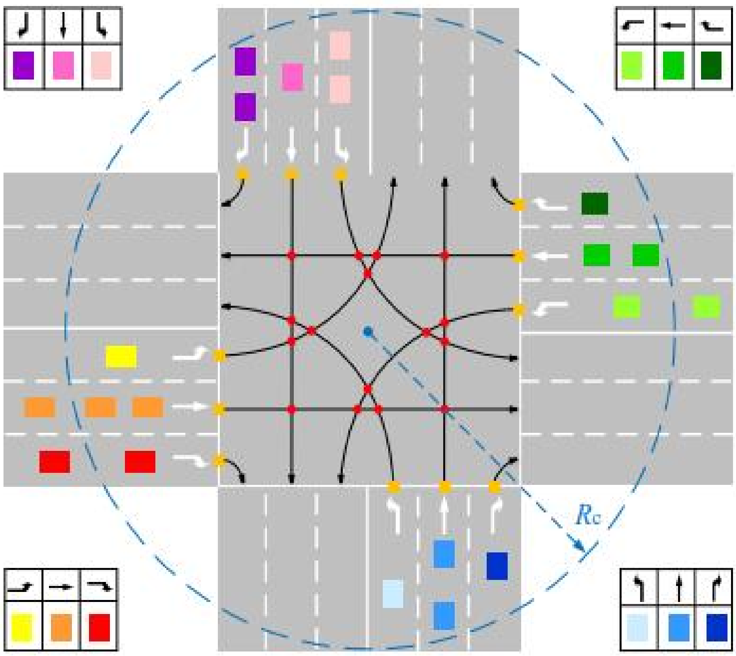

Figure 5.2: Collision points in the intersection [7]

Generally, there are four conflicting modes at intersections: merging, diverging, crossing, and following (cf. Figure 5.1). Since a vehicle may simultaneously conflict with multiple others, constructing a fully connected graph among all vehicles is inefficient. Instead, a contextual-based graph is introduced that links only pairs of vehicles at potential risk of collision, as determined by their entry and exit paths (cf. Figure 5.2). Any two conflicting vehicles are connected in this topological graph, and C_i denotes the set of vehicles that may conflict with vehicle i.

The conflicting path-based graph is denoted by $G_c = (V, E_c)$, where V is the set of nodes representing all CAVs within the buffer area (cf. Figure 3.2). E_c is the set of edges, each corresponding to a pair of vehicles with a potential risk of collision. By focusing solely on conflict-prone vehicles, the contextual-based graph reduces unnecessary communication and computation, thereby improving optimization efficiency.

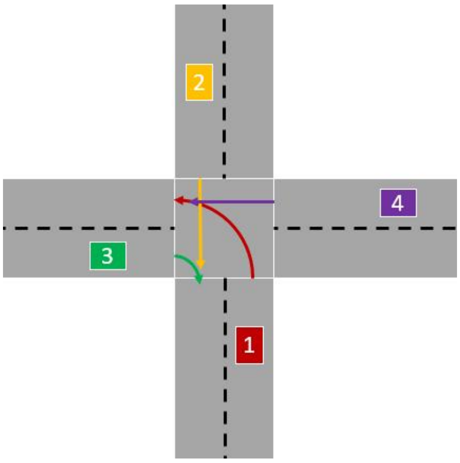

(a) Conflict relation at intersection

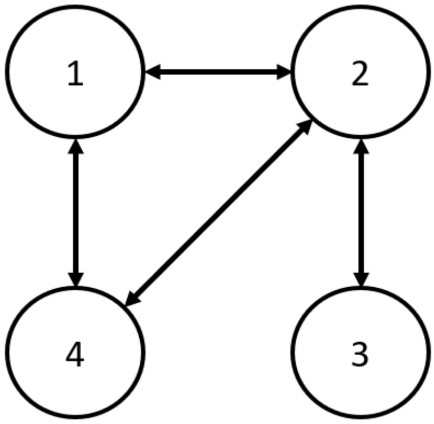

(b) Related topological graph

Figure 5.3: Conflict relation and related topological graph

An example is shown in Figure 5.3. Four vehicles enter the unsignalized intersection simultaneously from different directions. Vehicle 1 does not intersect with vehicle 3, therefore they are not linked in the topological graph; the same is true for vehicle 3 and 4 in this example. It should be emphasized that this topological graph is dynamic and is recalculated in real time based on current CAV desired paths and conflict relations. For instance, if vehicle 2 passes the intersection's conflict point before vehicles 1 and 4, it no longer needs to communicate with them, as they are no longer in conflict. If any vehicle leaves the intersection, it should be removed from the topological graph, not only from the vehicle list V but also from the edge list E. More details about the Contextual Risk Management Graph (CRMG) will be introduced in Section 5.2.3.

5.2.2 *Contextual Risk Management Graph based on PIDP*

Although the CRMG method significantly reduces unnecessary computations, further optimization is possible to decrease computational and time costs. When two CAVs are identified as having a potential collision risk, it does not necessarily imply that a collision will occur, this is where the previously introduced *mPIDP* plays a crucial role. Recognizing that a CAV's speed planning is typically localized rather than globally optimized, we focus on the speed profiles of both CAVs within a fixed time horizon $t_{horizon}$ to compute their PIDP curve and thereby derive the corresponding *mPIDP*. If the corresponding *mPIDP* exceeds the collision-free distance d_{cf}, further negotiation is unnecessary because the current situation has a sufficient Safety Margin. If the current *mPIDP* is less than d_{cf}, they should consider each other when they make decisions to reduce the potential risk of collision.

Similar to the CRMG, the Contextual Risk Management Graph based on PIDP (CRMG-PIDP) is denoted by $G_P = (V, E_P)$, where V is the set of nodes representing all CAVs within the buffer area (cf. Figure 3.2). E_P is the set of edges, each corresponding to a pair of vehicles whose *mPIDP* is less than d_{cf}. Since only pairs of vehicles with a potential risk of collision are considered in the CRMG-PIDP, it follows that $E_P \subseteq E_c$. The procedure for deriving E_P from E_c is given in Algorithm 5.

Algorithm 5 Definition of CRMG-PIDP

```
for all Pair (i, j) ∈ E_c do
    if mPIDP_ij(t < t_horizon) < d_cf then
        Add (i, j) to E_P
    end if
end for
```

5.2.3 *Graph-based Contextual Risk Management Updating Process*

Although we have already introduced how to construct the corresponding graphs based on vehicle entry–exit directions and the PIDP-based collision detection mechanism, it is important to emphasize—as noted earlier—that these graphs are not static but inherently dynamic. Therefore, a key focus of this section is how to update these graphs in real time according to the evolving traffic environment.

In a scenario that without any vehicle enters or leaves the intersection, the corresponding G_c and G_p can be easily computed. However, when a new vehicle enters the intersection, the vehicle list V must first be updated. Based on the entry–exit directions and trajectory of the new vehicle, the collision relation graph E_c with respect to all other vehicles in the list is then recalculated. Conversely, when a vehicle exits the intersection, it should be removed from the list V, along with all of its associated collision relations in E_p.

All the updating process is detailed in Algorithm 6. During each PIDP-based relation update, G_p can be dynamically modified according to the computed results. For example, if two vehicles i and j share a potential collision relation (i.e., $(i, j) \in E_c$) but their corresponding $mPIDP_{ij}$ is greater than d_{cf}, then (i, j) will not be included in E_p. As time evolves, if the updated $mPIDP_{ij}$ becomes less than or equal to d_{cf}, this indicates that, under their current strategies, vehicles i and j are inevitably exposed to a collision risk, and the pair should therefore be added to the collision-risk list E_p. Conversely, if a pair already included in E_p yields a new $mPIDP_{ij}$ greater than d_{cf}, it should be removed from E_p.The simulation results will be shown in Section 5.4.

This section sequentially introduces the CRMG and CRMG-PIDP methods, which progressively simplify the computational load of risk assessment. This lays the foundation for the real-time processing of inter-vehicle risk assessment in dense traffic flows. The following section will formally introduce how the macroscopic and microscopic layers are integrated, in order to analyze and solve traffic congestion in dense traffic from a multi-level perspective.

Algorithm 6 CRMG-PIDP updating process

while Infrastructure working **do**
  if Any vehicle arrives the intersection **then**
    Add the vehicle to the list V, calculate its conflicting relation and add them to collision relationship set E_p, update the conflicting path-based graph G_c
  end if
  if Any vehicle leaves the intersection **then**
    Remove the vehicle from the list V, remove all its corresponding relation from the set E_p, update the conflicting path-based graph G_c
  end if
  for all Vehicle $i \in V$ **do**
    for all Vehicle j & $(i, j) \in E_c$ **do**
      Calculate the $mPIDP_{ij}$
      if $mPIDP_{ij} \leq d_{cf}$ & $(i, j) \notin E_p$ **then**
        Add (i, j) to E_p
      else if $mPIDP_{ij} > d_{cf}$ & $(i, j) \in E_p$ **then**
        Remove (i, j) from E_p
      end if
    end for
  end for
  Update the PIDP-based graph G_p
end while

5.3 MULTI-SCALE COOPERATIVE DECISION-MAKING INTEGRATING TRAFFIC FLOW DYNAMICS

This section develops the core components of the proposed multi-scale architecture. We first establish a novel definition of traffic congestion specifically tailored to the unique characteristics of intersections fully populated by CAVs. Building upon this, a macroscopic control strategy is formulated to derive optimal, system-level directives for mitigating congestion. Finally, the Traffic Flow Coordination framework is introduced, detailing the mechanism that translates these high-level traffic flow objectives into actionable commands for the microscopic vehicle controllers. Figure 5.4 presents a diagram of the proposed integrated macroscopic and microscopic model.

5.3.1 *Definition of Traffic Congestion at Unsignalized Intersection for CAVs*

CAVs have fundamentally reshaped the dynamics of traffic flow, particularly at unsignalized intersections where traditional congestion metrics—designed for Human-Driven Vehicles (HDVs)—may no longer be directly applicable. Conventional indicators such as average delay, queue length, or stop-and-go frequency are intrinsically linked to human driving behavior and therefore fail to capture the cooperative, highly coordinated nature of CAV operations. This shift calls for a redefinition of congestion metrics that better reflect the operational efficiency, system stability, and coordination capabilities of CAV-dominated traffic.

To address this gap, we propose to quantify congestion at unsignalized intersections using the average speed within the intersection control area as the primary indicator, normalized by the free-flow speed v_f. At low to moderate levels of traffic flow and density,

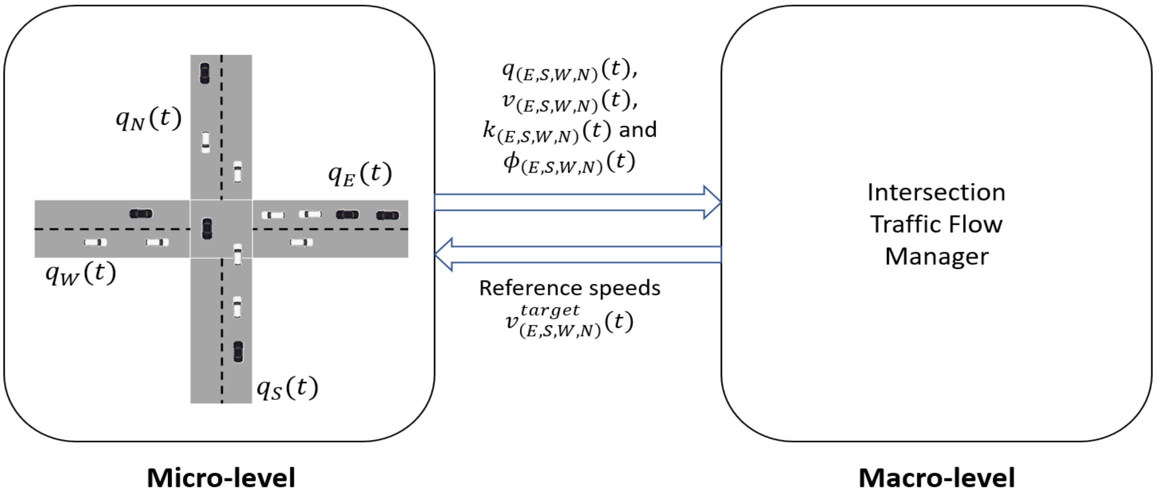

Figure 5.4: Micro- and Macro-level cooperative collaboration: (a) Micro-level: conflict risk assessment and management; (b) Macro-level: traffic flow optimization

the average speed of CAVs remains nearly constant, sustained by their precise motion control, short reaction times, and cooperative decision-making strategies. However, as traffic density approaches the critical congestion threshold, the average speed declines sharply, signaling the onset of instability and flow breakdown.

Based on the above characteristics, it becomes evident that the Greenshields model (cf. Section 2.6.1) is not fully applicable to traffic management at intersections exclusively composed of CAVs. Consequently, the congestion critical point q_m and its associated speed v_m do not necessarily correspond to $\frac{v_f}{2}$. Traditional approaches often rely on measures such as vehicle waiting time to characterize the degree of congestion at intersections. However, our aim is to employ indicators that can be directly obtained from traffic flow data to determine whether an intersection is operating under congested conditions.

In practice, the maximum traffic capacity of an intersection, q_m, is not a fixed value. Variations in intersection geometry, size, and the number of lanes can lead to different capacity levels across locations. Even within the same intersection, q_m may fluctuate depending on factors such as vehicle type composition (e.g., more tracks or personal vehicles with different dimensions) and the directional distribution of flows. As a result, it is not feasible to directly measure the maximum capacity q_m of an intersection. Instead, we seek to define congestion by extracting information from the observable traffic flow density and speed at the intersection, thereby providing a more practical and data-driven characterization of congestion states.

However, intersection management strategies based on vehicle platooning have demonstrated that traffic density alone is not strongly correlated with congestion under ideal conditions. When all vehicles maintain a fixed headway within a platoon and pass through the intersection in an orderly sequence, the traffic density at the intersection may approach its theoretical maximum. Nevertheless, the platoon can still sustain relatively high travel speeds, indicating that high density does not necessarily imply congestion in such coordinated scenarios. For instance, as illustrated in Figure 5.5, the traffic flow moving in the north-south direction maintains a relatively high velocity despite its significant density.

Let us now consider the unsignalized intersection scenario illustrated in Figure 5.5. At this moment, the traffic flow in the north–south direction is extremely high, nearly

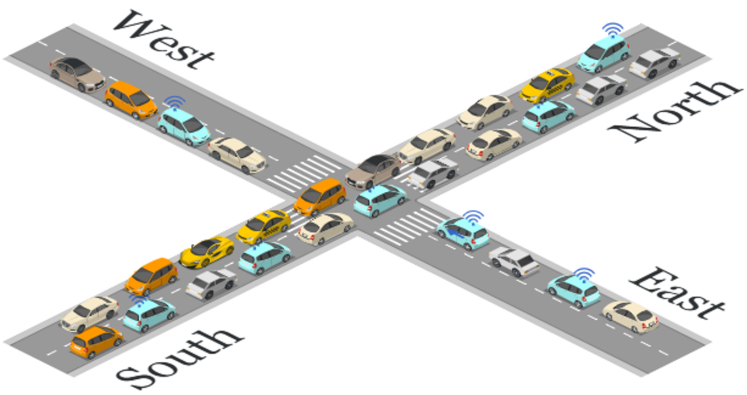

Figure 5.5: Special case for congestion

occupying the entire intersection and dominating its capacity, while vehicles traveling in the east–west direction are forced to stop and wait. For the north–south vehicles, the intersection remains uncongested, and their travel speed within the intersection can remain relatively high. However, for the east–west vehicles, the situation clearly represents congestion. From this scenario, the following insights can be systematically identified:

1. Traffic density is not strongly correlated with the presence or absence of congestion in the considered road, but depends on the bottleneck of the intersection interaction.

2. Congestion at an intersection should not be defined solely by the condition that all directional flows are impeded; rather, if congestion occurs in any single traffic direction, the intersection as a whole can reasonably be considered to be experiencing congestion.

3. Congestion may force vehicles to stop and queue in the action area or decision-making area in Figure 3.2 rather than within its core area only.

These three observations clearly establish that:

1. Traffic congestion at intersections should be determined based on traffic flow speed rather than traffic density.

2. The evaluation should incorporate the average speed of traffic flows across all four directions, rather than relying on the flow speed of a single direction.

3. The calculation should account for vehicle speeds within an extended area surrounding the intersection, rather than considering only the speeds of vehicles strictly within the intersection boundaries.

In this framework, we suggest defining congestion as the condition in which the average speed surrounding the intersection, $v_{intersection}$, drops to 70% of the free-flow (or maximum legal) speed v_{max} in the action area of the unsignalized intersection (cf. Figure 3.2). This threshold—significantly higher than the conventional 30–50% range commonly employed for HDVs—highlights the enhanced operational efficiency and resilience of CAVs, which are capable of sustaining higher throughput levels before congestion manifests. It should be emphasized, however, that the 70% threshold is not universally fixed; it may vary as a function of intersection geometry, traffic demand characteristics, and the penetration rate of CAVs in the traffic stream. This flexible definition therefore provides a more context-sensitive and system-appropriate measure of congestion for CAV-enabled urban traffic environments.

To this end, we define the characteristic speed under congested conditions as the "congestion speed", denoted by v_{con}. Furthermore, to effectively quantify the current degree of congestion at the intersection, we define the "congestion rate" ϕ as:

$$\phi = \left(2 - \frac{v(t)}{v_{con}(t)}\right) \times 100\% \tag{5.1}$$

when the congestion rate is below 100%, it indicates that while congestion has not yet occurred, there is a risk of its onset; the closer the rate is to 100%, the greater this risk becomes. Conversely, a rate exceeding 100% signifies that congestion has already materialized, with a higher value which corresponds to a more severe level of congestion.

5.3.2 *Congestion-Sensitive Flow Fusion*

We now turn to the derivation of a Congestion-Sensitive Flow Fusion model (CSFF) for unsignalized intersections with CAVs, starting from the Greenshields model and extending it to address congestion mitigation in CAV-dominated traffic flows.

Let us consider a scenario of maximum traffic density in conjunction with the Greenshields model, where the traffic flow in a specific direction near an unsignalized intersection reaches a complete standstill, with vehicles adhering to the minimum spacing. Equation (5.2) provides a method for calculating the jam density at the intersection based on the minimum safe distance:

$$k_{jam} = \frac{1}{d_{safety}} \tag{5.2}$$

Because the inter-vehicle distance reaches its minimum, the traffic density attains its theoretical maximum, and the vehicles are almost locked in place, unable to move, therefore we define it as the jam density at the intersection.

In an unsignalized intersection management system, if the goal is to alleviate congestion in one direction of travel, a feasible approach is to adjust the speeds of nearby vehicles and grant higher priority to vehicles in that direction. Assuming that the current traffic flow in the Greenshields model's equation (2.18) remains constant, we reformulate the expression to describe the relationship between vehicle density and average vehicle's speed as:

$$k = \frac{q}{v} \tag{5.3}$$

by differentiating both sides with respect to traffic flow speed, we obtain:

$$\frac{dk}{dv} = -\frac{q}{v^2} \tag{5.4}$$

$$dk = -\frac{q}{v^2}dv \tag{5.5}$$

where v_c is the current average vehicle speed when there is congestion. From equation (5.5), we can infer that increasing the expected average speed in the target direction can effectively reduce the vehicle density in that direction.

Considering that the target velocity we are studying is discontinuous, we therefore reformulate equation (5.5) from its continuous differential form into an approximate discretized expression:

$$\Delta k = -\frac{q}{v^2}\Delta v \tag{5.6}$$

Furthermore, based on equation (2.21), the maximum traffic flow is achieved when $k = \frac{k_{jam}}{2}$. Consequently, we can reformulate equation (5.6) as follows:

$$\Delta k = k_c - \frac{k_{jam}}{2} = -\frac{q}{v_c^2}\Delta v \tag{5.7}$$

$$\Delta v = v_c(1 - \frac{k_{jam}}{2k_c}) \tag{5.8}$$

$$v^{target} = v_c + \Delta v \tag{5.9}$$

where k_c is the current vehicle density when there is congestion and it satisfies $k_c > \frac{k_{jam}}{2}$ when there is congestion in the corresponding direction. v^{target} is the target average vehicle speed corresponding the maximum traffic flow for the direction with congestion based on current scenario from equation (2.21) and (5.5).

We now extend our focus to the entire unsignalized intersection. Typically, when traffic congestion occurs in one direction at an unsignalized intersection, it is because vehicles in that direction conflict with vehicles from other directions within the intersection, necessitating their deceleration to avoid collisions and thereby reducing the average speed in that direction. Consequently, we cannot solely focus on increasing the target average speed of vehicles in this direction to enhance their priority. We must also consider the impact on the target average speeds of vehicles in other directions, or the risk of collisions will increase.

Owing to the high complexity of traffic congestion causes at unsignalized intersections, it is challenging to employ a single, absolute constant for precise quantitative analysis. Nevertheless, we can assume that, during traffic congestion, the current total intersection traffic flow reflects the maximum carrying capacity of the intersection under that specific scenario, which we define as a constant C:

$$C = \sum q_i = \sum k_i v_i \tag{5.10}$$

where q_i, k_i, v_i are respectively the current observed traffic flow, density, and average speed for direction i in the buffer area. It should be noted that C is not an absolutely fixed value; its magnitude varies depending on intersection characteristics and may exhibit dynamic changes over time within the same intersection. Furthermore, each C is applicable only to describing the current traffic condition and cannot characterize past conditions or predict future traffic states at the intersection.

Using the constraint differentiation method, equation (5.10) can be rewritten with the following differential form:

$$0 = \sum k_i \Delta v_i \tag{5.11}$$

where Δv_i is the change in target speed in direction i. By reformulating equation (5.11) as an expression of the speed change in the congested direction and the speed changes in other directions:

$$\Delta v_{con} = -\frac{\sum_{i \neq con} k_i \Delta v_i}{k_{con}} \tag{5.12}$$

where k_{con} and Δv_{con} are the vehicle density and the change in target speed of the identified direction with congestion, and Δv_{con} is derived from equation (5.8). To simplify the calculation of how speed changes in the congested direction affect those in other directions, we assume that directions with higher traffic density k experience greater speed changes Δv.

Specifically, the traffic density k_i serves as the weight for the speed change Δv_i in direction i. This assumption leads to the derivation of equation (5.13):

$$\Delta v_j = -\frac{k_{con}\Delta v_{con} k_j}{\sum_{i\neq con} k_i^2} \tag{5.13}$$

where j represents any other direction different from the currently most congested direction. k_j and Δv_j are the vehicle density and the change in target speed for direction j. It is easy to find that equation (5.13) is a special set of solutions of equation (5.12).

We further investigate the scenario where traffic congestion occurs simultaneously in multiple directions. It is straightforward to rewrite equation (5.12) and (5.13) as follows:

$$\sum_{j\in cons} k_j \Delta v_j = -\sum_{i\notin cons} k_i \Delta v_i \tag{5.14}$$

$$\Delta v_j = -\frac{k_j \sum_{i\in cons} k_i \Delta v_i}{\sum_{i\notin cons} k_i^2} \tag{5.15}$$

where *cons* is the set of all directions with congestion.

Generally, the average vehicle speed is always positive in traffic, but it is possible to get a value of Δv_j which make v_j^{target} be negative from equation (5.15) if more than one direction has a risk of congestion. Another special case is when congestion is present in all four directions if each road is composed by two branches. In equation (5.11), since each direction experiences congestion, all Δv_i are derived from equation (5.8) and are positive, rendering equation (5.11) invalid, as the right-hand side consists entirely of positive values, contradicting the zero on the left-hand side. Both of the above special cases indicate that equation (5.11) is not applicable under certain conditions, necessitating its optimization. Consequently, we need to reassign priorities to all Δv_i, introducing new $\Delta\tilde{v}_i$ to replace the original Δv_i, ensuring that equation (5.11) remains valid.

In this scenario, we first assume that the total traffic flow at the intersection is not constant. After applying the differentiation method, equation (5.11) can be rewritten in the following form:

$$\Delta C = \sum k_i \Delta v_i \tag{5.16}$$

where ΔC denotes the assumed change in the total traffic flow at the intersection. Based on the relationship between ΔC and Δv_i, use the same method that we get equation (5.13) from equation (5.12) to apply proportional reweighting, we can derive the new $\Delta\tilde{v}_i$:

$$\Delta\tilde{v}_i = \Delta v_i - \frac{k_i \Delta C}{\sum k_i^2} \tag{5.17}$$

where $\Delta\tilde{v}_i$ represents the reweighted change in average speed for direction i, and $\Delta\tilde{v}_i$ satisfies:

$$\sum k_i \Delta\tilde{v}_i = 0 \tag{5.18}$$

$$v_i^{target} = v_i + \Delta\tilde{v}_i \tag{5.19}$$

where v_i^{target} denotes the target speed for direction i. And it can be noted that when ΔC is equal to 0, equation (5.17) is equal to (5.13) and (5.15).

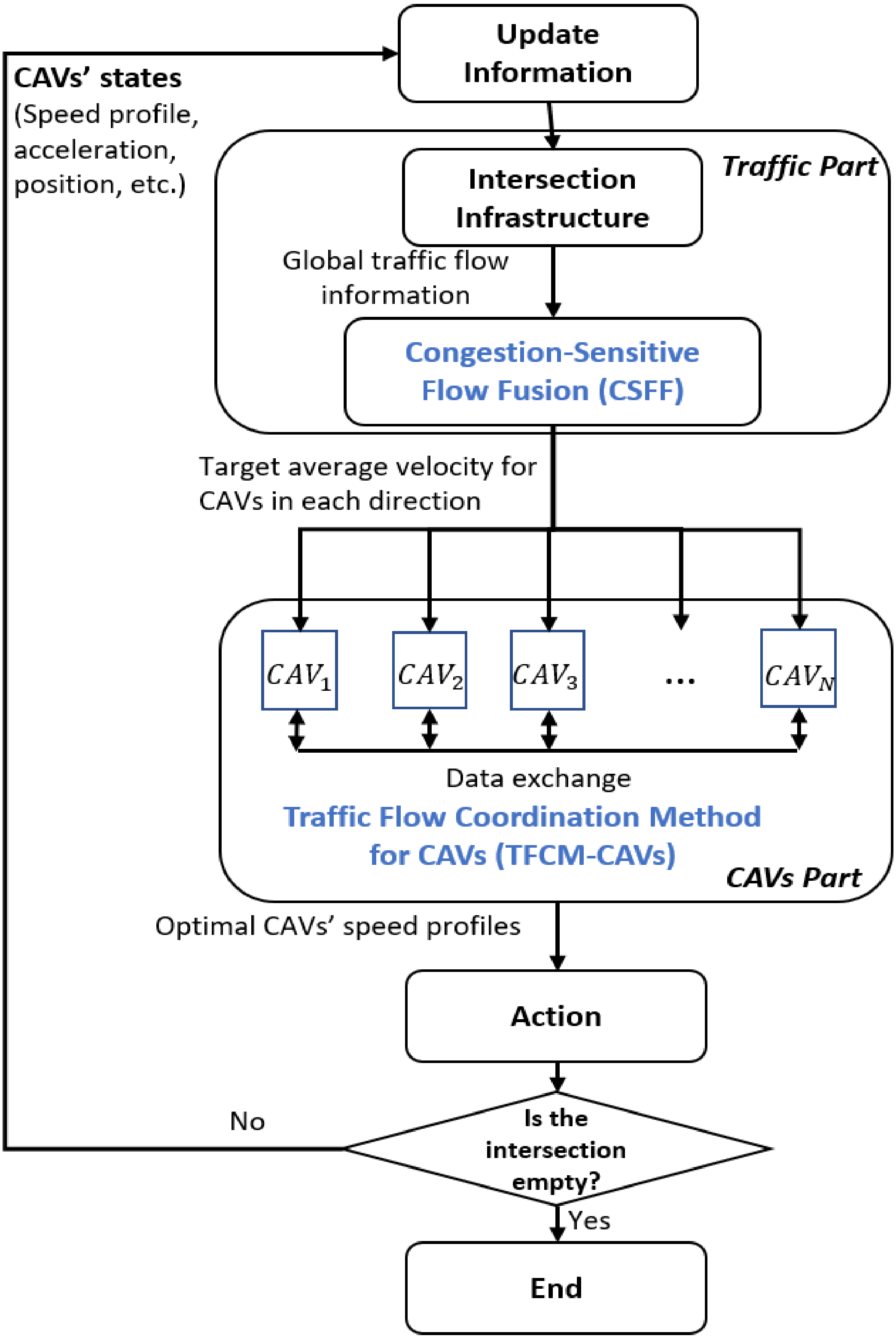

Figure 5.6: Proposed Traffic Flow Coordination Method for CAVs

5.3.3 *Traffic Flow Coordination Method for CAVs at Unsignalized Intersection*

In the previous sections, we developed CSFF to analyze and mitigate traffic congestion at unsignalized intersections. Now, we integrate this model with collision risk management to propose Traffic Flow Coordination Method for CAVs (TFCM-CAVs). This integration is realized through an optimization process, where objective functions and constraints are formulated to derive the optimal speed adjustment strategy. The goal is to ensure that all CAVs remain collision-free while allowing vehicles in each direction to achieve their target average speeds as closely as possible.

The proposed approach has two objectives:

1. Ensure at least one feasible solution free of collisions.
2. Identify solutions that allow CAVs to pass through intersections close to their current target speeds.

Based on the method for designing an objective function in Section 2.1.2 and the objective function (3.4) in Chapter 2, the objective function is consequently formulated in the following nonlinear model:

$$\begin{aligned} J(\mathbf{S}) =& W_{speed} \sum_{i \in V} \int_t (v_{d_i}^{target} - v_i(t)) + \\ & W_{penalty} \sum_{(i,j) \in E_C} (|ePIDP_{ij}^{ne}| + \frac{1}{t_{SNR_{ij}}}) \end{aligned} \tag{5.20}$$

where d_i is the direction of vehicle i and $v_{d_i}^{target}$ is the target average speed for direction d_i, $v_i(t)$ is speed profile of vehicle i. V is the set of all CAVs in the buffer circle, E_C denotes the set of all pairs of CAVs with a risk of collision between them. W_{speed} and $W_{penalty}$ are positive coefficients to balance between time efficiency and safety. $W_{penalty}$ is a large positive coefficient used to construct a penalty function. Whenever the proposed strategy entails a collision risk, this term generates an extremely high cost, rendering the strategy unacceptable. Thus, as evident from objective function (5.20), only a strategy that enables all vehicles to approach their respective target speeds as closely as possible while ensuring that all CAVs are free of collision risks will be deemed the current optimal strategy.

Having defined the objective function to balance speed optimization and collision avoidance for CAVs, we now outline how the TFCM-CAVs leverages the CSFF and the MRMCO-PIDP to fuse traffic flow dynamics and cooperative decision-making. Details of the TFCM-CAVs are given in Algorithm 7. The diagram of the TFCM-CAVs macroscopic and microscopic cooperative decision-making method is shown in Figure 5.6.

Firstly, according to the CSFF, it is necessary to obtain the current average speed, traffic density, and traffic flow for each direction of the intersection as well as the intersection center. The current traffic density k_i, average speed v_i, and traffic flow q_i in the direction i are given as:

$$v_i = \frac{N_i}{\sum_{j=1}^{N_i} \frac{1}{v_{i,j}}} \tag{5.21}$$

$$k_i = \frac{N_i}{r_{buffer}} \tag{5.22}$$

$$q_i = k_i v_i \tag{5.23}$$

Algorithm 7 Traffic Flow Coordination Method for CAVs (TFCM-CAVs)

while There are CAVs in the buffer circle of the intersection **do**
    Collect the current traffic flow q_i, traffic density k_i, and average speed v_i for each direction
    Collect the average vehicle speed of the intersection circle $v_{intersection}$
    \\ **CSFF part**
    if Traffic congestion at intersection ($v_{intersection} < 70\% * v_{max}$) **then**
        \\ Congestion happened
        Calculate Δv_i for each direction based on equation (5.8)
        if All Δv_i are positive or there exists a direction m such that $v_m^{target} < 0$ **then**
            Reweight $\Delta \tilde{v}_i$ based on equation (5.17)
            Replace all Δv_i by $\Delta \tilde{v}_i$
            for all Direction i with $\Delta v_i < 0$ **do**
                Update Δv_i using equation (5.13) and get the corresponding v_i^{target}
            end for
        end if
    else
        \\ No risk of congestion
        Set v_i^{target} to v_{max}
    end if
    \\ **TFCM-CAVs part**
    Compute the current best strategy S_{cur} for each CAV in the optimization circle using the MRMCO-PIDP
    Calculate the cost of the current best strategy $F(S_{cur})$ and the global best strategy $F(S_{best})$ for each vehicle in the optimization circle
    if $F(S_{cur}) < F(S_{best})$ **then**
        Replace the current global best strategy S_{best} with the current best strategy S_{cur}
    end if
end while

where N_i is the number of vehicles in the buffer circle from the direction i, $v_{i,j}$ is the speed of $j-th$ vehicle from the direction i. r_{buffer} is the radius of the buffer circle. The average speed within the intersection circle is given as:

$$v_{intersection} = \frac{N_v}{\sum_{i=1}^{N_v} \frac{1}{v_i}} \tag{5.24}$$

where $v_{intersection}$, N_v, and v_i are the average speed, the number of vehicles, and the speed of the $i-th$ vehicle in the intersection circle.

Secondly, if there is a risk of congestion in the intersection, which means the average speed in the intersection circle is less than the 70% maximum legal speed according to Section 5.3.1, the CSFF is applied and Δv_i for each direction of the intersection are then calculated.

Thirdly, we must check whether the current situation is one of the special scenarios discussed earlier. If it is, we need to reweight the Δv_i to $\Delta \tilde{v}_i$ from equation (5.17).

Then, the target speed for each direction in the intersection should be calculated from equation (5.9) or (5.19). If there is no risk of congestion at the intersection, meaning CAVs do not need to perform macroscopic traffic flow regulation, they can prioritize their own efficiency; therefore, the target speed should be set to the maximum legal speed of the intersection.

Finally, from the target speed for each direction of the intersection and the objective function (5.20), the MRMCO-PIDP will then determine the optimal speed profile for each CAV in the intersection to achieve collision avoidance and congestion mitigation.

5.4 SIMULATION RESULTS

In this section, simulations are conducted to validate both the CRMG-PIDP method, which is designed to reduce the computational load of risk assessment, and the TFCM-CAVs, which integrates macroscopic and microscopic traffic flow regulation. The former (CRMG-PIDP) provides the essential foundation for linking the proposed macroscopic approach with the microscopic layer. Without this method, the excessive computational load of risk assessment would severely limit the effectiveness of the interaction between traffic flow and intersection CAVs, thereby rendering the feasibility of the TFCM-CAVs method purely theoretical. Simulation results will be shown in Section 5.4.

5.4.1 *Simulation Environment*

Prior to commencing the simulation, it is necessary to introduce the simulation environment setup at the macroscopic level. In this new traffic flow simulation, the intersection-level topology introduced in Figure 3.2 remains valid. However, since the simulation adopts a method of estimating traffic flow based on vehicle frequency, we must extend the lane length used for vehicle counting. This extension is crucial to ensure that the acquired vehicle frequency data and the actual traffic flow data are as stable and undistorted as possible. The new intersection schematic is illustrated in Figure 5.7, which, compared to Figure 3.2, features a significantly extended measurement and control range for the intersection infrastructure.

In addition, considering that intervals between vehicles entering the intersection are random, extensive empirical data indicate that under low traffic density, these intervals

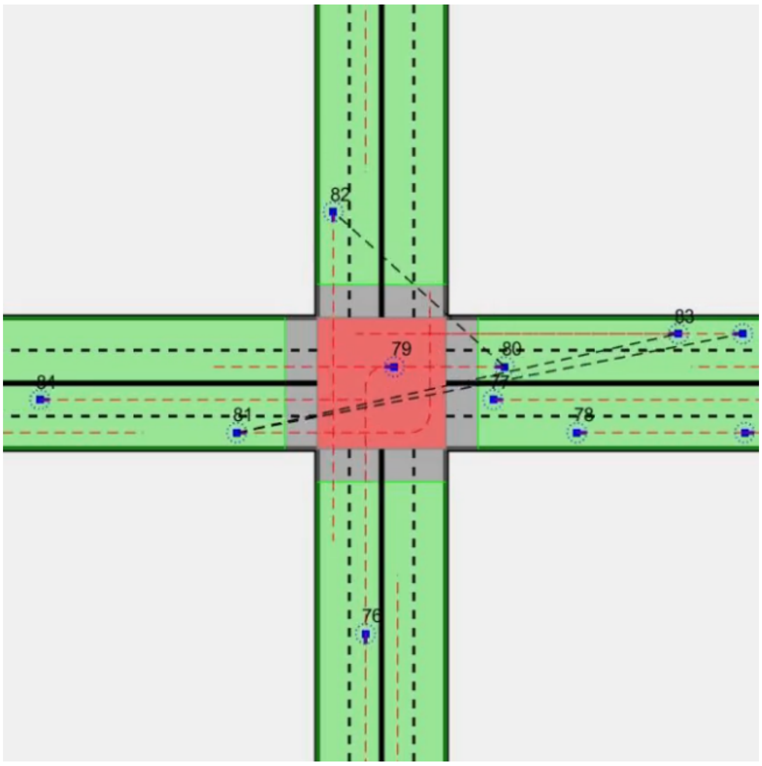

Figure 5.7: Example: The used intersection model and connectivity established by CAVs according to the possible risk of collision

closely follow a Poisson process [215]. Consequently, we use the Poisson distribution to model the relationship between vehicle arrival intervals and the average flow rate:

$$f_T(t_{gap}) = \lambda e^{-\lambda t}, t \geq 0 \tag{5.25}$$

where t_{gap} is the arrival interval between vehicles entering the buffer area (cf. Figure 3.2). λ is the traffic flow rate. f_T is the probability distribution corresponding to arrival intervals.

All the simulation videos in this chapter can be found in https://youtu.be/zTENIXb-kds.

5.4.2 *Analysis of Scalability and Computational Cost*

This subsection is dedicated to the critical validation of the proposed CRMG-PIDP framework under high-density traffic flow, which represents the most significant challenge for practical, real-world deployment. The analysis is structured to address the two primary objectives of this chapter: scalability (Can the method efficiently manage high traffic throughput?) and computational cost (Is the method fast enough for real-time control?).

To this end, we first qualitatively assess the resulting vehicle trajectories in a high-stress scenario to ensure stable and orderly coordination. We then quantitatively benchmark the framework's traffic efficiency against a standard FCFS baseline to measure its performance in mitigating control delays. Finally, a detailed statistical analysis of the computational iteration time is performed to rigorously verify the method's real-time feasibility and the effectiveness of the proposed optimization strategies.

Figures 5.8 provide a qualitative validation of the proposed CRMG-PIDP framework's behavior under a high-stress scenario, specifically a conflicting flow rate of 3000 veh/h. To ensure clarity and simplify the visualization, only the trajectories of vehicles entering the

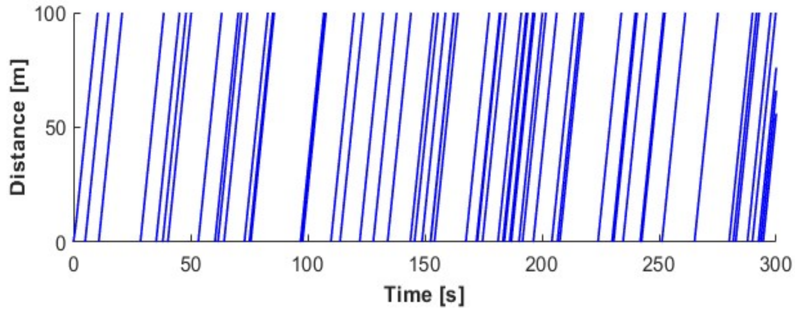

(a) The trajectories of vehicles from the east direction

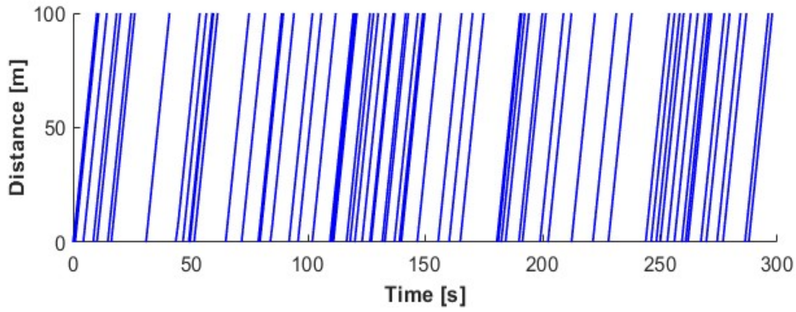

(b) The trajectories of vehicles from the north direction

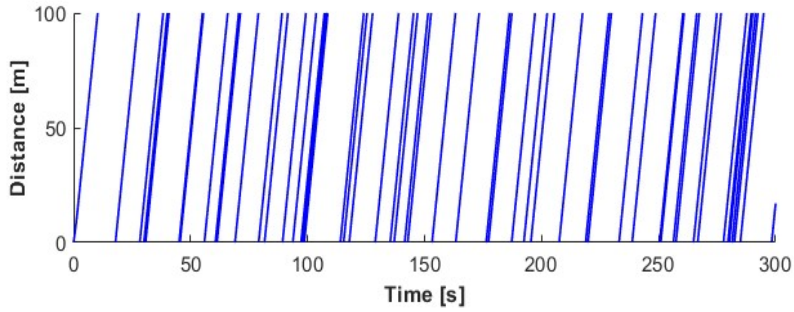

(c) The trajectories of vehicles from the west direction

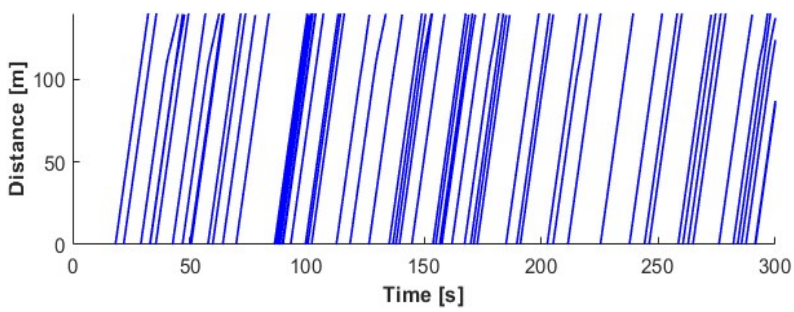

(d) The trajectories of vehicles from the south direction

Figure 5.8: Trajectories of CAVs from different entry directions

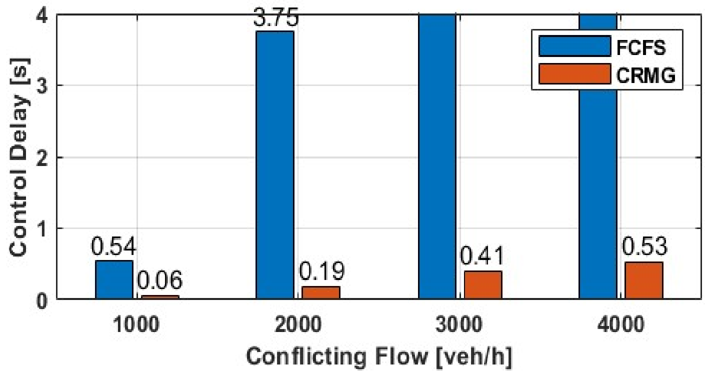

Figure 5.9: Control delay with different conflicting flow

system during the first 300 seconds of the simulation are represented. As depicted in the figure, the vast majority of vehicles exhibit smooth, continuous trajectories. This visual evidence indicates that the optimization framework is successfully resolving conflicts in an orderly and efficient manner, allowing vehicles to safely navigate the intersection without resorting to abrupt, hard-braking maneuvers or unnecessary stops.

Moving to a quantitative assessment of efficiency, Figure 5.9 presents a comparative analysis of the average control delay between the classic First Come First Serve (FCFS) method and the proposed CRMG method under a wide range of conflicting traffic flows. The FCFS method, serving as a standard baseline, performs adequately in low to moderate traffic conditions. However, its performance rapidly degrades as the traffic volume increases. A sharp inflection point is observed where the vehicle arrival rate surpasses the intersection's service capacity, leading to exponential queue growth and a sharp, unbounded increase in delay times. Consequently, when the traffic flow exceeds 2000 veh/h, the FCFS method becomes saturated and impractical for managing the intersection. In stark contrast, the CRMG method demonstrates superior performance, remaining effective and stable even under heavy conflicting flows of up to 4000 veh/h. More importantly, it achieves significantly lower control delays across the entire spectrum of traffic volumes. These results clearly indicate that the CRMG method not only outperforms the FCFS baseline but fundamentally redefines the intersection's operational capacity.

Finally, Figure 5.10 addresses the critical non-functional requirement of computational feasibility. This figure shows the statistical distribution (as a boxplot) of the computation time per iteration under three distinct optimization conditions, all tested at a high-stress load of 4000 veh/s and compared against the hard real-time constraint of the 0.1 s sampling interval ($t_{sampling}$).

1. **Unoptimized (MRMCO-PIDP):** We first observe that without any of the proposed optimizations, the base MRMCO-PIDP algorithm is computationally infeasible. Its average computation time of 0.23 s far exceeds the 0.1 s sampling interval, proving that a naive implementation is too long for real-time traffic applications.

2. **CRMG Optimization Only:** When only the CRMG method (the graph-based topology filtering) is employed, the average iteration time is successfully reduced to 0.064 s. While this average is below the 0.1 s threshold, the distribution reveals a significant stability problem. The variance remains considerable: the Q3 (75th percentile) reaches 0.1 s, and the upper whisker extends to 0.257 s. This indicates

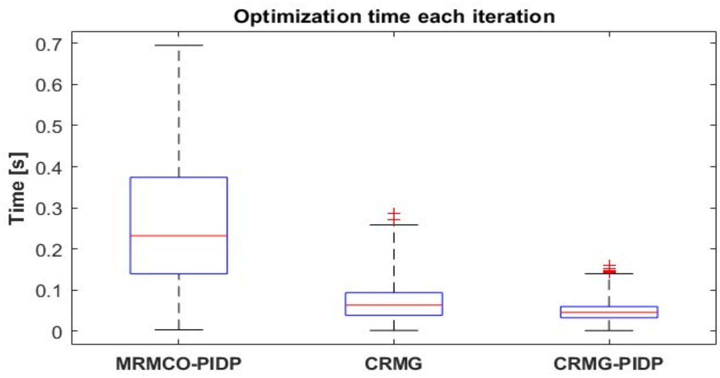

Figure 5.10: Time cost each iteration for different method

that in 25% of all cases, the iteration time still exceeds the sampling interval, making the system unreliable.

3. **Full Method (CRMG-PIDP):** In contrast, when the full CRMG-PIDP method is applied, the average iteration time further decreases to 0.046 s. More critically, the system's stability is substantially improved. The Q3 is reduced to 0.060 s and the upper whisker to 0.140 s.

Compared to both the unoptimized case and the intermediate CRMG-only scenario, the complete CRMG-PIDP method is the only one to demonstrate both high computational efficiency and, crucially, the safety required for real-world deployment. This proves that the combination of graph-based and PIDP-based filtering is essential for making the proposed cooperative framework feasible for real-time, complex, and dynamic environments.

5.4.3 *Multi-Scale Traffic Collaboration*

Having established the computational feasibility and real-time scalability of the CRMG-PIDP method in the previous section, the analysis now shifts to its ultimate objective: mitigating system-level congestion. The previous validation ensured the microscopic layer is fast enough to operate in dense traffic; this section validates whether the full, multi-scale architecture (TFCM-CAVs), which integrates this fast microscopic layer with macroscopic flow control, delivers superior performance compared to a purely microscopic approach (MRMCO-PIDP).

To quantify this system-level benefit, a comparative simulation was designed to benchmark the performance of the full TFCM-CAVs framework against the micro-only MRMCO-PIDP approach. Both methods were evaluated under challenging, high-density stochastic traffic flow conditions of 2000 and 3000 veh/h. The key performance indicators (KPIs) for this analysis were the average waiting delay and the intersection congestion rate. The congestion rate is formally defined as the ratio of time the intersection is in a congested state (i.e., $v_{intersection} < 70\% v_{max}$) to the total simulation time. All presented results are averaged from multiple replications of 1000 stochastic scenarios to ensure statistical robustness.

The results, summarized in Table 5.1, unequivocally demonstrate that the multi-scale TFCM-CAVs framework consistently outperforms the purely microscopic MRMCO-PIDP in terms of average waiting delay across all tested scenarios. This superior performance is attributed to the macroscopic layer's ability to proactively manage flow and provide

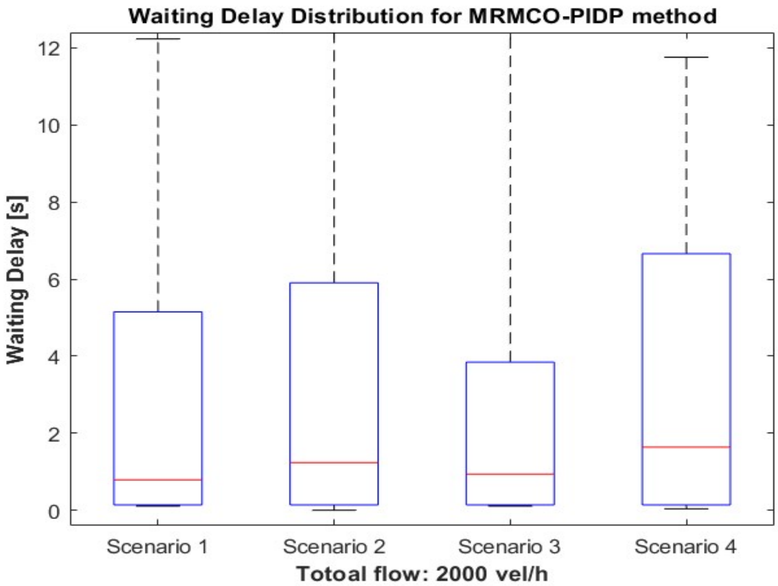

(a) MRMCO-PIDP architecture

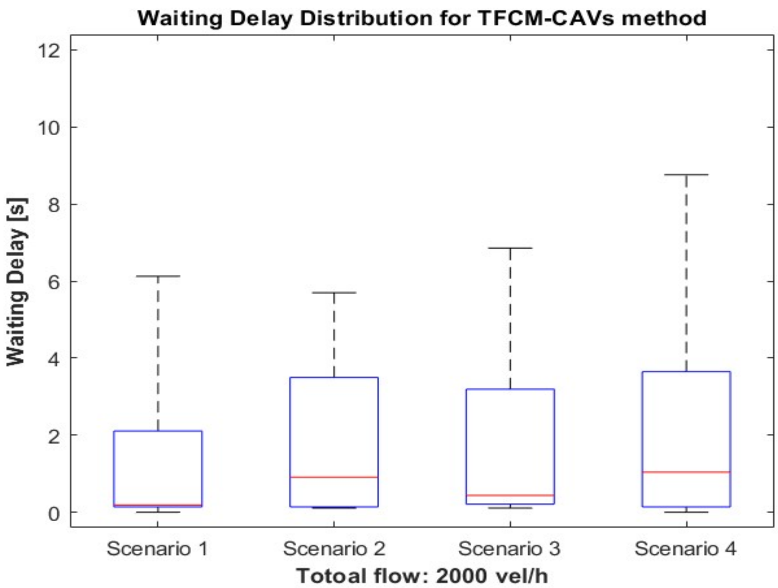

(b) TFCM-CAVs architecture

Figure 5.11: Distribution of time delays caused by traffic congestion at 2000 veh/h

Table 5.1: Evaluation of Congestion Mitigation Methods in Different Traffic Scenarios

Scenario	Total Flow (veh/h)	Direction	Flow (veh/h)	MRMCO-PIDP		TFCM-CAVs	
				Avg Delay (s)	Congestion Rate (%)	Avg Delay (s)	Congestion Rate (%)
1	2000	South East	1000 1000	2.56	6.84	1.89	3.34
2	2000	South East	1200 800	2.71	14.02	1.80	3.34
3	2000	South East	1500 500	2.8	13.19	1.85	4.17
4	2000	South East	1600 400	3.15	17.03	1.94	2.84
5	3000	South East	1500 1500	2.02	7.85	1.78	4.51
6	3000	South East	1800 1200	2.05	7.18	1.86	5.51
7	3000	South East	2250 750	2.11	6.68	1.56	6.01
8	3000	South East	2400 600	2.76	6.51	2.06	5.67

predictive speed guidance, preventing the onset of saturation. For instance, under the 2000 veh/h condition, the micro-only MRMCO-PIDP yielded an average delay of 2.5 to 3.2 s/veh, whereas TFCM-CAVs reduced this to 1.8 to 2.0 s/veh, achieving a significant reduction of approximately 37.5%. This performance gap is maintained even under the heavier 3000 veh/h flow, where TFCM-CAVs held delays to 1.6–2.0 s/veh compared to 2.0–2.8 s/veh for MRMCO-PIDP, representing a 25.0% improvement. The impact on the congestion rate was particularly pronounced, with the TFCM-CAVs framework reducing the total time the intersection spent in a congested state by approximately 40%.

Furthermore, beyond the average values, an analysis of the delay distribution, presented as boxplots in Figures 5.11 and 5.12, reveals another critical advantage. The TFCM-CAVs method produces a visibly more concentrated distribution of waiting delays, characterized by a smaller interquartile range. This tighter distribution is highly significant, as it indicates that the multi-scale approach not only reduces the average delay but also enhances the stability and predictability of the system, minimizing delay fluctuations across individual vehicles and ensuring a more equitable quality of service.

In summary, the TFCM-CAVs framework exhibits robust and superior performance across all tested traffic flow conditions. Its clear advantages in simultaneously reducing average delay, lowering the congestion rate, and optimizing the delay distribution affirm the feasibility, robustness, and significant benefit of the proposed multi-scale integration for congestion mitigation at dense unsignalized intersections.

5.5 CONCLUSION

This chapter extended the proposed architecture from the microscopic vehicle coordination frameworks developed in the previous chapters to a multi-scale architecture. This step was motivated by the necessity of integrating local, vehicle-level interactions with the broader context of system-level traffic dynamics. The work presented herein therefore investigated how to achieve this integration, developing the necessary methodologies to first ensure

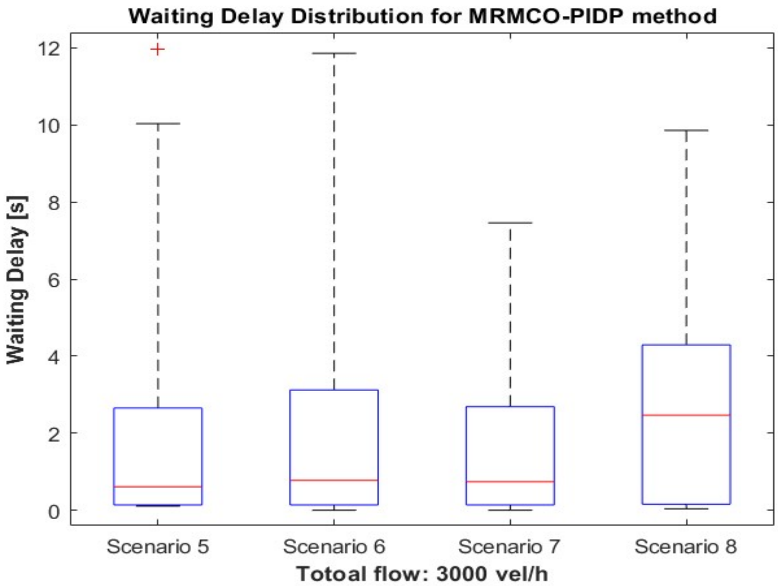

(a) MRMCO-PIDP architecture

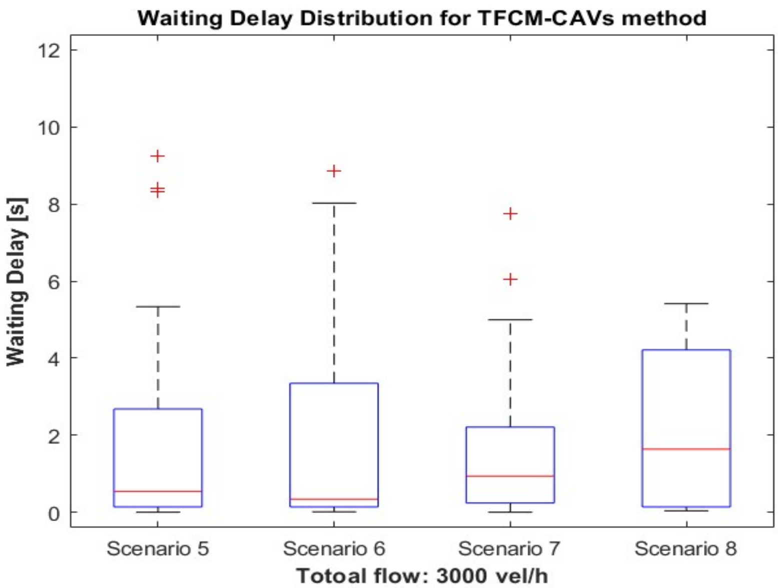

(b) TFCM-CAVs architecture

Figure 5.12: Distribution of time delays caused by traffic congestion at 3000 veh/h

the microscopic framework is scalable to high-density traffic, and second, to functionally connect it with macroscopic flow control.

First, to render a solution computationally feasible for high-density traffic, the graph-based Contextual Risk Management Graph (CRMG) and CRMG based on PIDP (CRMG-PIDP) methods were introduced. As the validation results confirmed, these methods are highly effective at characterizing collision risks while simultaneously and significantly reducing the computational burden of risk assessment. This optimization was proven to be a critical enabler, providing the real-time performance necessary for any practical, large-scale deployment.

Building upon this scalable and efficient microscopic foundation, the chapter then introduced the macroscopic control layer. The Congestion-Sensitive Flow Fusion (CSFF) model was proposed to formally analyze and define congestion risk at the intersection from a traffic flow perspective. This macroscopic insight was then operationalized via the Traffic Flow Coordination Method for CAVs (TFCM-CAVs). This framework successfully integrates the macroscopic speed directives from the CSFF model into the vehicles' cooperative decision-making logic. Simulation results demonstrated that this integrated multi-scale approach significantly outperforms purely microscopic strategies, achieving substantial reductions in both average waiting delays and overall congestion rates.

In summary, by bridging the gap between microscopic decision-making and macroscopic traffic dynamics, the methodologies developed in this chapter provide a complete and feasible framework for managing dense traffic at unsignalized intersections, achieving both local collision avoidance and system-level congestion mitigation.

CONCLUSION AND PROSPECTS

CONCLUSION

This PhD thesis proposes several contributions to multi-level cooperative decision-making for Connected Autonomous Vehicles (CAVs) in smart city mobility. It integrates the cooperative decision-making process of vehicles near urban intersections at the microscopic scale with the management and optimization of the overall intersection traffic flow at the macroscopic scale, thereby enabling a better solution for smart city mobility. The topics explored encompass a bottom-up, multi-level, yet holistically unified problem: progressing from single collision risk assessment of CAVs to multi-risk assessment and management and cooperative decision-making; from centralized to decentralized architectures; from cooperative decision-making under certainty to uncertainty; from enhancing risk management effectiveness with a limited number of CAVs to improving the computational efficiency of risk assessment in complex continuous traffic flows; and from specific CAV speed planning to urban intersection traffic flow management. This progression also represents the logical structure of this thesis, which builds a comprehensive solution layer by layer.

Chapter 1 begins by introducing the vehicle architecture, decision-making and planning of a single autonomous vehicle, gradually extending these concepts to CAVs. It further details the importance of CAVs in smart city mobility and related technologies, ultimately broadening the scope to include research on overall traffic flow management methods. This chapter comprehensively introduces the relevant research achievements, from microscopic individual vehicle behavior to macroscopic traffic flow management.

Building on the foundation of Chapter 1, Chapter 2 provides a detailed introduction to various methods proposed by other researchers that are relevant to this thesis. This includes foundational work that will be adopted as core components of this thesis's methodology, such as the Predicted Inter-Distance Profile (PIDP) and techniques for formulating objective functions in optimization algorithms.

Chapter 3 introduces the first core contribution: the Multi-Risk Management Cooperative Optimization based on PIDP (MRMCO-PIDP). This novel framework aims to quickly and efficiently manage complex, simultaneous, and overlapping collision risks among multiple CAVs. This method uses PIDP as the foundation for risk assessment and management, fully leverages the information-sharing characteristics of CAVs, and can make more rational risk assessments and more effective cooperative decisions through richer information. The method is then instantiated in two different architectures: the centralized Dynamic Collision-Free Cooperation (DCFC) and the decentralized Dynamic Multi-Risk Management Cooperative Optimization (D-MRMCO). Simulation results confirmed the method's feasibility and, critically, demonstrated that the decentralized D-MRMCO architecture provides exceptional computational scalability, a vital prerequisite for any practical application.

Chapter 4 directly addresses the deterministic limitations of the initial framework by confronting the challenge of uncertainty. This chapter proposes a PIDP-based Probabilistic Uncertainty Interval (PIDP-PUI) method as a novel hybrid methodology. This approach fuses the efficiency of probabilistic forecasting with the hard guarantees of set-based analysis, enabling robust decision-making even under severe stochastic disturbances. Its effectiveness was validated in critical communication loss scenarios, where the PIDP-PUI framework was shown to be capable of identifying and correcting the outputs of unreliable predictors. This allowed it to maintain a high safety margin in volatile situations where standard expectation-based methods failed.

Finally, Chapter 5 integrates these components into a complete, multi-scale architecture, thereby solving the remaining challenges of scalability and system-level integration. First, the Contextual Risk Management Graph (CRMG-PIDP) was introduced. This method, by analyzing vehicle turning strategies and trajectories at the intersection, effectively reduces the computational load of a large number of unnecessary risk assessment steps between vehicles, thereby saving valuable time in the optimization process. Second, the microscopic foundation from Chapters 3 and 4 was connected to the macroscopic layer. The Congestion-Sensitive Flow Fusion (CSFF) model was developed to analyze congestion from a traffic flow perspective, and the Traffic Flow Coordination Method (TFCM-CAVs) was proposed to translate these high-level directives into effective speed commands for CAVs in specific directions. Simulation results confirmed that this fully integrated framework significantly outperforms purely microscopic strategies, substantially reducing both average waiting delays and overall congestion rates.

In summary, this thesis successfully designed, developed, and validated a complete multi-level framework, enabling CAVs to act as cooperative agents to promote sustainable urban mobility. From the microscopic risk management of MRMCO-PIDP, to the robust uncertainty handling of PIDP-PUI, and culminating in the scalable, macro-micro integrated TFCM-CAVs architecture, this work provides a feasible and holistic solution. It demonstrates how cooperative decision-making can evolve beyond local conflict resolution to become an active and effective tool for managing systemic-level urban congestion.

PROSPECTS

The work in this thesis has yielded promising results for the proposed multi-level cooperative decision-making architecture, demonstrating effective improvements in urban traffic congestion within the simulation environment. The exceptional scalability of the MRMCO-PIDP method, in particular, confirms its viability for resolving complex multi-agent conflict problems. At the same time, we must recognize that the proposed methods still have limitations. For instance, the scope was confined to a homogeneous environment consisting entirely of CAVs, neglecting to explicitly deal with mixed-traffic more immediate reality of mixed-traffic scenarios with Human-Driven Vehicles (HDVs). Therefore, our future work will proceed along the following directions:

Improvement and Refinement of the CAV Multi-level Cooperative Decision-Making Architecture

1. **Integration of Heterogeneous Traffic with HDVs:** A critical next step is to extend the framework to heterogeneous traffic environments where CAVs and Human-Driven Vehicles (HDVs) coexist. The presence of non-cooperative human drivers introduces a high degree of stochasticity and unpredictable behavior. This scenario presents a clear opportunity to leverage the methodology developed in Chapter 4. An HDV can be modeled as an observable, yet non-communicating agent—functionally similar to a CAV that has suffered communication loss. Therefore, a

promising direction is to integrate the PIDP-PUI method into the proposed multi-level architecture to robustly manage these interactions. Furthermore, beyond treating HDVs as purely stochastic entities, future work could explore the development of reliable behavioral models based on different human driving styles. By observing an HDV's trajectory and actions, these models could be used to infer its likely driving style and generate more informed, less conservative predictions of its future behavior.

2. **Exploration of Hybrid Cooperative Architectures:** This thesis investigated distinct centralized (DCFC) and decentralized (D-MRMCO) architectures built upon the MRMCO-PIDP method. Future research could explore hybrid frameworks that strategically combine the strengths of both paradigms. For instance, a hybrid system might employ a centralized layer for high-level coordination or priority setting, while retaining decentralized negotiation for local trajectory adjustments. Another interesting direction involves coordinating traffic across adjacent intersections where different architectural choices (e.g., one centralized, one decentralized) might be implemented. Developing protocols for seamless inter-architecture cooperation would be essential for network-level scalability.

3. **Adoption of Advanced Multi-Level Models:** The current framework relies on the Greenshields model to describe macroscopic traffic flow. While simple and effective for a foundational study, a more precise description of the current traffic state would enable more accurate analysis and prediction. It is therefore necessary to replace this with more advanced macroscopic traffic flow models, such as the Daganzo-Newell triangular model or a complete Macroscopic Fundamental Diagram (MFD) for network-level control. Furthermore, in the current TFCM-CAVs model, the only link between the macroscopic flow management and microscopic decision-making is a target speed advisory. This is insufficient. It is necessary to develop richer connections, such as allowing the macroscopic layer to suggest strategic lane changes, which would alter the conflict point locations and further optimize vehicle throughput and congestion.

4. **Incorporation of Learning-Based Methods:** The current framework relies primarily on model-based optimization and analytical techniques (PIDP, interval analysis, graph methods, CSFF). There is significant potential in exploring the integration of machine learning, particularly Deep Reinforcement Learning, into the decision-making process. DRL agents could potentially learn highly effective, non-linear control policies for both microscopic risk management (potentially enhancing MRMCO-PIDP) and macroscopic traffic flow optimization (offering an alternative to the analytical CSFF model). Moreover, learning could be applied to improve the prediction models used within the PIDP-PUI framework, especially for complex HDV behaviors.

Simulations

The established simulation architecture provides a solid foundation for the testing and validation of the cooperative decision-making and control strategies for CAVs. However, these simulations have thus far been conducted exclusively within MATLAB and Simulink. To enhance the realism of these simulations and further strengthen the robustness assessment of the developed strategies, several extensions can be considered.

For instance, integrating the proposed methods into widely adopted frameworks such as ROS2[1], or potentially onto automotive-grade platforms adhering to standards like Adaptive AUTOSAR[2], would bridge the gap towards real-world implementation. Furthermore, to rigorously validate the PIDP-PUI method's performance in uncertain environments, these more advanced simulation platforms could be leveraged to incorporate inherent systemic uncertainties (such as localization uncertainty or communication noise), thereby enriching the test scenarios beyond communication loss alone. The complex urban environment also introduces significant challenges related to timing and synchronization in cooperative decision-making, which could be explored in these richer simulations. These extensions aim to make the simulations more representative of real-world conditions and facilitate a more comprehensive and exhaustive evaluation of the proposed control/command strategies.

Experiments

The implementation of the proposed D-MRMCO architecture on a fleet of small-scale autonomous vehicles (3 QCars) is currently underway. This critical step allows for testing the performance and efficiency of DCFC and D-MRMCO methods in complex real-world environments featuring various intersection scenarios. However, migrating this framework from simulation to the real world introduces numerous challenges that were justifiably ignored in this thesis, including, but not limited to, the specifics of CAV communication protocols and infrastructure-based sensing methods.

Beyond the previously mentioned communication challenges, another key issue is the integration of localization. We need to rely on an efficient localization system to simulate the functionality of intersection infrastructure. This will enable the CAVs to obtain relatively accurate information about other vehicles that are outside their own detection range.

Therefore, a more immediate and feasible application path is to adapt this framework to scenarios dominated by Autonomous Mobile Robot (AMR), such as in automated port terminal management or warehouse logistics. These environments are often human-free, mitigating the immediate safety risks associated with software or hardware failures. More importantly, such an application can be abstracted as a miniature smart city composed of dozens of intersections, providing a perfect testbed for validating the multi-level coordination and scalability of the proposed architecture in a controlled, real-world setting.

1 ROS2: https://www.ros.org/
2 AUTOSAR: https://www.autosar.org/

APPENDIX A

OBJECTIVE FUNCTION FOR ENERGY COST

As established in Section 3.3.1, energy cost is a significant component of a comprehensive objective function. This component was, however, intentionally omitted from the objective functions formulated in the preceding chapters. The primary reason for this omission stems from an inherent conflict: minimizing energy consumption typically involves reducing vehicle speeds, which directly opposes one of the primary research objectives of this thesis: ensuring the rapid passage of CAVs through the intersection. The inclusion of an energy cos term would have directly confounded the evaluation of the proposed methods' effectiveness in achieving this primary goal. Nevertheless, it is intended in the used objective function to avoid important acceleration increase or decrease, which ensure, in certain manner, the fact to optimize the consumed energy. This section will now detail the formulation of a new objective function that explicitly and properly integrates energy consumption.

First, equation (2.2) in Section 2.1.2 presented the vehicle's energy consumption model, where the integrand represents instantaneous power. For convenience and clarity, the equation is restated as follows:

$$f_{fuel}(t) = \int_{t_0} \frac{1}{\eta}(\frac{1}{2}\rho C_d A v(t)^3 + mgC_r v(t) + mv(t)|a(t)| + F_{idle})dt$$

It is evident that a vehicle's power consumption is positively correlated with its velocity. Consequently, if an energy-related objective function is naively designed to simply "minimize power", it will invariably drive the optimal vehicle speed towards zero. This leads to a trivial (but operationally useless) solution: all vehicles at the intersection would slow to a stop, achieving the minimum possible power draw (to maintain system operation) but failing to move and thus failing to complete their primary task. Therefore, it is essential that the energy consumption objective be linked to the completion of the task.

TASK-BASED ENERGY EFFICIENCY MANAGEMENT

In order to link the completion of the task and the energy consumption objective, this necessitates a reformulation of the problem. Previously, power was used to represent energy cost, which is effectively the derivative of energy with respect to time (dE/dt). The intuitive representation of the task ("crossing the intersection"), however, is distance. It is, therefore, necessary to express this objective as energy consumption relative to distance (dE/dx or $E(t)/x(t)$), not time. This concept is analogous to the real-world metric of "fuel consumption per 100 kilometers" (e.g., L/100 km). Based on this reasoning, a new expression can be formulated to optimize the vehicle's speed by minimizing its energy consumption per unit distance:

$$P_{fuel}(t) = \frac{f_{fuel}(t)}{\int_{t_0} v(t)dt}$$

Based on the aforementioned equation, it is evident that as the vehicle's velocity approaches zero, the resulting cost function (representing energy per unit distance) will tend towards infinity. This property inherently penalizes near-zero speeds, thus resolving the trivial solution ($v = 0$) problem encountered with the power-based model. Consequently, the optimization process will compel the vehicle to find an optimal speed profile that maximizes its energy efficiency (analogous to achieving the maximum travel distance for the minimum fuel consumption). Therefore, this expression can be directly adopted as the energy-cost component within the objective function for an optimization-based vehicle speed planning method.

BIBLIOGRAPHY

[1] S. He and L. Adouane, “A hybrid coordinated decision-making method for cavs at unsignalized intersection,” in *2024 European Control Conference (ECC)*, 2024, pp. 3769–3776. DOI: 10.23919/ECC64448.2024.10591063 (cit. on p. 19).

[2] S. He and L. Adouane, “Reactive cooperation of multi-vehicle system for efficient intersection crossing based on pidp speed space assessment,” in *2024 13th International Workshop on Robot Motion and Control (RoMoCo)*, 2024, pp. 142–148. DOI: 10.1109/RoMoCo60539.2024.10604427 (cit. on p. 19).

[3] S. He and L. Adouane, “A dynamic multi-risk management based on cooperative optimization architecture for cavs at unsignalized intersection,” *IFAC-PapersOnLine*, vol. 58, no. 18, pp. 71–77, 2024, 8th IFAC Conference on Nonlinear Model Predictive Control NMPC 2024, ISSN: 2405-8963. DOI: https://doi.org/10.1016/j.ifacol.2024.09.012. [Online]. Available: https://www.sciencedirect.com/science/article/pii/S2405896324013910 (cit. on p. 19).

[4] S. He and L. Adouane, “Energy efficiency of cavs in unsignalized intersections based on cooperative risk-assessment strategy,” in *Proceedings of the Symposium on Technological Systems, Sustainability and Safety (TS3 2024)*, Paris, France, 2024 (cit. on p. 19).

[5] S. He and L. Adouane, “Energy-efficient cooperative decision-making for cavs: a traffic flow optimization approach,” in *2025 20th Annual System of Systems Engineering Conference (SoSE)*, 2025, pp. 1–6. DOI: 10.1109/SoSE66311.2025.11083785 (cit. on pp. 19, 39).

[6] S. He and L. Adouane, “Safe cooperative decision-making in uncertain unsignalized intersection based on probabilistic and predictive risk assessment strategy,” in *2025 IEEE Intelligent Vehicles Symposium (IV)*, 2025, pp. 1140–1147. DOI: 10.1109/IV64158.2025.11097798 (cit. on p. 19).

[7] S. He and L. Adouane, “Contextual-graph topology for efficient and real-time cooperative intersection management,” *IFAC-PapersOnLine*, vol. 59, no. 3, pp. 151–156, 2025, 12th IFAC Symposium on Intelligent Autonomous Vehicles IAV 2025, ISSN: 2405-8963. DOI: https://doi.org/10.1016/j.ifacol.2025.07.026. [Online]. Available: https://www.sciencedirect.com/science/article/pii/S2405896325003659 (cit. on pp. 19, 123).

[8] S. He and L. Adouane, “Multi-scale cooperative decision-making in unsignalized intersections integrating traffic flow dynamics,” *Transportation Research Part D: Transport and Environment*, 2025, Submitted for publication, under review (cit. on p. 20).

[9] TomTom, *Tomtom traffic index: ranking 2024*, Accessed: 2025-10-08, 2024. [Online]. Available: https://www.tomtom.com/traffic-index/ranking/?country=FR%5C%2CUK (cit. on pp. 23, 24).

[10] U.S. Department of Transportation, "Critical reasons for crashes investigated in the national motor vehicle crash causation survey," National Highway Traffic Safety Administration, Tech. Rep., 2018 (cit. on p. 23).

[11] Statista Research Department. "Transportation emissions worldwide – statistics & facts." Published by Statista Research Department, Accessed: Oct. 10, 2025 (cit. on p. 23).

[12] H. Ritchie, "Cars, planes, trains: where do co_2 emissions from transport come from?" *Our World in Data*, 2020, https://ourworldindata.org/co2-emissions-from-transport (cit. on p. 23).

[13] E. COMMISSION, *White paper-roadmap to a single european transport area–towards a competitive and resource efficient transport system*, 2011 (cit. on p. 24).

[14] A. AbuLibdeh, "Traffic congestion pricing: methodologies and equity implications," in *Urban Transport Systems*, H. Yaghoubi, Ed., London: IntechOpen, 2017, ch. 11. DOI: 10.5772/66569. [Online]. Available: https://doi.org/10.5772/66569 (cit. on p. 24).

[15] S. Shaheen, A. Stocker, and R. Meza, "Social equity impacts of congestion management strategies," UC Berkeley Recent Work, Ph.D. dissertation, University of California, Berkeley, 2019. [Online]. Available: https://escholarship.org/uc/item/9z9618mn (cit. on p. 24).

[16] Y. Guo, Z. Tang, and J. Guo, "Could a smart city ameliorate urban traffic congestion? a quasi-natural experiment based on a smart city pilot program in china," *Sustainability*, vol. 12, no. 6, 2020, ISSN: 2071-1050. DOI: 10.3390/su12062291. [Online]. Available: https://www.mdpi.com/2071-1050/12/6/2291 (cit. on p. 24).

[17] S. Djahel et al., "Toward v2i communication technology-based solution for reducing road traffic congestion in smart cities," in *2015 International Symposium on Networks, Computers and Communications (ISNCC)*, 2015, pp. 1–6. DOI: 10.1109/ISNCC.2015.7238584 (cit. on p. 24).

[18] G. P. Rocha Filho et al., "Enhancing intelligence in traffic management systems to aid in vehicle traffic congestion problems in smart cities," *Ad Hoc Networks*, vol. 107, p. 102 265, 2020, ISSN: 1570-8705. DOI: https://doi.org/10.1016/j.adhoc.2020.102265. [Online]. Available: https://www.sciencedirect.com/science/article/pii/S1570870520302195 (cit. on p. 24).

[19] D. V. Gibson, G. Kozmetsky, and R. W. Smilor, *The technopolis phenomenon: Smart cities, fast systems, global networks*. Bloomsbury Publishing PLC, 1992 (cit. on p. 25).

[20] M. Ilyas, "Iot applications in smart cities," in *2021 International Conference on Electronic Communications, Internet of Things and Big Data (ICEIB)*, 2021, pp. 44–47. DOI: 10.1109/ICEIB53692.2021.9686400 (cit. on p. 25).

[21] Y. Mehmood et al., "Internet-of-things-based smart cities: recent advances and challenges," *IEEE Communications Magazine*, vol. 55, no. 9, pp. 16–24, 2017. DOI: 10.1109/MCOM.2017.1600514 (cit. on p. 25).

[22] Z. Zhang, "Research on the construction mode of intelligent traffic safety integration under the background of intelligent city," in *2020 International Conference on Intelligent Transportation, Big Data & Smart City (ICITBS)*, 2020, pp. 57–60. DOI: 10.1109/ICITBS49701.2020.00020 (cit. on p. 25).

[23] A. Kirimtat et al., "Future trends and current state of smart city concepts: a survey," *IEEE Access*, vol. 8, pp. 86 448–86 467, 2020. DOI: 10.1109/ACCESS.2020.2992441 (cit. on p. 25).

[24] C. Harrison et al., "Foundations for smarter cities," *IBM Journal of Research and Development*, vol. 54, no. 4, pp. 1–16, 2010. DOI: 10.1147/JRD.2010.2048257 (cit. on p. 25).

[25] L. Chen and C. Englund, "Cooperative intersection management: a survey," *IEEE Transactions on Intelligent Transportation Systems*, vol. 17, no. 2, pp. 570–586, 2016. DOI: 10.1109/TITS.2015.2471812 (cit. on p. 25).

[26] L. Banda, M. Mzyece, and F. Mekuria, "5g-iot and sustainability: smart city use case," in *2024 IEEE 100th Vehicular Technology Conference (VTC2024-Fall)*, 2024, pp. 1–5. DOI: 10.1109/VTC2024-Fall63153.2024.10757586 (cit. on p. 25).

[27] H. Chen, L. Yuan, and G. Jing, "5g boosting smart cities development," in *2020 2nd International Conference on Artificial Intelligence and Advanced Manufacture (AIAM)*, 2020, pp. 154–157. DOI: 10.1109/AIAM50918.2020.00038 (cit. on p. 25).

[28] T. Campisi et al., "The development of the smart cities in the connected and autonomous vehicles (cavs) era: from mobility patterns to scaling in cities," *Infrastructures*, vol. 6, no. 7, 2021, ISSN: 2412-3811. [Online]. Available: https://www.mdpi.com/2412-3811/6/7/100 (cit. on p. 25).

[29] A. Elawady, M. Abuzwidah, and W. Zeiada, "The benefits of using connected vehicles system on traffic delay and safety at urban signalized intersections," in *2022 Advances in Science and Engineering Technology International Conferences (ASET)*, 2022, pp. 1–6. DOI: 10.1109/ASET53988.2022.9734911 (cit. on p. 25).

[30] Y. Ren et al., "Green intelligence networking for connected and autonomous vehicles in smart cities," *IEEE Transactions on Green Communications and Networking*, vol. 6, no. 3, pp. 1591–1603, 2022. DOI: 10.1109/TGCN.2022.3148293 (cit. on p. 25).

[31] M. Matowicki and O. Pribyl, "The need for balanced policies integrating autonomous vehicles in cities," in *2020 Smart City Symposium Prague (SCSP)*, 2020, pp. 1–7. DOI: 10.1109/SCSP49987.2020.9134030 (cit. on p. 25).

[32] W. Gillan, "Prometheus and drive: their implications for traffic managers," in *Conference Record of papers presented at the First Vehicle Navigation and Information Systems Conference (VNIS '89)*, 1989, pp. 237–243. DOI: 10.1109/VNIS.1989.98769 (cit. on p. 26).

[33] Wikipedia contributors, *Darpa grand challenge*, Wikipedia, 2025. [Online]. Available: https://en.wikipedia.org/wiki/DARPA_Grand_Challenge (cit. on p. 26).

[34] Mobileye, *A brief history of autonomous vehicles – from renaissance to reality*, Accessed: 2023-02-27, mobileye, 2023. [Online]. Available: https://www.mobileye.com/blog/history-autonomous-vehicles-renaissance-to-reality/ (cit. on p. 27).

[35] I. SAE, *Taxonomy and definitions for terms related to driving automation systems for on-road motor vehicles*, Technical report J3016, 2021 (cit. on p. 26).

[36] Y. Cao et al., "L3pilot - code of practice for the development of automated driving functions," European Union, Technical Report L3Pilot Deliverable D2.3, 2021. DOI: 10.13140/RG.2.2.20815.41122 (cit. on p. 28).

[37] Mercedes-Benz, *Introducing drive pilot: an automated driving system for the highway*, Technical report, 2023 (cit. on p. 28).

[38] Autoraiders, *The evolution of waymo: pioneering level 4 autonomous cars*, Accessed: 2025-07-24, 2025. [Online]. Available: https://autoraiders.com/the-evolution-of-waymo-pioneering-level-4-autonomous-cars/ (cit. on p. 28).

[39] Autoevolution, *Understanding level 4 autonomous driving systems, from currently available to upcoming*, Accessed: 2025-07-24, 2025. [Online]. Available: https://www.autoevolution.com/news/understanding-level-4-autonomous-driving-systems-from-currently-available-to-upcoming-237939.html (cit. on p. 28).

[40] A. Mahmood and R. Szabolcsi, "A systematic review on risk management and enhancing reliability in autonomous vehicles," *Machines*, vol. 13, no. 8, 2025. DOI: 10.3390/machines13080646. [Online]. Available: https://www.mdpi.com/2075-1702/13/8/646 (cit. on pp. 28, 29).

[41] L. K. Sahoo and V. Varadarajan, "Deep learning for autonomous driving systems: technological innovations, strategic implementations, and business implications - a comprehensive review," *Complex Engineering Systems*, vol. 5, no. 1, 2025. DOI: 10.20517/ces.2024.83. [Online]. Available: https://www.oaepublish.com/articles/ces.2024.83 (cit. on p. 28).

[42] B. Paden et al., "A survey of motion planning and control techniques for self-driving urban vehicles," *IEEE Transactions on Intelligent Vehicles*, vol. 1, no. 1, pp. 33–55, 2016. DOI: 10.1109/TIV.2016.2578706. [Online]. Available: https://doi.org/10.1109/TIV.2016.2578706 (cit. on pp. 28, 29, 35).

[43] L. Adouane, *Autonomous Vehicle Navigation: From Behavioral to Hybrid Multi-Controller Architectures*. 2016. [Online]. Available: https://www.crcpress.com/Autonomous-Vehicle-Navigation-From-Behavioral-to-Hybrid-Multi-controller/Adouane/9781498715584 (cit. on p. 28).

[44] E. Yurtsever et al., "A survey of autonomous driving: common practices and emerging technologies," *IEEE Access*, vol. 8, pp. 58 443–58 469, 2020. DOI: 10.1109/ACCESS.2020.2983149. [Online]. Available: https://doi.org/10.1109/ACCESS.2020.2983149 (cit. on pp. 28, 29, 35).

[45] D. J. Yeong et al., "Sensor and sensor fusion technology in autonomous vehicles: a review," *Sensors*, vol. 21, no. 6, p. 2140, 2021. DOI: 10.3390/s21062140. [Online]. Available: https://doi.org/10.3390/s21062140 (cit. on pp. 28, 29).

[46] C. Chen et al., “Deepdriving: learning affordance for direct perception in autonomous driving,” *IEEE International Conference on Computer Vision (ICCV)*, pp. 2722–2731, 2017. DOI: 10.1109/ICCV.2015.312 (cit. on pp. 28, 29).

[47] W. Schwarting, J. Alonso-Mora, and D. Rus, “Planning and decision-making for autonomous vehicles,” *Annual Review of Control, Robotics, and Autonomous Systems*, vol. 1, pp. 187–210, 2018 (cit. on p. 29).

[48] L. Claussmann et al., “A review of motion planning for highway autonomous driving,” *IEEE Transactions on Intelligent Transportation Systems*, vol. 21, no. 5, pp. 1826–1848, 2020. DOI: 10.1109/TITS.2019.2913998. [Online]. Available: https://doi.org/10.1109/TITS.2019.2913998 (cit. on pp. 29, 36).

[49] D. González et al., “A review of motion planning techniques for automated vehicles,” *IEEE Transactions on Intelligent Transportation Systems*, vol. 17, no. 4, pp. 1135–1145, 2016. DOI: 10.1109/TITS.2015.2498841. [Online]. Available: https://doi.org/10.1109/TITS.2015.2498841 (cit. on pp. 29, 35).

[50] J. Van Brummelen et al., “Autonomous vehicle perception: the technology of today and tomorrow,” *Transportation Research Part C: Emerging Technologies*, vol. 89, pp. 384–406, 2018. DOI: 10.1016/j.trc.2018.02.012. [Online]. Available: https://doi.org/10.1016/j.trc.2018.02.012 (cit. on p. 29).

[51] J. Fayyad et al., “Deep learning sensor fusion for autonomous vehicle perception and localization: a review,” *Sensors*, vol. 20, no. 15, p. 4220, 2020. DOI: 10.3390/s20154220. [Online]. Available: https://doi.org/10.3390/s20154220 (cit. on p. 29).

[52] J. Levinson et al., “Towards fully autonomous driving: systems and algorithms,” *IEEE Intelligent Vehicles Symposium (IV)*, pp. 163–168, 2011. DOI: 10.1109/IVS.2011.5940562. [Online]. Available: https://doi.org/10.1109/IVS.2011.5940562 (cit. on p. 29).

[53] S. Kuutti et al., “A survey of the state-of-the-art localization techniques and their potentials for autonomous vehicle applications,” *IEEE Internet of Things Journal*, vol. 5, no. 2, pp. 829–846, 2018. DOI: 10.1109/JIOT.2018.2812300. [Online]. Available: https://doi.org/10.1109/JIOT.2018.2812300 (cit. on p. 29).

[54] B. Bright. “Driverless technology: key components of autonomous vehicles (a complete teardown).” Blog post, Fifth Level Consulting, Accessed: Dec. 19, 2024. [Online]. Available: https://fifthlevelconsulting.com/key-components-of-autonomous-vehicles/ (cit. on p. 30).

[55] M. Buehler, K. Iagnemma, and S. Singh, *The DARPA Urban Challenge: Autonomous Vehicles in City Traffic*. Berlin, Heidelberg: Springer, 2009, ISBN: 978-3-642-03990-4. DOI: 10.1007/978-3-642-03991-1. [Online]. Available: https://doi.org/10.1007/978-3-642-03991-1 (cit. on p. 29).

[56] M. Althoff et al., “Safety verification of autonomous vehicles using probabilistic motion primitives,” in *IEEE/RSJ International Conference on Intelligent Robots and Systems (IROS)*, 2009, pp. 3747–3752. DOI: 10.1109/IROS.2009.5354582. [Online]. Available: https://doi.org/10.1109/IROS.2009.5354582 (cit. on p. 30).

[57] S. M. LaValle and J. J. Kuffner, "Randomized kinodynamic planning," in *IEEE International Conference on Robotics and Automation (ICRA)*, 2001, pp. 473–479. DOI: 10.1109/ROBOT.2001.932632. [Online]. Available: https://doi.org/10.1109/ROBOT.2001.932632 (cit. on pp. 30, 35).

[58] J.-M. Vilca, L. Adouane, and Y. Mezouar, "Reactive navigation of mobile robot using elliptic trajectories andeffective on-line obstacle detection," *In Gyroscopy and Navigation Journal, Ed. Springer, Russia ISSN 2075 1087*, vol. 4, no. 1, pp. 14–25, 2013 (cit. on p. 30).

[59] D. Nguyen-Tuong and J. Peters, "Model learning for robot control: a survey," *Cognitive Processing*, vol. 12, no. 4, pp. 319–340, 2011. DOI: 10.1007/s10339-011-0404-1. [Online]. Available: https://doi.org/10.1007/s10339-011-0404-1 (cit. on p. 30).

[60] L. P. Kaelbling, M. L. Littman, and A. W. Moore, "Reinforcement learning: a survey," *Journal of Artificial Intelligence Research*, vol. 4, pp. 237–285, 1996. DOI: 10.1613/jair.301. [Online]. Available: https://doi.org/10.1613/jair.301 (cit. on p. 30).

[61] H. Kress-Gazit, G. E. Fainekos, and G. J. Pappas, "Temporal-logic-based reactive mission and motion planning," in *IEEE International Conference on Robotics and Automation (ICRA)*, 2009, pp. 2347–2352. DOI: 10.1109/ROBOT.2009.5152399. [Online]. Available: https://doi.org/10.1109/ROBOT.2009.5152399 (cit. on p. 30).

[62] R. Rajamani, *Vehicle Dynamics and Control*, 2nd ed. New York, NY: Springer, 2012, ISBN: 978-1-4614-1432-2. DOI: 10.1007/978-1-4614-1433-9. [Online]. Available: https://doi.org/10.1007/978-1-4614-1433-9 (cit. on p. 30).

[63] J. M. Snider, "Automatic steering methods for autonomous automobile path tracking," Robotics Institute, Carnegie Mellon University, Pittsburgh, PA, Tech. Rep. CMU-RI-TR-09-08, 2009. [Online]. Available: https://www.ri.cmu.edu/pub_files/2009/2/Jarrod_Snider_Master_Thesis.pdf (cit. on p. 30).

[64] R. Isermann, R. Schwarz, and S. Stolzl, "Fault-tolerant drive-by-wire systems," *IEEE Control Systems Magazine*, vol. 22, no. 5, pp. 64–81, 2002. DOI: 10.1109/MCS.2002.1035218. [Online]. Available: https://doi.org/10.1109/MCS.2002.1035218 (cit. on p. 30).

[65] J. Nilsson, P. Falcone, and J. Vinter, "Safe transitions from automated to manual driving using driver controllability estimation," *Intelligent Transportation Systems, IEEE Transactions on*, vol. 16, pp. 1806–1816, 2015. DOI: 10.1109/TITS.2014.2376877 (cit. on p. 30).

[66] K. Jo et al., "Development of autonomous car—part ii: a case study on the implementation of an autonomous driving system based on distributed architecture," *IEEE Transactions on Industrial Electronics*, vol. 62, no. 8, pp. 5119–5132, 2015. DOI: 10.1109/TIE.2015.2410258 (cit. on p. 31).

[67] Y. Zhou et al., "Advances in decision-making for autonomous vehicles: a review," in *2023 7th CAA International Conference on Vehicular Control and Intelligence (CVCI)*, 2023, pp. 1–8. DOI: 10.1109/CVCI59596.2023.10397250 (cit. on p. 31).

[68] X. Xing et al., “A hazard analysis approach based on stpa and finite state machine for autonomous vehicles,” in *2021 IEEE Intelligent Vehicles Symposium (IV)*, 2021, pp. 150–156. DOI: 10.1109/IV48863.2021.9575425 (cit. on pp. 32, 47).

[69] C. Hubmann et al., “A pomdp maneuver planner for occlusions in urban scenarios,” in *2019 IEEE Intelligent Vehicles Symposium (IV)*, 2019, pp. 2172–2179. DOI: 10.1109/IVS.2019.8814179 (cit. on pp. 32, 64).

[70] Z. Sunberg and M. J. Kochenderfer, “Improving automated driving through pomdp planning with human internal states,” *IEEE Transactions on Intelligent Transportation Systems*, vol. 23, no. 11, pp. 20 073–20 083, 2022. DOI: 10.1109/TITS.2022.3182687 (cit. on pp. 32, 64).

[71] M. Xiaoqiang et al., “Graph convolution reinforcement learning for decision-making in highway overtaking scenario,” in *2022 IEEE 17th Conference on Industrial Electronics and Applications (ICIEA)*, 2022, pp. 417–422. DOI: 10.1109/ICIEA54703.2022.10006015 (cit. on p. 32).

[72] P. Su, C. Xiang, and D. Chen, “Adopting graph neural networks to understand and reason about dynamic driving scenarios,” *IEEE Open Journal of Intelligent Transportation Systems*, vol. 6, pp. 579–589, 2025. DOI: 10.1109/OJITS.2025.3563428 (cit. on p. 32).

[73] B. Wang et al., “Can llms understand social norms in autonomous driving games?” In *2024 IEEE International Automated Vehicle Validation Conference (IAVVC)*, 2024, pp. 1–4. DOI: 10.1109/IAVVC63304.2024.10786452 (cit. on p. 32).

[74] N. Petrovic et al., “Llm-driven testing for autonomous driving scenarios,” in *2024 2nd International Conference on Foundation and Large Language Models (FLLM)*, 2024, pp. 173–178. DOI: 10.1109/FLLM63129.2024.10852505 (cit. on p. 32).

[75] M. M. Mayer, A. Buchner, and R. Bell, “Humans, machines, and double standards? the moral evaluation of the actions of autonomous vehicles, anthropomorphized autonomous vehicles, and human drivers in road-accident dilemmas,” *Frontiers in Psychology*, vol. Volume 13 - 2022, 2023, ISSN: 1664-1078. DOI: 10.3389/fpsyg.2022.1052729. [Online]. Available: https://www.frontiersin.org/journals/psychology/articles/10.3389/fpsyg.2022.1052729 (cit. on p. 32).

[76] Y. Chen et al., “Interaction-aware decision-making for autonomous vehicles,” *IEEE Transactions on Transportation Electrification*, vol. 9, no. 3, pp. 4704–4715, 2023. DOI: 10.1109/TTE.2023.3240454 (cit. on p. 32).

[77] J. A. Rodrigues da Silva, V. Grassi, and D. F. Wolf, “Maximum entropy inverse reinforcement learning using monte carlo tree search for autonomous driving,” *IEEE Transactions on Intelligent Transportation Systems*, vol. 25, no. 9, pp. 11 552–11 562, 2024. DOI: 10.1109/TITS.2024.3363497 (cit. on p. 33).

[78] J. Chen et al., “Spatial-temporal graph neural network for interaction-aware vehicle trajectory prediction,” in *2021 IEEE 17th International Conference on Automation Science and Engineering (CASE)*, 2021, pp. 2119–2125. DOI: 10.1109/CASE49439.2021.9551450 (cit. on p. 33).

[79] Y. Yoon et al., “Interaction-aware probabilistic trajectory prediction of cut-in vehicles using gaussian process for proactive control of autonomous vehicles,” *IEEE Access*, vol. 9, pp. 63 440–63 455, 2021. DOI: 10.1109/ACCESS.2021.3075677 (cit. on p. 33).

[80] J. Liang et al., “Interaction-aware trajectory prediction for safe motion planning in autonomous driving: a transformer-transfer learning approach,” *IEEE Transactions on Intelligent Transportation Systems*, pp. 1–16, 2025. DOI: 10.1109/TITS.2025.3588228 (cit. on p. 33).

[81] K. Min et al., “Interaction aware trajectory prediction of surrounding vehicles with interaction network and deep ensemble,” in *2020 IEEE Intelligent Vehicles Symposium (IV)*, 2020, pp. 1714–1719. DOI: 10.1109/IV47402.2020.9304713 (cit. on p. 33).

[82] J. C. Hayward, “Near miss determination through use of a scale of danger,” *Highway Research Record*, vol. 384, pp. 24–34, 1972, Presented at the 51st Annual Meeting of the Highway Research Board (cit. on pp. 33, 52).

[83] D. Iberraken, L. Adouane, and D. Denis, “Multi-level bayesian decision-making for safe and flexible autonomous navigation in highway environment,” in *2018 IEEE/RSJ International Conference on Intelligent Robots and Systems (IROS)*, 2018, pp. 3984–3990. DOI: 10.1109/IROS.2018.8593565 (cit. on p. 33).

[84] L. N. Peesapati, M. P. Hunter, and M. O. Rodgers, “Can post encroachment time substitute intersection characteristics in crash prediction models?” *Journal of Safety Research*, vol. 66, pp. 205–211, 2018, ISSN: 0022-4375. DOI: https://doi.org/10.1016/j.jsr.2018.05.002. [Online]. Available: https://www.sciencedirect.com/science/article/pii/S0022437517302281 (cit. on p. 33).

[85] C. Philippe et al., “Probability collectives algorithm applied to decentralized intersection coordination for connected autonomous vehicles,” in *2019 IEEE Intelligent Vehicles Symposium (IV)*, 2019, pp. 1928–1934. DOI: 10.1109/IVS.2019.8813827 (cit. on p. 33).

[86] H. Qin et al., “Review of autonomous path planning algorithms for mobile robots,” *Drones*, vol. 7, no. 3, 2023. DOI: 10.3390/drones7030211. [Online]. Available: https://www.mdpi.com/2504-446X/7/3/211 (cit. on p. 34).

[87] E. W. Dijkstra, “A note on two problems in connexion with graphs,” *Numerische Mathematik*, vol. 1, no. 1, pp. 269–271, 1959. DOI: 10.1007/BF01386390. [Online]. Available: https://doi.org/10.1007/BF01386390 (cit. on p. 34).

[88] P. E. Hart, N. J. Nilsson, and B. Raphael, “A formal basis for the heuristic determination of minimum cost paths,” *IEEE Transactions on Systems Science and Cybernetics*, vol. 4, no. 2, pp. 100–107, 1968. DOI: 10.1109/TSSC.1968.300136. [Online]. Available: https://doi.org/10.1109/TSSC.1968.300136 (cit. on p. 34).

[89] A. Stentz, “Optimal and efficient path planning for partially-known environments,” in *IEEE International Conference on Robotics and Automation (ICRA)*, 1994, pp. 3310–3317. DOI: 10.1109/ROBOT.1994.351742. [Online]. Available: https://doi.org/10.1109/ROBOT.1994.351742 (cit. on p. 34).

[90] S. Koenig, M. Likhachev, and D. Furcy, "Lifelong planning a*," in *IJCAI Workshop on Planning under Uncertainty and Incomplete Information*, 2001, pp. 1–8 (cit. on p. 34).

[91] D. Dolgov et al., "Practical search techniques in path planning for autonomous driving," in *AAAI Workshop on Search Techniques for Problem Solving*, 2008, pp. 1–6 (cit. on pp. 34, 35).

[92] M. Pivtoraiko and A. Kelly, "Generating near-minimal spanning control sets for constrained motion planning in discrete state spaces," in *IEEE/RSJ International Conference on Intelligent Robots and Systems (IROS)*, 2005, pp. 1421–1427. DOI: 10.1109/IROS.2005.1545298. [Online]. Available: https://doi.org/10.1109/IROS.2005.1545298 (cit. on p. 34).

[93] L. E. Kavraki et al., "Probabilistic roadmaps for path planning in high-dimensional configuration spaces," *IEEE Transactions on Robotics and Automation*, vol. 12, no. 4, pp. 566–580, 1996. DOI: 10.1109/70.508439. [Online]. Available: https://doi.org/10.1109/70.508439 (cit. on p. 35).

[94] S. M. LaValle, "Rapidly-exploring random trees: a new tool for path planning," Computer Science Department, Iowa State University, Tech. Rep. TR 98-11, 1998. [Online]. Available: http://janowiec.cs.iastate.edu/papers/rrt.ps (cit. on p. 35).

[95] S. Karaman and E. Frazzoli, *Sampling-based algorithms for optimal motion planning*, arXiv preprint arXiv:1105.1186, 2011. [Online]. Available: https://arxiv.org/abs/1105.1186 (cit. on p. 35).

[96] J. D. Gammell, S. S. Srinivasa, and T. D. Barfoot, *Informed rrt*: optimal sampling-based path planning focused via direct sampling of an admissible ellipsoidal heuristic*, arXiv preprint arXiv:1404.2334, 2014. [Online]. Available: https://arxiv.org/abs/1404.2334 (cit. on p. 35).

[97] J. J. Kuffner and S. M. LaValle, "Rrt-connect: an efficient approach to single-query path planning," in *IEEE International Conference on Robotics and Automation (ICRA)*, 2000, pp. 995–1001. DOI: 10.1109/ROBOT.2000.844730. [Online]. Available: https://doi.org/10.1109/ROBOT.2000.844730 (cit. on p. 35).

[98] L. Janson et al., "Fast marching tree: a fast marching sampling-based method for optimal motion planning in many dimensions," in *International Symposium on Robotics Research (ISRR)*, 2015. DOI: 10.1007/978-3-319-28872-7_33. [Online]. Available: https://doi.org/10.1007/978-3-319-28872-7_33 (cit. on p. 35).

[99] J. D. Gammell, S. S. Srinivasa, and T. D. Barfoot, "Batch informed trees (bit*): sampling-based optimal planning via the heuristically guided search of implicit random geometric graphs," in *IEEE International Conference on Robotics and Automation (ICRA)*, 2015, pp. 3067–3074. DOI: 10.1109/ICRA.2015.7139620. [Online]. Available: https://doi.org/10.1109/ICRA.2015.7139620 (cit. on p. 35).

[100] E. Aljalbout et al., "Non-uniform tree sampling for efficient path planning in dynamic environments," in *IEEE/RSJ International Conference on Intelligent Robots and Systems (IROS)*, 2020, pp. 8765–8772. DOI: 10.1109/IROS45743.2020.9341712. [Online]. Available: https://doi.org/10.1109/IROS45743.2020.9341712 (cit. on p. 35).

[101] L. E. Dubins, "On curves of minimal length with a constraint on average curvature, and with prescribed initial and terminal positions and tangents," *American Journal of Mathematics*, vol. 79, no. 3, pp. 497–516, 1957. DOI: 10.2307/2372560. [Online]. Available: https://doi.org/10.2307/2372560 (cit. on p. 35).

[102] J. A. Reeds and L. A. Shepp, "Optimal paths for a car that goes both forwards and backwards," *Pacific Journal of Mathematics*, vol. 145, no. 2, pp. 367–393, 1990. [Online]. Available: http://projecteuclid.org/euclid.pjm/1102635450 (cit. on p. 35).

[103] Y. Kanayama and N. Miyake, "Trajectory generation for mobile robots," *Robotics Research*, vol. 3, pp. 333–340, 1986 (cit. on p. 35).

[104] J.-W. Choi, R. E. Curry, and G. H. Elkaim, "Path planning based on gaussian elimination for autonomous ground vehicles," in *IEEE Advances in Control Systems*, Published in proceedings, 1990 (cit. on p. 35).

[105] K. Komoriya and K. Tanie, "Trajectory design and control of a wheeled mobile robot using b-spline curve," in *IEEE/RSJ International Workshop on Intelligent Robots and Systems (IROS)*, 1989, pp. 206–213. DOI: 10.1109/IROS.1989.637249. [Online]. Available: https://doi.org/10.1109/IROS.1989.637249 (cit. on p. 35).

[106] Y. Zhanhang and W. Jingyang. "In wuhan, robotaxis put china's self-driving ambitions to the test," Accessed: Dec. 19, 2024. [Online]. Available: https://www.sixthtone.com/news/1015767 (cit. on p. 36).

[107] National Transportation Safety Board, "Collision between vehicle controlled by developmental automated driving system and pedestrian tempe, arizona march 18, 2018," National Transportation Safety Board, Tech. Rep. NTSB/HAR-19/03 PB2019-101402, 2019, Accident date: March 18, 2018. [Online]. Available: https://www.ntsb.gov/investigations/AccidentReports/Reports/HAR1903.pdf (cit. on p. 36).

[108] European Commission, *Cooperative connected intelligent vehicles for safe and efficient road transport*, CORDIS project fact sheet. Accessed on 2025-08-27, European Commission, 2018. [Online]. Available: https://cordis.europa.eu/project/id/824019 (cit. on p. 36).

[109] T. Taleb et al., "Mobile edge computing potential in making cities smarter," *Comm. Mag.*, vol. 55, no. 3, pp. 38–43, 2017, ISSN: 0163-6804. DOI: 10.1109/MCOM.2017.1600249CM. [Online]. Available: https://doi.org/10.1109/MCOM.2017.1600249CM (cit. on p. 37).

[110] X. Sun, F. R. Yu, and P. Zhang, "A survey on cyber-security of connected and autonomous vehicles (cavs)," *IEEE Transactions on Intelligent Transportation Systems*, vol. 23, no. 7, pp. 6240–6259, 2022. DOI: 10.1109/TITS.2021.3085297 (cit. on p. 37).

[111] P. Sharma and J. Gillanders, "Cybersecurity and forensics in connected autonomous vehicles: a review of the state-of-the-art," *IEEE Access*, vol. 10, pp. 108 979–108 996, 2022. DOI: 10.1109/ACCESS.2022.3213843 (cit. on p. 37).

[112] T. Wang et al., “Survey on cooperatively v2x downloading for intelligent transport systems,” *IET Intelligent Transport Systems*, vol. 13, pp. 13–21, 1 2019. DOI: 10.1049/iet-its.2018.5104. [Online]. Available: https://digital-library.theiet.org/doi/abs/10.1049/iet-its.2018.5104 (cit. on p. 37).

[113] G. Thandavarayan, M. Sepulcre, and J. Gozalvez, “Cooperative perception for connected and automated vehicles: evaluation and impact of congestion control,” *IEEE Access*, vol. 8, pp. 197 665–197 683, 2020. DOI: 10.1109/ACCESS.2020.3035119 (cit. on p. 37).

[114] M. Wang et al., “Game-theoretic planning for self-driving cars in multivehicle competitive scenarios,” *IEEE Transactions on Robotics*, vol. 37, no. 4, pp. 1313–1325, 2021. DOI: 10.1109/TRO.2020.3047521 (cit. on p. 37).

[115] G. Bresson et al., “Simultaneous localization and mapping: a survey of current trends in autonomous driving,” *IEEE Transactions on Intelligent Vehicles*, vol. 2, no. 3, pp. 194–220, 2017. DOI: 10.1109/TIV.2017.2749181 (cit. on p. 37).

[116] V. Milanés et al., “Cooperative adaptive cruise control in real traffic situations,” *IEEE Transactions on Intelligent Transportation Systems*, vol. 15, no. 1, pp. 296–305, 2014. DOI: 10.1109/TITS.2013.2278494 (cit. on p. 38).

[117] Z. Wang et al., “A survey on cooperative longitudinal motion control of multiple connected and automated vehicles,” *IEEE Intelligent Transportation Systems Magazine*, vol. 12, no. 1, pp. 4–24, 2020. DOI: 10.1109/MITS.2019.2953562 (cit. on p. 38).

[118] B. Mendes et al., “Exploring v2x in 5g networks: a comprehensive survey of location-based services in hybrid scenarios,” *Vehicular Communications*, vol. 52, p. 100 878, 2025, ISSN: 2214-2096. DOI: https://doi.org/10.1016/j.vehcom.2025.100878. [Online]. Available: https://www.sciencedirect.com/science/article/pii/S2214209625000051 (cit. on p. 38).

[119] G. G. M. N. Ali et al., “A comprehensive study and analysis of the third generation partnership project’s 5g new radio for vehicle-to-everything communication,” *Future Internet*, vol. 16, no. 1, 2024, ISSN: 1999-5903. DOI: 10.3390/fi16010021. [Online]. Available: https://www.mdpi.com/1999-5903/16/1/21 (cit. on p. 38).

[120] H. Liu et al., “Improved consensus admm for cooperative motion planning of large-scale connected autonomous vehicles with limited communication,” *IEEE Transactions on Intelligent Vehicles*, vol. 9, no. 11, pp. 7222–7238, 2024. DOI: 10.1109/TIV.2024.3395479 (cit. on p. 38).

[121] B. Häfner et al., “A survey on cooperative architectures and maneuvers for connected and automated vehicles,” *IEEE Communications Surveys & Tutorials*, vol. 24, no. 1, pp. 380–403, 2022. DOI: 10.1109/COMST.2021.3138275 (cit. on p. 38).

[122] L. Gherardini, G. Cabri, and M. Montangero, “Decentralized approaches for autonomous vehicles coordination,” *Internet Technology Letters*, vol. 8, no. 1, e398, 2025. DOI: https://doi.org/10.1002/itl2.398. [Online]. Available: https://onlinelibrary.wiley.com/doi/abs/10.1002/itl2.398 (cit. on p. 38).

[123] Z. Huang, S. Shen, and J. Ma, “Decentralized ilqr for cooperative trajectory planning of connected autonomous vehicles via dual consensus admm,” *IEEE Transactions on Intelligent Transportation Systems*, vol. 24, no. 11, pp. 12 754–12 766, 2023. DOI: 10.1109/TITS.2023.3286898 (cit. on p. 38).

[124] V. P. Chellapandi et al., “Federated learning for connected and automated vehicles: a survey of existing approaches and challenges,” *IEEE Transactions on Intelligent Vehicles*, vol. 9, no. 1, pp. 119–137, 2024. DOI: 10.1109/TIV.2023.3332675 (cit. on p. 38).

[125] A. J. M. Muzahid et al., “Multiple vehicle cooperation and collision avoidance in automated vehicles: survey and an ai-enabled conceptual framework,” *Scientific Reports*, vol. 13, no. 1, p. 603, 2023, ISSN: 2045-2322. DOI: 10.1038/s41598-022-27026-9. [Online]. Available: https://doi.org/10.1038/s41598-022-27026-9 (cit. on p. 38).

[126] G. Wu et al., “Development of agent-based online adaptive signal control (asc) framework using connected vehicle (cv) technology,” University of California, Riverside, United States, Tech. Rep. CA16-2811, 2016, Funding: 65A0529-002. Collection: US Transportation Collection (cit. on p. 39).

[127] T. Chaanine et al., “A control-oriented highway traffic model with multiple clusters of cavs,” in *2023 IEEE 26th International Conference on Intelligent Transportation Systems (ITSC)*, 2023, pp. 5198–5203. DOI: 10.1109/ITSC57777.2023.10421830 (cit. on p. 39).

[128] Z. Zhu, L. Adouane, and A. Quilliot, “Decentralised cavs based on micro–macro flow control (mimafc) strategy for multi-intersection traffic network,” *IET Intelligent Transport Systems*, vol. 17, no. 3, pp. 503–521, 2023. DOI: https://doi.org/10.1049/itr2.12276. [Online]. Available: https://ietresearch.onlinelibrary.wiley.com/doi/abs/10.1049/itr2.12276 (cit. on p. 39).

[129] E. Scarlett, “Denmark to ban petrol and diesel cars by 2030,” *Power Technology*, 2018 (cit. on p. 39).

[130] BBC, *New diesel and petrol vehicles to be banned from 2040 in the uk*, https://www.bbc.com/news/uk-40723581, 2017 (cit. on p. 39).

[131] D. Zhao, Y. Dai, and Z. Zhang, “Computational intelligence in urban traffic signal control: a survey,” *IEEE Transactions on Systems, Man, and Cybernetics, Part C (Applications and Reviews)*, vol. 42, no. 4, pp. 485–494, 2012. DOI: 10.1109/TSMCC.2011.2161577 (cit. on p. 39).

[132] H. Yang et al., “Cooperative trajectory optimization for multiple connected vehicles at an unsignalized intersection,” *Advances in Mechanical Engineering*, vol. 17, no. 6, p. 16 878 132 251 349 330, 2025. DOI: 10.1177/16878132251349330 (cit. on p. 40).

[133] K. Dresner and P. Stone, “A multiagent approach to autonomous intersection management,” *Journal of Artificial Intelligence Research*, vol. 31, pp. 591–656, 2008 (cit. on pp. 40, 60).

[134] F. Alanazi, “A systematic literature review of autonomous and connected vehicles in traffic management,” *Applied Sciences*, vol. 13, no. 3, 2023, ISSN: 2076-3417 (cit. on p. 40).

[135] B. Donnelly, *Slot-based intersections*, Blog post. Accessed on 2025-08-20, 2016. [Online]. Available: https://brandondonnelly.com/slot-based-intersections (cit. on pp. 40, 74).

[136] D. Wesemeyer, M. Ortgiese, and S. Ruppe, “Slot-based dynamic traffic control - deriving generation rules from automated and connected driving and lane change behavior,” *Frontiers in Future Transportation*, vol. Volume 5 - 2024, 2024. DOI: 10.3389/ffutr.2024.1415375 (cit. on p. 40).

[137] X. Yang et al., “Research on vehicle-infrastructure cooperative traffic control for urban road travel reservation: frontiers and prospects,” *Journal of University of Shanghai for Science and Technology*, vol. 45, no. 4, pp. 307–320, 331, 2023 (cit. on p. 40).

[138] M. W. Levin, S. D. Boyles, and R. Patel, “Paradoxes of reservation-based intersection controls in traffic networks,” *Transportation Research Part A: Policy and Practice*, vol. 90, pp. 14–25, 2016, ISSN: 0965-8564. DOI: https://doi.org/10.1016/j.tra.2016.05.013. [Online]. Available: https://www.sciencedirect.com/science/article/pii/S0965856416303822 (cit. on p. 41).

[139] Z. Huang, S. Shen, and J. Ma, “Decentralized ilqr for cooperative trajectory planning of connected autonomous vehicles via dual consensus admm,” *IEEE Transactions on Intelligent Transportation Systems*, vol. 24, no. 11, pp. 12 754–12 766, 2023 (cit. on p. 41).

[140] E. Todorov and W. Li, “A generalized iterative LQG method for locally-optimal feedback control of constrained nonlinear stochastic systems,” *Proceedings of the 2005, American Control Conference, 2005.*, pp. 300–306, 2005. DOI: 10.1109/ACC.2005.1469949 (cit. on p. 41).

[141] W. Li and E. Todorov, “Iterative linear quadratic regulator design for nonlinear biological movement systems,” in *First International Conference on Informatics in Control, Automation and Robotics*, vol. 2, SciTePress, 2004, pp. 222–229 (cit. on p. 41).

[142] M. Doostmohammadian et al., “Fully distributed mpc with quantized communication for decentralized intersection coordination,” *arXiv preprint arXiv:2501.18889*, 2025 (cit. on p. 41).

[143] E. Nisyrios and K. Gkiotsalitis, “Optimization-based approaches for traffic and fleet management of connected and autonomous vehicles: a systematic literature review,” *International Journal of Intelligent Transportation Systems Research*, 2025 (cit. on p. 41).

[144] W. Bai et al., “An optimal scheduling model for connected automated vehicles at an unsignalized intersection,” *Algorithms*, vol. 18, no. 4, 2025, ISSN: 1999-4893 (cit. on p. 41).

[145] X. Pan et al., “A convex optimal control framework for autonomous vehicle intersection crossing,” *IEEE Transactions on Intelligent Transportation Systems*, vol. 24, no. 1, pp. 163–177, 2023. DOI: 10.1109/TITS.2022.3211272 (cit. on p. 41).

[146] T. Niels et al., “Optimization-based intersection control for connected automated vehicles and pedestrians,” *Transportation Research Record*, vol. 2678, no. 2, pp. 135–152, 2024. DOI: 10.1177/03611981231172956 (cit. on p. 41).

[147] G. R. Campos et al., “Cooperative receding horizon conflict resolution at traffic intersections,” in *53rd IEEE Conference on Decision and Control*, 2014, pp. 2932–2937. DOI: 10.1109/CDC.2014.7039840 (cit. on p. 42).

[148] R. Yao et al., “A path planning model based on spatio-temporal state vector from vehicles trajectories,” in *2019 IEEE 4th International Conference on Big Data Analytics (ICBDA)*, 2019, pp. 216–220. DOI: 10.1109/ICBDA.2019.8713199 (cit. on p. 42).

[149] W. Zhang, P. Yadmellat, and Z. Gao, “Spatial optimization in spatio-temporal motion planning,” in *2022 IEEE Intelligent Vehicles Symposium (IV)*, 2022, pp. 1248–1254. DOI: 10.1109/IV51971.2022.9827125 (cit. on p. 42).

[150] K. L. Keung, K. H. Chow, and C. K. M. Lee, “Collision avoidance and trajectory planning for autonomous mobile robot: a spatio-temporal deep learning approach,” in *2023 IEEE International Conference on Industrial Engineering and Engineering Management (IEEM)*, 2023, pp. 1042–1046. DOI: 10.1109/IEEM58616.2023.10406802 (cit. on p. 42).

[151] S. E. Li et al., “Dynamical modeling and distributed control of connected and automated vehicles: challenges and opportunities,” *IEEE Intelligent Transportation Systems Magazine*, vol. 9, no. 3, pp. 46–58, 2017. DOI: 10.1109/MITS.2017.2709781 (cit. on pp. 42, 62).

[152] Q. Li, Z. Chen, and X. Li, “A review of connected and automated vehicle platoon merging and splitting operations,” *IEEE Transactions on Intelligent Transportation Systems*, vol. 23, no. 12, pp. 22 790–22 806, 2022. DOI: 10.1109/TITS.2022.3193278 (cit. on p. 43).

[153] C. Wang, Y. Dai, and J. Xia, “A cav platoon control method for isolated intersections: guaranteed feasible multi-objective approach with priority,” *Energies*, vol. 13, no. 3, 2020, ISSN: 1996-1073. DOI: 10.3390/en13030625. [Online]. Available: https://www.mdpi.com/1996-1073/13/3/625 (cit. on p. 43).

[154] B. D. Greenshields, “A study in highway capacity,” *Highway Research Board Proceedings*, vol. 14, pp. 448–477, 1935 (cit. on pp. 44, 68).

[155] H. Greenberg, “An analysis of traffic flow,” *Operations Research*, vol. 7, no. 1, pp. 79–85, 1959. DOI: 10.1287/opre.7.1.79 (cit. on p. 44).

[156] R. T. Underwood, “Speed, volume, and density relationships: quality and theory of traffic flow,” in *Proceedings of the 1961 Symposium on the Theory of Traffic Flow*, New Haven, CT: Yale Bureau of Highway Traffic, 1961 (cit. on p. 44).

[157] M. J. Lighthill and G. B. Whitham, “On kinematic waves ii: a theory of traffic flow on long crowded roads,” *Proceedings of the Royal Society A*, vol. 229, no. 1178, pp. 317–345, 1955. DOI: 10.1098/rspa.1955.0089 (cit. on p. 44).

[158] P. I. Richards, “Shock waves on the highway,” *Operations Research*, vol. 4, no. 1, pp. 42–51, 1956. DOI: 10.1287/opre.4.1.42 (cit. on p. 44).

[159] C. F. Daganzo, "The cell transmission model: a dynamic representation of highway traffic based on hydrodynamic theory," *Transportation Research Part B: Methodological*, vol. 28, no. 4, pp. 269–287, 1994. DOI: 10.1016/0191-2615(94)90002-7 (cit. on p. 44).

[160] N. Geroliminis and C. F. Daganzo, "Existence of urban-scale macroscopic fundamental diagrams: some experimental findings," *Transportation Research Part B: Methodological*, vol. 42, no. 9, pp. 759–770, 2008. DOI: 10.1016/j.trb.2008.02.002 (cit. on pp. 44, 71).

[161] M. Johari, M. Keyvan-Ekbatani, and D. Ngoduy, "Impacts of bus stop location and berth number on urban network traffic performance," *IET Intelligent Transport Systems*, vol. 14, pp. 1546–1554, 12 2020. DOI: 10.1049/iet-its.2019.0860. Preprint: https://digital-library.theiet.org/doi/pdf/10.1049/iet-its.2019.0860. [Online]. Available: https://digital-library.theiet.org/doi/abs/10.1049/iet-its.2019.0860 (cit. on p. 44).

[162] J. Wang et al., "Macroscopic traffic flow modeling and empirical analysis of multiple modes of travel in urban road network," in *2022 4th International Academic Exchange Conference on Science and Technology Innovation (IAECST)*, 2022, pp. 513–517. DOI: 10.1109/IAECST57965.2022.10061880 (cit. on p. 44).

[163] H. Tu et al., "When to control the ramps on freeway corridors? a novel stability-and-mfd-based approach," *IEEE Transactions on Intelligent Transportation Systems*, vol. 15, no. 6, pp. 2572–2582, 2014. DOI: 10.1109/TITS.2014.2318752 (cit. on p. 44).

[164] Y. Yokoi and S. Yamamoto, "Control of a cyclic vehicular traffic flow based on the optimal velocity model — experiments by using lego nxt," in *2012 Proceedings of SICE Annual Conference (SICE)*, 2012, pp. 801–806 (cit. on p. 44).

[165] X. Hu, C. Huang, and A. Luo, "An area traffic signal optimum timing control model in mixed traffic flows and algorithm," in *2009 Second International Conference on Intelligent Computation Technology and Automation*, vol. 3, 2009, pp. 467–470. DOI: 10.1109/ICICTA.2009.913 (cit. on p. 44).

[166] S. Hwang et al., "Autonomous vehicle cut-in algorithm for lane-merging scenarios via policy-based reinforcement learning nested within finite-state machine," *IEEE Transactions on Intelligent Transportation Systems*, vol. 23, no. 10, pp. 17 594–17 606, 2022. DOI: 10.1109/TITS.2022.3153848 (cit. on p. 47).

[167] W. Sun et al., "Energy and mobility impacts of connected autonomous vehicles with co-optimization of speed and powertrain on mixed vehicle platoons," *Transportation Research Part C: Emerging Technologies*, vol. 142, p. 103 764, 2022, ISSN: 0968-090X. DOI: https://doi.org/10.1016/j.trc.2022.103764. [Online]. Available: https://www.sciencedirect.com/science/article/pii/S0968090X22001978 (cit. on p. 49).

[168] Y. Shimizu et al., "Jerk constrained velocity planning for an autonomous vehicle: linear programming approach," in *2022 International Conference on Robotics and Automation (ICRA)*, 2022, pp. 5814–5820. DOI: 10.1109/ICRA46639.2022.9812155 (cit. on p. 49).

[169] H. Jiang et al., “A multi-objective optimal control method for navigating connected and automated vehicles at signalized intersections based on reinforcement learning,” *Applied Sciences*, vol. 14, no. 7, 2024, ISSN: 2076-3417. [Online]. Available: https://www.mdpi.com/2076-3417/14/7/3124 (cit. on p. 49).

[170] C. S. Tan et al., “Pareto optimization with small data by learning across common objective spaces,” *Scientific Reports*, vol. 13, no. 1, p. 7842, 2023, ISSN: 2045-2322. DOI: 10.1038/s41598-023-33414-6. [Online]. Available: https://doi.org/10.1038/s41598-023-33414-6 (cit. on p. 49).

[171] C. Peng et al., “Drivers’ evaluation of different automated driving styles: is it both comfortable and natural?” *Human Factors*, vol. 66, no. 3, pp. 787–806, 2024. DOI: 10.1177/00187208221113448 (cit. on p. 50).

[172] H. A. Rakha et al., “Virginia tech comprehensive power-based fuel consumption model: model development and testing,” *Transportation Research Part D: Transport and Environment*, vol. 16, no. 7, pp. 492–503, 2011, ISSN: 1361-9209. DOI: https://doi.org/10.1016/j.trd.2011.05.008 (cit. on p. 50).

[173] A. M. Lekkas and T. I. Fossen, “Minimization of cross-track and along-track errors for path tracking of marine underactuated vehicles,” in *2014 European Control Conference (ECC)*, 2014, pp. 3004–3010. DOI: 10.1109/ECC.2014.6862594 (cit. on p. 51).

[174] Z. Zhu, “Hierarchical and hybrid decisional control architecture for cooperative navigation of autonomous vehicles in complex environments/situations,” Ph.D. dissertation, Université Clermont Auvergne, 2022 (cit. on pp. 53, 74).

[175] Y. Li et al., “Integrated cooperative adaptive cruise and variable speed limit controls for reducing rear-end collision risks near freeway bottlenecks based on micro-simulations,” *IEEE Transactions on Intelligent Transportation Systems*, vol. 18, no. 11, pp. 3157–3167, 2017. DOI: 10.1109/TITS.2017.2682193 (cit. on p. 53).

[176] C. Chai et al., “Evaluation and optimization of responsibility-sensitive safety models on autonomous car-following maneuvers,” *Transportation Research Record*, vol. 2674, no. 11, pp. 662–673, 2020. DOI: 10.1177/0361198120948507. Preprint: https://doi.org/10.1177/0361198120948507. [Online]. Available: https://doi.org/10.1177/0361198120948507 (cit. on p. 54).

[177] H. Behbahani et al., “Developing a new surrogate safety indicator based on motion equations,” *Promet - Traffic&Transportation*, vol. 26, no. 5, pp. 371–381, 2014. DOI: 10.7307/ptt.v26i5.1388. [Online]. Available: https://traffic2.fpz.hr/index.php/PROMTT/article/view/2489 (cit. on p. 54).

[178] K. Bellingard, L. Adouane, and F. Peyrin, “Safe overtaking maneuver for autonomous vehicle under risky situations based on adaptive velocity profile,” in *2021 IEEE International Intelligent Transportation Systems Conference (ITSC)*, 2021, pp. 304–311. DOI: 10.1109/ITSC48978.2021.9564964 (cit. on p. 54).

[179] D. Iberraken and L. Adouane, “Safe navigation and evasive maneuvers based on probabilistic multi-controller architecture,” *IEEE Transactions on Intelligent Transportation Systems*, vol. 23, no. 9, pp. 15 558–15 573, 2022. DOI: 10.1109/TITS.2022.3141893 (cit. on p. 54).

[180] M. Mouad et al., “Mobile robot navigation and obstacles avoidance based on planning and re-planning algorithm,” *IFAC Proceedings Volumes*, vol. 45, no. 22, pp. 622–628, 2012, 10th IFAC Symposium on Robot Control, ISSN: 1474-6670. DOI: https://doi.org/10.3182/20120905-3-HR-2030.00170. [Online]. Available: https://www.sciencedirect.com/science/article/pii/S1474667016336795 (cit. on p. 56).

[181] W. Ding et al., “Safe trajectory generation for complex urban environments using spatio-temporal semantic corridor,” *IEEE Robotics and Automation Letters*, vol. 4, no. 3, pp. 2997–3004, 2019. DOI: 10.1109/LRA.2019.2923954 (cit. on p. 56).

[182] M. Morsali, E. Frisk, and J. Åslund, “Spatio-temporal planning in multi-vehicle scenarios for autonomous vehicle using support vector machines,” *IEEE Transactions on Intelligent Vehicles*, vol. 6, no. 4, pp. 611–621, 2021. DOI: 10.1109/TIV.2020.3042087 (cit. on p. 56).

[183] B. Angulo, A. Panov, and K. Yakovlev, “Policy optimization to learn adaptive motion primitives in path planning with dynamic obstacles,” *IEEE Robotics and Automation Letters*, vol. 8, no. 2, pp. 824–831, 2023. DOI: 10.1109/LRA.2022.3233261 (cit. on p. 57).

[184] A. Botros and S. L. Smith, “Spatio-temporal lattice planning using optimal motion primitives,” *IEEE Transactions on Intelligent Transportation Systems*, vol. 24, no. 11, pp. 11 950–11 962, 2023. DOI: 10.1109/TITS.2023.3297068 (cit. on p. 57).

[185] K. Dresner and P. Stone, “Multiagent traffic management: an improved intersection control mechanism,” in *Proceedings of the Fourth International Joint Conference on Autonomous Agents and Multiagent Systems*, ser. AAMAS ’05, The Netherlands: Association for Computing Machinery, 2005, pp. 471–477, ISBN: 1595930930. DOI: 10.1145/1082473.1082545. [Online]. Available: https://doi.org/10.1145/1082473.1082545 (cit. on p. 61).

[186] I. H. Zohdy and H. Rakha, “Intersection management via vehicle connectivity: the intersection cooperative adaptive cruise control system concept,” *Journal of Intelligent Transportation Systems*, vol. 16, no. 4, pp. 221–232, 2012. DOI: 10.1080/15472450.2012.704336 (cit. on p. 61).

[187] J. Lee, B. Park, and I. Yun, “Cumulative travel-time models for intersection control of autonomous vehicles,” *Transportation Research Record*, vol. 2391, no. 1, pp. 67–77, 2013. DOI: 10.3141/2391-08 (cit. on p. 61).

[188] A. Abbas-Turki et al., “Autonomous intersection management: optimal trajectories and efficient scheduling,” *Sensors*, vol. 23, no. 3, 2023, ISSN: 1424-8220. DOI: 10.3390/s23031509. [Online]. Available: https://www.mdpi.com/1424-8220/23/3/1509 (cit. on p. 62).

[189] G. Lozenguez et al., “Punctual versus continuous auction coordination for multi-robot and multi-task topological navigation,” *Autonomous Robots*, vol. 40, no. 4, pp. 599–613, 2016 (cit. on p. 64).

[190] Z. Hu et al., “Cooperative-game-theoretic optimal robust path tracking control for autonomous vehicles,” *Journal of Vibration and Control*, vol. 28, no. 5-6, pp. 520–535, 2022. DOI: 10.1177/10775463211009383. [Online]. Available: https://doi.org/10.1177/10775463211009383 (cit. on p. 64).

[191] Z. Yang et al., “Design and optimization of robust path tracking control for autonomous vehicles with fuzzy uncertainty,” *IEEE Transactions on Fuzzy Systems*, vol. 30, no. 6, pp. 1788–1800, 2022. DOI: 10.1109/TFUZZ.2021.3067724 (cit. on p. 64).

[192] C. Hubmann et al., “Decision making for autonomous driving considering interaction and uncertain prediction of surrounding vehicles,” in *2017 IEEE Intelligent Vehicles Symposium (IV)*, 2017, pp. 1671–1678. DOI: 10.1109/IVS.2017.7995949 (cit. on p. 65).

[193] L. Jaulin et al., *Applied Interval Analysis: With Examples in Parameter and State Estimation, Robust Control and Robotics*. Springer, 2001 (cit. on p. 66).

[194] N. M. Ben Lakhal et al., “Safe and adaptive autonomous navigation under uncertainty based on sequential waypoints and reachability analysis,” *Robotics and Autonomous Systems*, vol. 152, p. 104 065, 2022, ISSN: 0921-8890. DOI: https://doi.org/10.1016/j.robot.2022.104065. [Online]. Available: https://www.sciencedirect.com/science/article/pii/S092188902200032X (cit. on p. 67).

[195] N. M. B. Lakhal et al., “Interval-based/data-driven risk management for intelligent vehicles: application to an adaptive cruise control system,” in *2019 IEEE Intelligent Vehicles Symposium (IV)*, 2019, pp. 239–244. DOI: 10.1109/IVS.2019.8814216 (cit. on p. 67).

[196] V. Narri et al., “Shared situational awareness with v2x communication and set-membership estimation,” in *2023 IEEE 26th International Conference on Intelligent Transportation Systems (ITSC)*, 2023, pp. 3335–3342. DOI: 10.1109/ITSC57777.2023.10422498 (cit. on p. 67).

[197] P. Vyas, L. Vachhani, and K. Sridharan, “Interval analysis technique for versatile and parallel multi-agent collision detection and avoidance,” *Journal of Intelligent & Robotic Systems*, vol. 98, no. 3, pp. 705–720, 2020, ISSN: 1573-0409. DOI: 10.1007/s10846-019-01091-1. [Online]. Available: https://doi.org/10.1007/s10846-019-01091-1 (cit. on p. 67).

[198] M.-J. Hao and B.-Y. Hsieh, “Greenshields model-based fuzzy system for predicting traffic congestion on highways,” *IEEE Access*, vol. 12, pp. 115 868–115 882, 2024. DOI: 10.1109/ACCESS.2024.3446843 (cit. on p. 69).

[199] M. Xu and Z.-K. Shi, “Outflow models based on velocity/density formulation used in dynamic traffic assignment,” in *2005 International Conference on Machine Learning and Cybernetics*, vol. 6, 2005, 3568–3573 Vol. 6. DOI: 10.1109/ICMLC.2005.1527560 (cit. on p. 69).

[200] B. S. Kerner, “Experimental features of self-organization in traffic flow,” *Physical Review Letters*, vol. 81, no. 17, pp. 3797–3800, 1998. DOI: 10.1103/PhysRevLett.81.3797 (cit. on p. 70).

[201] C. F. Daganzo and N. Geroliminis, “An analytical approximation for the macroscopic fundamental diagram of urban traffic,” *Transportation Research Part B: Methodological*, vol. 42, no. 9, pp. 771–781, 2008, ISSN: 0191-2615. DOI: https://doi.org/10.1016/j.trb.2008.06.008. [Online]. Available: https://www.sciencedirect.com/science/article/pii/S0191261508000799 (cit. on p. 71).

[202] M. Yildirimoglu and N. Geroliminis, "Approximating dynamic equilibrium conditions with macroscopic fundamental diagrams," *Transportation Research Part B: Methodological*, vol. 70, pp. 186–200, 2014, ISSN: 0191-2615. DOI: https://doi.org/10.1016/j.trb.2014.09.002. [Online]. Available: https://www.sciencedirect.com/science/article/pii/S0191261514001568 (cit. on p. 71).

[203] K. Bellingard, L. Adouane, and F. Peyrin, "Safe and adaptive roundabout insertion for autonomous vehicle based limit-cycle and predicted inter-distance profiles," in *2023 European Control Conference (ECC)*, 2023, pp. 1–7. DOI: 10.23919/ECC57647.2023.10178129 (cit. on p. 74).

[204] Z. Zhu, L. Adouane, and A. Quilliot, "Flexible multi-unmanned ground vehicles (mugvs) in intersection coordination based on ε-constraint probability collectives algorithm," *International Journal of Intelligent Robotics and Applications*, vol. 5, pp. 156–175, 2021. DOI: https://doi.org/10.1007/s41315-021-00181-4 (cit. on p. 75).

[205] S. Kirkpatrick, C. D. Gelatt, and M. P. Vecchi, "Optimization by simulated annealing," *Science*, vol. 220, no. 4598, pp. 671–680, 1983 (cit. on p. 89).

[206] Z. Zhu, L. Adouane, and A. Quilliot, "A decentralized multi-criteria optimization algorithm for multi-unmanned ground vehicles (mugvs) navigation at signal-free intersection," *IFAC-PapersOnLine*, vol. 54, no. 2, pp. 327–334, 2021, 16th IFAC Symposium on Control in Transportation Systems CTS 2021, ISSN: 2405-8963. DOI: https://doi.org/10.1016/j.ifacol.2021.06.038. [Online]. Available: https://www.sciencedirect.com/science/article/pii/S240589632100478X (cit. on p. 90).

[207] S. Shalev-Shwartz, S. Shammah, and A. Shashua, "On a formal model of safe and scalable self-driving cars," *ArXiv*, vol. abs/1708.06374, 2017. [Online]. Available: https://api.semanticscholar.org/CorpusID:1430623 (cit. on p. 102).

[208] R. Y. Rubinstein, "The cross-entropy method for combinatorial and continuous optimization," *Methodology and Computing in Applied Probability*, vol. 1, no. 2, pp. 127–190, 1999. DOI: 10.1023/A:1010091220143 (cit. on p. 105).

[209] J. Mockus, "On bayesian methods for seeking the extremum," in *Proceedings of the IFIP Technical Conference*, Berlin, Heidelberg: Springer-Verlag, 1974, pp. 400–404, ISBN: 3540071652 (cit. on pp. 105, 107).

[210] C. E. Rasmussen and C. K. I. Williams, *Gaussian Processes for Machine Learning*. The MIT Press, 2005, ISBN: 9780262256834. DOI: 10.7551/mitpress/3206.001.0001. [Online]. Available: https://doi.org/10.7551/mitpress/3206.001.0001 (cit. on p. 105).

[211] T. Gneiting and A. E. Raftery, "Strictly proper scoring rules, prediction, and estimation," *Journal of the American Statistical Association*, vol. 102, no. 477, pp. 359–378, 2007. DOI: 10.1198/016214506000001437 (cit. on p. 106).

[212] C. Guo et al., "On calibration of modern neural networks," in *Proceedings of the 34th International Conference on Machine Learning - Volume 70*, ser. ICML'17, Sydney, NSW, Australia: JMLR.org, 2017, pp. 1321–1330 (cit. on p. 106).

[213] A. Filos et al., “Can autonomous vehicles identify, recover from, and adapt to distribution shifts?” In *Proceedings of the 37th International Conference on Machine Learning*, ser. ICML’20, JMLR.org, 2020 (cit. on p. 106).

[214] J. Rios-Torres and A. A. Malikopoulos, “A survey on the coordination of connected and automated vehicles at intersections and merging at highway on-ramps,” *IEEE Transactions on Intelligent Transportation Systems*, vol. 18, no. 5, pp. 1066–1077, 2017. DOI: 10.1109/TITS.2016.2600504 (cit. on p. 121).

[215] Federal Highway Administration, “Traffic flow theory: a state-of-the-art report – chapter 9: traffic flow at signalized intersections,” 2010, Assumes Poisson arrivals at each lane, yielding (shifted) negative exponential headways. [Online]. Available: https://www.fhwa.dot.gov/publications/research/operations/tft/chap9.pdf (cit. on p. 136).